

**STRESS INTENSITY FACTORS AND
WEIGHT FUNCTIONS FOR SURFACE CRACKED
PLATES AND WELDED JOINTS**

by

Xin Wang

A thesis
presented to the University of Waterloo
in fulfillment of the
thesis requirement for the degree of
Doctor of Philosophy
in
Mechanical Engineering
Waterloo, Ontario, Canada, 1997

© Xin Wang, 1997



National Library
of Canada

Acquisitions and
Bibliographic Services

395 Wellington Street
Ottawa ON K1A 0N4
Canada

Bibliothèque nationale
du Canada

Acquisitions et
services bibliographiques

395, rue Wellington
Ottawa ON K1A 0N4
Canada

Your file Votre référence

Our file Notre référence

The author has granted a non-exclusive licence allowing the National Library of Canada to reproduce, loan, distribute or sell copies of this thesis in microform, paper or electronic formats.

The author retains ownership of the copyright in this thesis. Neither the thesis nor substantial extracts from it may be printed or otherwise reproduced without the author's permission.

L'auteur a accordé une licence non exclusive permettant à la Bibliothèque nationale du Canada de reproduire, prêter, distribuer ou vendre des copies de cette thèse sous la forme de microfiche/film, de reproduction sur papier ou sur format électronique.

L'auteur conserve la propriété du droit d'auteur qui protège cette thèse. Ni la thèse ni des extraits substantiels de celle-ci ne doivent être imprimés ou autrement reproduits sans son autorisation.

0-612-30658-5

Canada

The University of Waterloo requires the signatures of all persons using or photocopying this thesis. Please sign below, and give address and date.

Abstract

Weight function and stress intensity factor solutions for semi-elliptical surface cracks in flat plates and welded joints are developed, which account for the effect of two-dimensional stress distributions and load shedding.

Two methods are proposed to develop weight functions for the calculation of stress intensity factors for two-dimensional cracks under two-dimensional stress distributions: a general point load weight function and a Fourier series approach. In order to accommodate the effects of fixed boundary conditions into the weight functions, a compliance analysis method to obtain stress intensity factor solutions for fixed displacement boundary conditions from the available solutions for the same geometry with traction boundary conditions is developed for surface cracks. These methods are used to develop stress intensity factors and weight function solutions for embedded elliptical cracks, surface cracks in flat plates, T-plate, pipe-plate and tubular weld joints.

The solutions developed are suitable for fatigue life prediction or fracture assessment of these structures. The present approach is more efficient (in terms of computing and cost) than three-dimensional finite element analyses, yet more accurate and widely applicable than available empirical solutions.

Acknowledgements

I would like to express my sincere appreciation to my supervisor, Professor Stephan B. Lambert, for his strong support, guidance, encouragement, patience and kindness throughout the course of this work.

Financial support from the Natural Science and Engineering Research Council of Canada through a research grant to Prof. Lambert is gratefully acknowledged.

I would like also to thank Professor Gregory Glinka for his encouragement, support, advice, and helpful discussions.

Thanks go to Mr. Steve Hitchman for his technical computing support. I would like to acknowledge my thanks to all my fellow graduate students for their encouragement and support. In particular, I would like thank Jae-Boong Choi, Haojiang (John) Yuan, Roger Chen, Adam Kiciak, Hejin Yu, Duane Cronin, Xiaoying (Carolyn) Zhang, Yan Huang, and Hamid Jahedmotlagh for their help and friendship.

This work is dedicated to my parents who have encouraged and supported me throughout my educational and professional career, and to my wife, Ms. Rong Zhang, for her love and support over the many years.

Table of Contents

Abstract.....	iv
Acknowledgements.....	v
Table of Contents	vi
List of Tables	ix
List of Figures	xii
Nomenclature	xx
CHAPTER 1 INTRODUCTION	1
1.1 Objective	5
1.2 Thesis Outline.....	5
CHAPTER 2 BACKGROUND AND LITERATURE REVIEW	7
2.1 Stress Intensity Factors	7
2.2 Weight Functions	9
2.2.1 Theoretical Background.....	9
2.2.2 Determination of Weight Functions for Surface Cracks	14
2.3 Stress Intensity Factors and Weight Functions for Surface Cracks	19
2.3.1 Flat Plates	19
2.3.2 T-Plate Joints.....	22
2.3.3 Pipe-Plate and Tubular Joints	25
CHAPTER 3 THEORY AND DEVELOPMENT	38
3.1 Effect of Two-Dimensional Stress Distributions	39
3.1.1 General Approach.....	39

3.1.2 Fourier Series Approach	42
3.2 Effect of Boundary Conditions	47
3.2.1 Stress Intensity Factors for Fixed Boundary Conditions.....	48
3.2.2 Weight Functions for Cracks with Fixed Boundary Conditions	53
CHAPTER 4 EMBEDDED ELLIPTICAL CRACKS	62
4.1 Stress Intensity Factors for Embedded Elliptical Cracks	63
4.2 Proposed Weight Function.....	66
4.3 Validation of the Weight Function.....	68
CHAPTER 5 SURFACE CRACKS IN FLAT PLATES	81
5.1 Two-dimensional Stress Distributions	81
5.1.1 Stress Intensity Factor Solutions	83
5.1.2 Derivation of Weight Functions.....	87
5.1.3 Validation of Weight Functions.....	98
5.2 Fixed End Boundary Conditions.....	100
5.2.1 Stress Intensity Factor Solutions	101
5.2.2 Derivation of Weight Functions.....	109
5.2.3 Validation of Weight Functions.....	113
CHAPTER 6 SURFACE CRACKS IN T-PLATE JOINTS	157
6.1 Surface Cracks in T-plate Joints with Free Ends.....	157
6.1.1 Stress Intensity Factor Solutions	159
6.1.2 Derivation of Weight Functions.....	163
6.1.3 Validation of Derived Weight Functions.....	172
6.1.4 Discussion	173
6.2 Surface Cracks in T-plate Joints with Built-in Ends	175

6.2.1 Proposed Stress Intensity Factor Solutions	176
6.2.2 Verification of Proposed Stress Intensity Factor Solutions	177
6.2.3 Discussion	179
CHAPTER 7 SURFACE CRACKS IN PIPE-PLATE AND TUBULAR JOINTS	212
7.1 Surface Cracks in Pipe-plate Joints	212
7.1.1 Proposed Stress Intensity Factor Solution	213
7.1.2 Comparisons with Finite Element and Experimental Data	215
7.2 Surface Cracks in Tubular Joints	216
7.2.1 Proposed Stress Intensity Factor Solution	217
7.2.2 Comparisons with Experimental Data	218
7.3 Discussion	219
CHAPTER 8 CONCLUSIONS AND RECOMMENDATIONS	236
8.1 Conclusions	236
8.2 Recommendations	240
REFERENCES	241
APPENDIX LIST OF RELEVANT PAPERS PUBLISHED BY THE AUTHOR	253

List of Tables

<p>Table 5.1a. Boundary correction factors F for semi-elliptical surface cracks under stress distributions of $\sigma_0(1-x/a)^m \cos(\pi/c)$, $m = 0, 1, 2, 3$, $F = K/\sigma_0\sqrt{[\pi a/Q]}$, $a/c = 0.1$.</p> <p>..... 114</p>	114
<p>Table 5.1b. Boundary correction factors F for semi-elliptical surface cracks under stress distributions of $\sigma_0(1-x/a)^m \cos(\pi/c)$, $m = 0, 1, 2, 3$, $F = K/\sigma_0\sqrt{[\pi a/Q]}$, $a/c = 0.2$.</p> <p>..... 115</p>	115
<p>Table 5.1c. Boundary correction factors F for semi-elliptical surface cracks under stress distributions of $\sigma_0(1-x/a)^m \cos(\pi/c)$, $m = 0, 1, 2, 3$, $F = K/\sigma_0\sqrt{[\pi a/Q]}$, $a/c = 0.4$.</p> <p>..... 116</p>	116
<p>Table 5.1d. Boundary correction factors F for semi-elliptical surface cracks under stress distributions of $\sigma_0(1-x/a)^m \cos(\pi/c)$, $m = 0, 1, 2, 3$, $F = K/\sigma_0\sqrt{[\pi a/Q]}$, $a/c = 0.6$.</p> <p>..... 117</p>	117
<p>Table 5.1e. Boundary correction factors F for semi-elliptical surface cracks under stress distributions of $\sigma_0(1-x/a)^m \cos(\pi/c)$, $m = 0, 1, 2, 3$, $F = K/\sigma_0\sqrt{[\pi a/Q]}$, $a/c = 1$.</p> <p>..... 118</p>	118
<p>Table 5.2a. Boundary correction factors F for semi-elliptical surface cracks under stress distributions of $\sigma_0(1-x/a)^m \sin(\pi/c)$, $m = 0, 1, 2, 3$, $F = K/\sigma_0\sqrt{[\pi a/Q]}$, $a/c = 0.1$.</p> <p>..... 119</p>	119

Table 5.2b.	Boundary correction factors F for semi-elliptical surface cracks under stress distributions of $\sigma_0(1-x/a)^m \sin(\pi/c)$, $m = 0, 1, 2, 3$, $F = K/\sigma_0\sqrt{[\pi a/Q]}$, $a/c = 0.2$.	120
Table 5.2c.	Boundary correction factors F for semi-elliptical surface cracks under stress distributions of $\sigma_0(1-x/a)^m \sin(\pi/c)$, $m = 0, 1, 2, 3$, $F = K/\sigma_0\sqrt{[\pi a/Q]}$, $a/c = 0.4$.	121
Table 5.2d.	Boundary correction factors F for semi-elliptical surface cracks under stress distributions of $\sigma_0(1-x/a)^m \sin(\pi/c)$, $m = 0, 1, 2, 3$, $F = K/\sigma_0\sqrt{[\pi a/Q]}$, $a/c = 0.6$.	122
Table 5.2e.	Boundary correction factors F for semi-elliptical surface cracks under stress distributions of $\sigma_0(1-x/a)^m \sin(\pi/c)$, $m = 0, 1, 2, 3$, $F = K/\sigma_0\sqrt{[\pi a/Q]}$, $a/c = 1$.	123
Table 5.3	Comparison between the stress intensity factors calculated from present weight functions and finite element analyses from Shiratori (1987) under a residual stress field.	124
Table 6.1.	Boundary correction factors F for semi-elliptical surface cracks ($a/c = 0.05, 0.1, 0.2, 0.4, 0.6, 1.0$) in T-plate joints with $\pi/6$ weld angle under stress distributions of $\sigma_0(1-x/a)^n$, $n = 0, 1$, $F = K/\sigma_0\sqrt{[\pi a/Q]}$.	182
Table 6.2.	Boundary correction factors F for semi-elliptical surface cracks ($a/c = 0.05, 0.1, 0.2, 0.4, 0.6, 1.0$) in T-plate joints with $\pi/4$ weld angle under stress distributions of $\sigma_0(1-x/a)^n$, $n = 0, 1$, $F = K/\sigma_0\sqrt{[\pi a/Q]}$.	184

Table 6.3.	Boundary correction factors F for semi-elliptical surface cracks ($a/c = 0.2, 1.0$) in T-plate joints with $\pi/6$ weld angle under stress distributions of $\sigma(1-x/a)^n$, $n = 2, 3$, $F = K/\sigma\sqrt{[\pi a/Q]}$	186
Table 6.4.	Boundary correction factors F for semi-elliptical surface cracks ($a/c = 0.2, 1.0$) in T-plate joints with $\pi/4$ weld angle under stress distributions of $\sigma(1-x/a)^n$, $n = 2, 3$, $F = K/\sigma\sqrt{[\pi a/Q]}$	187
Table 6.5.	Weld toe magnification factors Mk for semi-elliptical surface cracks ($a/c = 0.2, 1.0$) in T-plate joints with $\pi/4$ weld angle under far field tension and bending.	188
Table 6.6.	Boundary correction factors F for semi-elliptical surface cracks ($a/c = 0.1, 0.2, 1.0$) in T-plate joints with $\pi/4$ weld angle and built-in ends under bending, $F = K/\sigma\sqrt{[\pi a/Q]}$	189
Table 7.1	Y factor for cracks in the pipe-plate weld joint (Lambert and Bell, 1993)....	222
Table 7.2	Crack Shape in the Pipe-plate Weld Joint (Forbes, 1991).....	223

List of Figures

Figure 1.1	Welded joints and flat plate geometries	6
Figure 2.1	Notation for semi-elliptical surface crack	28
Figure 2.2	Superposition method (Bueckner, 1970).....	29
Figure 2.3	Physical meaning of weight functions.....	30
Figure 2.4	Two-dimensional stress distribution	31
Figure 2.5	Weight function for mixed boundary conditions (Wu and Carlsson, 1991)....	32
Figure 2.6	Oore-Burns (1980a) weight function	33
Figure 2.7	Surface cracks in flat plate: (a) and (b) under residual stress field; (c) with fixed boundary conditions	34
Figure 2.8	(a) T-plate joint; (b) plate with an angular corner	35
Figure 2.9	Stress distribution in thickness direction (Haswell <i>et al.</i> , 1991)	36
Figure 2.10	Stress distribution around the weld toe	37
Figure 3.1	General two-dimensional crack	54
Figure 3.2	Weight functions for (a) half plane crack; (b) circular crack	55
Figure 3.3	Comparison between residual stress field Eq.(3.7) and Fourier approximation Eq. (3.8).....	56
Figure 3.4	Weight Function $M^c_I(x, P')$	57
Figure 3.5	Edge crack in flat plate with fixed boundary conditions	58

Figure 3.6	Superposition representation	59
Figure 3.7	Superposition of problem I	60
Figure 3.8	General arrangement for the calculation of the end displacements	61
Figure 4.1	Notation for an elliptical crack in an infinite solid, (a), (b)	71
Figure 4.2	Weight function for embedded elliptical crack	72
Figure 4.3	Comparison of the weight function based stress intensity factor and exact solution for $a/c = 0.8$ (Uniform and linear stress distributions).....	73
Figure 4.4	Comparison of the weight function based stress intensity factor and exact solution for $a/c = 0.8$ (2D non-linear and parabolic stress distributions).	74
Figure 4.5	Comparison of the weight function based stress intensity factor and exact solution for $a/c = 0.6$ (Uniform and linear stress distributions).....	75
Figure 4.6	Comparison of the weight function based stress intensity factor and exact solution for $a/c = 0.6$ (2D non-linear and parabolic stress distributions).	76
Figure 4.7	Comparison of the weight function based stress intensity factor and exact solution for $a/c = 0.4$ (Uniform and linear stress distributions).....	77
Figure 4.8	Comparison of the weight function based stress intensity factor and exact solution for $a/c = 0.4$ (2D non-linear and parabolic stress distributions).	78
Figure 4.9	Comparison of the weight function based stress intensity factor and exact solution for $a/c = 0.2$ (Uniform and linear stress distributions).....	79
Figure 4.10	Comparison of the weight function based stress intensity factor and exact solution for $a/c = 0.2$ (2D non-linear and parabolic stress distributions).	80
Figure 5.1	Geometry and co-ordinates system used	125
Figure 5.2	Typical mesh (part), $a/c = 0.1$, $a/t = 0.2$	126

Figure 5.3	Comparison of the weight function based stress intensity factor and FEM data for stress distribution $\sigma_0(1-x/a)^2 \cos(\pi/c)$, (deepest point).....	127
Figure 5.4	Comparison of the weight function based stress intensity factor and FEM data for stress distribution $\sigma_0(1-x/a)^2 \cos(\pi/c)$, (surface point).	128
Figure 5.5	Comparison of the weight function based stress intensity factors and FEM data for stress distribution $\sigma_0(1-x/a)^3 \cos(\pi/c)$, (deepest point).....	129
Figure 5.6	Comparison of the weight function based stress intensity factors and FEM data for stress distribution $\sigma_0(1-x/a)^3 \cos(\pi/c)$, (surface point).	130
Figure 5.7	Comparison of the weight function based stress intensity factor and FEM data for stress distribution $\sigma_0(1-x/a)^2 \sin(\pi/c)$, (surface point).	131
Figure 5.8	Comparison of the weight function based stress intensity factor and FEM data for stress distribution $\sigma_0(1-x/a)^3 \sin(\pi/c)$, (surface point).....	132
Figure 5.9	Fixed ends plate with surface crack (half)	133
Figure 5.10	Superposition representation	134
Figure 5.11	Superposition of problem I	135
Figure 5.12	General problem for calculation of displacements.....	136
Figure 5.13	Crack extension types.....	137
Figure 5.14	Localised displacements δ and θ	138
Figure 5.15	Distribution of N'	139
Figure 5.16	Deformed mesh	140
Figure 5.17	Comparison of the stress intensity factors from compliance analysis and finite element data for constant stress distribution $\sigma = \sigma_0$, $a/c = 0.1$, deepest point .	141

Figure 5.18	Comparison of the stress intensity factors from compliance analysis and finite element data for constant stress distribution $\sigma = \sigma_0$, $a/c = 0.1$, surface point	142
Figure 5.19	Comparison of the stress intensity factors from compliance analysis and finite element data for linear stress distribution $\sigma = \sigma_0(1-x/a)$, $a/c = 0.1$, deepest point	143
Figure 5.20	Comparison of the stress intensity factors from compliance analysis and finite element data for linear stress distribution $\sigma = \sigma_0(1-x/a)$, $a/c = 0.1$, surface point	144
Figure 5.21	Comparison of the stress intensity factors from compliance analysis and finite element data for constant stress distribution $\sigma = \sigma_0$, $a/c = 0.2$, deepest point	145
Figure 5.22	Comparison of the stress intensity factors from compliance analysis and finite element data for constant stress distribution $\sigma = \sigma_0$, $a/c = 0.2$, surface point	146
Figure 5.23	Comparison of the stress intensity factors from compliance analysis and finite element data for linear stress distribution $\sigma = \sigma_0(1-x/a)$, $a/c = 0.2$, deepest point	147
Figure 5.24	Comparison of the stress intensity factors from compliance analysis and finite element data for linear stress distribution $\sigma = \sigma_0(1-x/a)$, $a/c = 0.2$, surface point	148

Figure 5.25	Comparison of the stress intensity factors from compliance analysis and finite element data for constant stress distribution $\sigma = \sigma_0$, $a/c = 1.0$, deepest point	149
Figure 5.26	Comparison of the stress intensity factors from compliance analysis and finite element data for constant stress distribution $\sigma = \sigma_0$, $a/c = 1.0$, surface point	150
Figure 5.27	Comparison of the stress intensity factors from compliance analysis and finite element data for linear stress distribution $\sigma = \sigma_0(1-x/a)$, $a/c = 1.0$, deepest point	151
Figure 5.28	Comparison of the stress intensity factors from compliance analysis and finite element data for linear distribution $\sigma = \sigma_0(1-x/a)$, $a/c = 1.0$, surface point	152
Figure 5.29	Comparison of the stress intensity factors from weight function and finite element data for parabolic stress distribution $\sigma = \sigma_0(1-x/a)^2$, $a/c = 0.1$, deepest point	153
Figure 5.30	Comparison of the stress intensity factors from weight function analysis and finite element data for parabolic stress distribution $\sigma = \sigma_0(1-x/a)^2$, $a/c = 0.1$, surface point	154
Figure 5.31	Comparison of the stress intensity factors from weight function and finite element data for cubic stress distribution $\sigma = \sigma_0(1-x/a)^3$, $a/c = 0.1$, deepest point	155

Figure 5.32	Comparison of the stress intensity factors from weight function and finite element data for cubic stress distribution $\sigma = \alpha(1-x/a)^3$, $a/c = 0.1$, surface point	156
Figure 6.1	Geometry and co-ordinate system	190
Figure 6.2	Typical finite element mesh (part), $a/c = 0.2$, $a/t = 0.2$, 45 degree weld angle	191
Figure 6.3	Comparison of the weld toe magnification factor from the present FE calculation and Bowness and Lee (1996), (far field tension, $\pi/4$ weld angle, deepest point).	192
Figure 6.4	Comparison of the weld toe magnification factor from the present FE calculation and Bowness and Lee (1996), (far field tension, $\pi/4$ weld angle, surface point).	193
Figure 6.5	Comparison of the weld toe magnification factor from the present FE calculation and Bowness and Lee (1996), (far field bending, $\pi/4$ weld angle, deepest point).	194
Figure 6.6	Comparison of the weld toe magnification factor from the present FE calculation and Bowness and Lee (1996), (far field bending, $\pi/4$ weld angle, surface point).	195
Figure 6.7	Comparison of the weight function based stress intensity factor and FEM data for stress distribution $\alpha(1-x/a)^2$ ($\pi/4$ weld angle, deepest point).	196
Figure 6.8	Comparison of the weight function based stress intensity factor and FEM data for stress distribution $\alpha(1-x/a)^2$ ($\pi/4$ weld angle, surface point).	197
Figure 6.9	Comparison of the weight function based stress intensity factor and FEM data for stress distribution $\alpha(1-x/a)^3$ ($\pi/4$ weld angle, deepest point).	198
Figure 6.10	Comparison of the weight function based stress intensity factor and FEM data for stress distribution $\alpha(1-x/a)^3$ ($\pi/4$ weld angle, surface point).	199

Figure 6.11	Comparison of the weight function based weld toe magnification factor and FEM data (far field tension, $\pi/4$ weld angle, deepest point).....	200
Figure 6.12	Comparison of the weight function based weld toe magnification factor and FEM data (far field tension, $\pi/4$ weld angle, surface point).....	201
Figure 6.13	Comparison of the weight function based weld toe magnification factor and FEM data (far field bending, $\pi/4$ weld angle, deepest point).....	202
Figure 6.14	Comparison of the weight function based weld toe magnification factor and FEM data (far field bending, $\pi/4$ weld angle, surface point).	203
Figure 6.15	Geometry, boundary condition and load.....	204
Figure 6.16.	Proposed solution.....	205
Figure 6.17	Stress intensity factors for surface cracks in T-plate joints with built-in ends under bending, $\pi/4$ weld angle, ($a/c = 0.1, H/t = 10$, deepest point).....	206
Figure 6.18	Stress intensity factors for surface cracks in T-plate joints with built-in ends under bending, $\pi/4$ weld angle, ($a/c = 0.1, H/t = 10$, surface point).....	207
Figure 6.19	Stress intensity factors for surface cracks in T-plate joints with built-in ends under bending, $\pi/4$ weld angle, ($a/c = 0.2, H/t = 10$, deepest point).....	208
Figure 6.20	Stress intensity factors for surface cracks in T-plate joints with built-in ends under bending, $\pi/4$ weld angle, ($a/c = 0.2, H/t = 10$, surface point).....	209
Figure 6.21	Stress intensity factors for surface cracks in T-plate joints with built-in ends under bending, $\pi/4$ weld angle, ($a/c = 1.0, H/t = 10$, deepest point).....	210
Figure 6.22	Stress intensity factors for surface cracks in T-plate joints with built-in ends under bending, $\pi/4$ weld angle, ($a/c = 1.0, H/t = 10$, surface point).	211
Figure 7.1	Pipe-plate joint	224

Figure 7.2	T-plate with built-in ends model for pipe-plate joints.....	225
Figure 7.3	The pipe-plate specimen (Lambert, 1988)	226
Figure 7.4	Results for stress intensity factors for surface cracks in pipe-plate joints.....	227
Figure 7.5	Geometry of tubular joint	228
Figure 7.6	T-plate with built-in ends model for tubular joints	229
Figure 7.7	The tubular specimen (Forbes, 1991)	230
Figure 7.8	Results for stress intensity factors for surface cracks in tubular joints (axial loads)	231
Figure 7.9	Results for stress intensity factors for surface cracks in tubular joints (in plane bending loads)	232
Figure 7.10	Curvature of the surface crack	233
Figure 7.11	Typical two-dimensional stress distribution for pipe-plate and tubular joints	234
Figure 7.12	T-plate with built-in ends model, (a) two dimensional stress distribution, (b) one dimensional stress distribution.....	235

Nomenclature

a - crack length for an edge crack; crack depth for a semi-elliptical surface crack; half crack length of an embedded elliptical crack

A - deepest point of surface crack; area of crack face

A_0, A_1, A_2 - least squares fitting parameters for Y_I

$A_{k,l}^{(i,j)}$ - polynomial coefficients

B - surface point of surface crack

B_0, B_1, B_2 - least squares fitting parameters for Y_0

c - half crack length of a semi-elliptical crack; half crack length of an embedded elliptical crack

C - typical point at the major axis of the ellipse

C_0, C_1, C_2, C_3 - least squares fitting parameters for F_0

$C_{11}, C_{12}, C_{21}, C_{22}$ - plate compliances due to the existence of the crack

$C_{k,l}^{(i,j)}$ - coefficients in K solution for embedded elliptical cracks under polynomial stress distributions

D_0, D_1, D_2, D_3 - least squares fitting parameters for F_I

E - complete elliptical integral of the second kind; modulus of elasticity

F, F_s - boundary correction factors

F_0, F_1 - least squares fitting parameters for the reference stress intensity factors K_{1r}^B and K_{2r}^B

H - general elastic modulus; length of plate

J - J -integral

K - stress intensity factor

K^* - average stress intensity factor for surface crack

K_{1r}^A, K_{2r}^A - reference stress intensity factors at deepest point in a semi-elliptic surface

K_{1r}^B, K_{2r}^B - reference stress intensity factors at surface point in a semi-elliptic surface

K_r - reference stress intensity factor

L - plate length; length of chord

M - bending moment at the ends of a plate

$m(x; a), m(x, y; P'), M(x; P'), M_n^c(x; P'), M_n^s(x; P')$ - weight functions; c and s represent cos and sin in the Fourier series

m, n - Fourier series index

$M_1, M_2, M_3, M_{1P}, M_{2P}, M_{3P}, M_{4P}$ - weight function parameters

$M_{1A}, M_{2A}, M_{3A}, M_{1A}^c, M_{2A}^c, M_{3A}^c$ - weight function parameters for deepest point of a surface crack

$M_{1B}, M_{2B}, M_{3B}, M_{1B}^c, M_{2B}^c, M_{3B}^c, M_{1B}^s, M_{2B}^s, M_{3B}^s$ - weight function parameters for surface point of a surface crack

$M_{A0}, M_{A1}, M_{B0}, M_{B1}$ - parameters which account for the effect of the attachment for different weld angles

M_{k_t}, M_{k_b} - weld toe magnification factors for tension or bending

M_m, M_b - crack shape (depth and aspect ratio) correction factors for membrane or bending stresses

N - tension force at the ends of a plate

P - general point along crack front

p_0 - crack face pressure

Q - shape factor for an ellipse

r - distance between point (x, y) and any point on Γ

$R_{pipe}, R_{brace}, R_{chord}$ - radius of pipe, brace or chord

S - crack surface of a two-dimensional crack

s - shortest distance between the load point and the boundary of the crack

t - plate thickness

T - stress field

U - strain energy

u_r - reference crack opening displacement field

W, W_{eff} - plate width, effective plate width

Y_0, Y_1 - least squares fitting parameters for reference stress intensity factors $K_{I,r}^A$ and K_{2r}^A

Y_m, Y_b - boundary correction factors for stress intensity factors under tension or bending

Γ - contour corresponding to the crack front

α - factor to account for effect of built-in ends

β - factor to account for the effect of weldment

λ - parameter relating length of equivalent T-plate joints to radius of pipe or brace

ϕ - parametric angle of an ellipse; angle of the weldment for T-plate joints (degree)

ν - Poisson's ratio

θ - rotation at the ends of a plate

ρ - distance between load point and point P' ; weld radius

δ - variation symbol; displacement at the ends of a plate

$\sigma(x, y), \sigma(x)$ - local stress distribution normal to the prospective crack plane

σ_0 - characteristic stress or nominal stress

$\rho_1, \rho_2, \rho_3, \rho_4$ – parameters controlled by the shape of the ellipse

σ_m, σ_b - nominal tension or bending stresses

Chapter 1

Introduction

In practice, surface cracks are among the most common flaws in engineering structures such as plates and welded joints. The calculation of the stress intensity factor for such cracks is of major importance in fatigue and fracture assessment. Example welded joint geometries, including tubular, pipe-plate and plate-plate joints, and flat plates are shown in Fig. 1.1. The objective of the present research is to develop stress intensity factor and weight function solutions for semi-elliptical surface cracks in such geometries.

Stress intensity factors for semi-elliptical surface cracks in plates and welded joints depend on the geometry, including the geometry of the specimen and geometry of the crack, the loading and boundary conditions. Because of the complexity of the problem, rigorous closed form solutions for stress intensity factors are not possible even for the simplest geometries. Numerical methods, such as the finite element method, the finite element alternating method, the boundary element method, etc., are often used (Newman and Raju, 1979; Nishioka and Atluri, 1983; Aliabadi and Rooke, 1991). Alternatively, experimental methods involving the measurement of fatigue crack propagation rates and the

calculation of stress intensity factors by comparison with crack growth rate information from simple specimens can be used (Burns *et al.*, 1987).

Among the methods of calculating stress intensity factors, the finite element method is generally accepted as the most accurate. Although the finite element method can be applied to any complex geometry and loading condition, it is limited to a specific geometry, loading and boundary condition, is time consuming and, therefore, expensive.

Available finite element results for surface cracks in plates and welded joint geometries are quite limited. The most extensive analyses conducted on surface cracks so far are for flat plates (Newman and Raju, 1981; Shiratori *et al.*, 1987; Wang and Lambert, 1995a, 1997a). Some analyses have been conducted on T-plate joints (Smith, 1984; Bell, 1985; Dijkstra *et al.*, 1989; Fu *et al.*, 1993) and one for the pipe-plate model (Lambert and Bell, 1993). It is very difficult to find comprehensive analyses for tubular joints model (Ritchie *et al.*, 1987; Rhee, 1989). All of these results correspond to specific geometries and loading conditions.

Based on finite element results, empirical equations for stress intensity factors for surface cracks in flat plates and T-plate joints were derived for some specific loading cases, i.e., tension or bending (Newman and Raju, 1981; Fu *et al.*, 1993; Bowness and Lee, 1995). Because of limitations on available finite element results for pipe-plate or tubular joints, it is common practice to use the empirical equations developed for T-plates for these more complex joints. However, because of the difference in boundary conditions between T-plate joints and pipe-plate or tubular joints, the resulting stress intensity factors are over-predicted. This effect is referred to as load shedding (Aaghaakouchak *et al.*, 1989). The load shedding effect has to be considered whenever T-plate joint models are used to calculate stress intensity factors for pipe-plate or tubular joints. Another issue is that the

stress distributions on the uncracked plane in pipe-plate joints or tubular joints are two-dimensional (they vary through the thickness and along the weld toe); this effect on stress intensity factors cannot be addressed correctly using the results for T-plate joints, where only one-dimensional (through the thickness) stress distributions are generally considered (Haswell *et al.*, 1991).

Since empirical equations can be used to determine stress intensity factors only for limited loading cases, they cannot be used to calculate stress intensity factors for complex stress distributions that were not considered in the development of the empirical equations. The weight function method (Bueckner, 1970; Rice, 1972) enables the analysis of crack problems in a loading-independent way. The weight function depends only on the geometry and boundary conditions, and is independent of the applied load. The stress intensity factor for various different applied loads for a given geometry and boundary condition can be solved by integrating the product of the crack surface pressure and the weight function.

There are several methods to determine the weight functions for a given geometry and boundary condition (Aliabadi and Rooke, 1991). The most commonly used method is to extract them from existing stress intensity factor solutions in combination with actual or appropriate crack face displacement relations (Rice, 1972; Petroski and Achenbach, 1978). A method to determine weight functions for surface cracks by extracting them from appropriate reference stress intensity factor solutions alone has been developed in recent years (Shen and Glinka, 1991a, 1991b; Wang and Lambert, 1995b). However, the resulting weight functions are only applicable for one-dimensional stress variations. Some methods have been proposed to determine weight functions for two-dimensional stress distributions (Oore and Burns, 1980a; Rice, 1989; Vainshtok and Varfolomeyev, 1990; Vainshtok, 1991). Oore and Burns (1980a) proposed a method to determine approximate weight functions for two-dimensional stress distributions for embedded irregular cracks in an

infinite body. To date, this is the only approach that is being used in engineering applications. However, since this approximate weight function is only applicable to embedded cracks, it must be corrected empirically for application to surface cracks.

Available weight function solutions for surface cracks in flat plates and welded joints are more difficult to find than stress intensity factor solutions. Weight functions at the deepest and surface points of a surface crack in a flat plate for one-dimensional stress distributions have been developed recently by Shen and Glinka (1991a, 1991b) and Wang and Lambert (1995a, 1997). The weight function solution for one-dimensional stress distributions at the deepest point of a surface crack in flat plates with an angular corner is available, and has been used for the solution of T-plate welded joint problems (Niu and Glinka, 1990). No weight functions are available for pipe-plate or tubular joints.

To calculate the stress intensity factors for complex geometries (T-plate, pipe-plate and tubular joints), it is common practice to use weight functions developed for relatively simple geometries (flat plates) in conjunction with stress distributions from corresponding uncracked T-plate, pipe-plate or tubular joint geometries. Although reasonable results were obtained for T-plate welded joints (Forbes *et al.*, 1991), the resulting stress intensity factors were not acceptable for pipe-plate or tubular joints because of the load shedding effect and the lack of consideration for the stress variation along the weld toe (Haswell *et al.*, 1991; Forbes *et al.*, 1992). It is, therefore, necessary to develop weight functions which can account for the effect of two-dimensional stress distributions and the load shedding effect for surface cracks in these structures.

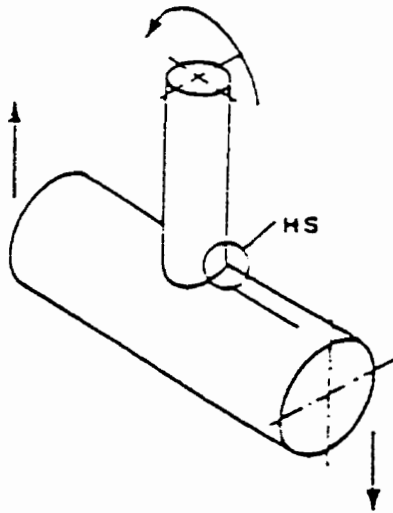
1.1 Objective

The aim of the present research is to develop stress intensity factor and weight function solutions for embedded and semi-elliptical surface cracks in flat plates and welded joints which can account for the effect of two-dimensional stress distributions, and the effect of load shedding. These stress intensity factor and weight function solutions may then be used for the fatigue life prediction and fracture assessment of these structures. This approach will be more efficient (in terms of computing time and cost) than three-dimensional finite element analyses, yet more accurate and widely applicable than available empirical solutions.

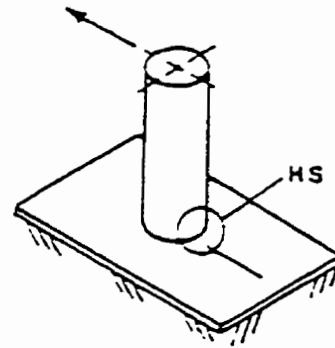
1.2 Thesis Outline

This thesis is divided into eight chapters. In chapter 2, an overview of stress intensity factors and weight functions is presented. Chapter 3 presents the theory and development of weight function methods which can accommodate two-dimensional stress distributions and load shedding effects. The following chapters presents the application of these methods to calculate stress intensity factors for embedded elliptical cracks in infinite body (chapter 4), surface cracks in flat plates (chapter 5), surface cracks in T-plate joints (chapter 6), and surface cracks in pipe-plate and tubular joints (chapter 7). Conclusions are made in chapter 8 along with some recommendations.

Figure 1.1 Welded joint and flat plate geometries



TUBULAR JOINT



PIPE-PLATE JOINT

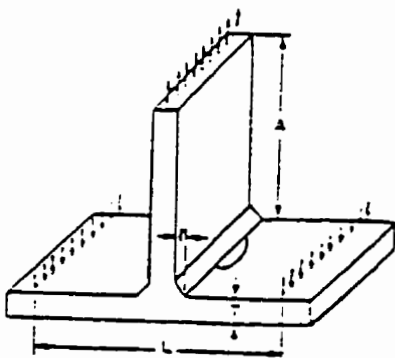
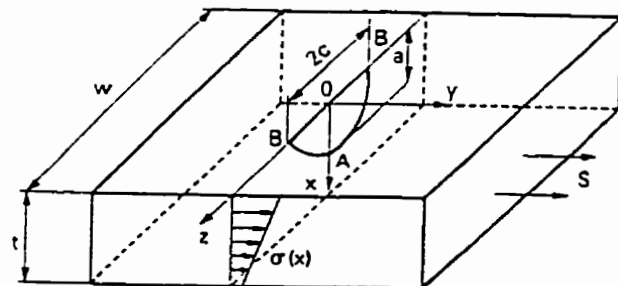


PLATE-PLATE JOINT



FLAT PLATE

Chapter 2

Background and Literature Review

2.1 Stress Intensity Factors

A cracked body can be loaded in any one or combination of three displacement modes. Most crack problems of engineering interest involve primarily Mode I (opening mode). In the present research, only Mode I will be considered. Stress intensity factors for cracks in a given specimen depend on the geometry of the specimen, including the global specimen geometry and the crack geometry, the loading and boundary conditions. For one-dimensional edge cracks or central cracks, the stress intensity factor, K , is represented as

$$K = F \sigma_0 \sqrt{\pi a} \quad (2.1)$$

where the factor F is needed to account for geometry, stress distribution, and boundary conditions, σ_0 is the nominal stress and a is the crack length. For semi-elliptical surface cracks, as shown in Figure 2.1, K is represented as

$$K = F\sigma_0\sqrt{\frac{\pi a}{Q}} \quad (2.2)$$

where Q is the shape factor for the ellipse, approximated by (Newman and Raju, 1979)

$$Q = 1.0 + 1.464\left(\frac{a}{c}\right)^{1.65} \quad (a/c \leq 1) \quad (2.3)$$

Note that the stress intensity factor changes along the crack front; usually the values at the deepest and surface points are the most important values.

For some simple geometry and loading conditions, exact closed form solutions from elasticity theory are available for K . However, for many cases of practical interest, it is necessary to perform numerical analyses. Among all numerical methods available, the finite element method has emerged as one of the most powerful tools for the solution of one-dimensional (edge or through cracks) or two-dimensional (surface or embedded cracks) crack problems in fracture mechanics. Special techniques have been developed to treat the crack tip singularity and to extract stress intensity factors (Barsoum, 1977; Shih, *et al.*, 1986; Banks-Sills, 1991). Throughout the present research, the finite element method will be used to provide stress intensity factor data from which the weight functions are derived, and to verify stress intensity factor and weight function solutions.

2.2 Weight Functions

2.2.1 Theoretical Background

The weight function method was originally proposed for one-dimensional crack problems (edge or through cracks). Bueckner (1970) first demonstrated that for a cracked body as shown in Figure 2.2(a), loaded by a stress field S , the stress intensity factor for this problem is the same as that for the same cracked body loaded by a crack surface pressure, $\sigma(x)$, as shown in Figure 2.2(b). The stress distribution, $\sigma(x)$, is the stress distribution acting on the prospective crack plane in the uncracked geometry. Therefore, the calculation of stress intensity factor for a given crack geometry under any applied load is equivalent to the calculation of stress intensity factor for the same crack geometry with the corresponding crack pressure, $\sigma(x)$, acting on the crack surface. The stress intensity factor for a cracked body with loading on the crack surface can be calculated by integrating the product of the weight function, $m(x,a)$, and the stress distribution, $\sigma(x)$, on the crack plane:

$$K = \int_0^a \sigma(x)m(x,a)dx \quad (2.4)$$

The weight function, $m(x, a)$, depends only on the geometry and boundary conditions for the cracked body. Once the weight function has been determined, the stress intensity factor for this geometry can be obtained from Eq.(2.4) for any stress distribution, $\sigma(x)$. Mathematically, the weight function, $m(x, a)$, is the generalized Green's function for the present stress intensity factor problem. It is the stress intensity factor at the crack tip for a pair of unit point loads acting on the surface at x as shown in Figure 2.3(a).

For a two-dimensional crack (surface or embedded crack), the stress intensity factors vary along the crack front, as shown in Fig. 2.1. The counterpart to equation (2.4) for two-dimensional cracks is

$$K(P) = \iint_S \sigma(x, y) m(x, y; P) dS \quad (2.5)$$

where weight function $m(x, y; P)$ is the stress intensity factor at point P on the crack front for a pair of unit point loads acting on the crack surface at (x, y) as shown in Figure 2.3(c), $\sigma(x, y)$ is a two-dimensional stress distribution as shown in Figure 2.4, and the integration becomes an area integration over the crack surface, S . If the stress distribution acting on the two-dimensional crack surface is only a function of x , then equation (2.5) can be simplified:

$$K(P) = \int_a^c \sigma(x) \left(\int_c^c m(x, y; P) dy \right) dx = \int_a^c \sigma(x) M(x; P) dx \quad (2.6)$$

where $M(x, P)$ is the stress intensity factor at point P for a unit line load at x as shown in Figure 2.3(b). $M(x, P)$ is the weight function for a two-dimensional crack subject to a one-dimensional stress distribution.

Generating the weight function through point-wise stress intensity factor calculations is impractical. The determination of the weight function for a one-dimensional crack, $m(x, a)$, can be simplified by using the relation derived by Rice(1972):

$$m(x, a) = \frac{H}{K_r} \frac{\partial u_r(x, a)}{\partial a} \quad (2.7)$$

where H is the generalized elastic modulus, which equals E for plane stress or $E/(1-\nu^2)$ for plane strain, K_r and u_r are the stress intensity factor and corresponding crack face displacement for one reference stress distribution. The relationship between the weight function and the displacement field for two-dimensional cracks was also found by Rice (1972):

$$m(x, y; P') = \frac{H}{K_r(P')} \frac{\delta u_r(x, y)}{\delta F_{P'}} \quad (2.8)$$

where $\delta F_{P'}$ is the local variation of the crack area in the vicinity of point P' .

Originally, the relationships developed by Rice, (1972), Eq. (2.4), (2.7) for one-dimensional cracks and (2.5), (2.8) for two-dimensional cracks, were developed for a cracked body loaded by surface tractions. They cannot be used directly for a cracked body subject to mixed boundary conditions (involving both prescribed tractions and displacements). Generalisation of the weight function theory to mixed boundary conditions involving both prescribed surface tractions and displacements was later made by a number of researchers (for example, Bowie and Freese, 1981). For a one-dimensional crack, as summarised by Wu and Carlsson (1991), the stress intensity factor for any cracked body loaded by surface tractions, $\sigma(x)$ on the crack face and prescribed displacements u_i on boundary Γ (as shown in Figure 2.5), can be calculated from

$$K = \frac{H}{K_r} \left[\int_0^a \sigma(x) \frac{\partial u_r(x,a)}{\partial a} dx - \int_{\Gamma} u_i \cdot \frac{\partial (\sigma_r)_{ij}}{\partial a} n_j d\Gamma \right] \quad (2.9)$$

where K_r and u_r are the reference stress intensity factor and corresponding crack face displacement as before, and $(\sigma_r)_{ij}$ are the stresses at prescribed displacement boundary for the reference case.

For the special case where the prescribed displacements, u_i , on boundary Γ are zero (zero displacement boundary), then the second term in Eq. (2.9) becomes zero, and Eq. (2.9) becomes

$$K = \frac{H}{K_r} \int_0^a \sigma(x) \frac{\partial u_r(x,a)}{\partial a} dx \quad (2.10)$$

which is a combination of Eq.(2.4) and (2.7).

In other words, for a one dimensional crack with zero displacement boundary conditions, stress intensity factors can be calculated using standard weight functions (Eq. (2.4)). The weight function can be calculated from a reference stress intensity factor solution, K_r , and displacement, u_r , using Eq.(2.7). But these reference solutions must be obtained for a crack problem with the same zero displacement boundary conditions. Similarly, for a two-dimensional crack with zero displacement boundary conditions, the stress intensity factors can be calculated using weight functions (Eqs. (2.5) and (2.6)); and these weight functions can be obtained from Eq. (2.8).

For one-dimensional cracks, equation (2.7) provides an efficient way to determine weight functions from a reference stress intensity factor solution and the corresponding displacement field. For a given problem, an appropriate reference stress intensity factor K_r can often be found either in the literature or by numerical calculation. However, the corresponding analytical expression for the crack opening displacement function $u_r(x, a)$ is more difficult to obtain, since it is a field function which varies along the crack length and is seldom published together with stress intensity factor solutions. To overcome this difficulty, several authors (Petroski and Achenbach, 1978; Shen and Glinka, 1991b) have proposed approximate expressions for the displacement, $u_r(x, a)$, or the weight function, $m(x, a)$, which can be evaluated when combined with only reference stress intensity factors.

For two-dimensional crack problems, it is much more difficult to apply the relationship between the weight function and a set of reference stress intensity factor solutions with a corresponding displacement field as shown in equation (2.8). The complete solution for the first order variation in $u_r(x, y)$ corresponding to arbitrary variations in F_p along the crack front has to be known, but is more difficult to obtain than $\partial u_r / \partial a$ for one-dimensional crack problems (Rice, 1989). Further work is required in this area.

The key property of the weight function method by Bueckner (1970) and Rice (1972) described here is that all information required to determine the weight function for a given geometry and boundary condition is stored completely in one set of solutions for stress intensity factor, K_r , and displacement field, u_r , for any one reference loading case. The resulting weight function can be used to predict the stress intensity factors for other loading cases with the same accuracy as the reference stress intensity factor solutions. Reference stress intensity factor solutions therefore play an important role in determining weight functions.

2.2.2 Determination of Weight Functions for Surface Cracks

Methods to determine weight functions, $M(x; P')$, for two-dimensional surface cracks under one-dimensional stress distributions are well developed. The resulting weight functions are obviously only applicable to one-dimensional stress distributions. A few methods have been proposed to determine the weight function, $m(x, y; P')$, for two-dimensional stress distributions, but no technique has achieved general acceptance or been fully developed. If the reference stress intensity factors are the solutions from traction type boundary conditions only, the resulting weight functions are restricted to traction type boundary conditions as well.

One-Dimensional Stress Distributions

If the stress distribution is one-dimensional, the weight function $M(x; P')$ described in Eq.(2.6) can be used. Shen and Glinka (1991a) found that the weight function at the deepest point (that is, P' corresponds to point A in Figure 2.1) of a semi-elliptical surface crack could be approximated based on the general expression:

$$M(x, a; A) = \frac{2}{\sqrt{2\pi(a-x)}} \left[1 + M_{1A} \left(1 - \frac{x}{a}\right)^{\frac{1}{2}} + M_{2A} \left(1 - \frac{x}{a}\right) + M_{3A} \left(1 - \frac{x}{a}\right)^{\frac{3}{2}} \right] \quad (2.11)$$

The three parameters, M_{1A} , M_{2A} and M_{3A} , depend only on the geometry of the semi-elliptical surface crack (a/t and a/c). They can be obtained from three reference stress intensity factor solutions at the deepest point or two solutions plus an additional condition.

For the surface point, B , of a semi-elliptical surface crack, the weight function can be approximated using the following expression (Shen and Glinka, 1991a):

$$M(x, a; B) = \frac{2}{\sqrt{\pi a}} \left[1 + M_{1B} \left(\frac{x}{a} \right)^{\frac{1}{2}} + M_{2B} \left(\frac{x}{a} \right) + M_{3B} \left(\frac{x}{a} \right)^{\frac{3}{2}} \right] \quad (2.12)$$

Again, the three parameters, M_{1B} , M_{2B} and M_{3B} , depend only on the geometry of the crack. They can be obtained from three reference stress intensity factor solutions or two solutions plus an additional condition.

As explained by Shen and Glinka (1991a), the third condition for the weight function at the deepest point, $M(x, a; A)$, is that the second derivative of the weight function be zero at $x = 0$, which leads to

$$M_{2A} = 3 \quad (2.13)$$

The third condition (Shen and Glinka, 1991) for weight function at the surface point $M^c(x, a; B)$ is that the weight function equals zero at $x = a$, which gives

$$1 + M_{1B} + M_{2B} + M_{3B} = 0 \quad (2.14)$$

In addition, the author (Wang and Lambert, 1995b) developed local weight functions for every point along the crack front. By analyzing the closed formed weight function for an embedded circular crack in an infinite three-dimensional body for any point, P' , in the range $0 < \phi < \pi/2$, along the crack front in a semi-elliptical surface crack as shown in Fig. 2.1, the following forms were proposed to approximate the weight function $M(x, a; P')$:

for $0 \leq x \leq a \sin \phi$

$$M(x, a; P') = \frac{\sqrt{\sin \phi + 1}}{\sqrt{\pi(a \sin \phi - x)}} \left[1 + M_{1P'} \left(1 - \frac{x}{a \sin \phi} \right) + M_{2P'} \left(1 - \frac{x}{a \sin \phi} \right)^2 \right] \quad (2.15a)$$

for $a \sin \phi \leq x \leq a$

$$M(x, a; P') = \frac{\sqrt{1 - \sin \phi}}{\sqrt{\pi(x - a \sin \phi)}} \left[1 + M_{3P'} \left(\frac{x}{a \sin \phi} - 1 \right)^{\frac{1}{2}} + M_{4P'} \left(\frac{x}{a \sin \phi} - 1 \right)^2 \right] \quad (2.15b)$$

This functional form depends not only on x and a , but also on the position of the local point, P' , in terms of ϕ . This piecewise function is employed due to the singular nature of the weight function. Both parts of the weight function, $M(x, a; P')$ – (2.15a) and (2.15b), must be used to perform the integration to calculate the stress intensity factor. In order to determine the four parameters, $M_{1P'}$, $M_{2P'}$, $M_{3P'}$ and $M_{4P'}$ in Eq.(2.15), two reference stress intensity factor solutions and two additional conditions are necessary.

The accuracy of the above approach of determining weight functions for deepest point and surface point has been verified for surface cracks in flat plates (Wang and Lambert, 1995a, 1997a), thin pipes (Wang and Lambert, 1995c) and thick pipes (Zheng and Glinka, 1995; Kiciak *et al.*, 1995) using finite element results. The accuracy of the weight functions for every point along the crack front has been verified for surface cracks in flat plates (Wang and Lambert, 1995b). It was found that the accuracy of the predicted stress intensity factors using the weight functions derived was of the same order as the reference stress intensity factor solutions. The drawback of this approach is that two-dimensional stress distributions cannot be considered explicitly.

Two-Dimensional Stress Distributions

For a two-dimensional stress distribution acting on the crack surface, the approximate weight function, $m(x,y; P')$, proposed by Oore and Burns (1980a) can be used. They considered available analytical solutions for embedded three-dimensional, planar cracks and proposed a point load weight function for any embedded crack in an infinite three-dimensional body (Figure 2.6):

$$m(x, y; P') = \frac{\sqrt{2}}{\pi} \frac{1}{[(x-x')^2 + (y-y')^2] \left(\int_{\Gamma} \frac{d\Gamma}{r^2} \right)^{\frac{1}{2}}} \quad (2.16)$$

where x' , y' are the coordinates of point P' , Γ is the contour corresponding to the crack front, and r is the distance between point (x, y) and any point on contour Γ . This weight function is only applicable for embedded cracks. For surface cracks, Oore and Burns (1980b) proposed a magnification factor technique:

$$K_{sv} = M_s K_{ev} \quad (2.17)$$

where K_{sv} is the stress intensity factor for a surface crack; K_{ev} is the stress intensity factor for an equivalent embedded crack subjected to the equivalent symmetric stress field, and M_s is a free surface magnification factor. Originally, Oore and Burns (1980b) assumed that M_s depended on the geometry but not on loading conditions, and M_s could be obtained from finite element results for surface cracks by Newman and Raju (1981). It was later found that M_s depended on loading conditions as well, and more sophisticated modification techniques were required to obtain the stress intensity factors for surface cracks (Grueter *et*

al., 1981; Forbes *et al.*, 1991). Nevertheless, this approach has been successfully used in many applications for the calculation of stress intensity factors (Desjardins, 1988).

However, a few drawbacks to this approach remain. First, the resulting weight function is only an approximate weight function for embedded cracks in an infinite body. For low aspect ratio embedded elliptical cracks ($a/c = 0.1$), the difference between the stress intensity factors predicted by the Oore-Burns weight function and theoretical results was as high as 25% (Desjardins, 1988) for a linear stress distribution. Second, the weight function can only be used directly to calculate stress intensity factors for embedded cracks. Correction techniques are required to correct the solution for surface cracks (Grueter *et al.*, 1981; Forbes, 1991). Third, a complex line integration along the crack front contour must be conducted to obtain the weight function $m(x,y; P')$, and special numerical techniques must be employed (Desjardins, 1988).

More research effort is required to develop more accurate and efficient weight functions for two-dimensional stress distributions.

The Effect of Fixed Boundary Conditions

The methods of determining weight functions discussed in this section were widely used to determine the weight functions for surface cracks in flat plates without any prescribed displacement boundary conditions, since the reference stress intensity factors used were calculated from only prescribed tractions boundary conditions. If the reference stress intensity factors used were calculated from a cracked body with zero displacement along a certain boundary, then the derived weight function would have accommodated the effect of the corresponding zero displacement boundary conditions.

2.3 Stress Intensity Factors and Weight Functions for Surface Cracks

Below is a brief review of stress intensity factors and weight functions solutions for surface cracks in flat plates, T-plate, pipe-plate and tubular joints.

2.3.1 Flat Plates

Stress Intensity Factors

The most accepted stress intensity factor solutions for semi-elliptic surface cracks in finite thickness plates were obtained by Raju and Newman (1979) and Shiratori *et al.* (1987) using the finite element method. Newman and Raju obtained results for remote tension and bending loading only. Shiratori *et al.* obtained results for constant, linear, parabolic or cubic stress distributions on the crack face. This data is available for aspect ratios, a/c , of 0.2, 0.4, 0.6 and 1.0, and relative crack depths, a/t , of 0.2, 0.4, 0.6 and 0.8. Recently, stress intensity factors for low aspect ratio ($a/c = 0.1$ or 0.05) and high aspect ratio ($a/c = 1.5$ or 2.0) semi-elliptical surface cracks in a finite thickness plate with relative crack depths a/t of 0.2, 0.4, 0.6 or 0.8 subjected to constant, linear, quadratic or cubic stress distributions were determined by the author (Wang and Lambert, 1995a, 1997a).

Interpolation of this finite element data in terms of aspect ratio, a/c and relative depth, a/t is required to get general solutions for a specific region of a/c and a/t . Newman and Raju (1981), and Wang and Lambert (1995b, 1997a) presented stress intensity factor equations for bending (linear stress distribution on the crack plane in the Wang and Lambert formula) and tension based on curve fitting to the finite element data. The Newman and Raju formula is

$$K = [M_m \left(\frac{a}{c}, \frac{a}{t}\right) \sigma_m + M_b \left(\frac{a}{c}, \frac{a}{t}\right) \sigma_b] \sqrt{\frac{\pi a}{Q}} \quad (2.18)$$

where a is the crack depth, and σ_m and σ_b denote tension and bending stress components of the nominal stress distribution, respectively.

For most calculations for surface cracks in flat plates, the loading distribution is one-dimensional, i.e., it does not vary in the plate width direction. However, more complex stress distributions, such as when residual stresses are present, may occur where stress distributions change in the plate width direction. Figures 2.7(a) and (b) shows a typical distribution for residual stresses due to a butt weld in a flat plate (Shiratori *et al.*, 1987). Wu (1984) and Shiratori *et al.* (1987) conducted finite element calculations for surface cracks in flat plates under two-dimensional stress distributions, but insufficient data is available to generate empirical equations for stress intensity factors for two-dimensional stress distributions. More finite element results are required to obtain systematic solutions for stress intensity factors of surface cracks in flat plates under two-dimensional stress distributions.

No finite element solution exists for surface cracks in flat plates with built-in end (zero displacement) boundary conditions. Stress intensity factors for surface cracks in flat plates with built-in ends can be calculated using plates with built-in ends subject to crack face pressure as shown in Figure 2.7(c). The available stress intensity factor solutions for surface cracks in flat plates with free ends are not appropriate. Further work is required on the analysis of the effects of the zero displacement boundary conditions on stress intensity factors.

Weight Functions

Based on available finite element results from Shiratori *et al.* (1987), Shen and Glinka (1991a) derived one-dimensional weight functions for the deepest and surface points of semi-elliptical surface cracks in finite thickness plates using the method outlined in section 2.2.2. The weight functions derived by Shen and Glinka (1991a) are only valid for $0.2 \leq a/c \leq 1$. The author refined this analysis by performing finite element calculations to obtain reference stress intensity factor solutions for both low aspect ratio and high aspect ratio semi-elliptical cracks, and derived weight functions for the deepest and surface points (Wang and Lambert, 1995a, 1997a) to cover a wide range of aspect ratios, a/c , from 0 to 2.0. None of these weight functions consider a stress distribution which varies in the width direction of the plate.

By applying the magnification factor technique or Grueter's correction, the O-integral weight function can be used to calculate stress intensity factors for surface cracks in flat plates (Desjardins, 1988; Forbes, 1991). Differences between stress intensity factors from finite element calculations and predictions using the magnification factor technique were found to be less than 5% only for the case of shallow cracks with $a/t \leq 0.3$ and $0.2 \leq a/c \leq 1$. Grueter's correction technique gave better predictions (within 5% of the finite element results for $a/t \leq 0.7$, $0.2 \leq a/c \leq 1$), but can only be used to compute stress intensity factors at the deepest point and cannot handle stresses that vary in the width direction. General weight functions need to be developed which can address two-dimensional stress distributions and cover a wide region of a/c and a/t .

The available weight functions were developed based on the reference stress intensity factors for surface cracks in flat plates with free ends. Therefore, these weight

functions are only suitable for the calculation of stress intensity factors of surface cracks in flat plates with traction boundary conditions.

2.3.2 T-plate Joints

The T-plate model represents a simple welded joint and is often used as a model for more complex welded joint behavior. A schematic of the weld toe geometry, uncracked stress field, and crack location is given in Fig. 2.8(a). In the calculation of stress intensity factors, the model is either loaded by far-field tension or bending. On the prospective crack plane, the actual stress distribution has a stress concentration which depends on the weld toe geometry.

Stress Intensity Factors

Three-dimensional finite element analyses were used to calculate the stress intensity factors for surface cracks in T-plate joints by several authors (Smith, 1984; Bell, 1985; Dijkstra *et al.*, 1989; and Fu *et al.*, 1993). The resulting stress intensity factors for this geometry are generally summarized by a format proposed by Maddox (1975):

$$K = [Y_m \sigma_m + Y_b \sigma_b] \sqrt{\frac{\pi a}{Q}} \quad (2.19)$$

Y_m and Y_b are given by

$$Y_m = M_{k_m} \cdot M_m \quad (2.20)$$

and

$$Y_b = M_{k_b} \cdot M_b \quad (2.21)$$

where subscripts m and b denote tension and bending stress; σ_m and σ_b are the nominal tension and bending stresses; M_{k_m} and M_{k_b} denote the weld toe correction factors; and M_m and M_b denote the crack shape (depth and aspect ratio) correction factors. The M_m and M_b factors are usually based on the work of Newman and Raju for flat plates, Eq.(2.16). Parametric equations are available for M_{k_m} and M_{k_b} in terms of the relative crack depth, a/t , and aspect ratio, a/c (Fu *et al.*, 1993; Bowness and Lee, 1997).

It must be noted that all the available solutions are for T-plate joints with free ends; no solutions are available for T-plate joints with built-in ends. The T-plate models with built-in ends would likely provide a better model for more complex pipe-plate and tubular joints, since they incorporate some load shedding effects.

Weight Functions

The only weight function developed specifically for welded joints was derived by Niu and Glinka (1990). The actual geometry considered was a flat plate with an angular corner as shown in Figure 2.8(b). Considering an approximate stress intensity factor solution at the deepest point of a surface crack, Niu and Glinka (1987,1990) extracted one-dimensional weight functions for the deepest point of surface cracks in plates with an angular corner. They verified this weight function using finite element data from Smith

(1984). The weight function for flat plates with an angular corner was then used as the weight function for surface cracks in T-plate joints (Niu and Glinka, 1987, 1990).

It is common practice to calculate stress intensity factors for surface cracks in T-plate joints using weight functions derived for flat plates in conjunction with stress distributions from corresponding uncracked T-plate joints (Forbes *et al.*, 1991). It is argued that by using the stress distribution, $\sigma(x)$, calculated for the uncracked T-joints and the weight function for flat plates, the effect of the weldment geometry on the stress intensity factor would be accounted for satisfactorily. For surface cracks in a welded geometry incorporating a 45° weld angle and a toe radius ratio, $\rho/t = 1/38$, as shown in Figure 2.8(a), Forbes *et al.* (1991) compared the predicted stress intensity factors at the deepest point using the weight function for plates with an angular corner by Niu and Glinka (1990), the weight function for flat plates by Shen and Glinka (1991a), the weight function for embedded elliptical cracks by Oore-Burns (1980a) with an improved surface correction scheme for flat plates, and three-dimensional finite element predictions by Smith (1984) and Bell (1985). For a wide range of relative crack depths ($0 \leq a/t \leq 0.8$) and crack aspect ratios ($0.2 \leq a/c \leq 1.0$), under far field tension and bending, the results from the three weight functions were in fairly good agreement with each other and with finite element results. Therefore, the weight function for a flat plate provided acceptable results at the deepest point for the T-joint geometry considered. They made no comment regarding the surface point since more detailed finite element calculations are required for such a comparison. In the absence of specific weight functions for T-plate joints, such an approximation provides a quick and acceptable estimate of stress intensity factors.

In the presence of two-dimensional stress distributions, more general weight functions for two-dimensional stress distributions must be developed for surface cracks in T-plate joints. For T-plate welded joints with a finite width, it was found that the

uncracked stress distribution changes along the width direction even in the absence of residual stresses (Lecsek, 1993). It is, therefore, necessary to investigate the effect of the stress variation along the width on the stress intensity factors. Also, available weight functions are based on stress intensity factors for surface cracks in T-plate joints without any end constraints. If the ends of the T-plate joint are fixed, these weight functions cannot be used directly.

2.3.3 Pipe-Plate and Tubular Joints

The pipe-plate specimen (Figure 1.1) has been considered as a simplified model for a tubular joint (Lambert *et al.*, 1987). It has several important features in common with full tubular joints while remaining relatively simple to analyze. These features include a non-uniform, yet symmetrical, stress distribution along the weld toe and the potential for load redistribution once significant crack growth has occurred.

Stress Intensity Factors

There is a limited set of finite element solutions for stress intensity factors for surface cracks in pipe-plate joints (Lambert and Bell, 1993) or tubular joints (Ritchie *et al.*, 1987; Rhee, 1989). Some full scale experimental data also exists for pipe-plate (Lambert and Bell, 1993) or tubular joints (Dover *et al.*, 1978; Forbes, 1991). These results cover only very specific geometries and, therefore, cannot be used to obtain general solutions. Instead, it is common practice to use empirical equations developed for T-plate joints, Eq.(2.19), to calculate the stress intensity factors for surface cracks in pipe-plate or tubular joints (Cheaitani *et al.*, 1995).

Because of the difference between the boundary conditions for T-plate joints and pipe-plate or tubular joints, several authors (Aaghaakouchak *et al.*, 1989; Haswell *et al.*, 1991; Forbes *et al.*, 1992) have found that the use of such empirical equations results in a conservative estimation of stress intensity factor for deep cracks, $a/t > 0.5$, and hence an underestimation of fatigue life and fracture strength. This effect has been referred to as load shedding, which redistributes the load as the crack develops and thus reduces the crack driving force. This is not addressed in the empirical equations developed from T-plate joints.

Based on full scale experimental results by Dover (1978), Aaghaakouchak *et al.* (1989) proposed a relationship to account for the load shedding effect. They treat the membrane component of stress, σ_m , as being unaffected by the crack while the bending component, σ_b , is allowed to decrease using the relationship:

$$\sigma_b = \sigma_b^0 (1 - a/t) \quad (2.22)$$

where σ_b and σ_b^0 are the bending stresses in the cracked and uncracked body, respectively; and a/t is the non-dimensional crack depth. This modification gives better agreement between stress intensity factors from the combined equation approach and those from 3-D finite element calculations or experiments. However, since this empirical relationship was proposed based on limited experimental results, it gives unconservative estimations of stress intensity factors for some cases (Maddox, 1997).

There is another issue which has not been accounted for in this analysis: the two-dimensional stress distributions on the uncracked plane. Since the nominal stresses σ_m and σ_b , used in Eq. (2.19) represent only the stresses at the hot spot location, they cannot

describe the two-dimensional changes of stress distributions shown in Figure 2.9 (through the thickness) and 2.10 (along the weld toe)(Haswell *et al.*, 1991; Hellier *et al.*, 1990).

Weight Functions

No weight functions are available for pipe-plate or tubular joints. Several authors have used the Oore-Burns weight function developed for embedded elliptical cracks (Dover *et al.*, 1986; Burdekin *et al.*, 1986; Forbes *et al.*, 1992) to calculate stress intensity factors for surface cracks in tubular joints. Since none of these weight functions consider the load shedding effect, the resulting stress intensity factors are conservative (Haswell *et al.*, 1991; Forbes *et al.*, 1992).

Figure 2.1 Notation for semi-elliptical surface crack

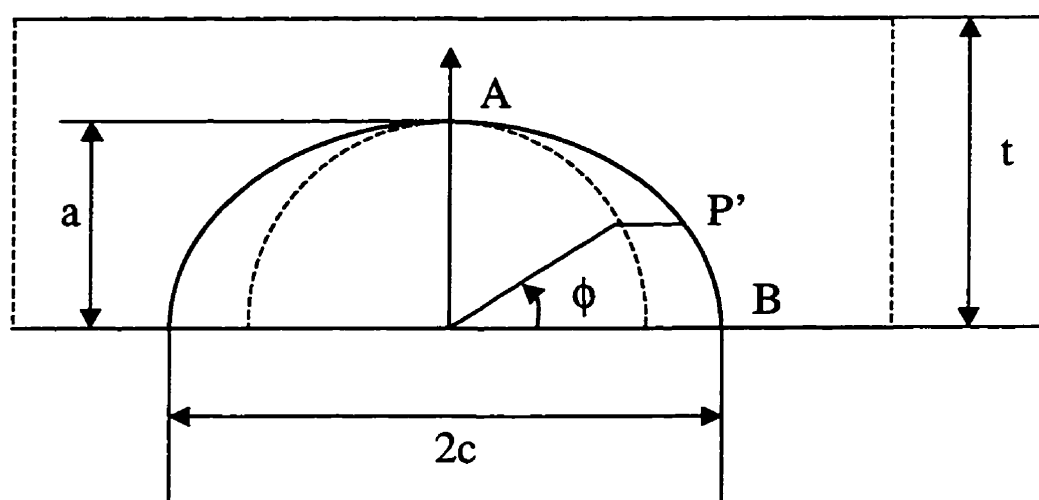


Figure 2.2 Superposition method (Bueckner, 1970)

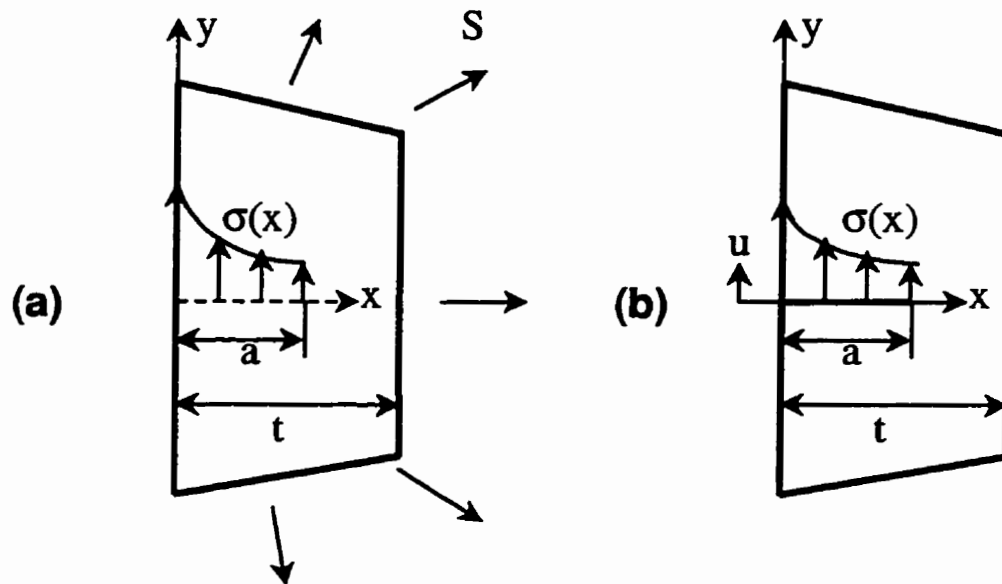
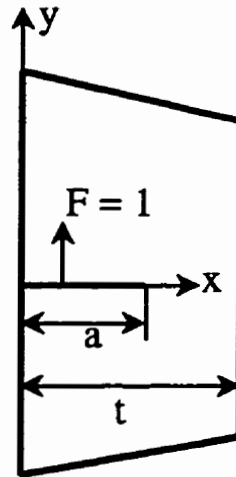
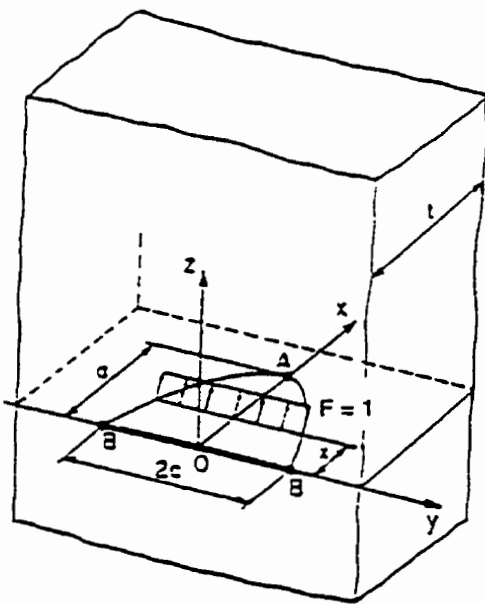


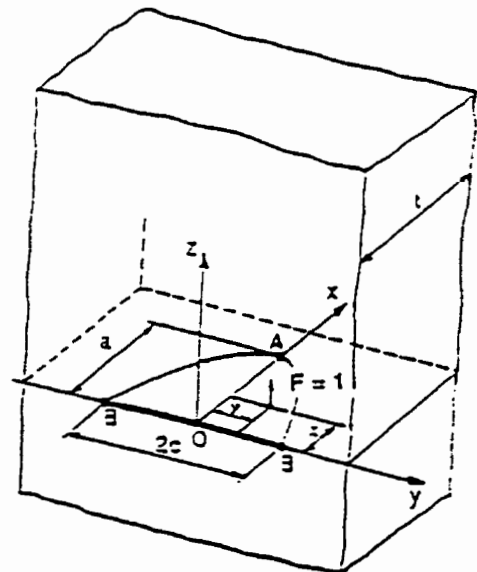
Figure 2.3 Physical meaning of weight functions, (a) for 1D crack; (b) for 2D crack under one-dimensional stress; (c) for 2D crack under two-dimensional stress



(a)



(b)



(c)

Figure 2.4 Two-dimensional stress distribution

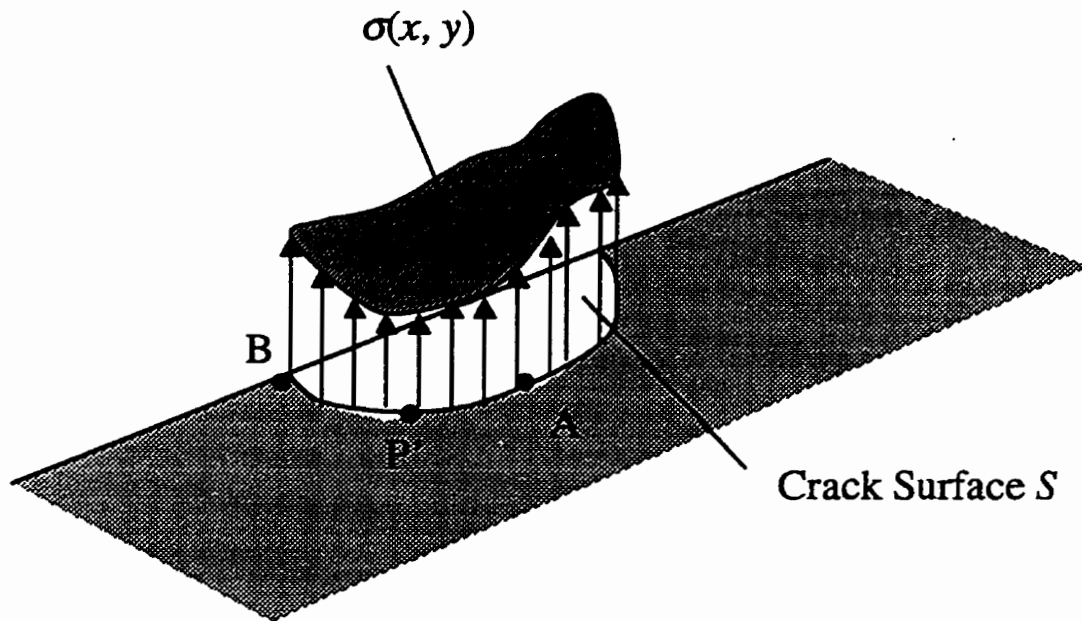


Figure 2.5 Weight function for mixed boundary conditions (Wu and Carlsson, 1991)

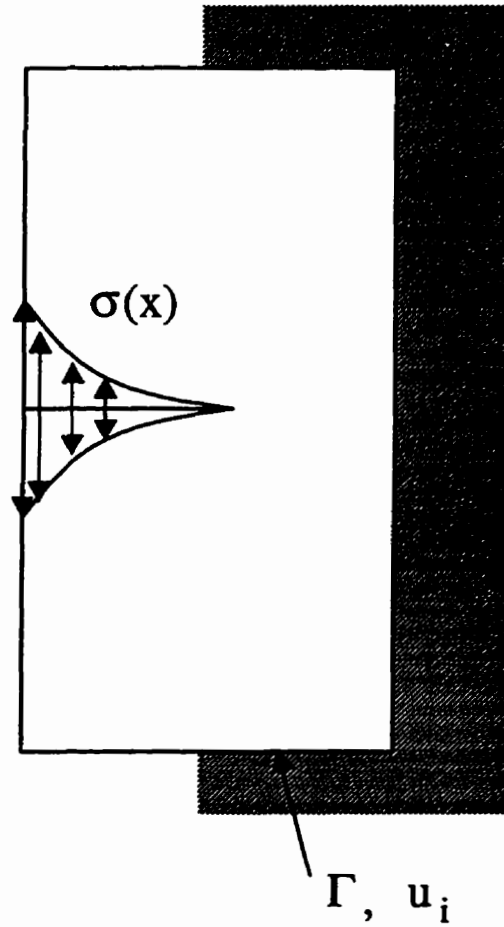


Figure 2.6 Oore-Burns (1980a) weight function

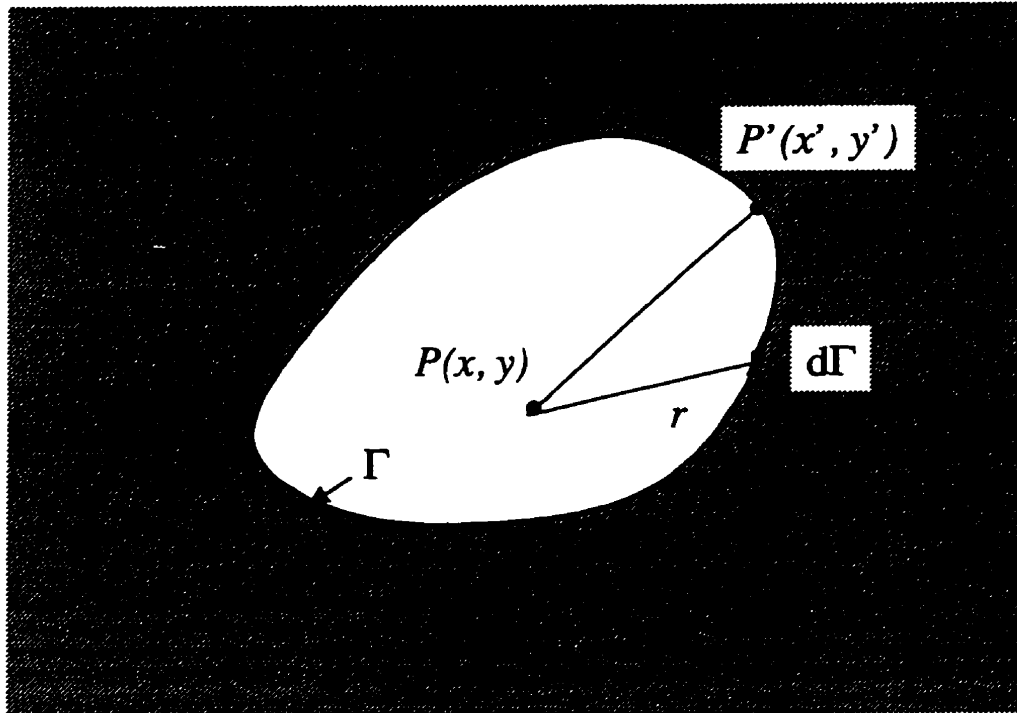
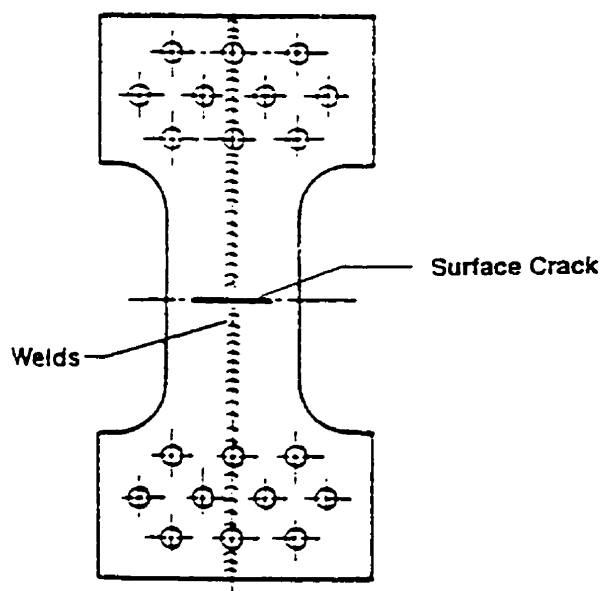
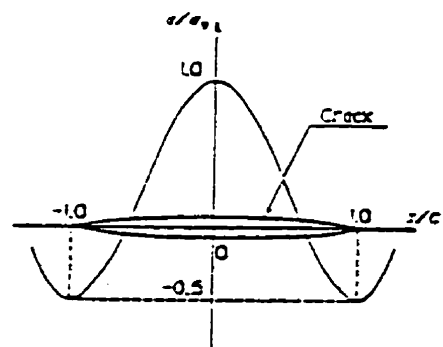


Figure 2.7 Surface cracks in flat plate: (a) and (b) under residual stress field; (c) with fixed boundary conditions

a)



b)



c)

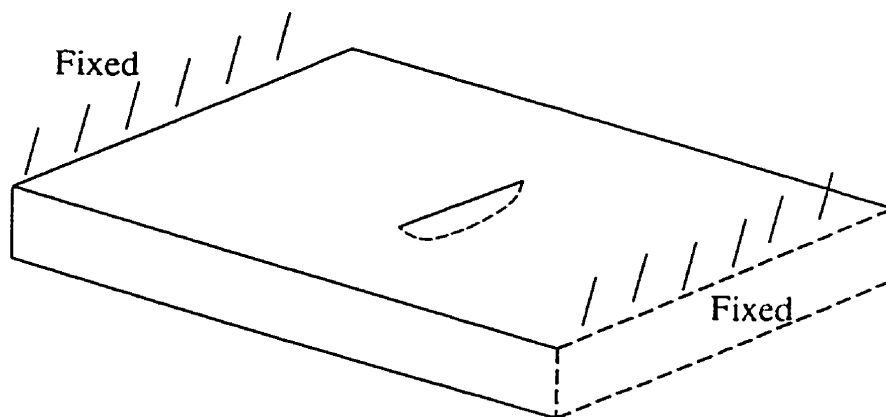
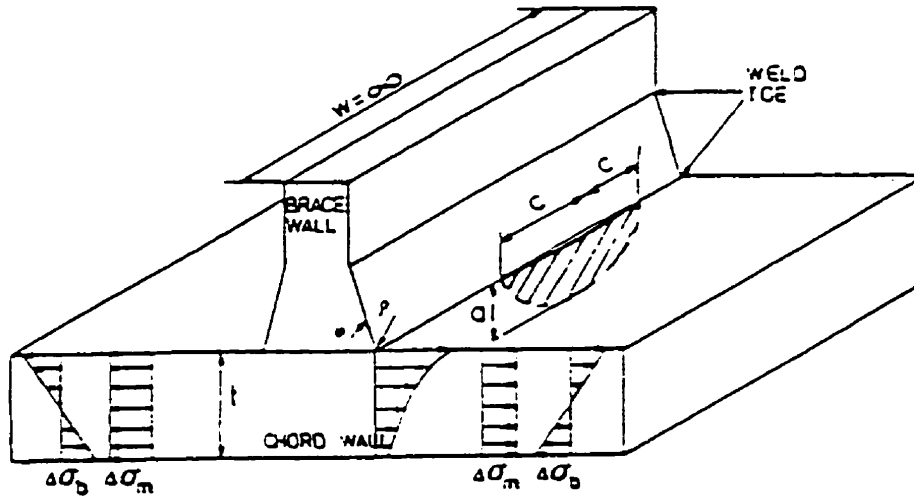
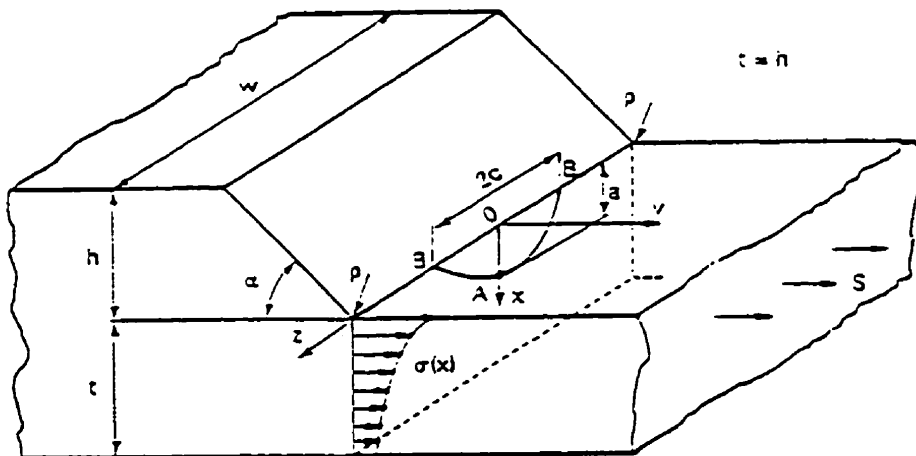


Figure 2.8 (a) T-plate joint; (b) plate with an angular corner



a) T-Plate Joint (Dijkstra et al, 1989)



b) Plate with an Angular Corner (Niu and Glinka, 1990)

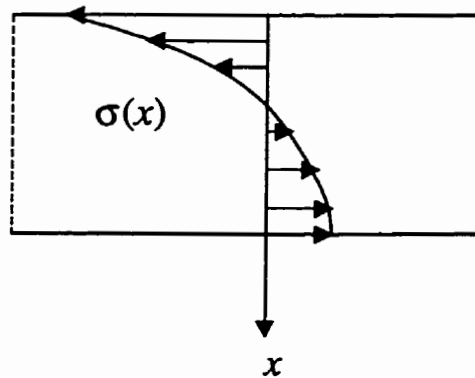
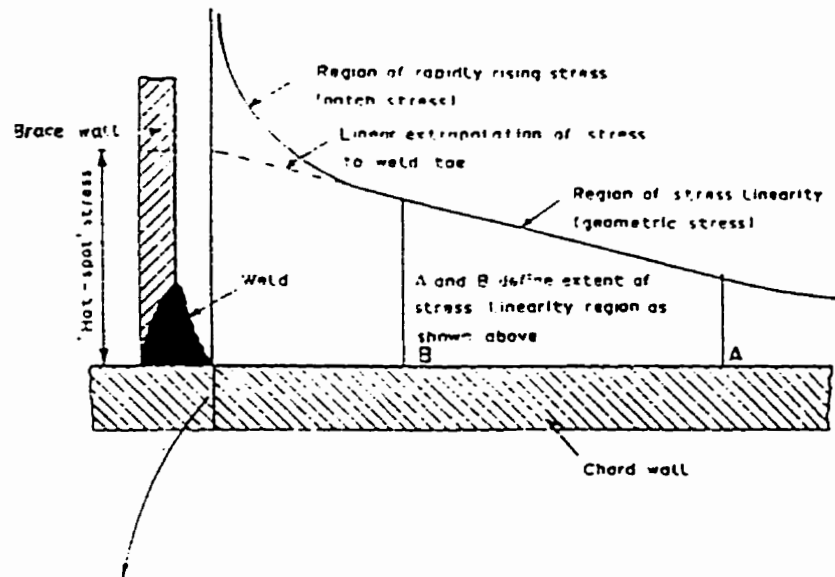
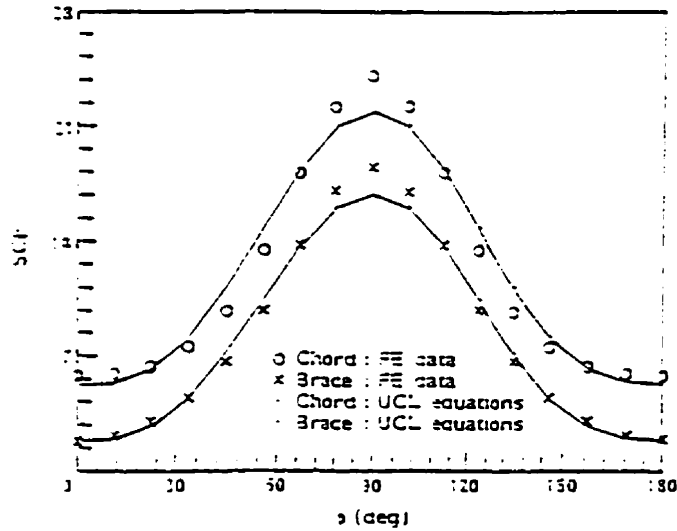
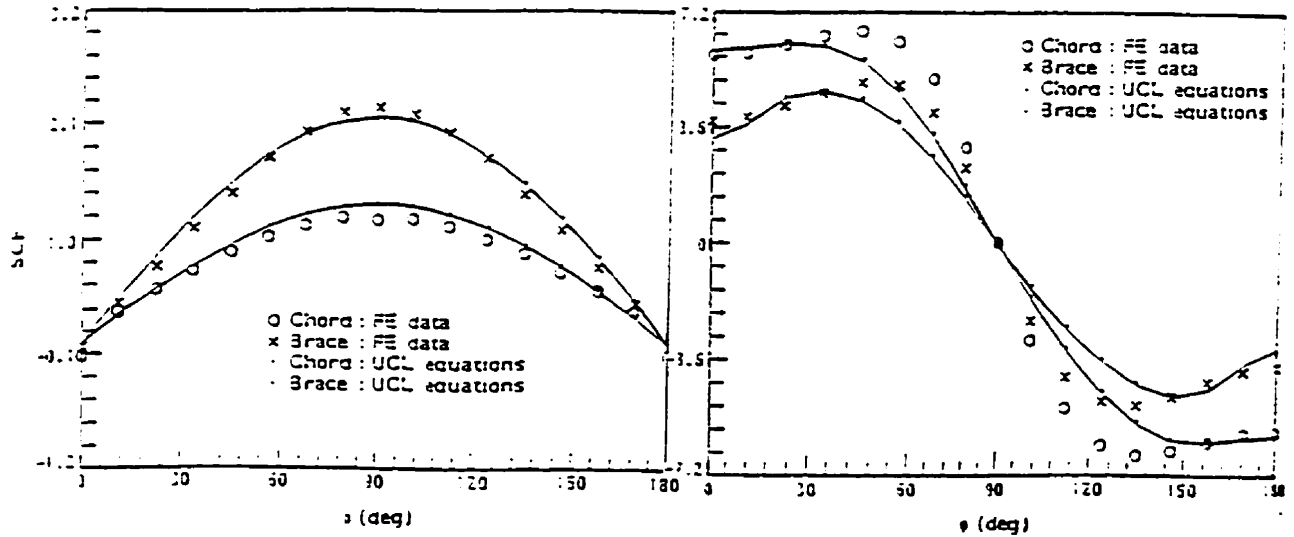
Figure 2.9 Stress distribution in thickness direction (Haswell *et al.*, 1991)

Figure 2.10 Stress distribution around the weld toe



a). Normal stress along the crack toe for axially loading (Hellier et al., 1990)



b). Normal stress along the crack toe for out-of-plane bending

c). Normal stress along the crack toe for in-plane bending (Hellier et al., 1990)

Chapter 3

Theory and Development

The objective of the present research is to develop weight functions for the calculation of stress intensity factors for surface cracks in flat plates and welded joints, including T-plate, pipe-plate and tubular joints. The resulting weight functions will consider two-dimensional stress distributions and include the load shedding effect for pipe-plate and tubular joints. In this chapter, a general methodology to accommodate the effects of two-dimensional stress distribution and prescribed zero displacement boundary conditions on weight functions is discussed.

Since there are no general methods to determine two-dimensional weight functions for surface cracks, approaches have been developed to address two-dimensional stress distributions. In the present research, two methods are proposed to treat two-dimensional stress distributions: the Fourier series approach and the general point load weight function approach. These two approaches are presented in section 3.1.

In order to accommodate the effects of prescribed zero displacement boundary conditions into weight functions, reference stress intensity factor solutions for the same

prescribed zero displacement boundary conditions must be used to derive weight functions. In section 3.2, a method to obtain stress intensity factor solutions for prescribed zero displacement boundary conditions based on available stress intensity factors for traction type boundary condition is discussed.

3.1 Effect of Two-dimensional Stress Distributions

3.1.1 General Approach

For two-dimensional cracks, stress intensity factors for any two-dimensional stress field, $\sigma(x, y)$, can be calculated using the two-dimensional weight function $m(x, y; P')$ in Eq. (2.5):

$$K(P') = \iint_s \sigma(x, y) m(x, y; P') dx dy \quad (2.5)$$

In order to obtain the point load weight function, $m(x, y; P')$, for surface cracks in any complex geometry, a general form must to be recognized and used to determine the weight functions from reference stress intensity factor solutions.

Properties of Weight Functions for Two-Dimensional Cracks

By analyzing the properties of weight functions for two dimensional crack problems, Rice (1989) pointed out that s and ρ (Fig. 3.1) were key parameters in the weight function expression, $m(x, y; P')$, where s is the shortest distance between the load point and the boundary of the crack front, and ρ is the distance between the load and the point P' as

shown in Fig. 3.1. These two parameters can be used to describe available analytical weight functions.

For the half-plane crack in an infinite body as shown in Figure 3.2(a)

$$m(x, y; P') = \frac{\sqrt{2s}}{\pi^{3/2} \rho^2} \quad (3.1)$$

For the penny shape crack as shown in Figure 3.2(b)

$$m(x, y; P') = \frac{\sqrt{2s}}{\pi^{3/2} \rho^2} \sqrt{1 - \frac{s}{2a}} \quad (3.2)$$

where a is the radius of the circular crack.

Rice (1989) has also shown that the weight function for an arbitrary planar crack embedded in an infinite body (Fig. 3.1) can be generally written as

$$m(x, y; P') = \frac{\sqrt{2s}}{\pi^{3/2} \rho^2} w(x, y; P') \quad (3.3)$$

It is apparent from Eq. (3.3) that the singularity term in all the weight functions is of the order \sqrt{s}/ρ^2 , and the weight function tends to infinity when ρ approaches zero. When s equals zero and ρ is not zero, the weight function value is zero, and the stress intensity factor is also zero.

The function $w(x, y; P')$ describes the geometry effect for the shape of the embedded crack. For a half-plane crack

$$w(x, y; P') = 1 \quad (3.4)$$

and for a penny shaped crack

$$w(x, y; P') = \sqrt{1 - \frac{s}{2a}} \quad (3.5)$$

It was also found (Rice, 1989) that the function $w(x, y; P')$ has a well-defined limit, when point (x, y) approaches the crack boundary, i.e., s approaches 0. For both cases of half plane or penny shaped crack,

$$\lim_{s \rightarrow 0} [w(x, y; P')] = 1 \quad (3.6)$$

For a given two-dimensional crack, if the function $w(x, y; P')$ can be determined, then the general weight function $m(x, y; P')$ can be obtained from Eq. (3.3). Note that approach represented by Eq. (3.3), derived by Rice (1989), is very similar to the O-integral proposed by Oore and Burns (1980). Both can give the correct weight function for the half-plane or penny-shaped cracks.

In the present thesis, this general approach was used to develop weight functions for embedded elliptical cracks in an infinite body, as presented in Chapter 4. However, the determination of $m(x, y; P')$ for surface cracks requires more effort. In order to avoid these difficulties, a Fourier series approach was developed.

3.1.2 Fourier Series Approach

As discussed previously, the direct determination of $m(x, y; P')$ for a surface crack is rather difficult. A Fourier series approach is proposed to avoid this difficulty. Any stress field, $\sigma(x, y)$, in the region S : $0 \leq x \leq a$, and $-c \leq y \leq c$, can always be presented using a Fourier series to represent the variation in the y -direction.

For example, the residual stress distribution shown in Figure 2.7(b) was given by Shiratori et al. (1987):

$$\sigma(x, y) = \sigma_y \left[3 \left(\frac{y}{c} \right)^3 - \frac{9}{2} \left(\frac{y}{c} \right)^2 + 1 \right] \quad (3.7)$$

where σ_y is the yield stress of the material. This stress distribution can be represented using the following simple two-term Fourier series with a maximum difference of one percent:

$$\sigma(x, y) = \sigma_y \left[\frac{1}{4} + \frac{72}{\pi^4} \cos\left(\frac{\pi y}{c}\right) \right] \quad (3.8)$$

Figure 3.3 shows the comparison between these two stress distributions. For the two-dimensional stress distributions encountered in pipe-plates and tubular joints shown in Figure 2.10, simple Fourier series with two (or at most three) terms can be used to represent the variation along the weld toe.

In general, the Fourier series expansion in the y -direction for any stress distribution $\sigma(x, y)$ can be expressed as:

$$\sigma(x, y) = a_0(x) + \sum_{n=1}^{\infty} (a_n(x) \cos(\frac{n\pi y}{c}) + b_n(x) \sin(\frac{n\pi y}{c})) \quad (3.9)$$

where the Fourier constants, which are functions of x , can be calculated from (Spiegel, 1992)

$$\begin{aligned} a_0(x) &= \frac{1}{2c} \int_{-c}^c \sigma(x, y) dy \\ a_n(x) &= \frac{1}{c} \int_{-c}^c \sigma(x, y) \cos \frac{n\pi y}{c} dy \quad (n = 1, 2, \dots) \\ b_n(x) &= \frac{1}{c} \int_{-c}^c \sigma(x, y) \sin \frac{n\pi y}{c} dy \quad (n = 1, 2, \dots) \end{aligned}$$

After substituting for the stress field using the Fourier expansion, Eq. (2.5) can be written as

$$K(P') = \int_0^a \int_{l_y} (a_0(x) + \sum_{n=1}^{\infty} (a_n(x) \cos(\frac{n\pi y}{c}) + b_n(x) \sin(\frac{n\pi y}{c}))) m(x, y; P') dy dx \quad (3.10)$$

By integrating with respect to y first, we can define the following series of weight functions:

$$\begin{aligned} M_n^c(x, P') &= \int_{l_y} \cos(\frac{n\pi y}{c}) m(x, y; P') dy \quad n = 0, 1, 2, 3, \dots \\ M_n^s(x, P') &= \int_{l_y} \sin(\frac{n\pi y}{c}) m(x, y; P') dy \quad n = 1, 2, 3, \dots \end{aligned} \quad (3.11)$$

where superscripts c and s represent “cos” and “sin”, n represents the n th term in the Fourier series, and l_y is the region of integration for y for a given x value. The newly

defined weight functions, $M_n^c(x;P')$, and $M_n^s(x;P')$ are the stress intensity factors at point P' for a line load varying as $\cos(n\pi y/c)$ or $\sin(n\pi y/c)$ at x . Fig. 3.4 shows the line load corresponding to weight function $M_n^c(x;P')$. After introducing the series of weight functions, Eq. (3.10) becomes

$$K(P') = \int_0^a a_0(x)M_0^c(x;P')dx + \sum_{n=1}^{\infty} \left[\int_0^a a_n(x)M_n^c(x;P')dx + \int_0^a b_n(x)M_n^s(x;P')dx \right] \quad (3.12)$$

Instead of the determination of weight function $m(x,y;P')$, the problem has been reduced to the determination of weight functions $M_n^s(x;P')$ and $M_n^c(x;P')$. It can be seen immediately that $M_0^c(x;P')$ is actually the one dimensional weight function $M(x;P')$ discussed previously, which is available for surface cracks in flat plates (Wang and Lambert, 1995a, 1995b, 1997). Since for most engineering applications the stress variation in the y -direction can be represented accurately using a Fourier series with a maximum $n = 1$, only $M_1^s(x;P')$ and $M_1^c(x;P')$ are required for most applications. In fatigue and fracture analyses, the stress intensity factors at the deepest and surface points are generally the most important values. Therefore, in the following discussion, only $M_1^s(x;P')$ and $M_1^c(x;P')$ at points $P' = A$ and $P' = B$ will be developed.

Now, the stress intensity factor for any two-dimensional stress field, which can be presented by:

$$\sigma(x,y) = a_0(x) + a_1(x) \cdot \cos\left(\frac{\pi y}{c}\right) + b_1(x) \cdot \sin\left(\frac{\pi y}{c}\right) \quad (3.13)$$

can be calculated as follows:

at the deepest point

$$K(A) = \int_0^a a_0(x)M(x; A)dx + \int_0^a a_1(x)M_1^c(x; A)dx + \int_0^a b_1(x)M_1^s(x; A)dx \quad (3.14)$$

and at the surface point

$$K(B) = \int_0^a a_0(x)M(x; B)dx + \int_0^a a_1(x)M_1^c(x; B)dx + \int_0^a b_1(x)M_1^s(x; B)dx \quad (3.15)$$

The weight functions, $M^s_I(x; P')$ and $M^c_I(x; P')$, can be obtained using reference stress intensity factor solutions in the same manner as for $M(x; P')$.

Weight function $M^c_I(x; P')$.

In a similar way to the development of the functional expression for $M(x; P')$, the following forms are proposed for the weight function $M^c_I(x; P')$. At the deepest point, A,

$$M_1^c(x, a; A) = \frac{1}{\sqrt{2\pi(a-x)}} \left[1 + M_{1A}^c \left(1 - \frac{x}{a}\right)^{\frac{1}{2}} + M_{2A}^c \left(1 - \frac{x}{a}\right) + M_{3A}^c \left(1 - \frac{x}{a}\right)^{\frac{3}{2}} \right] \quad (3.16)$$

where M_{1A}^c , M_{2A}^c and M_{3A}^c are geometry dependent parameters which can be decided from two reference stress intensity factor solutions plus a third condition. At the surface point, B,

$$M_1^c(x, a; B) = \frac{-2}{\sqrt{\pi x}} \left[1 + M_{1B}^c \left(\frac{x}{a} \right)^{\frac{1}{2}} + M_{2B}^c \left(\frac{x}{a} \right) + M_{3B}^c \left(\frac{x}{a} \right)^{\frac{3}{2}} \right] \quad (3.17)$$

where M_{1B}^c , M_{2B}^c and M_{3B}^c can similarly be decided from two reference stress intensity factor solutions plus a third condition.

Fett *et al.* (1987) showed that the curvature of the crack surface at the crack mouth is zero. Consequently, from Eq. (2.8), the third condition for the weight function at the deepest point, $M_I^c(x, a; A)$, is that the second derivative of the weight function be zero at $x = 0$, which leads to

$$M_{2A}^c = 3 \quad (3.18)$$

The third condition (Shen and Glinka, 1991) for weight function at the surface point $M_I^c(x, a; B)$ is that the weight function equals zero at $x = a$, since the stress intensity factor at the surface point is zero for a point load acting at the deepest point (on the crack front). This gives

$$1 + M_{1B}^c + M_{2B}^c + M_{3B}^c = 0 \quad (3.19)$$

Weight function $M_I^f(x; P')$.

The weight function $M_I^f(x; P')$ represents the stress intensity factors at point P' caused by a line load varying with $\sin(\pi y/c)$ on the crack surface. From symmetry considerations, it can be seen that $M_I^f(x; P')$ is zero at the deepest point, A , i.e.,

$$M_1^s(x, a; A) = 0 \quad (3.20)$$

The proposed weight function for surface point B is, similar to $M(x; P')$:

$$M_1^s(x, a; B) = \frac{\sqrt{2}}{\sqrt{\pi a}} \left[1 + M_{1B}^s \left(\frac{x}{a} \right)^{\frac{1}{2}} + M_{2B}^s \left(\frac{x}{a} \right) + M_{3B}^s \left(\frac{x}{a} \right)^{\frac{3}{2}} \right] \quad (3.21)$$

where M_{1B}^s , M_{2B}^s and M_{3B}^s are parameters dependent on geometry which can be decided from two reference solutions and a third condition. The third condition for $M_1^s(x, a; B)$ is that the weight function equals zero at $x = a$ (Shen and Glinka, 1991), which gives

$$1 + M_{1B}^s + M_{2B}^s + M_{3B}^s = 0 \quad (3.22)$$

So, if two reference stress intensity factors are available, the series of weight functions can be determined, and may be used to calculate stress intensity factors under two-dimensional stress distributions.

This approach was applied to develop weight functions for surface cracks in flat plates under two-dimensional stress distributions. Details of the development will be presented in Chapter 5.

3.2 Effect of Boundary Conditions

All available stress intensity factor solutions for cracks in flat plates and T-plates are for a cracked body under traction type loads. Therefore, the cracked geometry is statically determinate and the applied stresses are known *a priori*. However, for a cracked body with

fixed displacement boundary conditions, the problem becomes statically indeterminate, and the applied stresses are not known *a priori*. The stresses applied to the cracked geometry change due to the change in stiffness of the cracked section.

Although finite element analyses can be applied to calculate stress intensity factors for any cracked geometry with fixed boundary conditions, there is a simpler approach. The stress intensity factors for fixed displacement boundary conditions can be calculated from available stress intensity factor solutions for applied stress loads. By using a compliance analysis, the applied stresses on the fixed boundary can be solved for a given crack geometry (Okamura *et al.*, 1975; Marchand *et al.*, 1986). Once the applied stresses are obtained, the fixed displacement boundary conditions can be replaced by applied stress boundary conditions, and the corresponding stress intensity factors can be solved from the available solutions for applied stress loads.

The application of this method to calculate the stress intensity factors for single edge cracked specimen with fixed displacement boundary conditions was developed by Marchand *et al.* (1986), and is summarised in this section. These stress intensity factor solutions were used by the author to derive weight functions, which include the effects of fixed displacement boundary conditions.

3.2.1 Stress Intensity Factors for Fixed Displacement Boundary Conditions

Superposition Method

Consider an edge cracked flat plate restrained from moving at the ends with crack depth a , thickness t and width W . A constant distributed load is applied to the crack face as shown in Figure 3.5. This problem can be represented by the superposition of problems I

and II, as shown in Figure 3.6. The unknown tension and moment, N' and M' , can be obtained from compatibility conditions at the ends.

The displacements for problem I, δ_I and θ_I , can be calculated from a further superposition of problems I-A and I-B, shown in Figure 3.7. Since the calculation of the displacements for problem I-B is a classical problem with a standard solution, the key issue here is the calculation of the displacements for problems I-A and II, which can be obtained from the solution of the general problem shown in Figure 3.8.

Compliance Analysis

The relative displacement δ and rotation θ for the problem shown in Figure 3.8 can be obtained from the summation of “cracked” and “uncracked” components:

$$\begin{pmatrix} \delta_{total} \\ \theta_{total} \end{pmatrix} = \begin{pmatrix} \delta_c \\ \theta_c \end{pmatrix} + \begin{pmatrix} \delta_{nc} \\ \theta_{nc} \end{pmatrix} \quad (3.23)$$

The compliance of the “uncracked” beam has a standard solution given by

$$\begin{pmatrix} \delta_{nc} \\ \theta_{nc} \end{pmatrix} = \begin{bmatrix} L/EA & 0 \\ 0 & L/EI \end{bmatrix} \begin{pmatrix} N \\ M \end{pmatrix} \quad (3.24)$$

The compliance for the “cracked” beam is obtained by considering the complementary energy of the specimen, U , in terms of N and M :

$$U(N, M) = \frac{1}{2} [N \ M] \left(\begin{bmatrix} \delta_c \\ \theta_c \end{bmatrix} + \begin{bmatrix} \delta_{nc} \\ \theta_{nc} \end{bmatrix} \right) \quad (3.25)$$

If we introduce a crack extension da , we have

$$\frac{\partial U}{\partial a} = \frac{1}{2} [N \ M] \begin{pmatrix} \frac{\partial \delta_c}{\partial a} \\ \frac{\partial \theta_c}{\partial a} \end{pmatrix} \quad (3.26)$$

On the other hand, from the relation between stress intensity factor and strain energy release rate under plane stress conditions

$$\frac{\partial U}{\partial a} = \frac{K_I^2}{E} \quad (3.27)$$

Here K_I is the stress intensity factor solution for the problem shown in Figure 3.8, which is a cracked geometry loaded remotely by surface tractions. For the present problem, this solution is available (Tata *et al.*, 1973). Writing the stress intensity factor solution in matrix form following the notation used by Marchand *et al.* (1986):

$$K_I = \begin{bmatrix} \frac{\partial K}{\partial N} & \frac{\partial K}{\partial M} \end{bmatrix} \begin{pmatrix} N \\ M \end{pmatrix} \quad (3.28)$$

the energy change, Eq. (3.27), becomes

$$\frac{\partial U}{\partial a} = \frac{1}{E} [N \ M] \begin{bmatrix} \left(\frac{\partial K}{\partial N}\right)^2 & \left(\frac{\partial K}{\partial N}\right)\left(\frac{\partial K}{\partial M}\right) \\ \left(\frac{\partial K}{\partial N}\right)\left(\frac{\partial K}{\partial M}\right) & \left(\frac{\partial K}{\partial M}\right)^2 \end{bmatrix} \begin{pmatrix} N \\ M \end{pmatrix} \quad (3.29)$$

Comparing Eqs. (3.26) and (3.29) gives

$$\begin{pmatrix} \frac{\partial \delta_c}{\partial a} \\ \frac{\partial \theta_c}{\partial a} \end{pmatrix} = \frac{2}{E} \begin{bmatrix} \left(\frac{\partial K}{\partial N}\right)^2 & \left(\frac{\partial K}{\partial N}\right)\left(\frac{\partial K}{\partial M}\right) \\ \left(\frac{\partial K}{\partial N}\right)\left(\frac{\partial K}{\partial M}\right) & \left(\frac{\partial K}{\partial M}\right)^2 \end{bmatrix} \begin{pmatrix} N \\ M \end{pmatrix} \quad (3.30)$$

Integrating with respect to a gives

$$\begin{pmatrix} \delta_c \\ \theta_c \end{pmatrix} = \begin{bmatrix} \int_0^a \frac{2}{E} \left(\frac{\partial K}{\partial N}\right)^2 da & \int_0^a \frac{2}{E} \left(\frac{\partial K}{\partial N}\right)\left(\frac{\partial K}{\partial M}\right) da \\ \int_0^a \frac{2}{E} \left(\frac{\partial K}{\partial N}\right)\left(\frac{\partial K}{\partial M}\right) da & \int_0^a \frac{2}{E} \left(\frac{\partial K}{\partial M}\right)^2 da \end{bmatrix} \begin{pmatrix} N \\ M \end{pmatrix} \quad (3.31)$$

or

$$\begin{pmatrix} \delta_c \\ \theta_c \end{pmatrix} = \begin{bmatrix} C_{11} & C_{12} \\ C_{21} & C_{22} \end{bmatrix} \begin{pmatrix} N \\ M \end{pmatrix} \quad (3.33)$$

From Eq. (3.23) we have

$$\begin{pmatrix} \delta_{total} \\ \theta_{total} \end{pmatrix} = \begin{bmatrix} L/EA & 0 \\ 0 & L/EI \end{bmatrix} \begin{pmatrix} N \\ M \end{pmatrix} + \begin{bmatrix} C_{11} & C_{12} \\ C_{21} & C_{22} \end{bmatrix} \begin{pmatrix} N \\ M \end{pmatrix} \quad (3.34)$$

which gives the total relative displacements.

Stress Intensity Factors

Now, going back to the original problem, the displacement solution for problem I is

$$\begin{pmatrix} \delta_I \\ \theta_I \end{pmatrix} = \begin{bmatrix} C_{11} & C_{12} \\ C_{21} & C_{22} \end{bmatrix} \begin{pmatrix} \sigma W t \\ 0 \end{pmatrix} + \begin{bmatrix} L/EA & 0 \\ 0 & L/EI \end{bmatrix} \begin{pmatrix} \sigma W t \\ 0 \end{pmatrix} - \begin{bmatrix} L/EA & 0 \\ 0 & L/EI \end{bmatrix} \begin{pmatrix} \sigma W t \\ 0 \end{pmatrix} \quad (3.35)$$

and for problem II

$$\begin{pmatrix} \delta_{II} \\ \theta_{II} \end{pmatrix} = - \begin{bmatrix} C_{11} & C_{12} \\ C_{21} & C_{22} \end{bmatrix} \begin{pmatrix} N' \\ M' \end{pmatrix} - \begin{bmatrix} L/EA & 0 \\ 0 & L/EI \end{bmatrix} \begin{pmatrix} N' \\ M' \end{pmatrix} \quad (3.36)$$

Applying the zero displacement boundary conditions gives

$$\begin{bmatrix} C_{11} & C_{12} \\ C_{21} & C_{22} \end{bmatrix} \begin{pmatrix} \sigma W t \\ 0 \end{pmatrix} - \begin{bmatrix} C_{11} & C_{12} \\ C_{21} & C_{22} \end{bmatrix} \begin{pmatrix} N' \\ M' \end{pmatrix} - \begin{bmatrix} L/EA & 0 \\ 0 & L/EI \end{bmatrix} \begin{pmatrix} N' \\ M' \end{pmatrix} = 0 \quad (3.37)$$

For a given geometry alt and L/t , Eq. (3.37) can be solved to obtain N' and M' . Stress intensity factors can then be evaluated as a combination of solutions for problems I and II:

$$K = \frac{\partial K}{\partial N} (\sigma W t - N') + \frac{\partial K}{\partial M} (-M') \quad (3.38)$$

This method was developed by Okamura *et al.* (1975) for edge cracks in beams and provides an efficient way to calculate K for fixed boundary conditions. It has been extended by the author to surface cracks in flat plates, and is discussed in Chapter 5.

3.2.2 Weight Functions for Cracks with Fixed Boundary Conditions

Weight functions for a cracked geometry can be derived from reference stress intensity solutions. If the reference stress intensity factors used in the derivation of these weight functions incorporate fixed boundary conditions, the corresponding weight function will include the effects of the fixed boundary conditions.

Usually, two reference stress intensity factor solutions are required to derive weight functions; one for a uniform load and one for a linearly varying load acting on the crack face. Section 3.2.1 presented a method to calculate the stress intensity factor for uniform loads. Similarly, stress intensity factors for the case of a linearly distributed load applied to the crack face may be solved using the same superposition and compliance analysis technique. Based on these two stress intensity factor solutions, weight functions for the given geometry can be obtained in the standard way, as discussed in Chapter 2.

This method will be used to develop weight functions for semi-elliptical surface cracks under fixed displacement boundary conditions. The development for surface cracks in flat plates will be presented in Chapter 5, and for surface cracks in T-plate joints will be presented in Chapter 6.

Figure 3.1 General two-dimensional crack

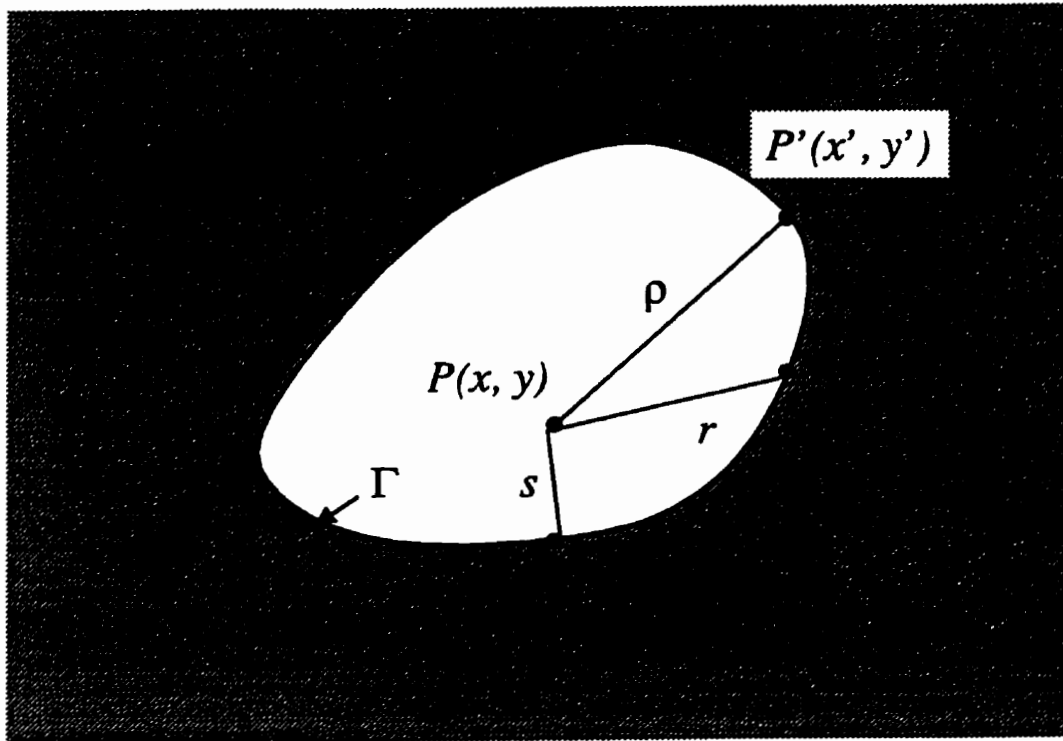


Figure 3.2 Weight functions for (a) half plane crack; (b) circular crack

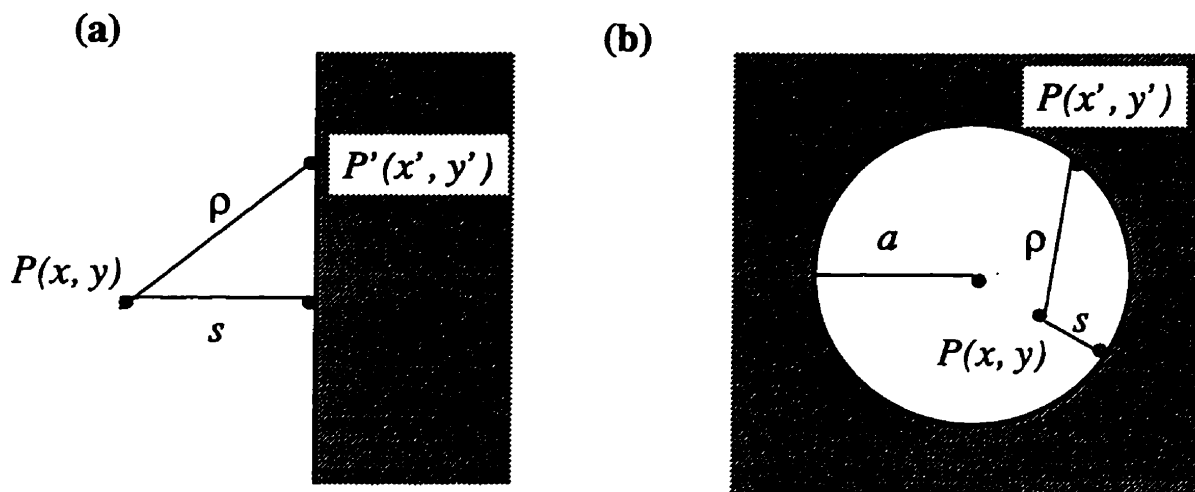


Figure 3.3 Comparison between residual stress field Eq.(3.7) and Fourier approximation Eq. (3.8).

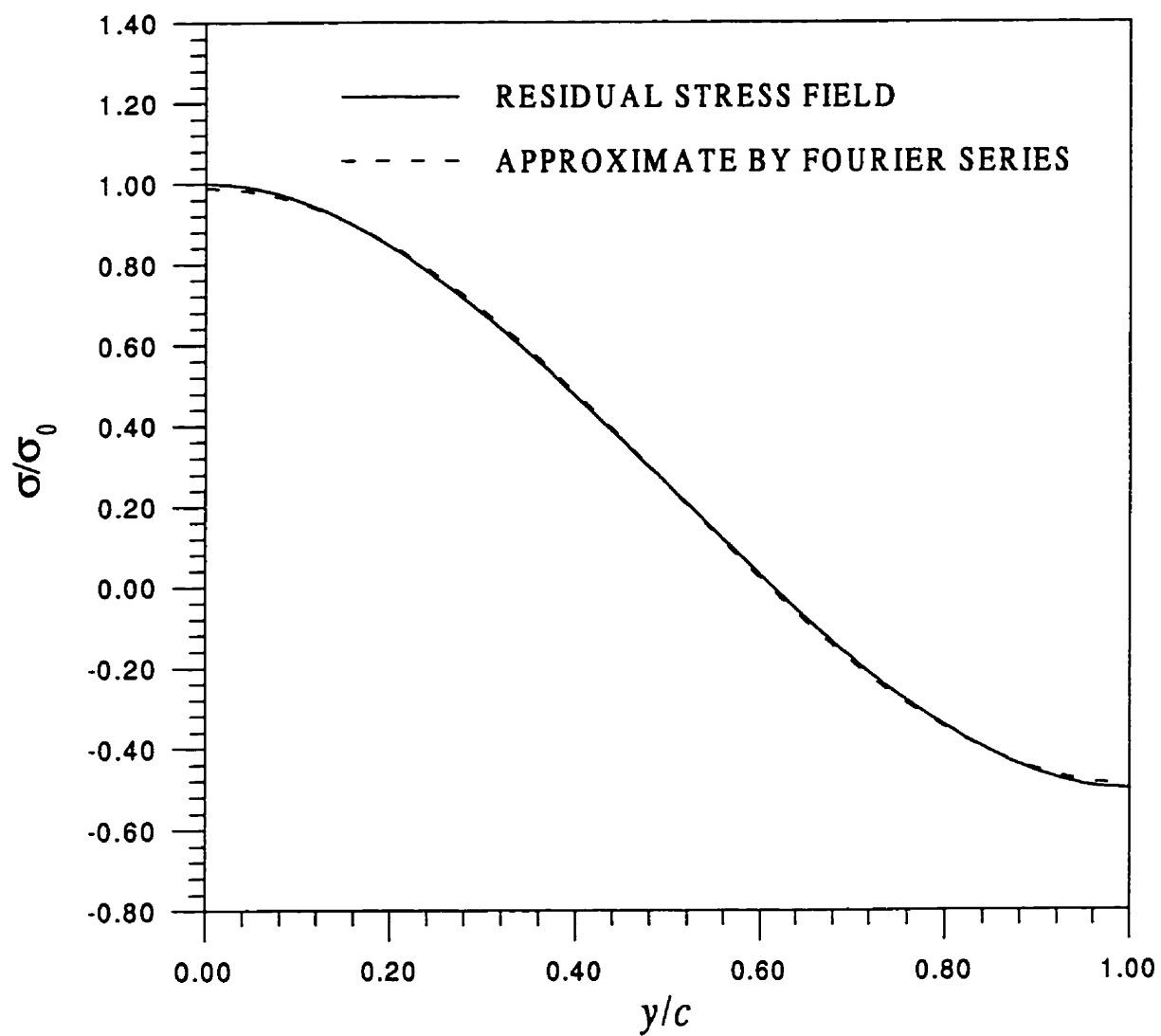


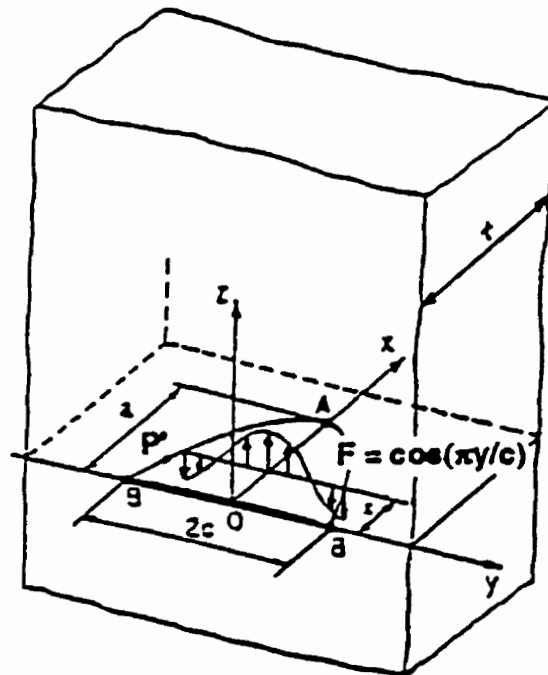
Figure 3.4 Weight Function $M^c_1(x, P')$.

Figure 3.5 Edge crack in flat plate with fixed boundary conditions

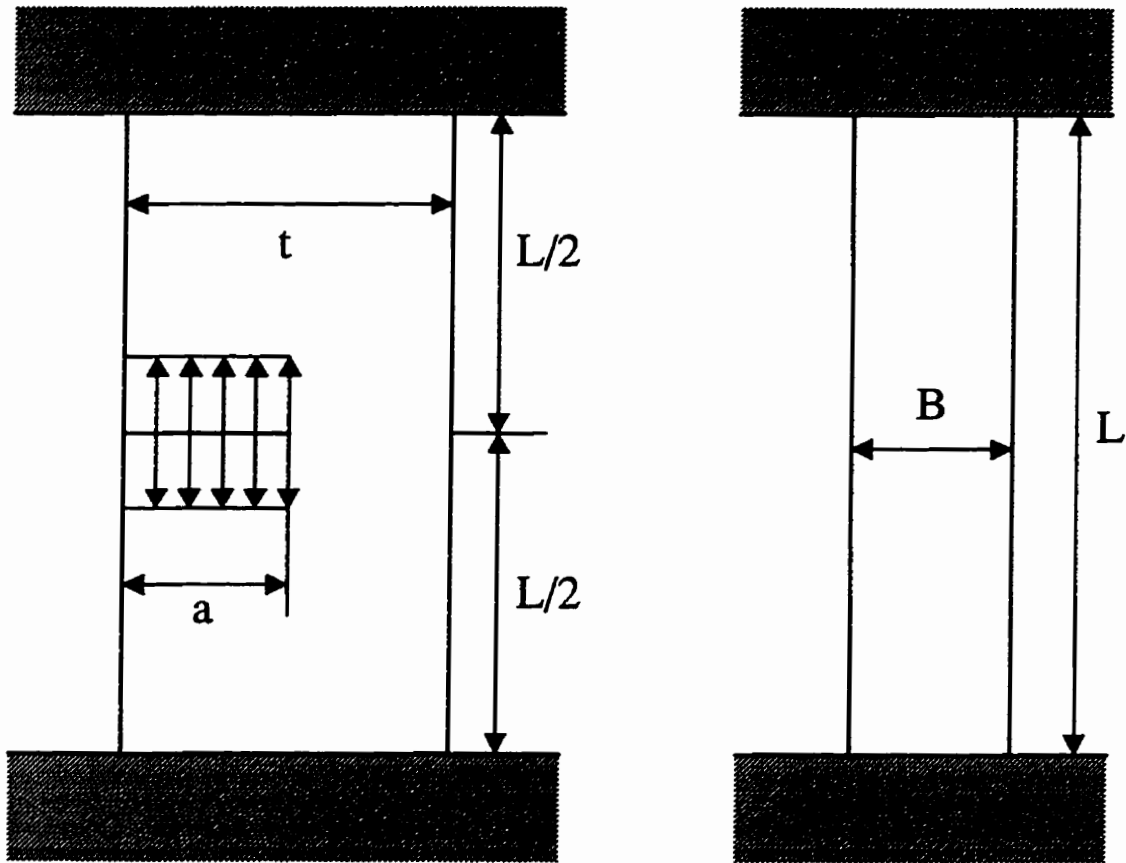


Figure 3.6 Superposition representation

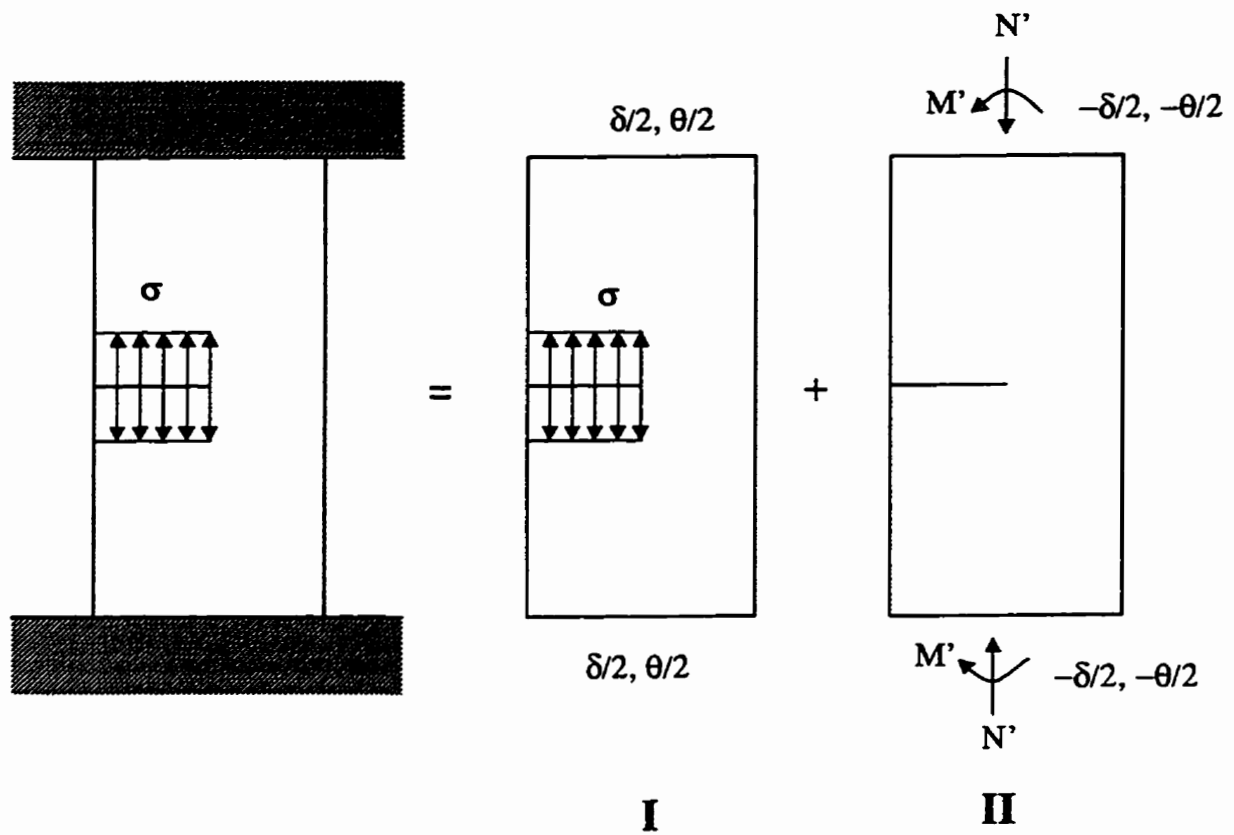


Figure 3.7 Superposition of problem I

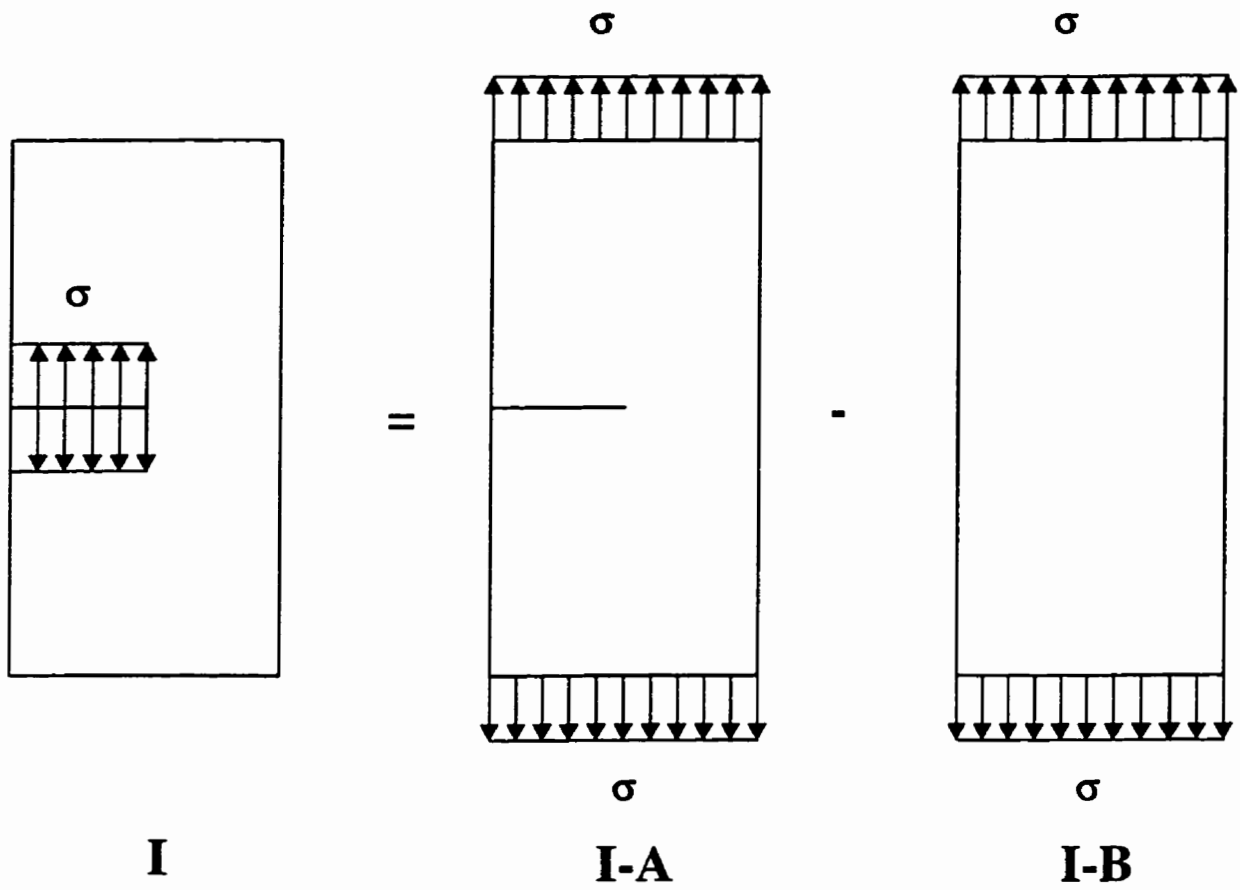


Figure 3.8 General arrangement for the calculation of the end displacements



Chapter 4

Embedded Elliptical Cracks

A problem frequently encountered in applied fracture and fatigue analysis is the estimation of stress intensity factors for elliptical cracks embedded in a thick plate and subjected to a complex stress distribution (Fig. 4.1). This geometry is the simplest since there are no free surface effects on the crack, and therefore is a useful starting point for more complex surface cracks to be discussed later.

When the uncracked stress distribution in the area to be occupied by the elliptical crack is simple, such as uniform uniaxial tension or a one-dimensional linearly varying stress field $\sigma(y)$, then the available explicit solutions of Green and Sneddon (1950), or Kassir and Shih (1967) can be used to determine the stress intensity factors along the crack front. When the stress distribution is two-dimensional, $\sigma(x, y)$, which is the case in many engineering applications, more involved calculations must be made. By applying the potential function method, exact stress intensity factor solutions for polynomial stress distributions up to the order of three were provided by Shah and Kobayashi (1971) and for polynomial stress distributions of any order of n were provided by Vijaykumar and Atluri (1981) and Nishioka and Atluri (1983). For a general stress distribution represented by a

polynomial with N terms, the calculation of stress intensity factor involves the determination of the solution of N linear equations with N unknowns, and the parameters of the linear equations require tedious evaluations of elliptic integrals (Nishioka and Atluri, 1983). In addition, there are stress distributions which cannot be easily represented by polynomials or need a large number of terms.

Another method of determining stress intensity factors due to complex stress distributions is the weight function method. For two-dimensional cracks in an infinite body, exact close-form weight function solutions are available only for very limited cases: the circular crack and the half plane crack (Bueckner, 1987).

In this Chapter, an approximate weight function for embedded elliptical cracks is proposed based on the properties of weight functions discussed in Section 3.1.1. The function makes it possible to calculate stress intensity factors for embedded elliptical cracks under arbitrary 2-D stress distributions by integrating the product of the weight function and the stress distribution on the crack plane.

4.1 Stress Intensity Factors for Embedded Elliptical Cracks

From the three-dimensional theory of elasticity, stress intensity factors for an embedded elliptical crack in an infinite body under polynomial loading can be obtained using the potential function method (Vijayakumar and Atluri, 1981). For an embedded elliptical crack in an infinite body as shown in Figure 4.1, if the pressure distribution can be represented using the following polynomial

$$p(x, y) = \sum_{i=0}^1 \sum_{j=0}^1 \sum_{n=0}^M \sum_{m=0}^m A_{m-n,n}^{(i,j)} x^{2m-2n+i} y^{2n+j} \quad (4.1)$$

where $A_{m,n}^{(i,j)}$ are coefficients and the parameters i and j specify the symmetries of the load with respect to the ellipse, then the corresponding stress intensity factor along the crack front can be written as

$$K(P') = 8\mu \left(\frac{\pi}{ac}\right)^{1/2} (a^2 \sin^2 \theta + c^2 \cos^2 \theta)^{1/4} \sum_{i=0}^1 \sum_{j=0}^1 \sum_{k=0}^M \sum_{l=0}^k (-2)^{2k+i+j} \\ \times (2k+i+j+1) \frac{1}{ac} \left(\frac{\cos \theta}{a}\right)^{2k-2l+i} \left(\frac{\sin \theta}{c}\right)^{2l+j} C_{k-l,l}^{(i,j)} \quad (4.2)$$

where the coefficients $C_{k,l}^{(i,j)}$ depend only on the coefficients $A_{m,n}^{(i,j)}$ as used in Eq. (4.1). The relation between the parameters $A_{m,n}^{(i,j)}$ and the parameters $C_{k,l}^{(i,j)}$ can be summarized in matrix form as

$$\begin{matrix} (N \times 1) & (N \times N) & (N \times 1) \\ \{A\} & = [B] \cdot \{C\} \end{matrix} \quad (4.3)$$

where N is the total number of coefficients $A_{m,n}^{(i,j)}$ or $C_{k,l}^{(i,j)}$ (they have the same number of non-zero members). In addition to the solution of N linear equations with N unknowns, generally the determination of the components of $[B]$ requires “tedious evaluation of elliptical integrals of different kinds and different orders which involves exorbitant, if not unpleasant, algebraic work” (Nishoika and Atluri, 1983). Only for certain very simple loading cases is the application of Eq.(4.2) straight forward.

For the simplest case where an elliptical crack is subjected to a constant applied pressure $p(x, y) = -p_0$, the only non-zero component of $A^{(ij)}_{m,n}$ is $A^{(0,0)}_{0,0} = -p_0$. As a result, the only non-zero component of $C^{(ij)}_{k,l}$ is

$$C_{0,0}^{(0,0)} = \frac{p_0 a c^2}{8\mu E(k)} \quad (4.4)$$

where $E(k)$ is the complete elliptical integral of the second kind and

$$k^2 = 1 - \left(\frac{c}{a}\right)^2 \quad (4.5)$$

The stress intensity factor can then be derived from Eq.(2) as

$$K(P^*) = \frac{\pi^{1/2}}{E(k)} \left(\frac{c}{a}\right)^{1/2} p_0 (a^2 \sin^2 \theta + c^2 \cos^2 \theta)^{1/4} \quad (4.6)$$

which was also derived by Irwin (1962) based on the solution by Green and Snedden (1950).

For the case where a linear varying pressure was applied on the elliptical crack surface, $p(x, y) = -p_0 y/c$, the only non-zero component of $A^{(ij)}_{m,n}$ is $A^{(0,1)}_{0,0} = -p_0$. The only resulting non-zero component of $C^{(ij)}_{k,l}$ is

$$C_{0,0}^{(0,1)} = \frac{p_0 a^3 c^2 k k'^2}{8\mu[(1+k)E(k) - k'^2 K(k)]} \quad (4.7)$$

where $K(k)$ is the complete elliptical integral of the first kind and $k' = c/a$. The stress intensity factor is

$$K(P') = \frac{\pi^{1/2} \sin \theta k^2}{(1+k^2)E(k) - k'^2 K(k)} \left(\frac{c}{a}\right)^{1/2} p_0 (a^2 \sin^2 \theta + c^2 \cos^2 \theta)^{1/4} \quad (4.8)$$

which was also derived by Kassir and Sih (1966). For complex stress distributions, where a high order polynomial must be used, the solutions represented by Eq.(4.2) can be very difficult to obtain and the weight function method should be considered.

4.2 Proposed Weight Function

From Chapter 2, stress intensity factors for any stress field, $\sigma(x, y)$, can be calculated using a two-dimensional weight function $m(x, y; P')$ by Eq. (2.5):

$$K(P') = \iint_S \sigma(x, y) m(x, y; P') dx dy \quad (2.5)$$

In Chapter 3, section, 3.1.1, the following general form for the weight function for an arbitrary planar crack embedded in an infinite body (Fig. 3.1) was presented

$$m(x, y; P') = \frac{\sqrt{2s}}{\pi^{3/2} \rho^2} w(x, y; P') \quad (3.3)$$

where s is the shortest distance between the load point and the boundary of the crack front, and ρ is the distance between the load and the point P' as shown in Fig. 3.1.

It was postulated that the general weight function for embedded elliptical cracks would depend on geometric parameters, ρ_1 to ρ_4 , which are controlled by the shape of the ellipse as shown in Figure 4.2. They are the distances between the point C , where the line representing the shortest distance from load point (x, y) to the crack front intersects the major axis of the ellipse, and those four points on the crack front where the line connecting point C to the point is normal to the tangent of the crack front at that point. In addition, the proposed solution must be consistent with available analytical weight function solutions for limiting cases for elliptical cracks: circular and half-plane cracks.

Several possible functional forms were considered. They following produced the most accurate stress intensity factor results as presented in the next section:

$$m(x, y; P') = \frac{\sqrt{2s}}{\pi^{3/2} \rho^2} \cdot \sqrt{1 - \frac{s}{8\rho_1} - \frac{s}{8\rho_2} - \frac{s}{8\rho_3} - \frac{s}{8\rho_4}} \quad (4.9)$$

In terms of Eq. (3.3), the function $w(x, y; P')$ for embedded elliptical crack is

$$w(x, y; P') = \sqrt{1 - \frac{s}{8\rho_1} - \frac{s}{8\rho_2} - \frac{s}{8\rho_3} - \frac{s}{8\rho_4}} \quad (4.10)$$

The limit of $w(x, y; P')$ when s approaches zero is 1, which is the same as that for circular and half plane cracks.

Note that when $a = c$, the case of a penny shape crack, ρ_1 to ρ_4 all equal a and Eq. (4.9) tends to Eq. (3.2). When a and c go to infinity, which is the case of a half plane crack,

ρ_1 to ρ_4 all go to infinity and Eq. (4.9) tends to Eq (3.1). Thus the proposed equation is consistent with all known relevant analytical weight functions.

4.3 Validation of the Weight Function

In order to calculate stress intensity factors using Eq. (2.5), numerical integration must be conducted. A computer program was developed to perform the integration based on the standard Gauss-Legendre quadrature technique. Instead of using rectangular or triangular elements over the domain of integration (which are not efficient in handling the curved boundaries), curved elements were used.

The analytical weight function for an embedded penny shaped crack represented by Eq. (3.2) was used to verify the integration algorithm. For constant load, the maximum difference between the analytical solution and the calculation based on the present integration routine was less than 0.8% along the whole crack front. For one-dimensional linearly varying load, the maximum difference was less than 1.1%. These results indicate that the integration routine is sufficiently accurate for the integration of weight functions.

To validate the proposed weight function, Eq. (4.9), six different loading cases were applied to the surface of the elliptical crack. Applying Eq. (2.5), stress intensity factors along the crack front of an embedded elliptical crack of aspect ratio $a/c = 0.2, 0.4, 0.6$ and 0.8 were calculated for the following stress fields:

uniform stress field

$$\sigma(x, y) = \sigma_0 \quad (4.11)$$

one-dimensional linear stress field depending on coordinate x

$$\sigma(x, y) = \sigma_0 \frac{x}{a} \quad (4.12)$$

one-dimensional linear stress field depending on coordinate y

$$\sigma(x, y) = \sigma_0 \frac{y}{c} \quad (4.13)$$

Two-dimensional non-linear stress field

$$\sigma(x, y) = \sigma_0 \frac{xy}{ac} \quad (4.14)$$

one-dimensional quadratic stress field depending on coordinate x

$$\sigma(x, y) = \sigma_0 \left(\frac{x}{a}\right)^2 \quad (4.15)$$

and one-dimensional quadratic stress field depending on coordinate y

$$\sigma(x, y) = \sigma_0 \left(\frac{y}{c}\right)^2 \quad (4.16)$$

The resulting stress intensity factors were normalized as follows,

$$F(\phi) = \frac{K(\phi)}{(\sigma_0 \sqrt{\pi a} / E)} \quad (4.17)$$

where F is the boundary correction factor, E is the complete elliptical integral of the second kind and is given by the following empirical equation (Newman and Raju, 1981).

$$E = \sqrt{1.0 + 1.464 \left(\frac{a}{c}\right)^{1.65}} \quad (4.18)$$

The boundary correction factors from the weight function calculations were compared with exact solutions (Shah and Kobayashi, 1967). As shown in Figures 4.3-4.10, the difference between the predictions and the exact solution were generally within 5% for aspect ratios, a/c , of 0.8 or 0.6 and within 10% for aspect ratios, a/c , of 0.4 or 0.2. Therefore, the proposed weight function was validated for embedded elliptical cracks. For low aspect ratio cracks, $a/c = 0.2$, the present weight function gave better accuracy (within 10%) than the O-integral (18%) (Desjardins, 1988).

The proposed weight function can also serve as the foundation for the further development of weight functions for two-dimensional surface cracks, corner cracks and other part-through cracks in engineering structures. However, no further development is contained in the present thesis. The Fourier series approach presented in Chapter 3 was applied to develop weight functions for surface cracks under two-dimensional stress distributions.

Figure 4.1 Notation for an elliptical crack in an infinite solid, (a), (b)

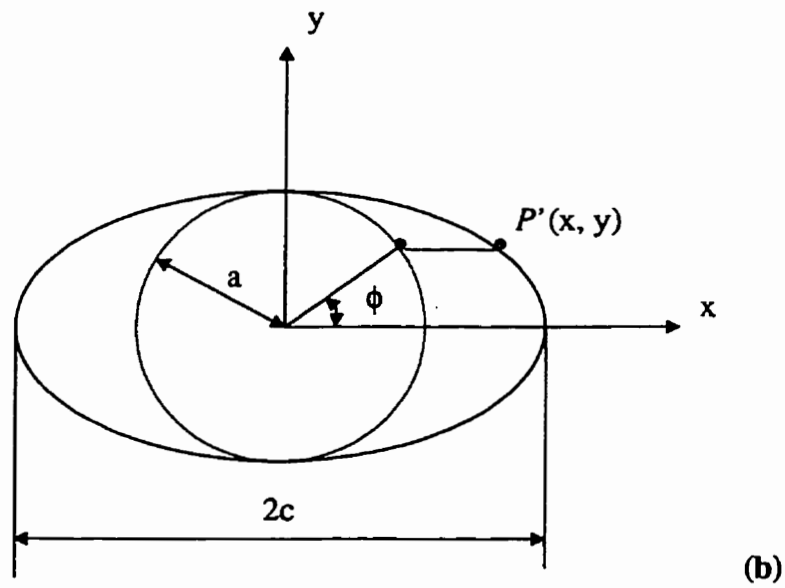
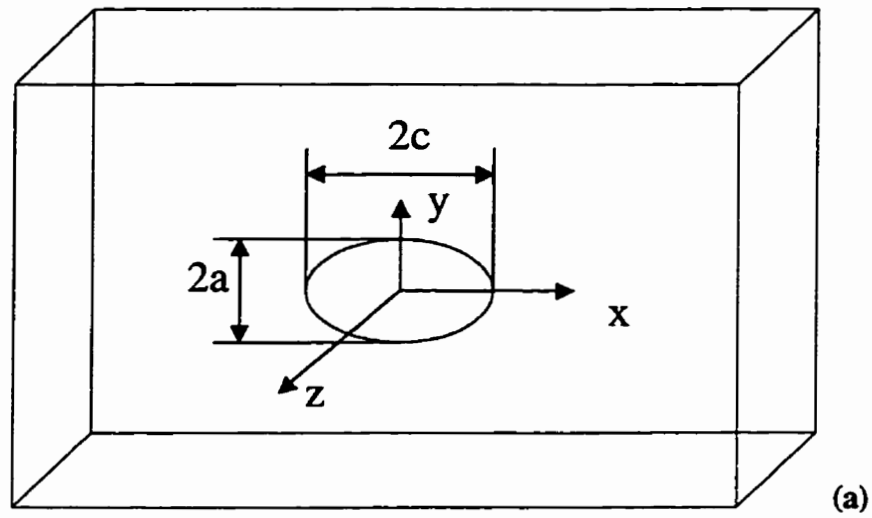


Figure 4.2 Weight function for embedded elliptical crack

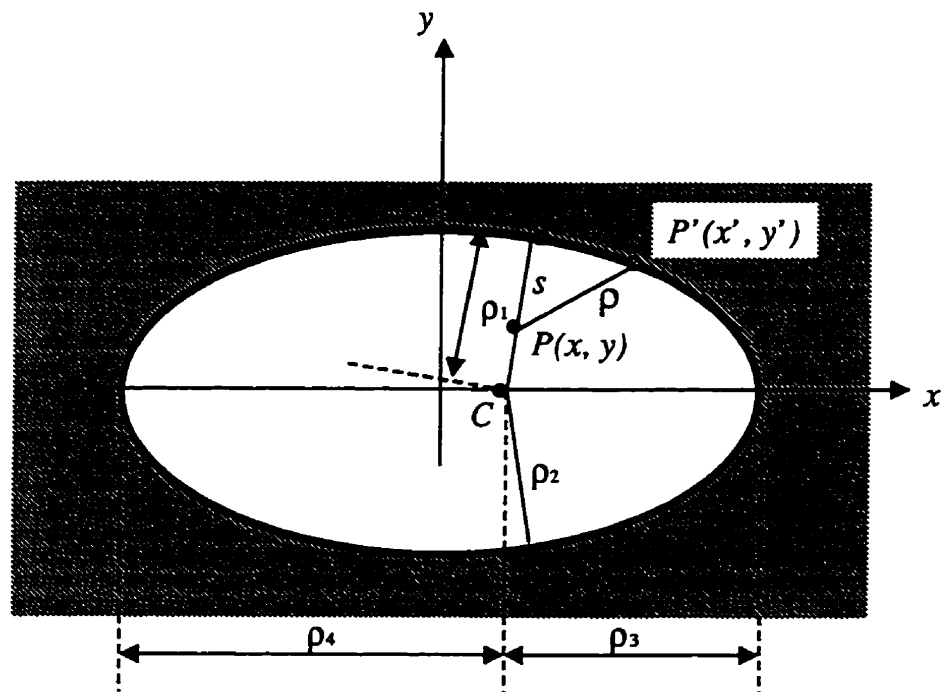


Figure 4.3 Comparison of the weight function based stress intensity factor and exact solution for $a/c = 0.8$ (Uniform and linear stress distributions).

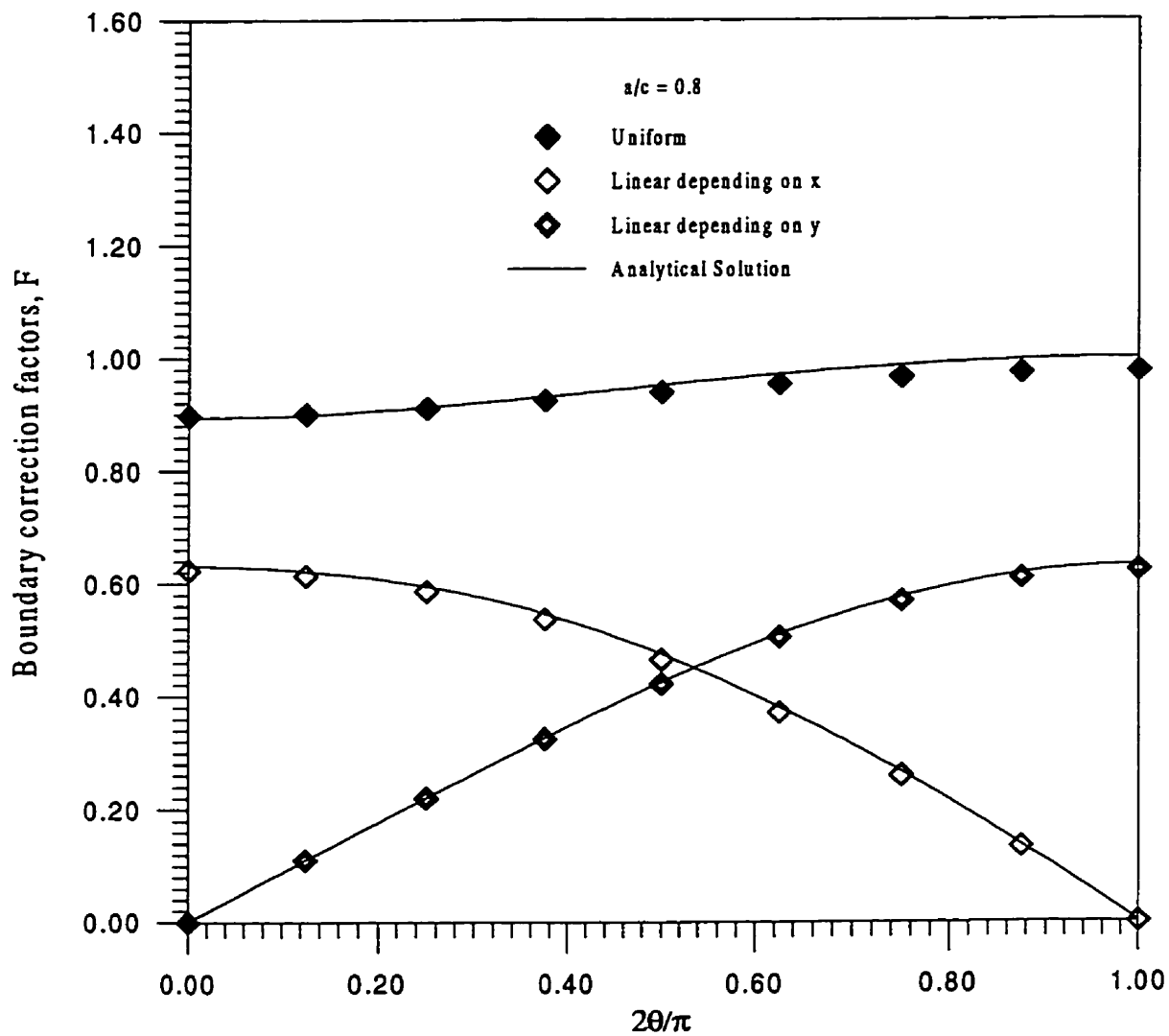


Figure 4.4 Comparison of the weight function based stress intensity factor and exact solution for $a/c = 0.8$ (2D non-linear and parabolic stress distributions).

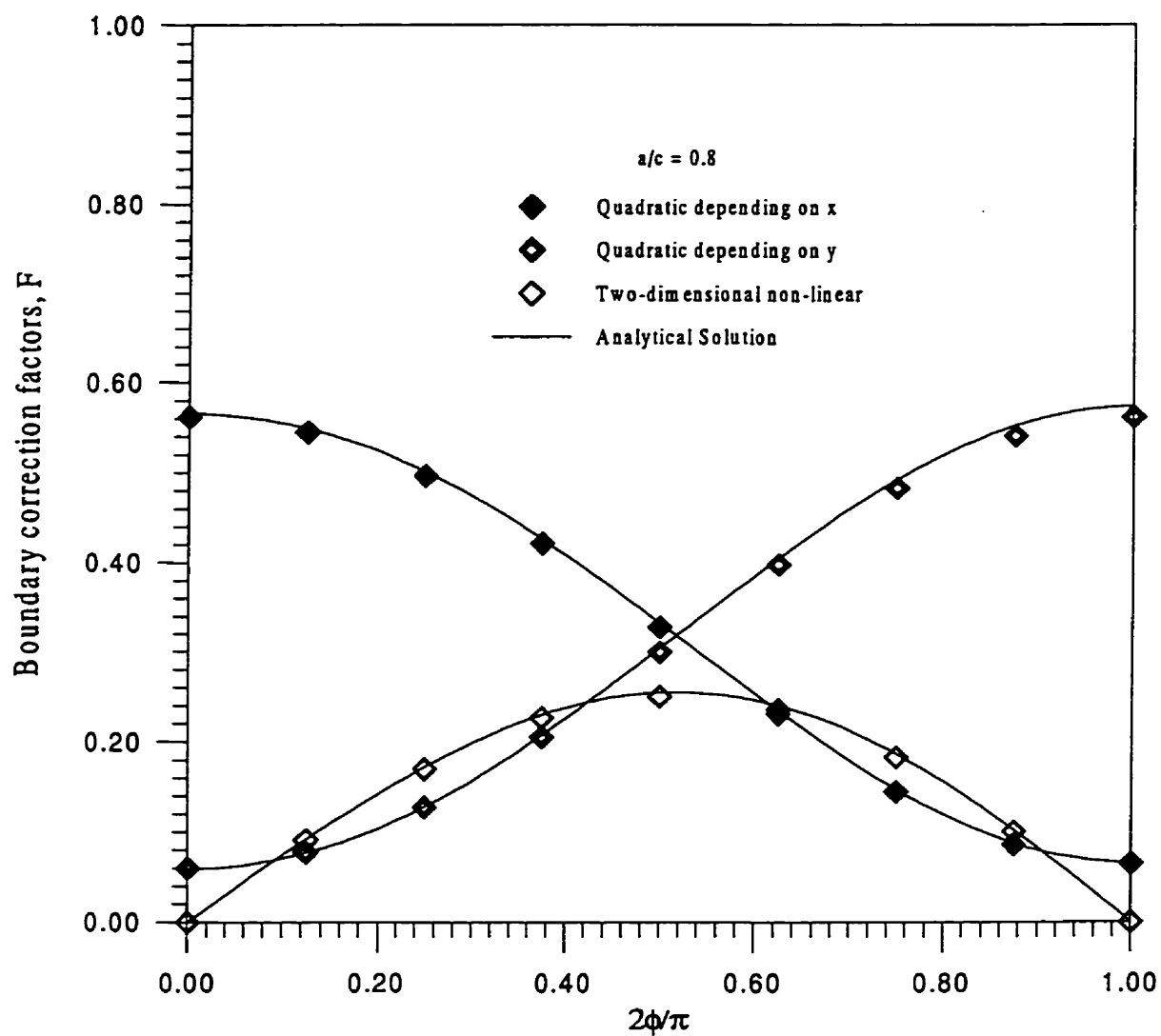


Figure 4.5 Comparison of the weight function based stress intensity factor and exact solution for $a/c = 0.6$ (Uniform and linear stress distributions).

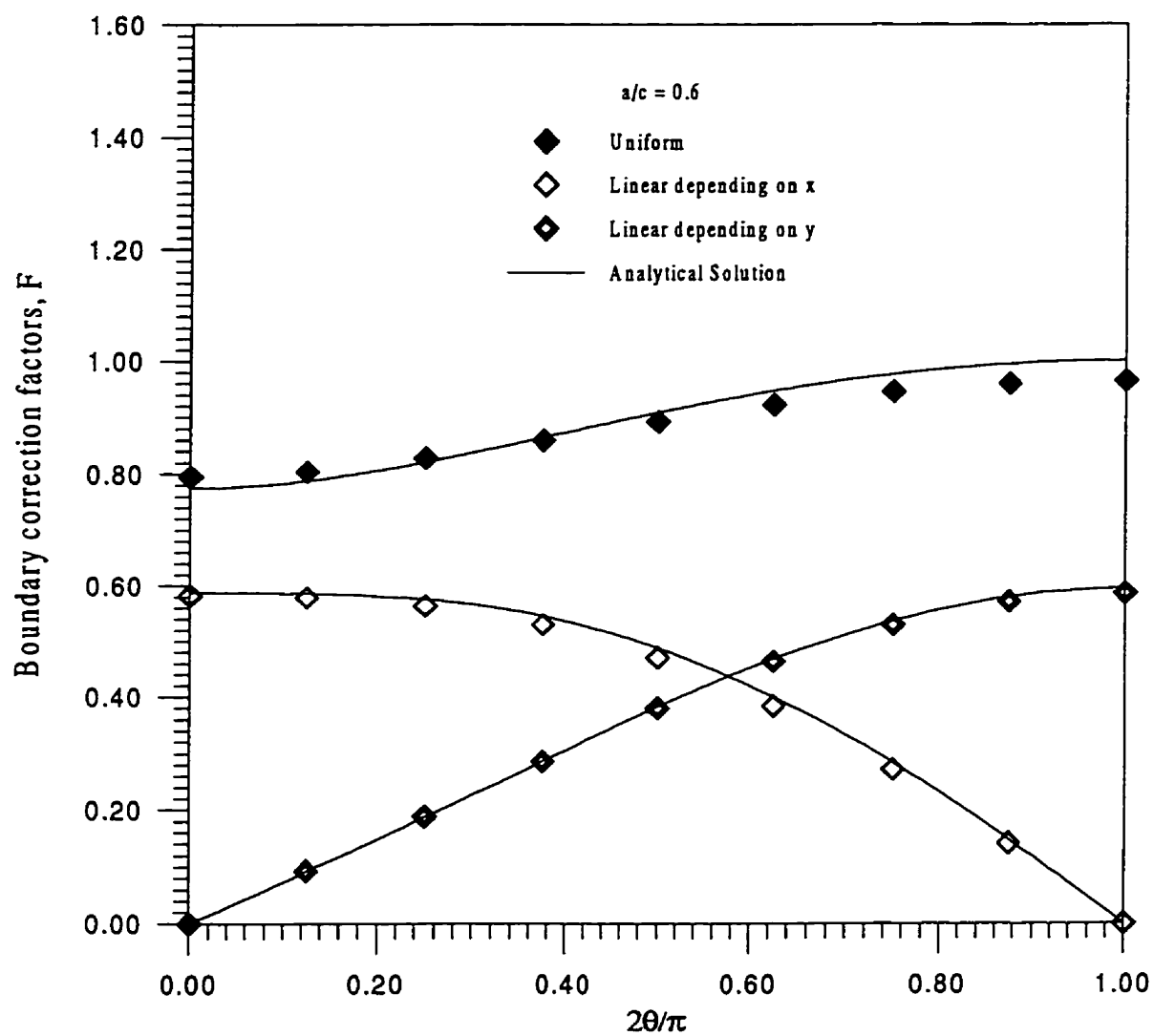


Figure 4.6 Comparison of the weight function based stress intensity factor and exact solution for $a/c = 0.6$ (2D non-linear and parabolic stress distributions).

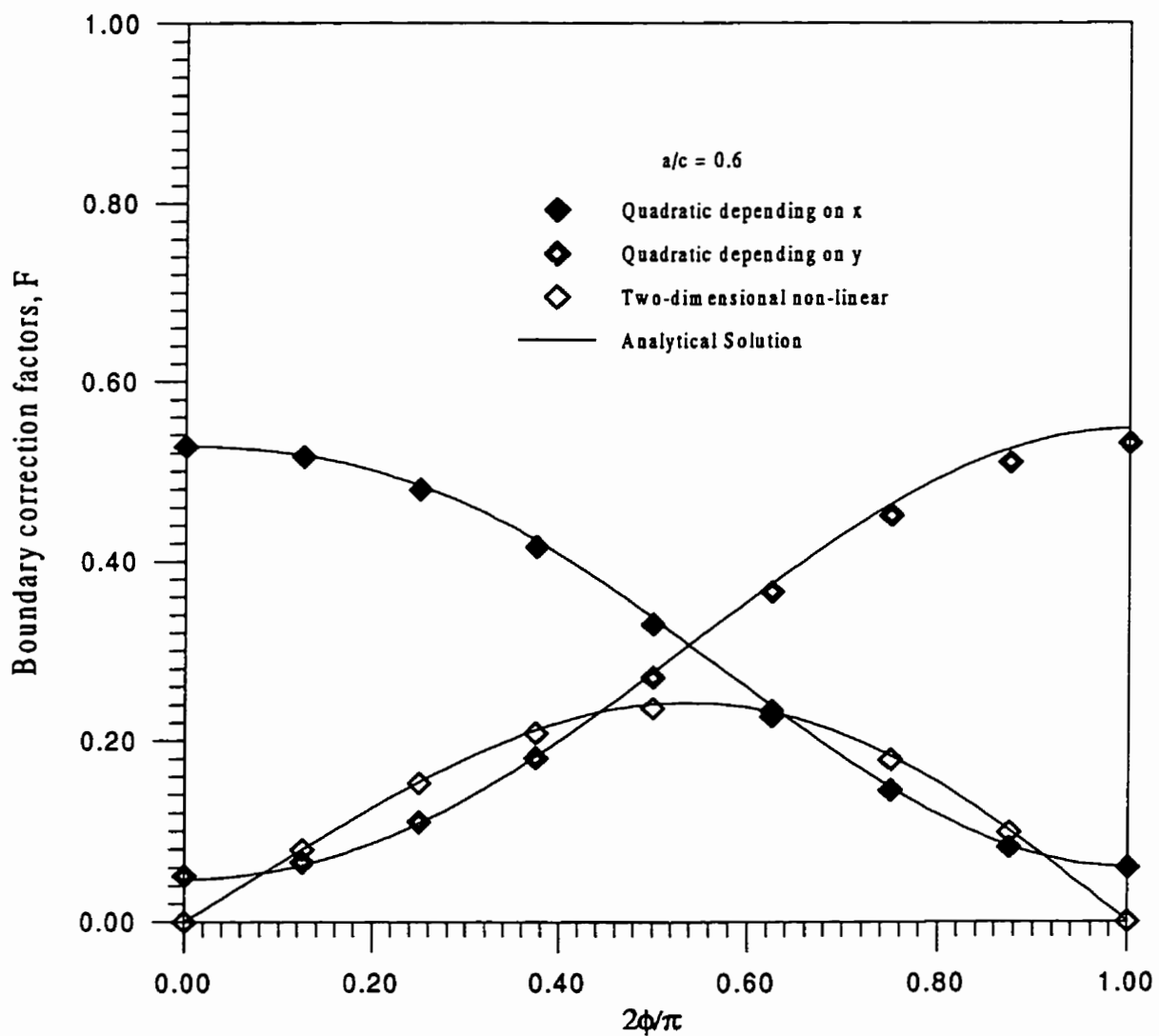


Figure 4.7 Comparison of the weight function based stress intensity factor and exact solution for $a/c = 0.4$ (Uniform and linear stress distributions).

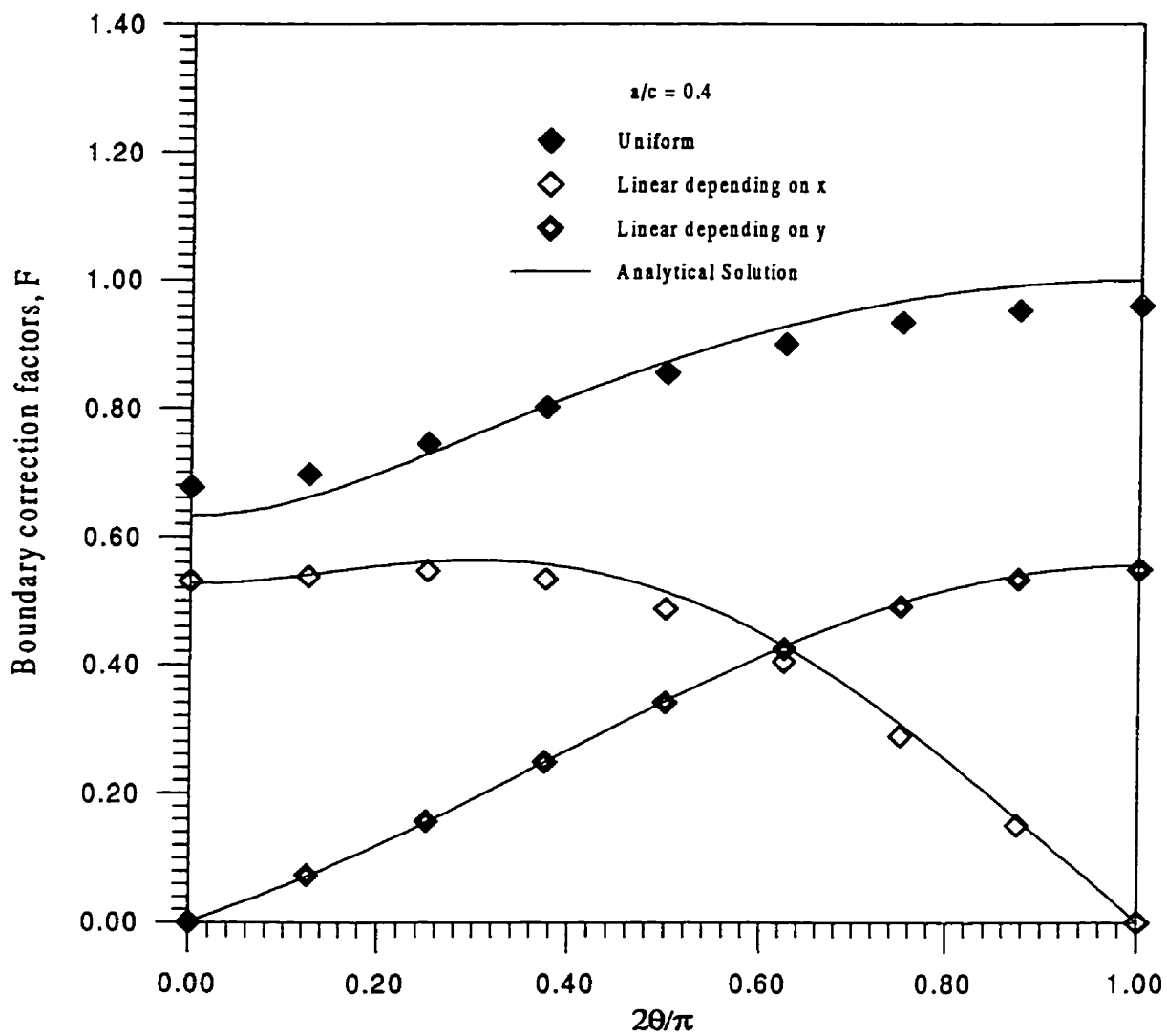


Figure 4.8 Comparison of the weight function based stress intensity factor and exact solution for $a/c = 0.4$ (2D non-linear and parabolic stress distributions).

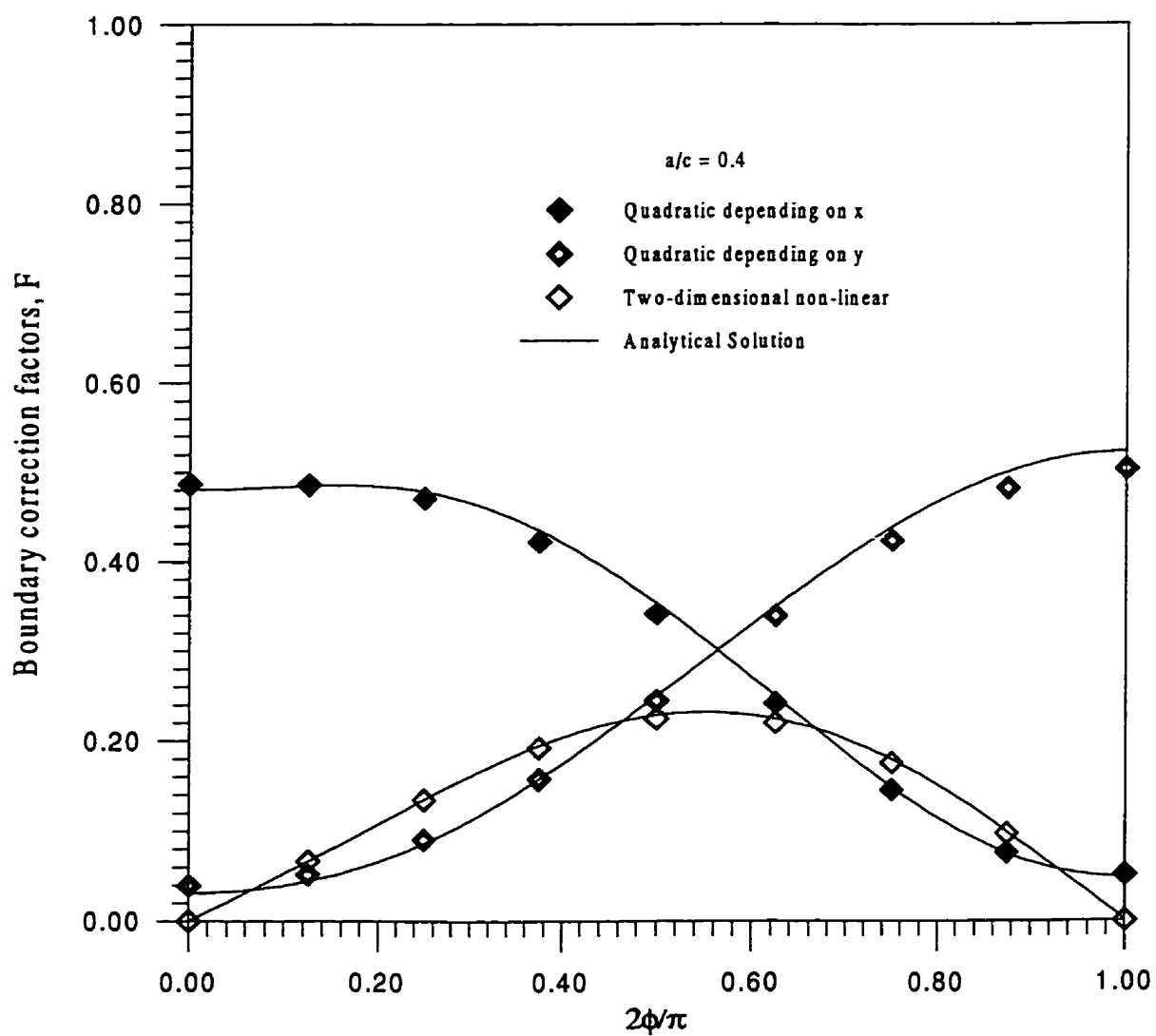


Figure 4.9 Comparison of the weight function based stress intensity factor and exact solution for $a/c = 0.2$ (Uniform and linear stress distributions).

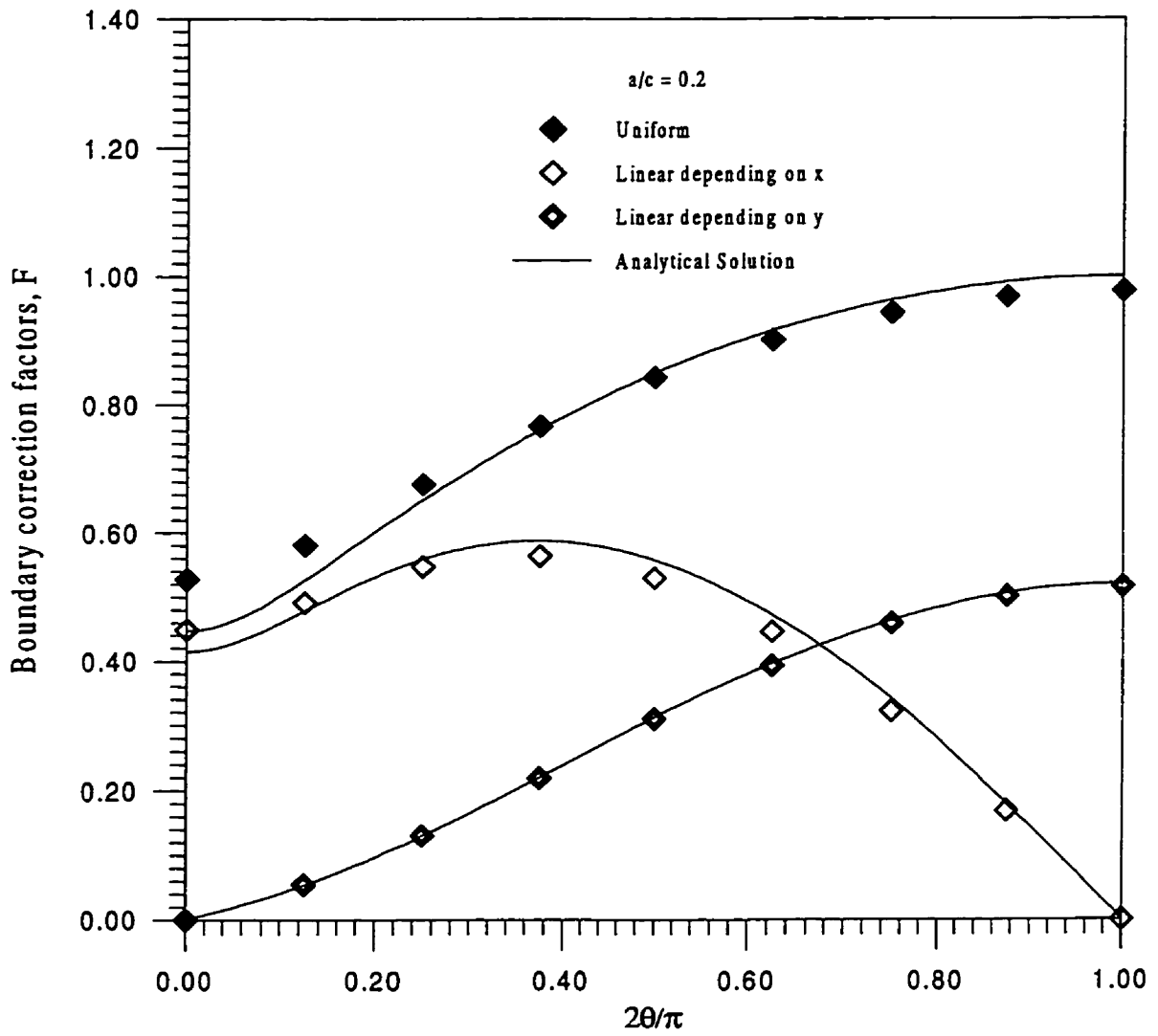
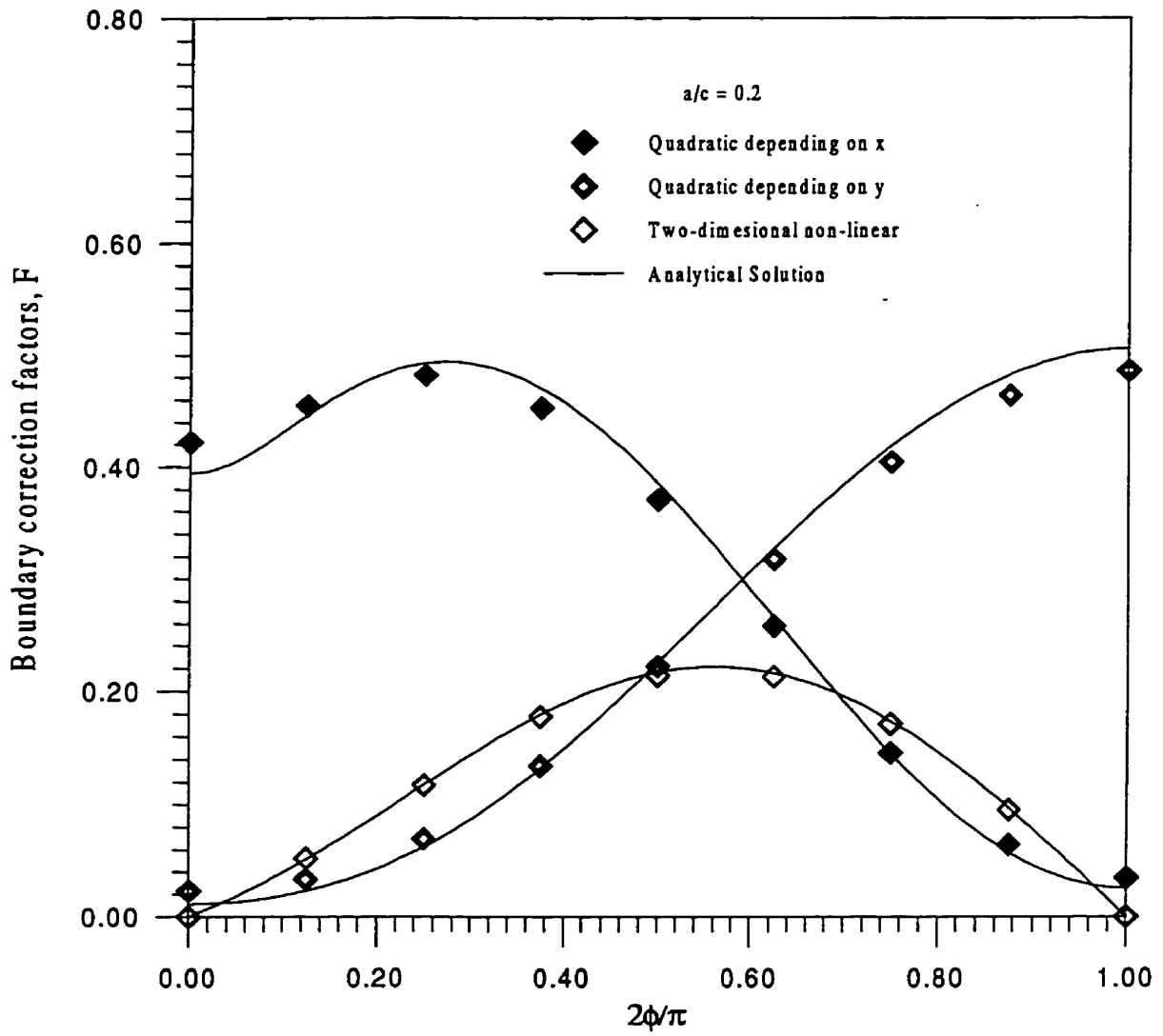


Figure 4.10 Comparison of the weight function based stress intensity factor and exact solution for $a/c = 0.2$ (2D non-linear and parabolic stress distributions).



Chapter 5

Surface Cracks in Flat Plates

In this chapter, stress intensity factors and weight functions for surface cracks in flat plates under two-dimensional stress distributions (section 5.1) or with fixed boundary conditions (section 5.2) are presented.

5.1 Two-Dimensional Stress Distributions

For semi-elliptical surface cracks, stress intensity factors for any two-dimensional stress field, $\sigma(x, y)$, can be calculated using a two-dimensional weight function $m(x, y; P')$ by Eq. (2.5)

$$K(P') = \iint_S \sigma(x, y) m(x, y; P') dx dy \quad (2.5)$$

As discussed in Section 3.1, the direct determination of $m(x, y; P')$ for a surface crack is rather difficult. A Fourier series approach was proposed to avoid this difficulty. For any stress field, $\sigma(x, y)$, in the region S : $0 \leq x \leq a$, and $-c \leq y \leq c$, can be presented using a Fourier series to represent the variation in the y -direction by Eq. (3.9):

$$\sigma(x, y) = a_0(x) + \sum_{n=1}^{\infty} (a_n(x) \cos(\frac{n\pi y}{c}) + b_n(x) \sin(\frac{n\pi y}{c})) \quad (3.9)$$

The stress intensity factor can then be calculated by

$$K(P') = \int_0^a a_0(x) M_0^c(x; P') dx + \sum_{n=1}^{\infty} [\int_0^a a_n(x) M_n^c(x; P') dx + \int_0^a b_n(x) M_n^s(x; P') dx] \quad (3.10)$$

Most two-dimensional stress fields encountered in practice can be represented by a Fourier series of order one:

$$\sigma(x, y) = a_0(x) + a_1(x) \cdot \cos(\frac{\pi y}{c}) + b_1(x) \cdot \sin(\frac{\pi y}{c}) \quad (3.13)$$

The stress intensity factor at the deepest and surface points can be calculated as follows:

at the deepest point

$$K(A) = \int_0^a a_0(x) M(x; A) dx + \int_0^a a_1(x) M_1^c(x; A) dx + \int_0^a b_1(x) M_1^s(x; A) dx \quad (3.14)$$

and at the surface point

$$K(B) = \int_0^a a_0(x)M(x; B)dx + \int_0^a a_1(x)M_1^c(x; B)dx + \int_0^a b_1(x)M_1^s(x; B)dx \quad (3.15)$$

$M_0^c(x; P')$ is actually the one dimensional weight function $M(x; P')$ discussed previously, which is available for surface cracks in flat plates (Wang and Lambert, 1995a, 1995b, 1997). Only $M_1^s(x; P')$ and $M_1^c(x; P')$ remain to be determined.

The weight functions, $M_1^s(x; P')$ and $M_1^c(x; P')$, can be obtained using reference stress intensity factor solutions in the same manner as for $M(x; P')$, as discussed in Section 3.1.2. In this section, weight functions $M_1^s(x; P')$ and $M_1^c(x; P')$ are developed for surface cracks in flat plates.

5.1.1 Stress Intensity Factor Solutions

In order to determine and validate weight functions $M_1^c(x; P')$ and $M_1^s(x; P')$, three dimensional finite element calculations were conducted. The resulting stress intensity factors for two basic loading cases were used as reference solutions to derive the weight functions. These weight functions were then validated using solutions for other loading cases and a set of finite element data by Shiratori (1986).

Three dimensional finite elements were used to model the symmetric quarter of a plate containing a semi-elliptic surface crack. Figure 5.1 shows the geometry and the co-ordinate system used. The finite element analyses were made using ABAQUS version 5.4 (H.K.S., 1994) with 20-noded isoparametric three-dimensional solid elements and reduced integration. In order

to model the square root singularity at the crack tip, three-dimensional prism elements with four mid-side nodes at the quarter points (a degenerate cube with one face collapsed) were used and the separate crack tip nodal points were constrained to have the same displacement (Barsoum, 1977).

The stress intensity factor, K , was calculated from the J -integral which was calculated using the domain integral method (Moran and Shih, 1987). The analyses were made with a linear elastic material model with a Young's modulus, E , of 207 GPa and Poisson's ratio, ν of 0.3. The relationship for plane strain between J and K was used to calculate K

$$K = \sqrt{\frac{J E}{(1 - \nu^2)}} \quad (5.1)$$

except at the surface point of the crack where the relationship for plane stress was used

$$K = \sqrt{J E} \quad (5.2)$$

The loads were applied directly to the crack surface. Eight types of loading were applied to each crack geometry, with the following two-dimensional stress distributions

$$\sigma(x, y) = \sigma_0 \left(1 - \frac{x}{a}\right)^m \cos\left(\frac{\pi y}{c}\right) \quad m = 0, 1, 2, 3 \quad (5.3)$$

and

$$\sigma(x, y) = \sigma_0 \left(1 - \frac{x}{a}\right)^m \sin\left(\frac{\pi y}{c}\right) \quad m = 0, 1, 2, 3 \quad (5.4)$$

where σ_0 is the nominal stress, a is the crack depth and c is the half length.

A mesh generator was developed to generate all required input files for the analysis. An elliptical transformation was used to form the crack tip mesh. Therefore, the lines of elements around the crack tip were elliptic or hyperbolic, so that intersecting lines were orthogonal as required for the evaluation of the stress intensity factors (Banks-Sills, 1991). A typical model for the present analysis used about 15,000 degrees-of-freedom. A typical mesh is plotted in Fig. 5.2.

The stress intensity factor results have been normalised as follows,

$$F = \frac{K}{\sigma_0 \sqrt{\pi a} / Q} \quad (5.5)$$

where F is the boundary correction factor, and Q is the shape factor of an ellipse given by the square of the complete elliptic integral of second kind. The following empirical equation for Q was used, for $0 \leq a/c \leq 1.0$:

$$Q = 1.0 + 1.464 \left(\frac{a}{c}\right)^{1.65} \quad (5.6)$$

Note that the $r^{-1/2}$ singularity vanishes at the intersection of three free surfaces (Sih and Lee, 1989) such as the surface point of the crack. That is, the $r^{-1/2}$ singularity occurs only near crack front points embedded entirely in the material. However, as shown by Sih and Lee (1989), for engineering materials with a Poisson ratio, $\nu = 0.3$, the dominant singularity near the surface point of a surface crack was $r^{-0.4523}$, which in practical terms does not represent a dramatic departure from the $r^{-1/2}$ singularity. Also, in the present calculation, the domain integral method was used to evaluate stress intensity factors. Therefore the stress intensity factor calculated for the surface point was in fact an average value over the element size. The stress intensity factor for the surface point of the surface crack should be considered a reasonable physical approximation of the state of affairs at the surface.

In previous work (Wang and Lambert, 1995), the finite element model was extensively verified with exact solutions (by calculating the stress intensity factors for embedded circular and elliptical cracks in an infinite body under tension), and with approximate solutions (by calculating the stress intensity factors for semi-elliptical surface cracks with non-linear loads applied to the crack surface). Based on this, the accuracy of the present finite element calculation is expected to be within a few (5%) percent of the actual solutions.

Stress intensity factors for semi-elliptical surface cracks ($a/c = 0.1, 0.2, 0.4, 0.6$ or 1.0) in a finite thickness plate with relative crack depths, a/t , of $0.2, 0.4, 0.6$ or 0.8 subjected to two-dimensional stress distributions as expressed in Eqs. (5.3) and (5.4) were determined. The results are summarised in Tables 5.1(a)-5.1(e) and Tables 5.2(a)-5.2(e).

5.1.2 Derivation of Weight Functions

Determination of Weight Functions $M^c_I(x; A)$ and $M^c_I(x; B)$

As described in section 3.1.2, weight functions $M^c_I(x; A)$ and $M^c_I(x; B)$ can be derived in the form of Eqs.(3.16) and (3.17).

$$M^c_I(x, a; A) = \frac{1}{\sqrt{2\pi(a-x)}} \left[1 + M^c_{1A} \left(1 - \frac{x}{a}\right)^{\frac{1}{2}} + M^c_{2A} \left(1 - \frac{x}{a}\right) + M^c_{3A} \left(1 - \frac{x}{a}\right)^{\frac{3}{2}} \right] \quad (3.16)$$

$$M^c_I(x, a; B) = \frac{-2}{\sqrt{\pi x}} \left[1 + M^c_{1B} \left(\frac{x}{a}\right)^{\frac{1}{2}} + M^c_{2B} \left(\frac{x}{a}\right) + M^c_{3B} \left(\frac{x}{a}\right)^{\frac{3}{2}} \right] \quad (3.17)$$

The parameters were determined from two reference stress intensity factors and the conditions represented by Eqs.(3.18) and (3.19).

$$M^c_{2A} = 3 \quad (3.18)$$

$$1 + M^c_{1B} + M^c_{2B} + M^c_{3B} = 0 \quad (3.19)$$

The weight function at the deepest point $M^c_I(x; A)$

In order to determine $M^c_I(x; A)$ using Eq.(3.16), two reference solutions were used to evaluate M^c_{1A} , M^c_{2A} and M^c_{3A} : constant or linearly decreasing stress through thickness while varying as $\cos(\pi y/c)$ along the width, corresponding to $m = 0$ or $m = 1$ in Eq. (5.3). When

expanded into a Fourier series in the y -direction, the non-zero Fourier constants for these two stress fields are $a_1(x) = \sigma_0$, and $a_1(x) = \sigma_0(1 - x/a)$, respectively.

Reference stress intensity factors. For the deepest point of a surface crack, the numerical solutions for $a/c = 0.1, 0.2, 0.4, 0.6$ or 1.0 presented previously (Table 5.1) were approximated by empirical formulas fitted with an accuracy of 3% or better. The range of applicability for these equations is $0.1 \leq a/c \leq 1.0$ and $0 \leq a/t \leq 0.8$. The results as a/t approached zero were interpolated from finite element data.

The results for a stress distribution constant through the thickness while varying as $\cos(\pi y/c)$ in the width direction

$$\sigma(x, y) = \sigma_0 \cos\left(\frac{\pi y}{c}\right) \quad (5.7)$$

are

$$K_{Ir}^A = \sigma_0 \sqrt{\frac{\pi a}{Q}} Y_0 \quad (5.8)$$

where

$$Y_0 = B_0 + B_1\left(\frac{a}{t}\right)^2 + B_2\left(\frac{a}{t}\right)^4$$

$$B_0 = 1.0488 - 0.6994\left(\frac{a}{c}\right) + 0.3985\left(\frac{a}{c}\right)^2$$

$$B_1 = -1.2626 - 0.3042\left(\frac{a}{c}\right) + 0.5850\left(\frac{a}{c}\right)^2 + \frac{1.0}{\left(0.01134 + \frac{a}{c}\right)^{0.5375}}$$

$$B_2 = -1.3984 + 4.2159\left(\frac{a}{c}\right) - 2.7520\left(\frac{a}{c}\right)^2$$

The results for a stress distribution linearly decreasing through the thickness while varying as $\cos(\pi y/c)$ in the width direction

$$\sigma(x, y) = \sigma_0 \left(1 - \frac{x}{a}\right) \cos\left(\frac{\pi y}{c}\right) \quad (5.9)$$

are

$$K_{2r}^A = \sigma_0 \sqrt{\frac{\pi a}{Q}} Y_1 \quad (5.10)$$

where

$$Y_1 = A_0 + A_1\left(\frac{a}{t}\right)^2 + A_2\left(\frac{a}{t}\right)^4$$

$$A_0 = 0.4297 - 0.4977\left(\frac{a}{c}\right) + 0.2368\left(\frac{a}{c}\right)^2$$

$$A_1 = -1.232 - 0.1897\left(\frac{a}{c}\right) + 0.4603\left(\frac{a}{c}\right)^2 + \frac{1.0}{\left(-0.007422 + \frac{a}{c}\right)^{0.3880}}$$

$$A_2 = -1.0565 + 2.9244\left(\frac{a}{c}\right) - 1.9589\left(\frac{a}{c}\right)^2$$

Weight function. By substituting Eqs. (5.8), (5.10), and the corresponding Fourier constants into Eq. (3.14) plus the condition represented by Eq. (3.18), three equations with three unknowns were established. The parameters in the weight function expressions were solved for and are

$$M_{1A}^c = \frac{\sqrt{2\pi}}{\sqrt{Q}}(4Y_0 - 6Y_1) - \frac{24}{5} \quad (5.11)$$

$$M_{2A}^c = 3 \quad (5.12)$$

$$M_{3A}^c = 2\left(\frac{\sqrt{2\pi}}{\sqrt{Q}}Y_0 - M_{1A} - 4\right) \quad (5.13)$$

The weight function for the deepest point of a semi-elliptic surface crack can then be determined directly from Eq. (3.16).

The weight function for the surface point $M_I^c(x; B)$

The two reference stress intensity factor solutions used to determine weight function $M_I^c(x; B)$, in the form of Eq. (3.17), were constant or linearly decreasing stress fields through the thickness while varying as $\cos(\pi y/c)$ in the width direction; these are the same stress fields used for the determination of $M_I^c(x; A)$.

Reference Stress Intensity Factors. For the surface point of the surface crack, the finite element results presented previously (Table 5.1) for surface cracks ($a/c = 0.1, 0.2, 0.4, 0.6$ or 1.0) were approximated as follows, with an accuracy of 3% or better. The range of applicability for these equations is $0.1 \leq a/c \leq 1.0$ and $0 \leq a/t \leq 0.8$.

The results for a stress distribution constant through the thickness while varying as $\cos(\pi y/c)$ in the width direction

$$\sigma(x, y) = \sigma_0 \cos\left(\frac{\pi y}{c}\right) \quad (5.14)$$

are

$$K_{Ir}^B = \sigma_0 \sqrt{\frac{\pi a}{Q}} F_0 \quad (5.15)$$

where

$$F_0 = \frac{C_0 + C_1}{C_2 + C_3}$$

$$C_0 = -0.5061 - 0.1557\left(\frac{a}{t}\right) + 0.1127\left(\frac{a}{t}\right)^2$$

$$C_1 = -0.7517\left[\ln\left(\frac{a}{c}\right)\right] - 0.5450\left[\ln\left(\frac{a}{c}\right)\right]^2 - 0.1145\left[\ln\left(\frac{a}{c}\right)\right]^3$$

$$C_2 = 1.0 + 0.2928\left(\frac{a}{t}\right)$$

$$C_3 = 1.506\left[\ln\left(\frac{a}{c}\right)\right] + 1.069\left[\ln\left(\frac{a}{c}\right)\right]^2 + 0.2025\left[\ln\left(\frac{a}{c}\right)\right]^3$$

The results for a stress distribution linearly decreasing through the thickness while varying as $\cos(\pi y/c)$ in the width direction

$$\sigma(x, y) = \sigma_0 \left(1 - \frac{x}{a}\right) \cos\left(\frac{\pi y}{c}\right) \quad (5.16)$$

are

$$K_{2r}^B = \sigma_0 \sqrt{\frac{\pi a}{Q}} F_1 \quad (5.17)$$

where

$$F_1 = \frac{D_0 + D_1}{D_2 + D_3}$$

$$D_0 = -0.5040 - 0.1749\left(\frac{a}{t}\right) + 0.04722\left(\frac{a}{t}\right)^2$$

$$D_1 = -0.8456\left[\ln\left(\frac{a}{c}\right)\right] - 0.5473\left[\ln\left(\frac{a}{c}\right)\right]^2 - 0.09502\left[\ln\left(\frac{a}{c}\right)\right]^3$$

$$D_2 = 1.0 + 0.3775\left(\frac{a}{t}\right)$$

$$D_3 = 1.6307\left[\ln\left(\frac{a}{c}\right)\right] + 0.9936\left[\ln\left(\frac{a}{c}\right)\right]^2 + 0.1353\left[\ln\left(\frac{a}{c}\right)\right]^3$$

Weight Function. By substituting Eqs. (5.15), (5.17), and the corresponding Fourier constants into Eq. (3.15), and applying the condition represented by Eq. (3.19), three equations with three unknowns were established. The weight function parameters for the surface point were solved for and are

$$M_{1B}^c = -\frac{\pi}{2\sqrt{Q}}(30 F_1 - 18 F_0) - 8 \quad (5.18)$$

$$M_{2B}^c = -\frac{\pi}{2\sqrt{Q}}(60 F_0 - 90 F_1) + 15 \quad (5.19)$$

$$M_{3B}^c = - (1 + M_{1B} + M_{2B}) \quad (5.20)$$

The weight function for the surface point can then be determined directly from Eq. (3.17).

Determination of Weight Functions $M_{1B}^s(x; A)$ and $M_{1B}^s(x; B)$

As discussed previously, weight function $M_{1B}^s(x; A)$ is always zero. The determination of $M_{1B}^s(x; B)$ is based on the form of Eq.(3.21) and the condition represented by Eq.(3.22):

$$M_{1B}^s(x, a; B) = \frac{\sqrt{2}}{\sqrt{\pi x}} \left[1 + M_{1B}^s \left(\frac{x}{a} \right)^{\frac{1}{2}} + M_{2B}^s \left(\frac{x}{a} \right) + M_{3B}^s \left(\frac{x}{a} \right)^{\frac{3}{2}} \right] \quad (3.21)$$

$$1 + M_{1B}^s + M_{2B}^s + M_{3B}^s = 0 \quad (3.22)$$

The weight function for the surface point $M_{1B}^s(x; B)$

The two reference stress intensity factor solutions used to determine weight function $M_{1B}^s(x; B)$ for the surface point of a semi-elliptic crack in the form of Eq. (3.21) were stress fields which were constant or linearly decreasing through the thickness while varying as $\sin(\pi y/c)$ in the width direction, corresponding to $m = 0$ or $m = 1$ in Eq. (5.4). When expanded into a Fourier series in the y -direction, the non-zero Fourier constants for these two stress fields are $b_1(x) = \sigma_0$, and $b_1(x) = \sigma_0(1 - x/a)$, respectively

Reference Stress Intensity Factors. For the surface point of a surface crack, the finite element results presented previously (Table 5.2) for surface cracks ($a/c = 0.1, 0.2, 0.4, 0.6$ or 1.0) were approximated as follows, with an accuracy of 2% or better. The range of applicability for these equations is $0.1 \leq a/c \leq 1.0$ and $0 \leq a/t \leq 0.8$.

The results for a stress distribution constant through the thickness while varying as $\sin(\pi y/c)$ in the width direction

$$\sigma(x, y) = \sigma_0 \sin\left(\frac{\pi y}{c}\right) \quad (5.21)$$

are

$$K_{I,r}^B = \sigma_0 \sqrt{\frac{\pi a}{Q}} F_0 \quad (5.22)$$

where

$$F_0 = C_0 + C_1\left(\frac{a}{t}\right)^2 + C_2\left(\frac{a}{t}\right)^4$$

$$C_0 = -0.03269 - 0.7112\left(\frac{a}{c}\right) - 0.2526\left(\frac{a}{c}\right)^2$$

$$C_1 = 0.28875 - 0.3987\left(\frac{a}{c}\right) + 0.08353\left(\frac{a}{c}\right)^2$$

$$C_2 = -0.01265 + 1.582\left(\frac{a}{c}\right) - 0.4132\left(\frac{a}{c}\right)^2 + 2.5667\left(\frac{a}{c}\right)^3$$

The results for a stress distribution linearly decreasing through the thickness while varying as $\sin(\pi y/c)$ in the width direction

$$\sigma(x, y) = \sigma_0 \left(1 - \frac{x}{a}\right) \sin\left(\frac{\pi y}{c}\right) \quad (5.23)$$

are

$$K_{2r}^B = \sigma_0 \sqrt{\frac{\pi a}{Q}} F_1 \quad (5.24)$$

where

$$F_1 = D_0 + D_1\left(\frac{a}{t}\right)^2 + D_2\left(\frac{a}{t}\right)^4$$

$$D_0 = -0.02135 + 0.5267\left(\frac{a}{c}\right) - 0.1481\left(\frac{a}{c}\right)^2$$

$$D_1 = 0.1954 - 0.2617\left(\frac{a}{c}\right) + 0.03613\left(\frac{a}{c}\right)^2$$

$$D_2 = 0.00978 - 1.0629\left(\frac{a}{c}\right) - 2.9257\left(\frac{a}{c}\right)^2 + 1.8114\left(\frac{a}{c}\right)^3$$

Weight Function. By substituting Eqs. (5.22), (5.24) and the corresponding Fourier constants into Eq. (14), and applying the condition represented by Eq. (3.22), three equations with three unknowns were established. The weight function parameters were solved for and are

$$M_{1B}^s = \frac{\sqrt{2\pi}}{\sqrt{Q}}(30 F_1 - 18 F_0) - 8 \quad (5.25)$$

$$M_{2B}^s = \frac{\sqrt{2\pi}}{\sqrt{Q}}(60 F_0 - 90 F_1) + 15 \quad (5.26)$$

$$M_{3B}^s = - (1 + M_{1B} + M_{2B}) \quad (5.27)$$

The weight function for the surface point can then be determined directly from Eq. (3.21).

5.1.3 Validation of Derived Weight Functions

Comparison with present FEM data The weight functions for the deepest and surface points derived were validated using finite element results for four two-dimensional non-linear stress fields. Using Eqs. (3.14) and (3.15), stress intensity factors were calculated for the following stress fields:

$$\sigma(x, y) = \sigma_0 \left(1 - \frac{x}{a}\right)^2 \cos\left(\frac{\pi y}{c}\right) \quad (5.28)$$

$$\sigma(x, y) = \sigma_0 \left(1 - \frac{x}{a}\right)^3 \cos\left(\frac{\pi y}{c}\right) \quad (5.29)$$

$$\sigma(x, y) = \sigma_0 \left(1 - \frac{x}{a}\right)^2 \sin\left(\frac{\pi y}{c}\right) \quad (5.30)$$

and

$$\sigma(x, y) = \sigma_0 \left(1 - \frac{x}{a}\right)^3 \sin\left(\frac{\pi y}{c}\right) \quad (5.31)$$

The corresponding non-zero Fourier constants for the above four stress distributions are $a_1(x) = \sigma_0(1 - x/a)^2$, $a_1(x) = \sigma_0(1 - x/a)^3$, $b_1(x) = \sigma_0(1 - x/a)^2$ and $b_1(x) = \sigma_0(1 - x/a)^3$, respectively. The stress intensity factors for the deepest and surface points calculated from weight functions and from the present finite element calculations for the above stress distribution are shown in Figs. 5.3 to 5.8. For the a/c range from 0.1 to 1 and $0 \leq a/t \leq 0.8$, the differences between the

boundary correction factors calculated from the weight function and the finite elements results were less than 4% for the surface point and 6% for the deepest point. Note that for these cases, the boundary correction factors span at least two orders of magnitude. Consequently, the 'percentage difference' was obtained by dividing the absolute difference by the maximum absolute value in each case.

Comparison with Shiratori's Results. In the paper by Shiratori (1986), stress intensity factors for semi-elliptical surface cracks with $a/c = a/t = 0.2$ and $a/c = a/t = 0.6$ under the following residual stress field distribution were calculated using three-dimensional finite element methods:

$$\sigma(x, y) = \sigma_0 \left[3 \left(\frac{y}{c} \right)^3 - \frac{9}{2} \left(\frac{y}{c} \right)^2 + 1 \right] \quad (5.32)$$

As discussed in Section 3.1.2, this stress distribution can be expanded accurately using the following Fourier series with non-zero Fourier constants, $a_0 = (1/4)\sigma_0$ and $a_1 = (72/\pi^4)\sigma_0$:

$$\sigma(x, y) = \frac{\sigma_0}{4} + \frac{72\sigma_0}{\pi^4} \cos\left(\frac{\pi y}{c}\right) \quad (5.33)$$

Figure 3.3 shows the comparison between these two stress distributions. By applying Eq.(3.14) and (3.15), stress intensity factors at the deepest point and surface point were calculated using the present weight functions. A comparison between the finite element results from Shiratori and from the present weight functions are given in Table 5.3. Excellent agreement was achieved with a maximum difference of 3.9%.

5.2 Fixed Ends Boundary Conditions

Although the stress intensity factors for surface cracks in flat plates have been analysed extensively over the last two decades (Newman and Raju, 1978; Shiratori, 1982; Wang and Lambert, 1995a, 1995b, 1997), most of the work has focused on cracked plates under traction type loads. No solutions are available for surface cracks in flat plates with fixed end boundary conditions.

In this section, weight functions $M(x, A)$ and $M(x, B)$ for surface cracks in flat plates with fixed ends are derived. Stress intensity factors for any one-dimensional stress distribution can then be calculated using Eq. (2.6):

$$K(P') = \int_0^a \sigma(x) M(x; P') dx \quad (2.6)$$

Here P' is any general point along the crack front, but will be restricted to the deepest or surface points (A or B) in the following.

Stress intensity factor solutions for surface cracks in flat plates with zero displacement at the ends under crack face pressure as shown in Figure 5.9 are calculated based on the superposition method and compliance analyses as described in section 3.2. These stress intensity factor solutions were then used as reference stress intensity factors to derive weight functions for surface cracks in flat plates with fixed boundary conditions. The weight functions were validated using finite element data.

5.2.1 Stress Intensity Factor Solutions

Stress intensity factor solutions for surface cracks in flat plates are available for traction loads. These solutions can be used to produce stress intensity factor solutions for fixed end boundary conditions if superposition and compliance analyses as described in section 3.2 are applied. Since the methods described there were for edge cracks in flat plates (Marchand, *et al.*, 1986), it is necessary to generalise them to surface cracks.

Superposition Method

Consider a surface cracked flat plate with crack depth a , crack half length c , thickness t , length H , and width W . A constant load is applied to the crack face as shown in Figure 5.9. Similar to the problem discussed for edge cracks in section 3.2, this problem can be represented by the superposition of problems I and II as shown in Figure 5.10. The unknowns are the tension, N' , and moment, M' , which can be obtained from compatibility conditions at the ends.

As for edge cracks, the displacements for problem I, δ_t and θ_t , can be calculated from the superposition of problems I-A and I-B, as shown in Figure 5.11. Here the calculation of displacements for problem I-B is a classical problem with a standard solution, since no crack is involved. The key problem here is the calculation of displacements for problems I-A and II, which can be represented generally as shown in Figure 5.12. Note the problem here is different from the one discussed in section 3.2, Figure 3.8, since this is a surface crack instead of an edge crack.

As an approximation, the bending moment and axial force along the width direction are assumed to be uniform; N and M represent the total forces. Also, the displacements,

δ and θ , are assumed to be constant along the width direction. The justification for this simplification will be discussed later.

Compliance Analysis

As discussed in section 3.2 for edge cracks, relative displacement, δ , and rotation, θ , for the problem shown in Figure 5.12 can be taken as the summation of “cracked” and “uncracked” components:

$$\begin{pmatrix} \delta_{total} \\ \theta_{total} \end{pmatrix} = \begin{pmatrix} \delta_c \\ \theta_c \end{pmatrix} + \begin{pmatrix} \delta_{nc} \\ \theta_{nc} \end{pmatrix} \quad (5.34)$$

The compliance of the “uncracked” plate gives

$$\begin{pmatrix} \delta_{nc} \\ \theta_{nc} \end{pmatrix} = \begin{bmatrix} L/EA & 0 \\ 0 & L/EI \end{bmatrix} \begin{pmatrix} N \\ M \end{pmatrix} \quad (5.35)$$

An expression for the cracked terms are obtained by considering the complementary energy, U , of the specimen in terms of N and M :

$$U(N, M) = \frac{1}{2} [N \ M] \left(\begin{bmatrix} \delta_c \\ \theta_c \end{bmatrix} + \begin{bmatrix} \delta_{nc} \\ \theta_{nc} \end{bmatrix} \right) \quad (5.36)$$

If we introduce a crack extension over a certain area, dA , since the uncracked displacement will not change, we have

$$\frac{\partial U}{\partial A} = \frac{1}{2} [N M] \begin{pmatrix} \frac{\partial \delta_c}{\partial A} \\ \frac{\partial \theta_c}{\partial A} \end{pmatrix} \quad (5.37)$$

There are several different possible crack extension patterns for semi-elliptical cracks, as shown in Figure 5.13 (Fett, 1992). If we chose pattern I, which keeps c constant, we have

$$\Delta A = \frac{1}{2} \pi c \Delta a \quad (5.38)$$

Substituting this relation into Eq. (5.37), we get

$$\frac{\partial U}{\partial a} = \frac{1}{2} [N M] \begin{pmatrix} \frac{\partial \delta_c}{\partial a} \\ \frac{\partial \theta_c}{\partial a} \end{pmatrix} \quad (5.39)$$

On the other hand, from the relation between stress intensity factors and energy release rates, for crack extension dA ,

$$\frac{\partial U}{\partial A} = \frac{1}{E(\Delta A)} \int_{\Delta A} K^2 d(\Delta A) \quad (5.40)$$

This integration is along the entire crack front, ΔA follows the assumed extension pattern, and K is the stress intensity factor solution along the crack front for surface cracks shown in Figure 5.12.

If we define the following averaged stress intensity factor:

$$K^* = \frac{1}{(\Delta A)} \int_{\Delta A} K^2 d(\Delta A) \quad (5.41)$$

From the relationship between ΔA and Δa for the assumed crack extension pattern, Eq. (5.38), Eq. (5.40) can be simplified to

$$\frac{\partial U}{\partial a} = \frac{1}{2} \pi c \frac{(K^*)^2}{E} \quad (5.42)$$

For the present problem, the solution for K along the crack front is available (Newman and Raju, 1981; Wang and Lambert, 1995b), and the averaged stress intensity factors K^* can be calculated. If we write the averaged stress intensity factor solution for a combined load M and N , in matrix form:

$$K^* = \begin{bmatrix} \frac{\partial K^*}{\partial N} & \frac{\partial K^*}{\partial M} \end{bmatrix} \begin{pmatrix} N \\ M \end{pmatrix} \quad (5.43)$$

Then the energy change, Eq. (5.42), becomes

$$\frac{\partial U}{\partial a} = \frac{\pi c}{2E} [N \ M] \begin{bmatrix} \left(\frac{\partial K^*}{\partial N}\right)^2 & \left(\frac{\partial K^*}{\partial N}\right)\left(\frac{\partial K^*}{\partial M}\right) \\ \left(\frac{\partial K^*}{\partial N}\right)\left(\frac{\partial K^*}{\partial M}\right) & \left(\frac{\partial K^*}{\partial M}\right)^2 \end{bmatrix} \begin{pmatrix} N \\ M \end{pmatrix} \quad (5.44)$$

Comparing Eqs. (5.39) and (5.44) gives

$$\begin{pmatrix} \frac{\partial \delta_c}{\partial a} \\ \frac{\partial \theta_c}{\partial a} \end{pmatrix} = \frac{\pi c}{E} \begin{bmatrix} \left(\frac{\partial K^*}{\partial N}\right)^2 & \left(\frac{\partial K^*}{\partial N}\right)\left(\frac{\partial K^*}{\partial M}\right) \\ \left(\frac{\partial K^*}{\partial N}\right)\left(\frac{\partial K^*}{\partial M}\right) & \left(\frac{\partial K^*}{\partial M}\right)^2 \end{bmatrix} \begin{pmatrix} N \\ M \end{pmatrix} \quad (5.45)$$

If we introduce the aspect ratio of the surface crack, $a/c = n$, and integrate with respect to a , we obtain

$$\begin{pmatrix} \delta_c \\ \theta_c \end{pmatrix} = \begin{bmatrix} \int_0^a \frac{\pi a}{nE} \left(\frac{\partial K^*}{\partial N}\right)^2 da & \int_0^a \frac{\pi a}{nE} \left(\frac{\partial K^*}{\partial N}\right)\left(\frac{\partial K^*}{\partial M}\right) da \\ \int_0^a \frac{\pi a}{nE} \left(\frac{\partial K^*}{\partial N}\right)\left(\frac{\partial K^*}{\partial M}\right) da & \int_0^a \frac{\pi a}{nE} \left(\frac{\partial K^*}{\partial M}\right)^2 da \end{bmatrix} \begin{pmatrix} N \\ M \end{pmatrix} \quad (5.46)$$

or

$$\begin{pmatrix} \delta_c \\ \theta_c \end{pmatrix} = \begin{bmatrix} C_{11} & C_{12} \\ C_{21} & C_{22} \end{bmatrix} \begin{pmatrix} N \\ M \end{pmatrix} \quad (5.47)$$

These are the additional displacements due to the existence of the surface crack, where C_{11} to C_{22} are the corresponding compliances. From Eq. (5.34)

$$\begin{pmatrix} \delta_{total} \\ \theta_{total} \end{pmatrix} = \begin{bmatrix} L/EA & 0 \\ 0 & L/EI \end{bmatrix} \begin{pmatrix} N \\ M \end{pmatrix} + \begin{bmatrix} C_{11} & C_{12} \\ C_{21} & C_{22} \end{bmatrix} \begin{pmatrix} N \\ M \end{pmatrix} \quad (5.48)$$

These are the total relative displacements for the problem shown in Figure 5.12.

Note that the expressions for crack-introduced compliance were derived based on one possible crack extension type, which keeps the crack length constant, as shown in Figure 5.13(a). These results should be independent of the crack extension type. If we use type II crack extension, as shown in Figure 5.13(b), which keeps the aspect ratio, n , constant, a different relationship between ΔA and Δa will be obtained, and also a different averaged K solution will be introduced. The integrations in Eq.(5.46) must then be conducted for a constant aspect ratio. This alternative analysis was carried out and it was found that the resulting compliances and, consequently, displacements were the same.

Stress Intensity Factors

Going back to the problem shown in Figure 5.10, the displacement solution for problem I is

$$\begin{pmatrix} \delta_I \\ \theta_I \end{pmatrix} = \begin{bmatrix} C_{11} & C_{12} \\ C_{21} & C_{22} \end{bmatrix} \begin{pmatrix} \sigma W t \\ 0 \end{pmatrix} + \begin{bmatrix} L/EA & 0 \\ 0 & L/EI \end{bmatrix} \begin{pmatrix} \sigma W t \\ 0 \end{pmatrix} - \begin{bmatrix} L/EA & 0 \\ 0 & L/EI \end{bmatrix} \begin{pmatrix} \sigma W t \\ 0 \end{pmatrix} \quad (5.49)$$

and for problem II

$$\begin{pmatrix} \delta_{II} \\ \theta_{II} \end{pmatrix} = - \begin{bmatrix} C_{11} & C_{12} \\ C_{21} & C_{22} \end{bmatrix} \begin{pmatrix} N' \\ M' \end{pmatrix} - \begin{pmatrix} L/EA & 0 \\ 0 & L/EI \end{pmatrix} \begin{pmatrix} N' \\ M' \end{pmatrix} \quad (5.50)$$

Applying the boundary condition gives

$$\begin{bmatrix} C_{11} & C_{12} \\ C_{21} & C_{22} \end{bmatrix} \begin{pmatrix} \sigma W t \\ 0 \end{pmatrix} - \begin{bmatrix} C_{11} & C_{12} \\ C_{21} & C_{22} \end{bmatrix} \begin{pmatrix} N' \\ M' \end{pmatrix} - \begin{pmatrix} L/EA & 0 \\ 0 & L/EI \end{pmatrix} \begin{pmatrix} N' \\ M' \end{pmatrix} = 0 \quad (5.51)$$

For a given geometry represented by a/c , a/t , H/t and W/t , Eq. (5.51) can be solved for N' and M' . The stress intensity factors are obtained from a combination of solutions for problems I and II:

$$K = \frac{\partial K}{\partial N}(\sigma W t - N') + \frac{\partial K}{\partial M}(-M') \quad (5.52)$$

Note that the expression for K , Eq.(5.52), can be applied to any point along the crack front as long as the corresponding $\partial K/\partial N$ and $\partial K/\partial M$ at the same point are used. The resulting K is the regular stress intensity factor, not the average stress intensity factors K^* . K^* is only used in the calculation of compliance.

The Effective Width W_{eff}

Note that, unlike edge cracks, the assumption that extension and rotation do not change along the width direction is not always true for surface cracks. For surface cracks, rotation and extension are localised around the area corresponding to the surface crack position, as illustrated in Figure 5.14. Consequently, the reaction forces N' and M' shown in Figure 5.10 are also localised around the area corresponding to the surface crack position.

Finite element calculations for surface cracks in flat plates with fixed boundary conditions and constant crack surface traction loads as shown in Figure 5.9 were conducted. The reaction forces within the local area corresponding to the surface crack location were found. Figure 5.15 shows the distribution of N' along the width direction for a geometry with $a/c = 0.1$, $a/t = 0.8$, $H/t = 10$ and $W/t = 60$. Problem I in the superposition representation (Figure 5.10) was also analysed. The additional deformation due to the

existence of the surface crack was also found to be restricted to the region corresponding to the crack location. Figure 5.16 shows the deformed mesh for $a/c = 0.2$, $a/t = 0.8$, $H/t = 10$ and $W/t = 60$.

Based on these calculations, an effective width, W_{eff} , was proposed for the analysis of surface cracked plates. It was assumed that W_{eff} would depend on some combination of crack half-length c , and plate thickness t . A similar assumption was used for the effective area calculation in the plastic collapse analysis of a surface cracked plate in C.E.G.B./R6 (Miller, 1988). A number of expressions for W_{eff} , based on discrete combination of c and t , were examined by comparing the analysis results with appropriate finite element calculations. The following expression produced the best results:

$$W_{eff} = 4c + 4t \quad (5.53)$$

Validation of the Method

The present compliance analysis method and superposition model in conjunction with available stress intensity factor solutions for free end boundaries were applied to calculate the stress intensity factors for surface cracks in flat plates with fixed boundary conditions for constant and linear loading conditions:

$$\sigma(x, y) = \sigma_0 \quad (5.54)$$

and

$$\sigma(x, y) = \sigma_0 \left(1 - \frac{x}{a}\right) \quad (5.55)$$

The resulting stress intensity factors will depend on a/c , a/t and H/t . Since W_{eff} was used for all plate widths, W , ($W > W_{eff}$ for all cases), the resulting stress intensity factors were independent of W/t .

Finite element calculations were conducted for $a/c = 0.1, 0.2$ and 1.0 , $a/t = 0.4, 0.6$ and 0.8 , and $H/t = 10$ and 20 . Comparisons of stress intensity factors at the deepest and surface points between predictions from the compliance analysis and finite element calculations are shown in Figures 5.17 - 5.28. The differences for all these cases were within 10%.

Note that load shedding depends on strongly on the a/t ratio. When a/t is less than 0.4, load shedding is not significant. Load shedding also depends on aspect ratio, lower aspect ratio cracks experience more load shedding.

5.2.2 Derivation of Weight Functions

By applying the method described in Section 2.2, weight functions $M(x; A)$ and $M(x; B)$ for surface cracks in plates with fixed ends were derived based on the stress intensity factor solutions obtained from the compliance analysis.

Determination of Weight Functions $M(x; A)$ and $M(x; B)$

Weight functions $M(x; A)$ and $M(x; B)$ were derived in the form of Eqs.(2.11) and (2.12):

$$M(x, a; A) = \frac{2}{\sqrt{2\pi(a-x)}} \left[1 + M_{1A} \left(1 - \frac{x}{a}\right)^{\frac{1}{2}} + M_{2A} \left(1 - \frac{x}{a}\right) + M_{3A} \left(1 - \frac{x}{a}\right)^{\frac{3}{2}} \right] \quad (2.11)$$

$$M(x, a; B) = \frac{2}{\sqrt{\pi a}} \left[1 + M_{1B} \left(\frac{x}{a}\right)^{\frac{1}{2}} + M_{2B} \left(\frac{x}{a}\right) + M_{3B} \left(\frac{x}{a}\right)^{\frac{3}{2}} \right] \quad (2.12)$$

The parameters were determined from two reference stress intensity factors and the conditions represented by Eqs.(2.13) and (2.14):

$$M_{2A} = 3 \quad (2.13)$$

$$M_{1B} + M_{2B} + M_{3B} + 1 = 0 \quad (2.14)$$

Weight function at the deepest point $M(x; A)$

In order to determine $M(x; A)$ using Eq.(2.11), two reference solutions were used to decide M_{1A} , M_{2A} and M_{3A} : constant or a linearly decreasing stress through thickness.

Reference stress intensity factors. For the deepest point of a surface crack, the results for a constant stress distribution, Eq. (5.54), can be represented as

$$K_{Ir}^A = \sigma_0 \sqrt{\frac{\pi a}{Q}} Y_0 \quad (5.56)$$

where Y_0 was obtained from the compliance analysis presented in Section 5.2.1.

The results for a stress distribution linearly decreasing through the thickness in the width direction, Eq.(5.55), can be represented as

$$K_{2r}^A = \sigma_0 \sqrt{\frac{\pi a}{Q}} Y_1 \quad (5.57)$$

where Y_0 was also obtained from the compliance analysis presented in Section 5.2.1. The weight functions were derived from these reference stress intensity factor solutions.

Weight function. By substituting Eqs. (5.56) and (5.57) into Eq. (2.6) plus the condition represented by Eq. (2.13), three equations with three unknowns were established. The parameters in the weight function expressions were solved for and are

$$M_{1A} = \frac{\pi}{\sqrt{2Q}} (4Y_0 - 6Y_1) - \frac{24}{5} \quad (5.58)$$

$$M_{2A} = 3 \quad (5.59)$$

$$M_{3A} = 2 \left(\frac{\pi}{\sqrt{2Q}} Y_0 - M_{1A} - 4 \right) \quad (5.60)$$

The weight function for the deepest point of a semi-elliptic surface crack can then be determined directly from Eq. (2.11).

Weight function for the surface point $M(x; B)$

The two reference stress intensity factor solutions used to determine the weight function $M(x; B)$, in the form of Eq. (2.12), were stress fields of constant or linear decreasing through the thickness; these are the same stress fields used for the determination of $M(x; A)$.

Reference Stress Intensity Factors. For the surface point of the surface crack, the results for a stress distribution constant through the thickness, Eq.(5.54), can be represented as

$$K_{1r}^B = \sigma_0 \sqrt{\frac{\pi a}{Q}} F_0 \quad (5.61)$$

The results for a stress distribution linearly decreasing through the thickness, Eq. (5.55), can be represented as:

$$K_{2r}^B = \sigma_0 \sqrt{\frac{\pi a}{Q}} F_1 \quad (5.62)$$

where F_0 and F_1 in Eqs. (5.61) and (5.62) were obtained from the compliance analysis presented in Section 5.2.1.

Weight Function. By substituting Eqs. (5.61) and (5.62) into Eq. (2.6), and then applying the condition represented by Eq. (2.14), three equations with three unknowns were established. The weight function parameters for the surface point were determined to be

$$M_{1B} = \frac{\pi}{2\sqrt{Q}}(30F_1 - 18F_0) - 8 \quad (5.63)$$

$$M_{2B} = \frac{\pi}{2\sqrt{Q}}(60F_0 - 90F_1) + 15 \quad (5.64)$$

$$M_{3B} = -(1 + M_{1B} + M_{2B}) \quad (5.65)$$

The weight function for the surface point can then be determined directly from Eq. (2.12).

5.2.3 Validation of Weight Functions

The weight functions for the deepest and surface points derived in Sections 5.2.2 were validated using finite element results for two non-linear stress fields. Using Eq. (2.6), stress intensity factors were calculated for the following stress fields:

$$\sigma(x, y) = \sigma_0 \left(1 - \frac{x}{a}\right)^2 \quad (5.66)$$

$$\sigma(x, y) = \sigma_0 \left(1 - \frac{x}{a}\right)^3 \quad (5.67)$$

The stress intensity factors for the deepest and surface points calculated from weight functions and from the present finite element calculations for the above stress distribution are shown in Figures 5.29 to 5.32. The difference between the boundary correction factors calculated from the weight function and the finite element results were less than 10% for both the surface and the deepest points.

m	position	a/t=0.2	a/t=0.4	a/t=0.6	a/t=0.8
0	surface	-0.3693	-0.3682	-0.3594	-0.3300
	deepest	1.0708	1.2778	1.5787	1.8178
1	surface	-0.3513	-0.3531	-0.3545	-0.3555
	deepest	0.4387	0.5656	0.7488	0.8684
2	surface	-0.3345	-0.3369	-0.3410	-0.3503
	deepest	0.2739	0.3653	0.5008	0.5853
3	surface	-0.3195	-0.3220	-0.3270	-0.3394
	deepest	0.2010	0.2725	0.3795	0.4442

Table 5.1a. Boundary correction factors F for semi-elliptical surface cracks under stress distributions of $\sigma_0(1-x/a)^m \cos(\pi/c)$, $m = 0, 1, 2, 3$, $F = K/\sigma_0 \sqrt{[\pi a/Q]}$, $a/c = 0.1$.

m	position	a/t=0.2	a/t=0.4	a/t=0.6	a/t=0.8
0	surface	-0.4610	-0.4425	-0.4179	-0.3858
	deepest	0.9581	1.0462	1.1871	1.3095
1	surface	-0.4299	-0.4221	-0.4111	-0.4001
	deepest	0.3626	0.4174	0.4944	0.5317
2	surface	-0.4025	-0.3988	-0.3932	-0.3903
	deepest	0.2184	0.2573	0.3148	0.3366
3	surface	-0.3790	-0.3776	-0.3744	-0.3759
	deepest	0.1577	0.1879	0.2332	0.2471

Table 5.1b. Boundary correction factors F for semi-elliptical surface cracks under stress distributions of $\sigma_0(1-x/a)^m \cos(\pi/c)$, $m = 0, 1, 2, 3$, $F = K/\sigma_0 \sqrt{[\pi a/Q]}$, $a/c = 0.2$.

m	position	a/t=0.2	a/t=0.4	a/t=0.6	a/t=0.8
0	surface	-0.5130	-0.4855	-0.4467	-0.4068
	deepest	0.8415	0.8746	0.9246	0.9799
1	surface	-0.4793	-0.4639	-0.4430	-0.4208
	deepest	0.2725	0.2915	0.3117	0.3196
2	surface	-0.4467	-0.4363	-0.4321	-0.4099
	deepest	0.1518	0.1650	0.1819	0.1859
3	surface	-0.4183	-0.4105	-0.4016	-0.3939
	deepest	0.1056	0.1157	0.1295	0.1309

Table 5.1c. Boundary correction factors F for semi-elliptical surface cracks under stress distributions of $\infty(1-x/a)^m \cos(\pi/c)$, $m = 0, 1, 2, 3$, $F = K/\infty\sqrt{[\pi a/Q]}$, $a/c = 0.4$.

m	position	a/t=0.2	a/t=0.4	a/t=0.6	a/t=0.8
0	surface	-0.5125	-0.4894	-0.4549	-0.4181
	deepest	0.7822	0.7996	0.8254	0.8645
1	surface	-0.4897	-0.4766	-0.4574	-0.4350
	deepest	0.2221	0.2319	0.2367	0.2365
2	surface	-0.4617	-0.4527	-0.4402	-0.4262
	deepest	0.1141	0.1209	0.1273	0.1271
3	surface	-0.4354	-0.4287	-0.4199	-0.4114
	deepest	0.0763	0.0815	0.0874	0.0860

Table 5.1d. Boundary correction factors F for semi-elliptical surface cracks under stress distributions of $\sigma_0(1-x/a)^m \cos(\pi/c)$, $m = 0, 1, 2, 3$, $F = K/\sigma_0 \sqrt{[\pi a/Q]}$, $a/c = 0.6$.

m	position	a/t=0.2	a/t=0.4	a/t=0.6	a/t=0.8
0	surface	-0.5063	-0.4920	-0.4680	-0.4540
	deepest	0.7416	0.7484	0.7595	0.7842
1	surface	-0.5028	-0.4948	-0.4790	-0.4706
	deepest	0.1704	0.1743	0.1684	0.1594
2	surface	-0.4852	-0.4796	-0.4677	-0.4639
	deepest	0.0752	0.0778	0.0777	0.0737
3	surface	-0.4653	-0.4612	-0.4511	-0.4509
	deepest	0.0465	0.0485	0.0496	0.0462

Table 5.1e. Boundary correction factors F for semi-elliptical surface cracks under stress distributions of $\sigma_0(1-x/a)^m \cos(\pi/c)$, $m = 0, 1, 2, 3$, $F = K/\sigma_0\sqrt{[\pi a/Q]}$, $a/c = 1$.

m	position	a/t=0.2	a/t=0.4	a/t=0.6	a/t=0.8
0	surface	0.0438	0.0778	0.1329	0.2337
1	surface	0.0346	0.0584	0.0980	0.1723
2	surface	0.0289	0.0471	0.0777	0.1362
3	surface	0.0249	0.0396	0.0645	0.1126

Table 5.2a. Boundary correction factors F for semi-elliptical surface cracks under stress distributions of $\sigma_0(1-x/a)^m \sin(\pi/c)$, $m = 0, 1, 2, 3$, $F = K/\sigma_0\sqrt{[\pi a/Q]}$, $a/c = 0.1$.

m	position	a/t=0.2	a/t=0.4	a/t=0.6	a/t=0.8
0	surface	0.1071	0.1391	0.2010	0.3056
1	surface	0.0839	0.1061	0.1499	0.2262
2	surface	0.0694	0.0863	0.1199	0.1796
3	surface	0.0594	0.0731	0.1003	0.1491

Table 5.2b. Boundary correction factors F for semi-elliptical surface cracks under stress distributions of $\sigma_0(1-x/a)^m \sin(\pi/c)$, $m = 0, 1, 2, 3$, $F = K/\sigma_0 \sqrt{[\pi a/Q]}$, $a/c = 0.2$.

m	position	a/t=0.2	a/t=0.4	a/t=0.6	a/t=0.8
0	surface	0.2251	0.2406	0.2782	0.3331
1	surface	0.1754	0.1862	0.2128	0.2533
2	surface	0.1449	0.1530	0.1735	0.2054
3	surface	0.1239	0.1305	0.1470	0.1732

Table 5.2c. Boundary correction factors F for semi-elliptical surface cracks under stress distributions of $\sigma_0(1-x/a)^m \sin(\pi/c)$, $m = 0, 1, 2, 3$, $F = K/\sigma_0\sqrt{[\pi a/Q]}$, $a/c = 0.4$.

m	position	a/t=0.2	a/t=0.4	a/t=0.6	a/t=0.8
0	surface	0.3012	0.3076	0.3256	0.3480
1	surface	0.2392	0.2437	0.2560	0.2725
2	surface	0.2002	0.2037	0.2128	0.2256
3	surface	0.1730	0.1759	0.1830	0.1933

Table 5.2d. Boundary correction factors F for semi-elliptical surface cracks under stress distributions of $\sigma_0(1-x/a)^m \sin(\pi/c)$, $m = 0, 1, 2, 3$, $F = K/\sigma_0\sqrt{[\pi a/Q]}$, $a/c = 0.6$.

m	position	a/t=0.2	a/t=0.4	a/t=0.6	a/t=0.8
0	surface	0.4239	0.4254	0.4083	0.3883
1	surface	0.3549	0.3560	0.3392	0.3208
2	surface	0.3079	0.3087	0.2927	0.2756
3	surface	0.2729	0.2736	0.2585	0.2428

Table 5.2e. Boundary correction factors F for semi-elliptical surface cracks under stress distributions of $\sigma_0(1-x/a)^m \sin(\pi/c)$, $m = 0, 1, 2, 3$, $F = K/\sigma_0\sqrt{[\pi a/Q]}$, $a/c = 1$.

Crack Geometry	Position	Shiratori, (1987) F_s	Present Approach F	Difference (%) $100 \cdot F - F_s / F_s$
a/c=0.2, a/t=0.2	Deepest	1.0416	1.0073	3.2
	Surface	-0.2012	-0.1933	3.9
a/c=0.6, a/t=0.6	Deepest	0.9408	0.9116	3.1
	Surface	-0.0376	-0.0382	1.6

Table 5.3 Comparison between the stress intensity factors calculated from present weight functions and finite element analyses from Shiratori (1987) under a residual stress field (Eq. (5.23)).

Figure 5.1 Geometry and co-ordinates system used

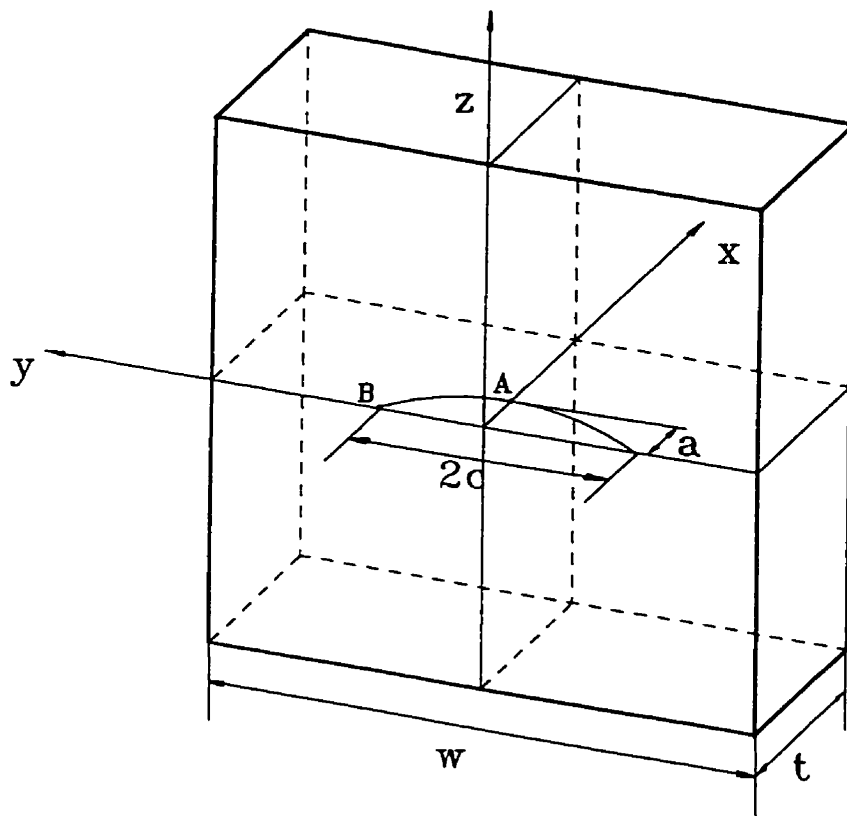


Figure 5.2 Typical mesh (part), $a/c = 0.1$, $a/t = 0.2$

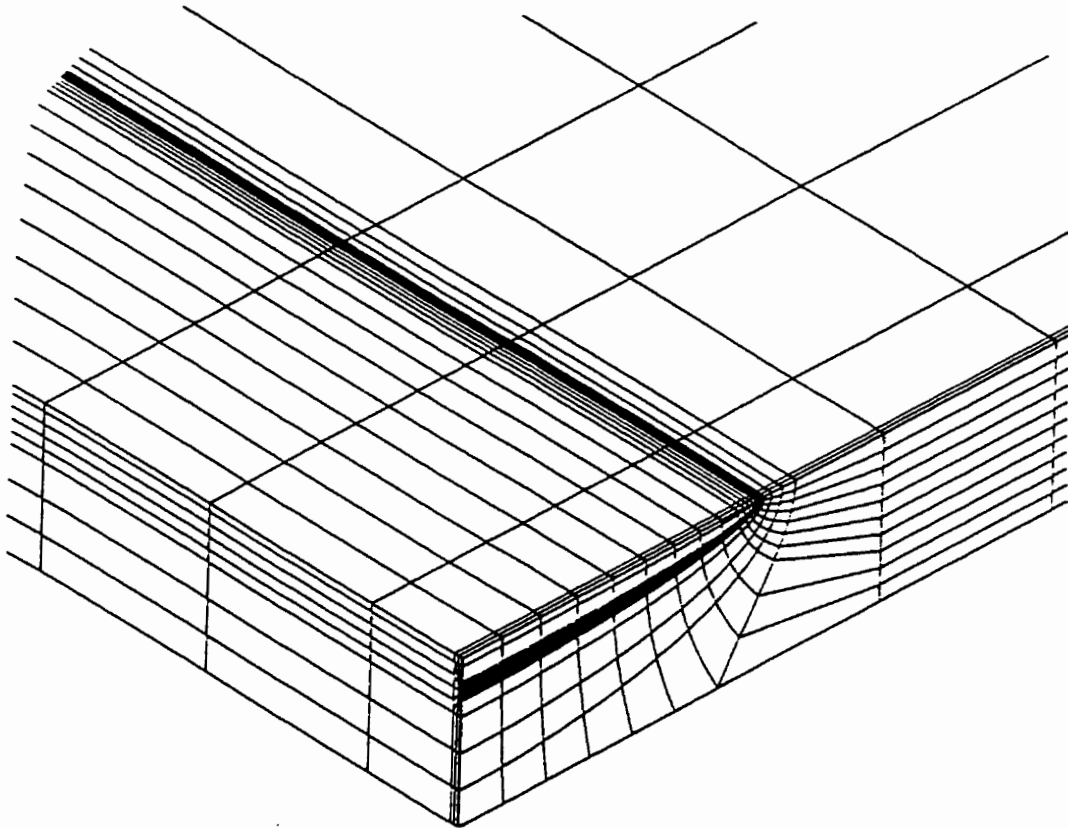


Fig. 5.3 Comparison of the weight function based stress intensity factor and FEM data for stress distribution $\propto (1-x/a)^2 \cos(\pi/c)$, (deepest point).

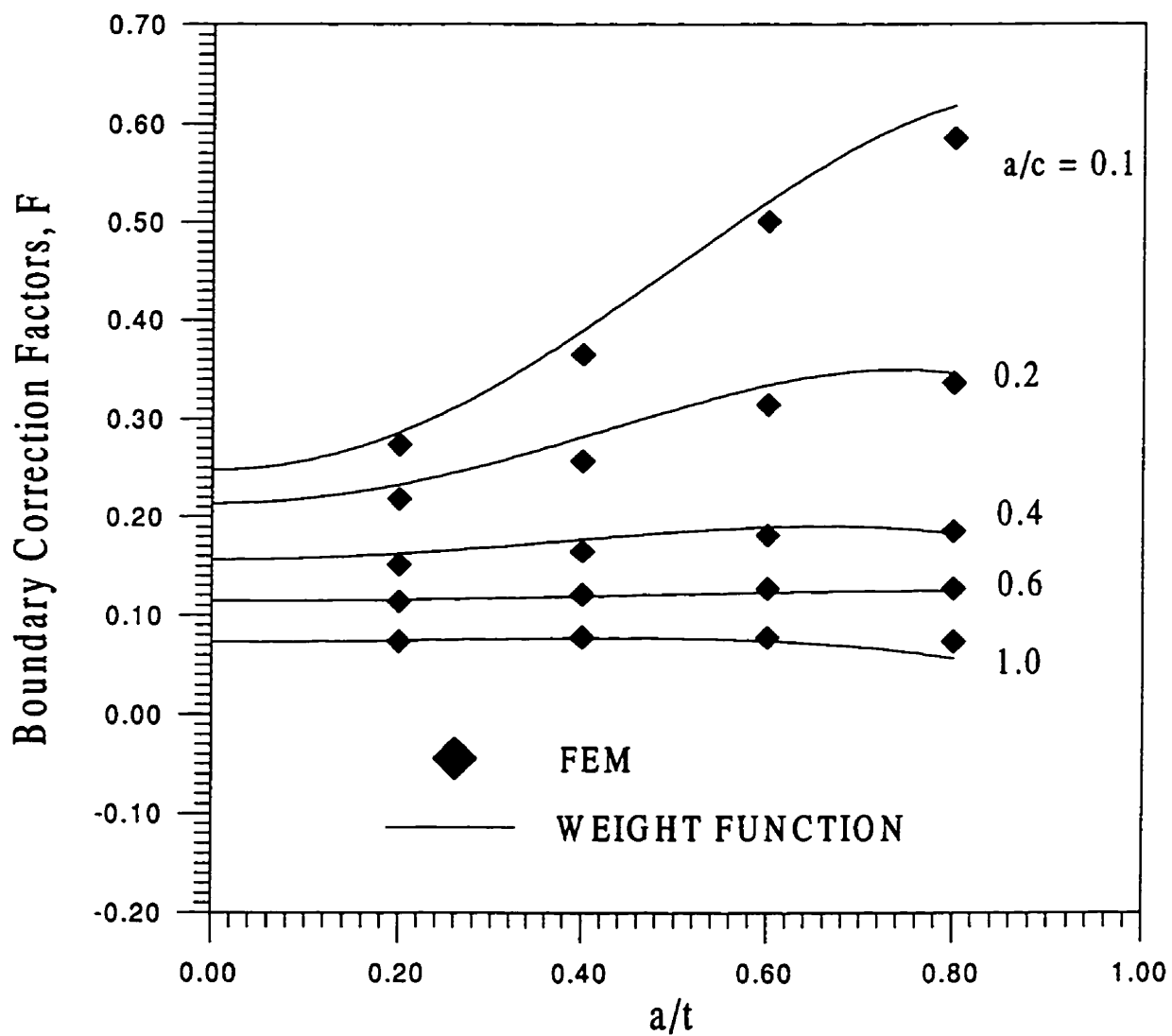


Fig. 5.4 Comparison of the weight function based stress intensity factor and FEM data for stress distribution $\sigma_0(1-x/a)^2 \cos(\pi/c)$, (surface point).

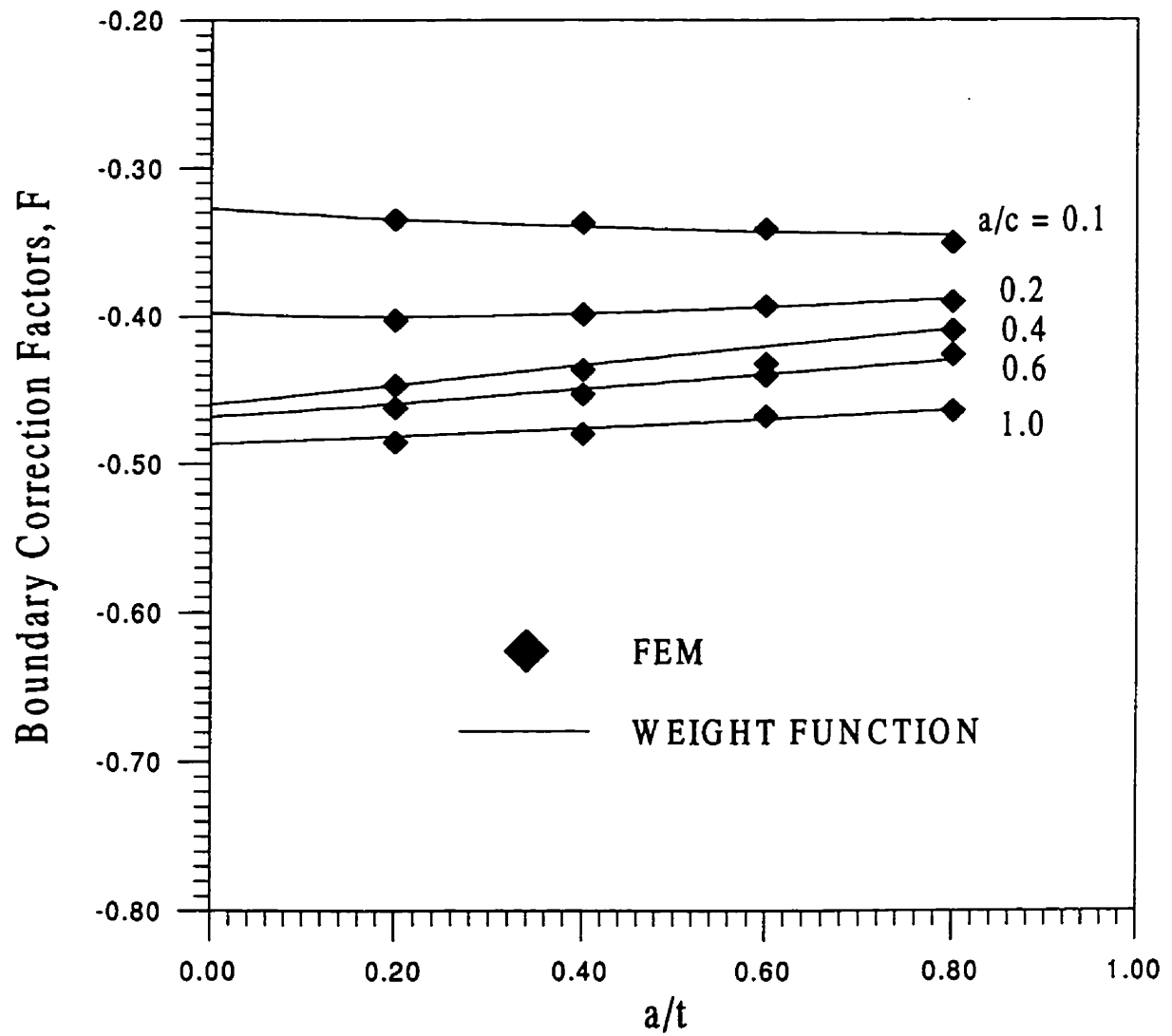


Fig. 5.5 Comparison of the weight function based stress intensity factors and FEM data for stress distribution $\sigma(1-x/a)^3 \cos(\pi/c)$, (deepest point).

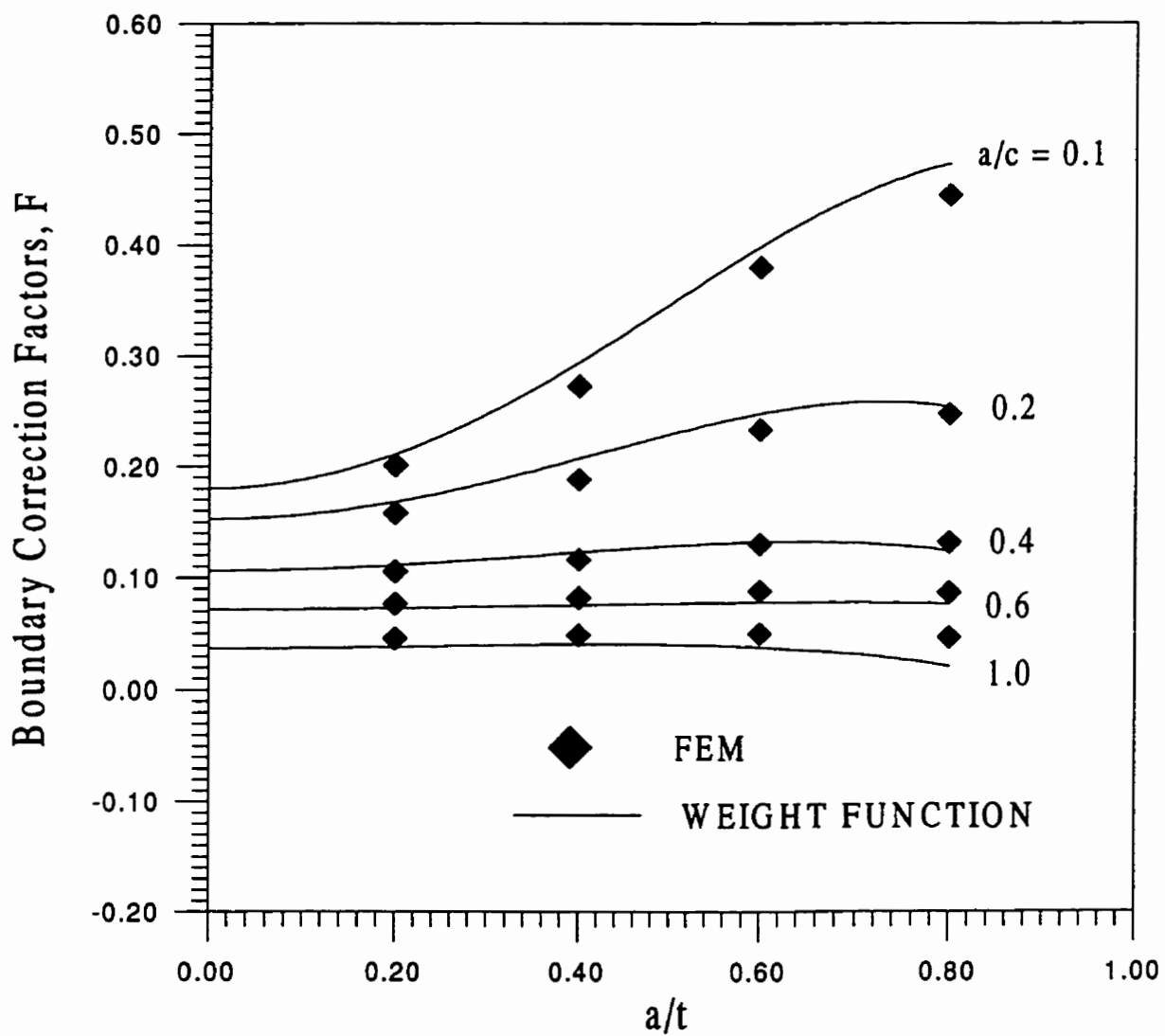


Fig. 5.6 Comparison of the weight function based stress intensity factors and FEM data for stress distribution $\sigma_0(1-x/a)^3 \cos(\pi/c)$, (surface point).

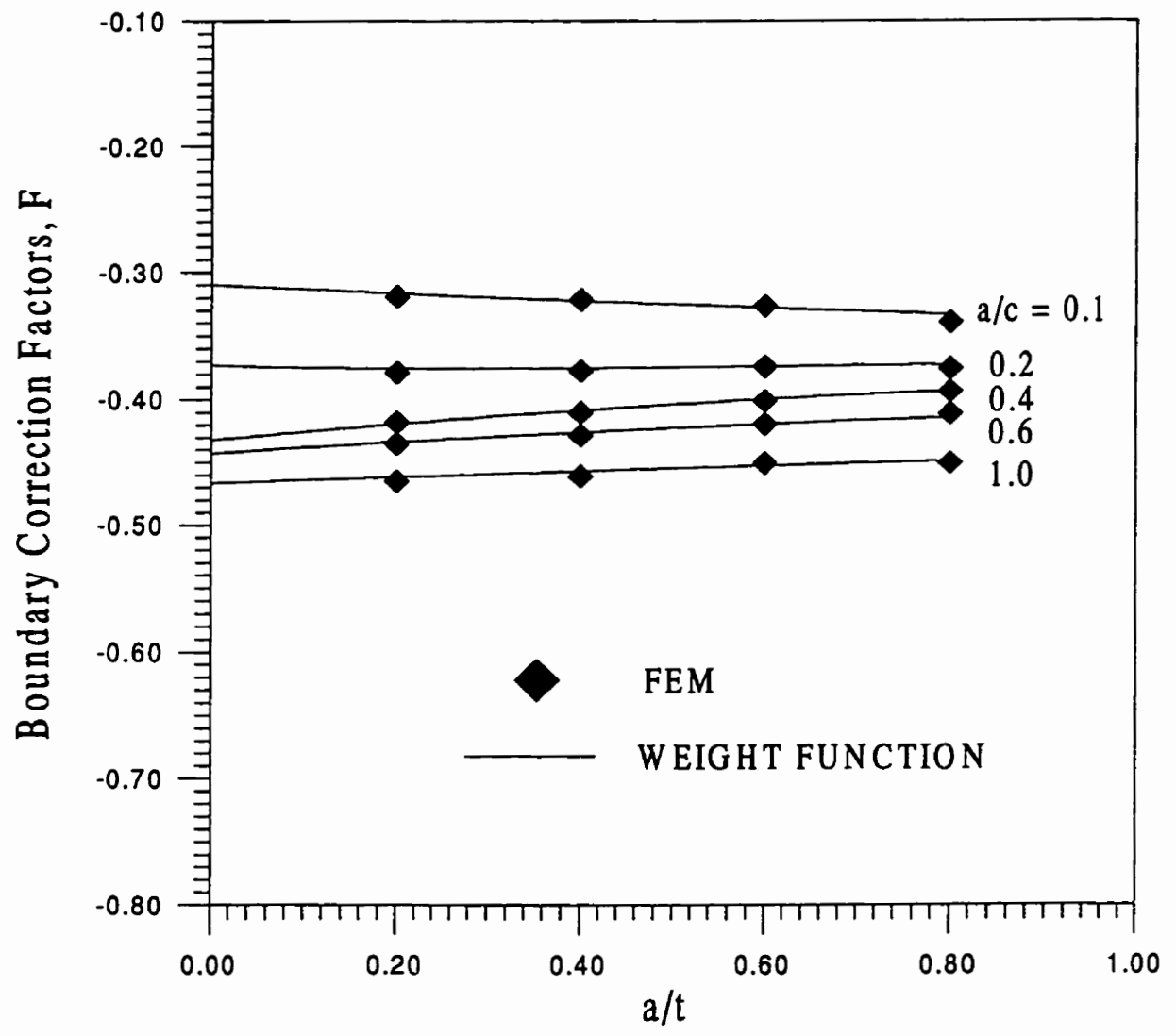


Fig. 5.7 Comparison of the weight function based stress intensity factor and FEM data for stress distribution $\propto (1-x/a)^2 \sin(\pi/c)$, (surface point).

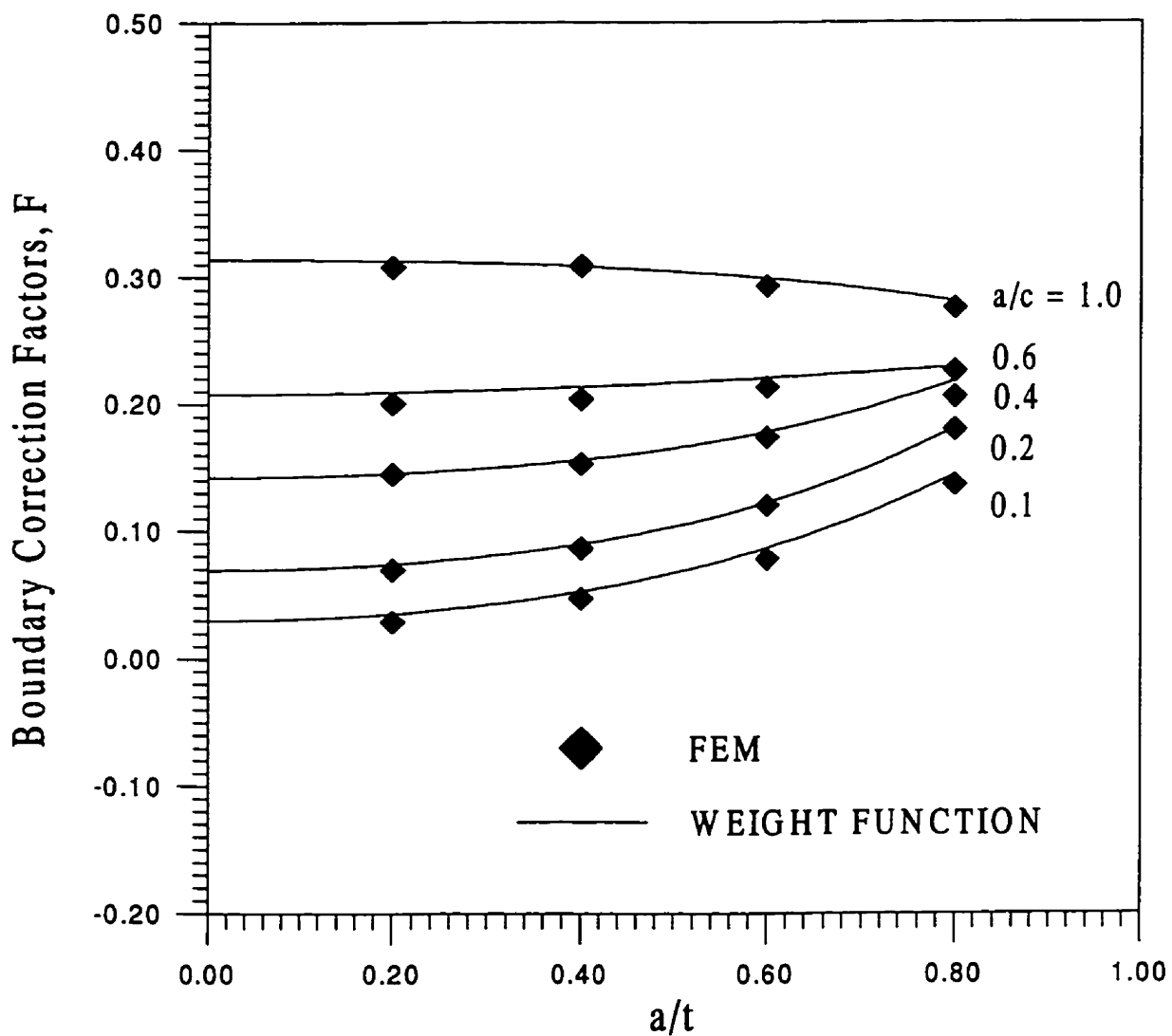


Fig. 5.8 Comparison of the weight function based stress intensity factor and FEM data for stress distribution $\sigma_0(1-x/a)^3 \sin(\pi/c)$, (surface point).

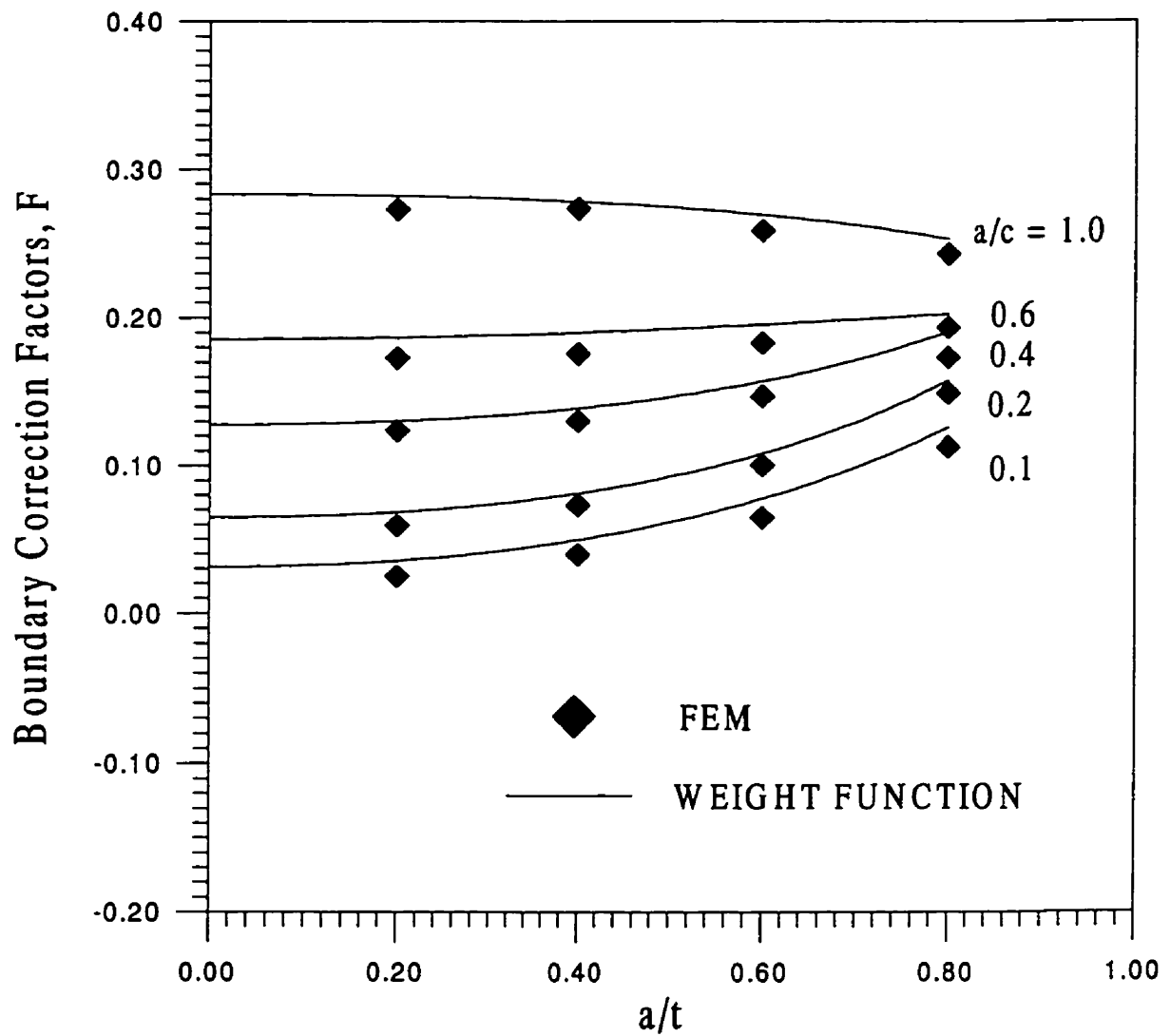


Figure 5.9 Fixed ends plate with surface crack (half)

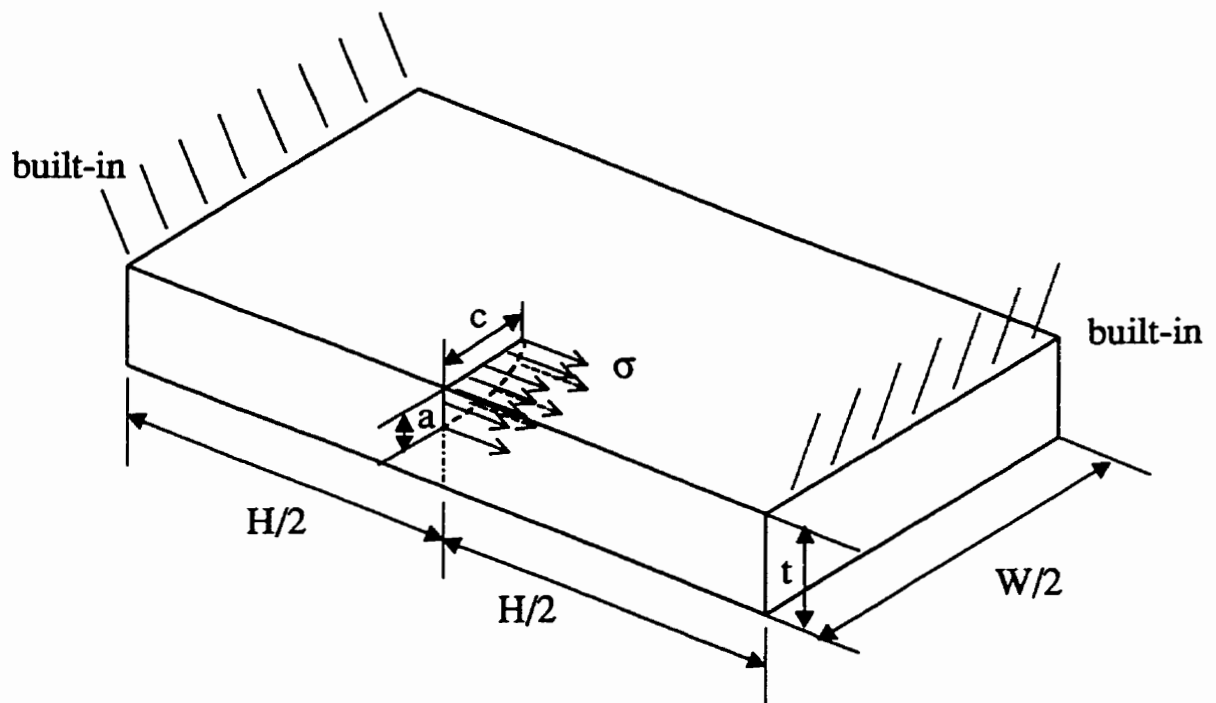


Figure 5.10 Superposition representation

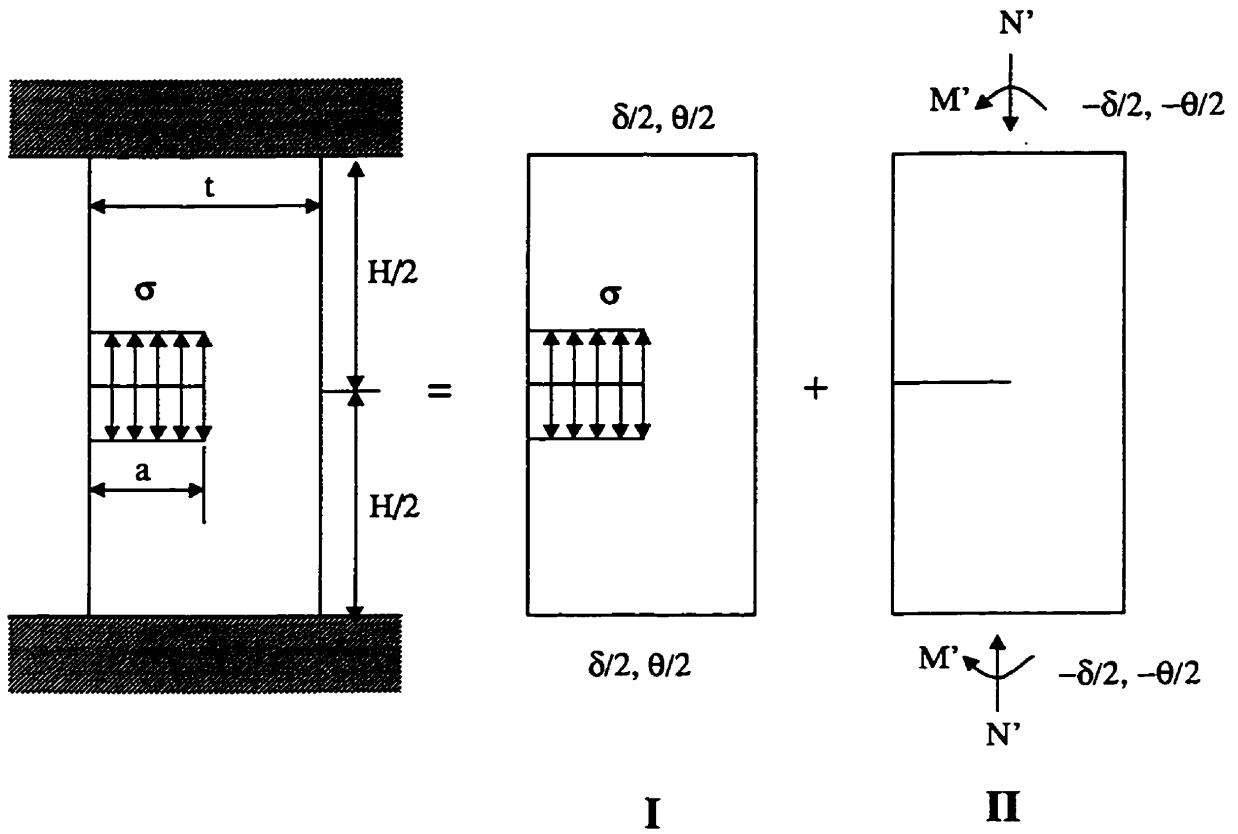


Figure 5.11 Superposition of problem I

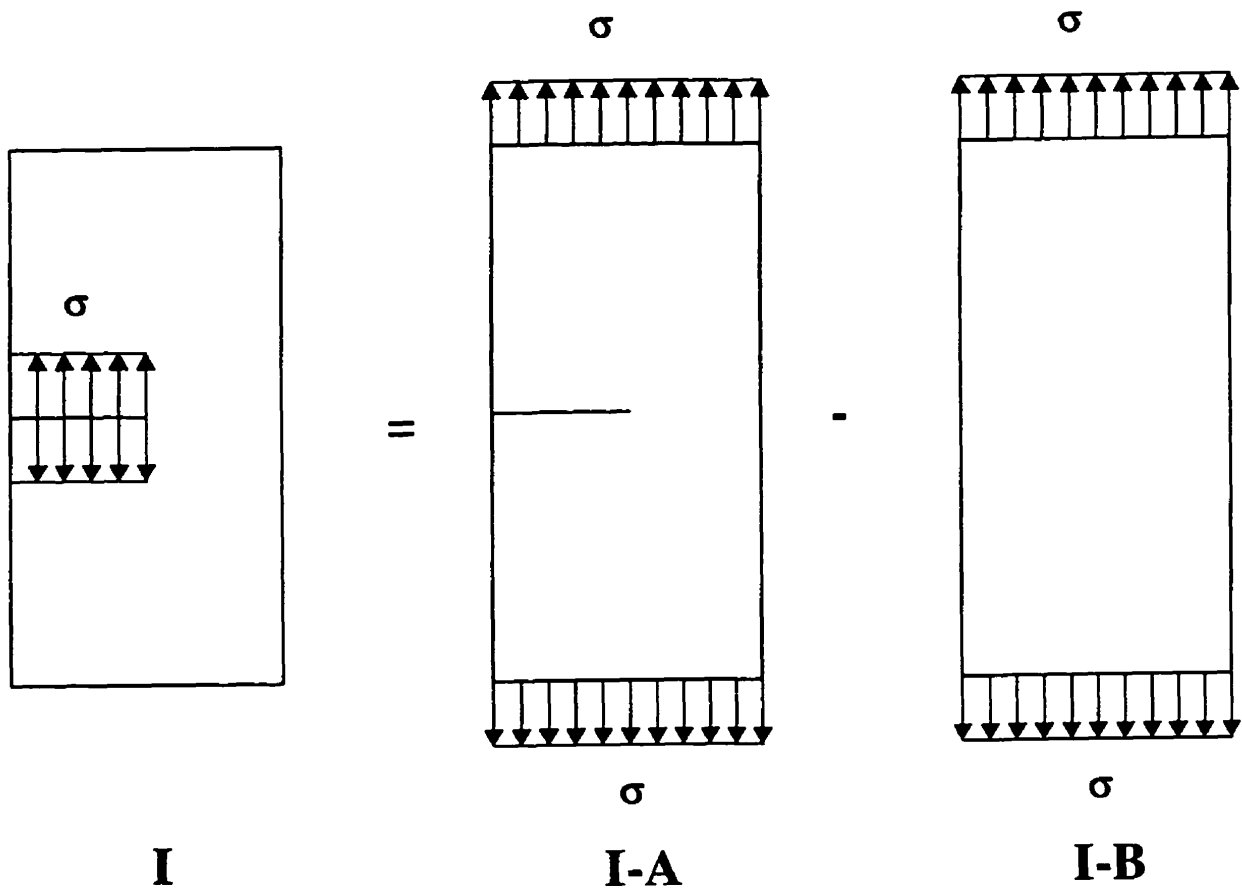


Figure 5.12 General problem for calculation of displacements

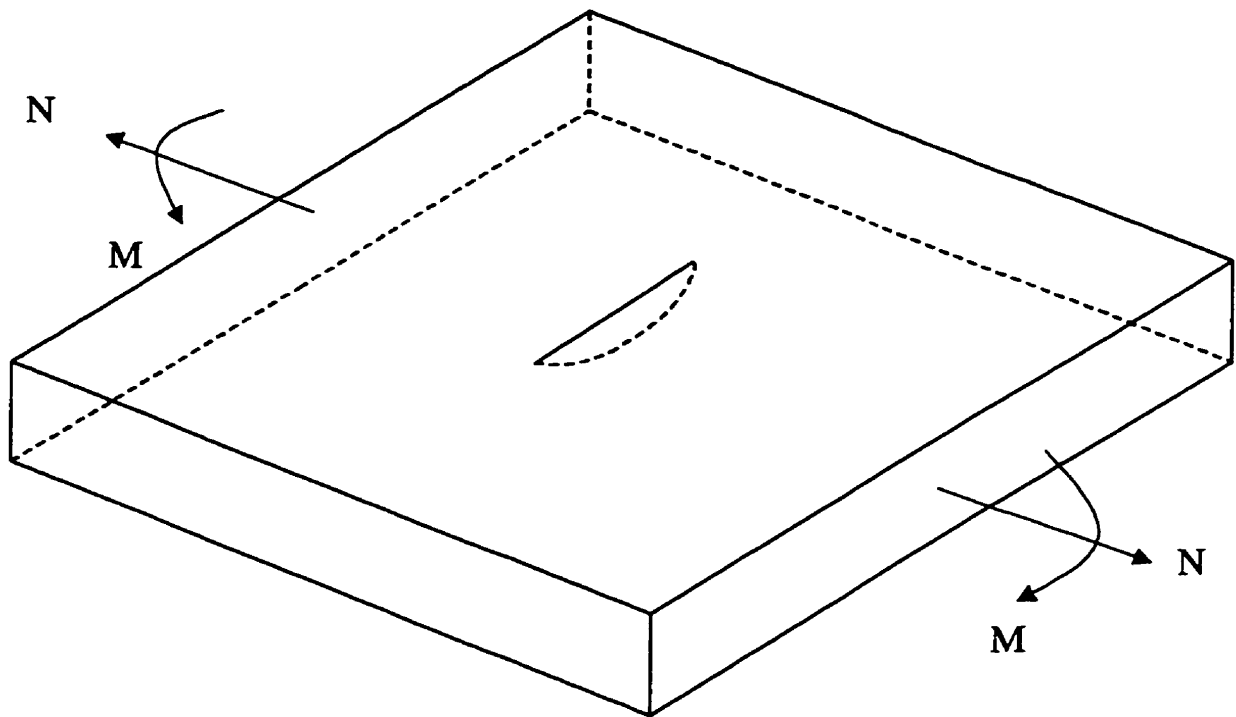
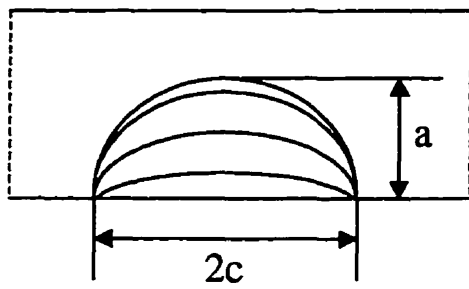
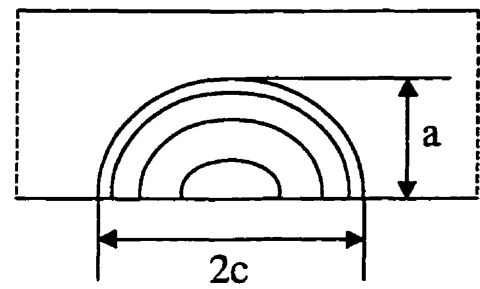


Figure 5.13 Crack extension types



(a) Pattern I



(b) Pattern II

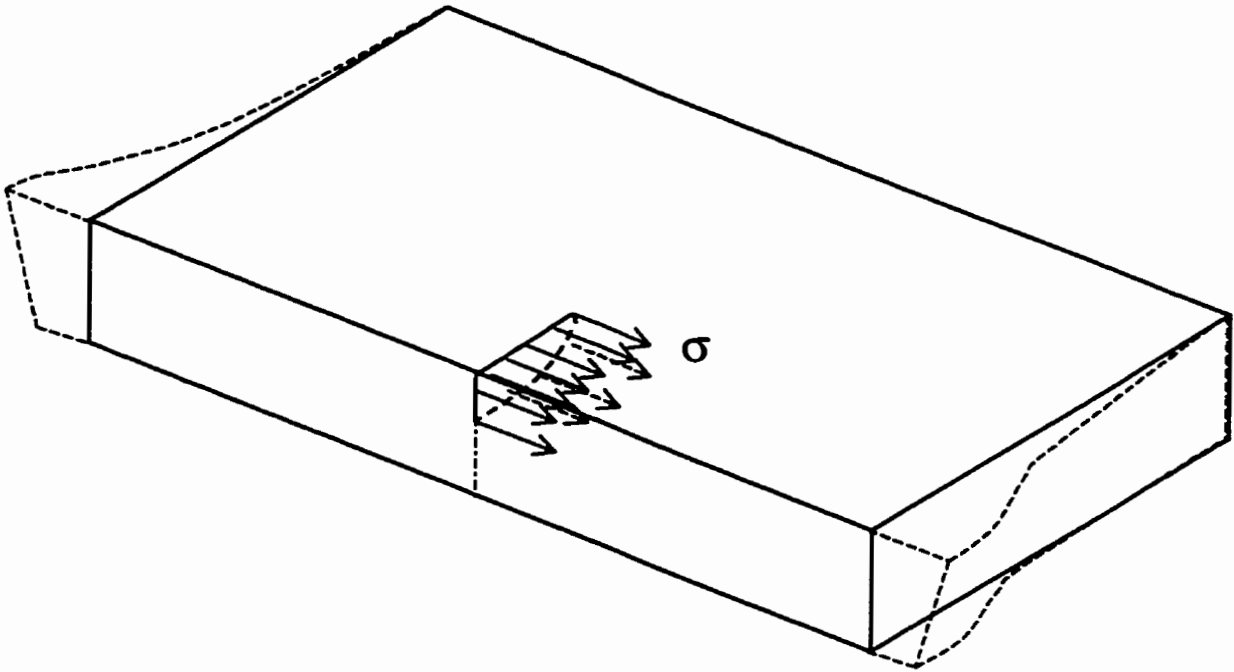
Figure 5.14 Localised displacements δ and θ 

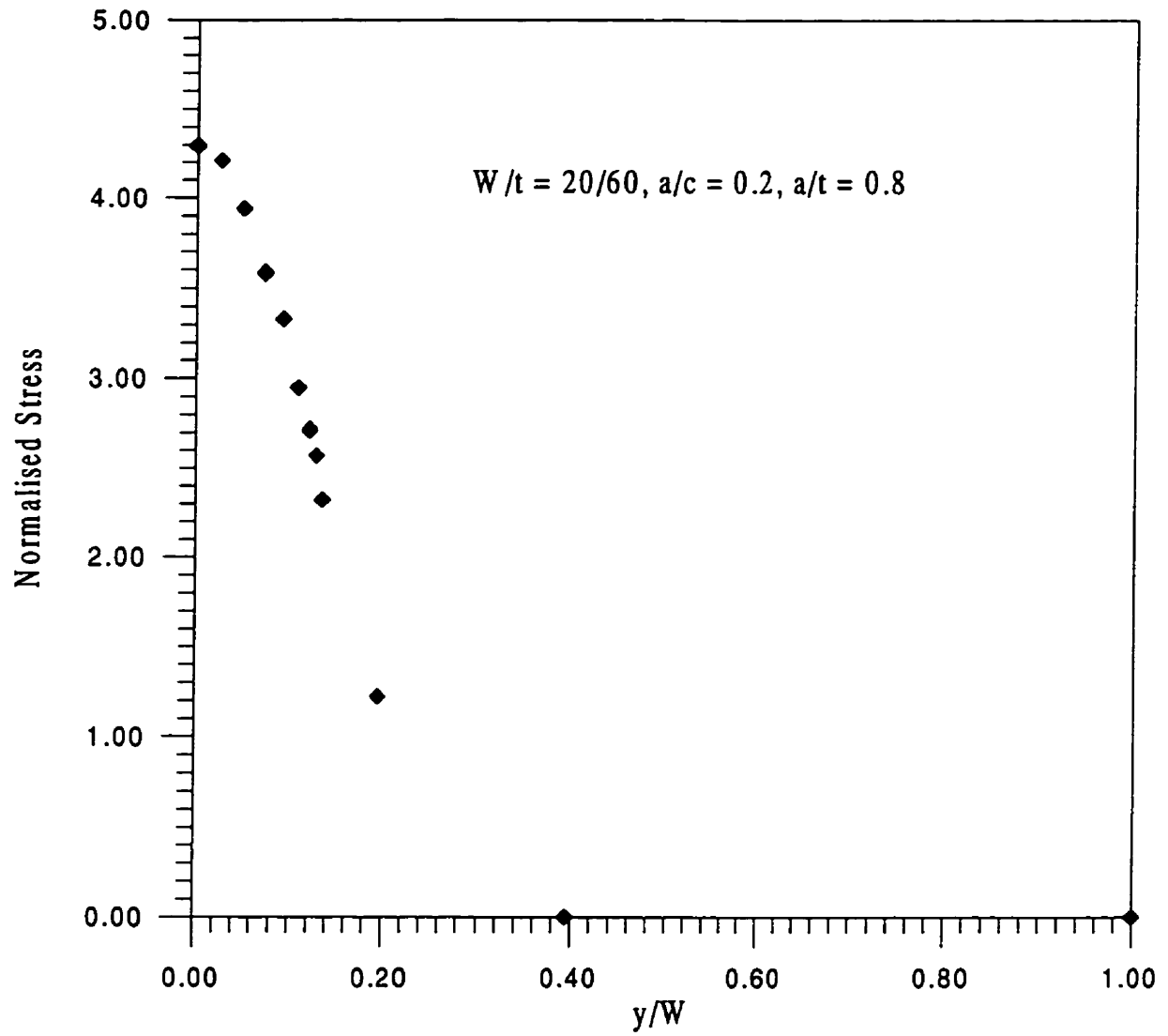
Figure 5.15 Distribution of N' 

Figure 5.16 Deformed mesh

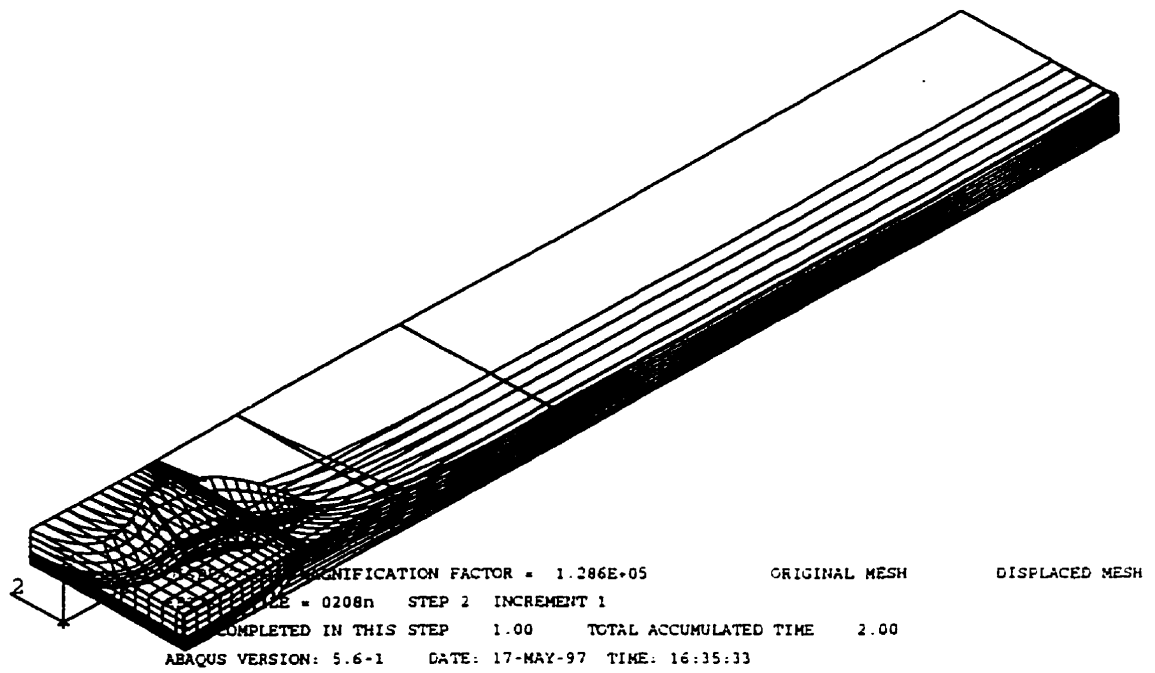


Figure 5.17 Comparison of the stress intensity factors from compliance analysis and finite element data for constant stress distribution $\sigma = \sigma_0$, $a/c = 0.1$, deepest point

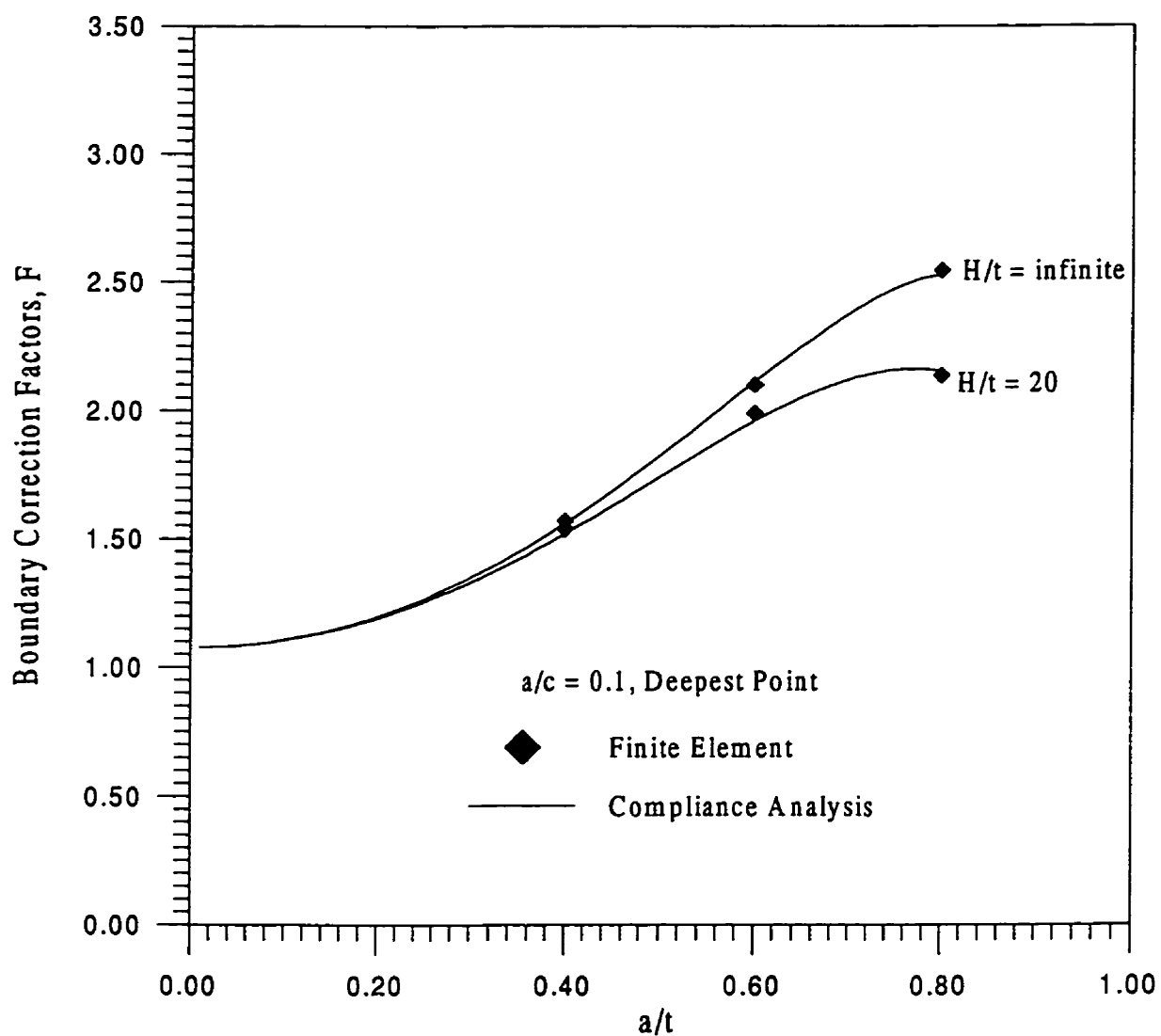


Figure 5.18 Comparison of the stress intensity factors from compliance analysis and finite element data for constant stress distribution $\sigma = \sigma_0$, $a/c = 0.1$, surface point

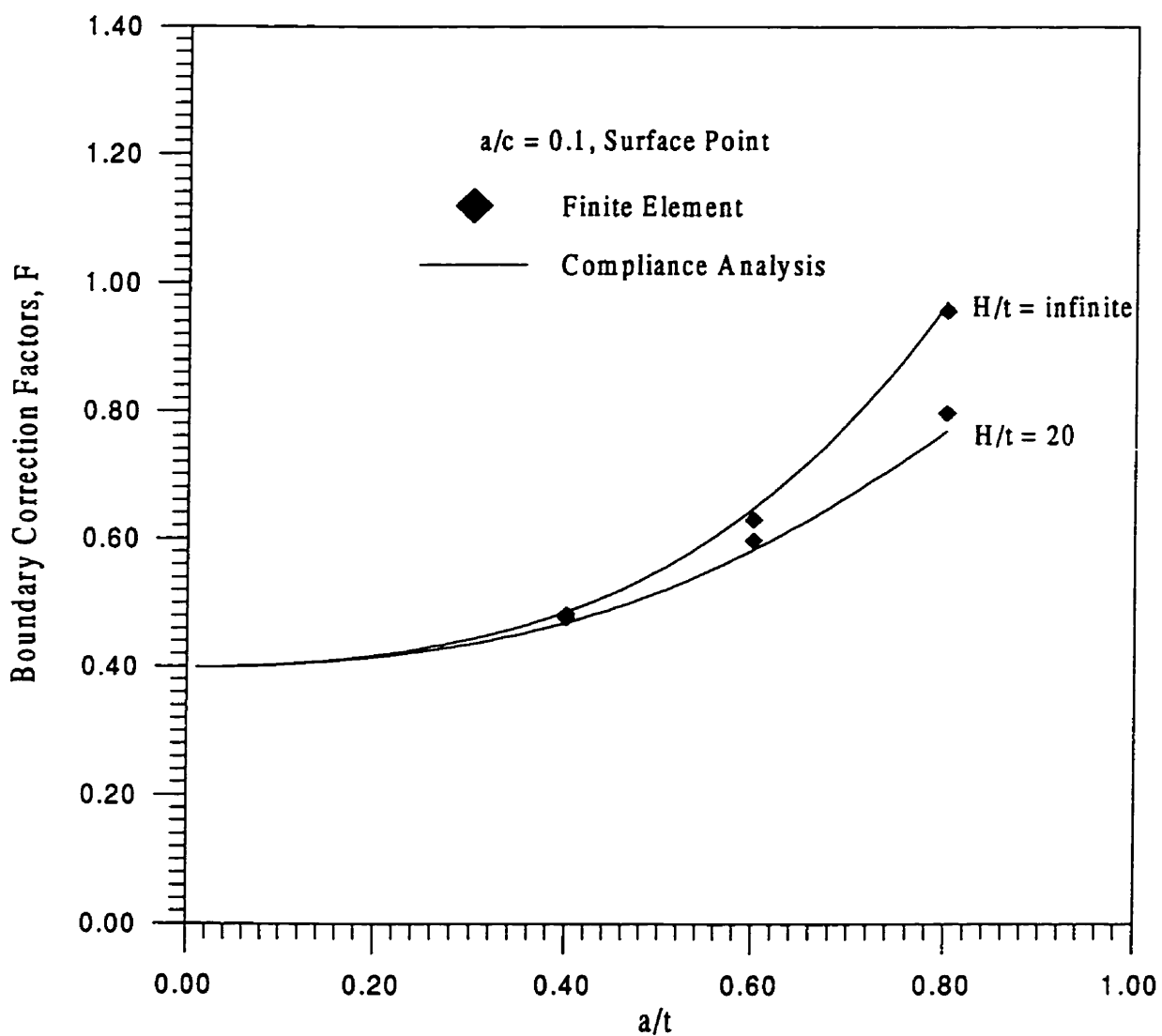


Figure 5.19 Comparison of the stress intensity factors from compliance analysis and finite element data for linear stress distribution $\sigma = \sigma_0(1-x/a)$, $a/c = 0.1$, deepest point

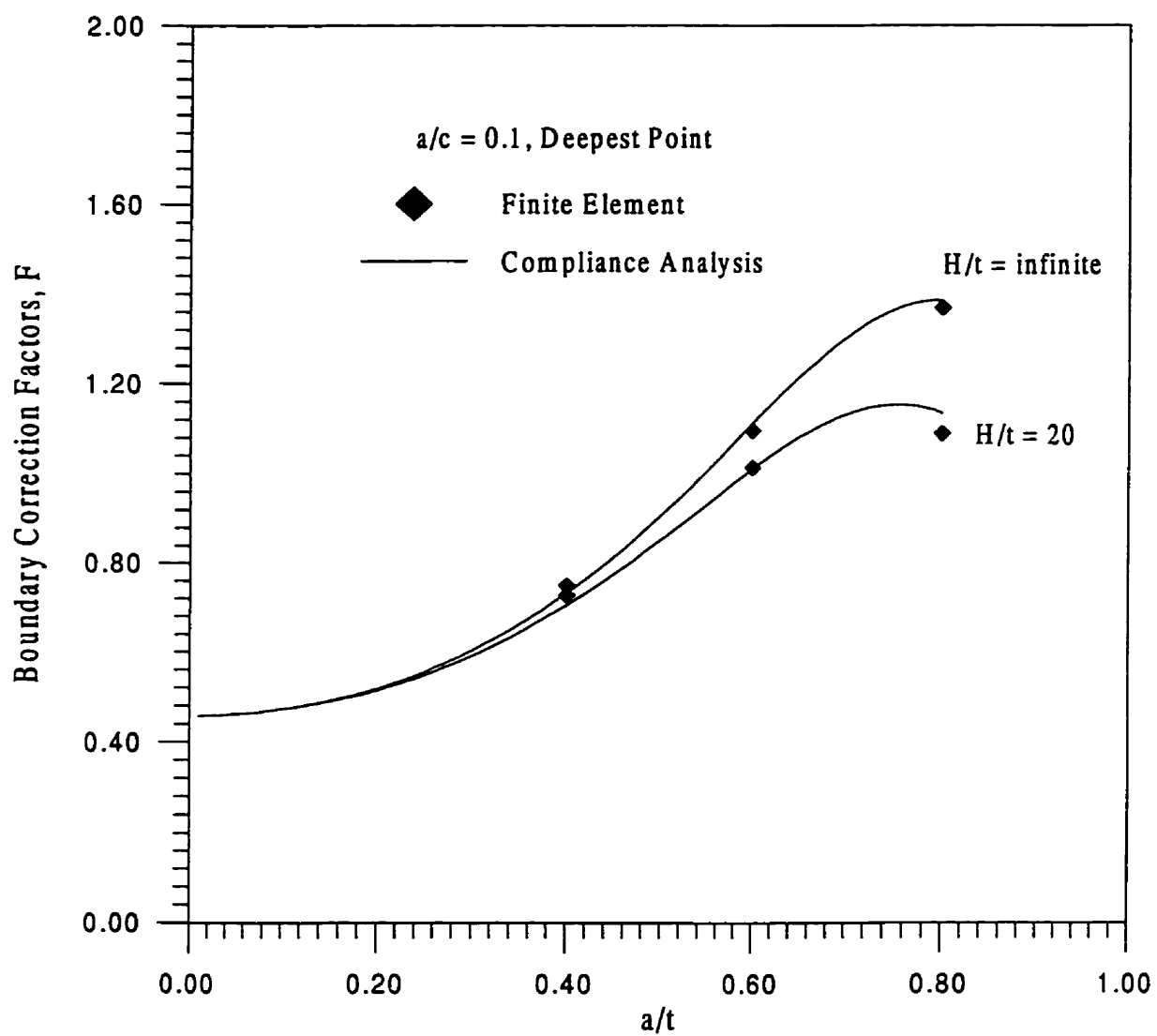


Figure 5.20 Comparison of the stress intensity factors from compliance analysis and finite element data for linear stress distribution $\sigma = \sigma_0(1-x/a)$, $a/c = 0.1$, surface point

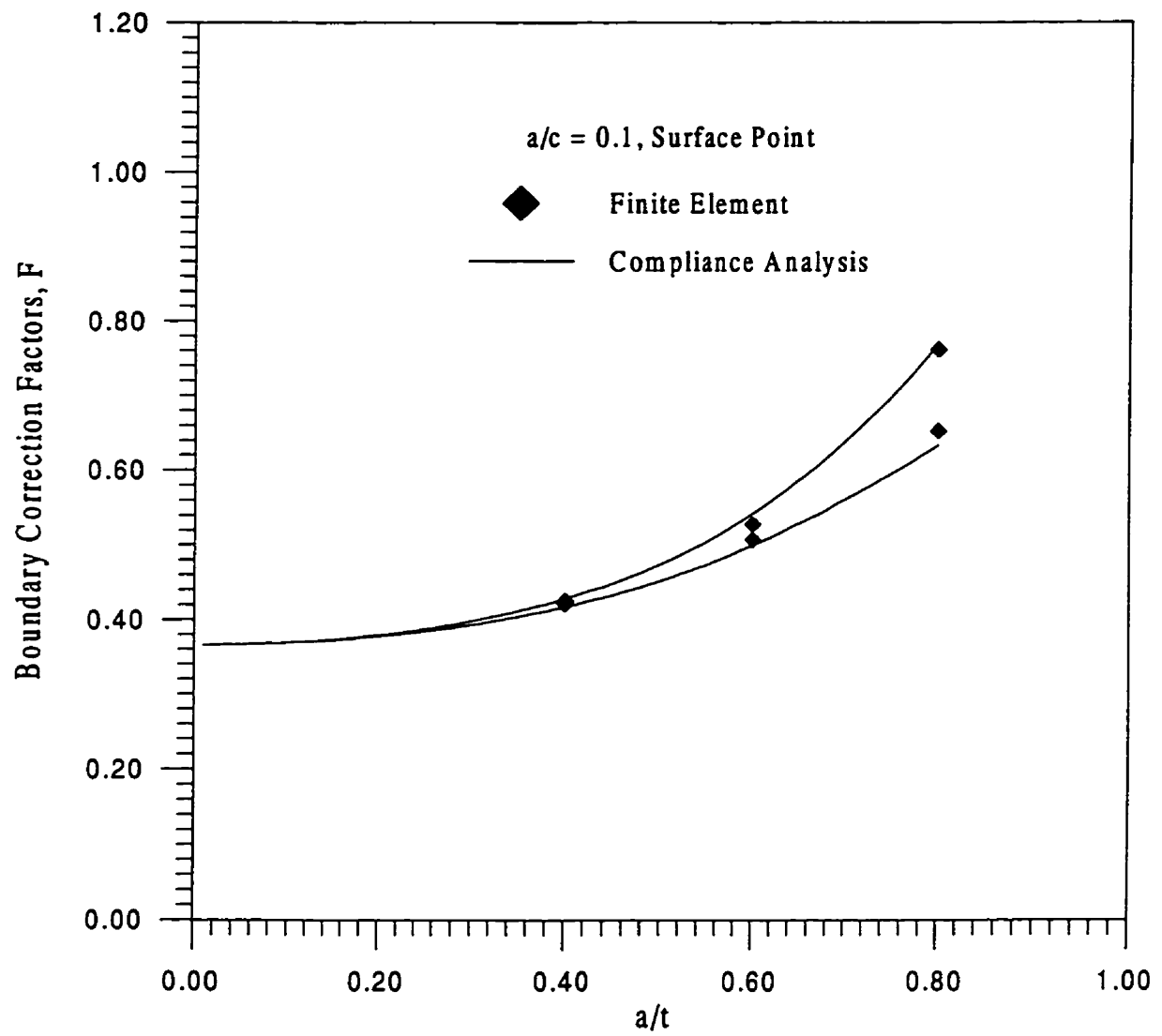


Figure 5.21 Comparison of the stress intensity factors from compliance analysis and finite element data for constant stress distribution $\sigma = \sigma_0$, $a/c = 0.2$, deepest point

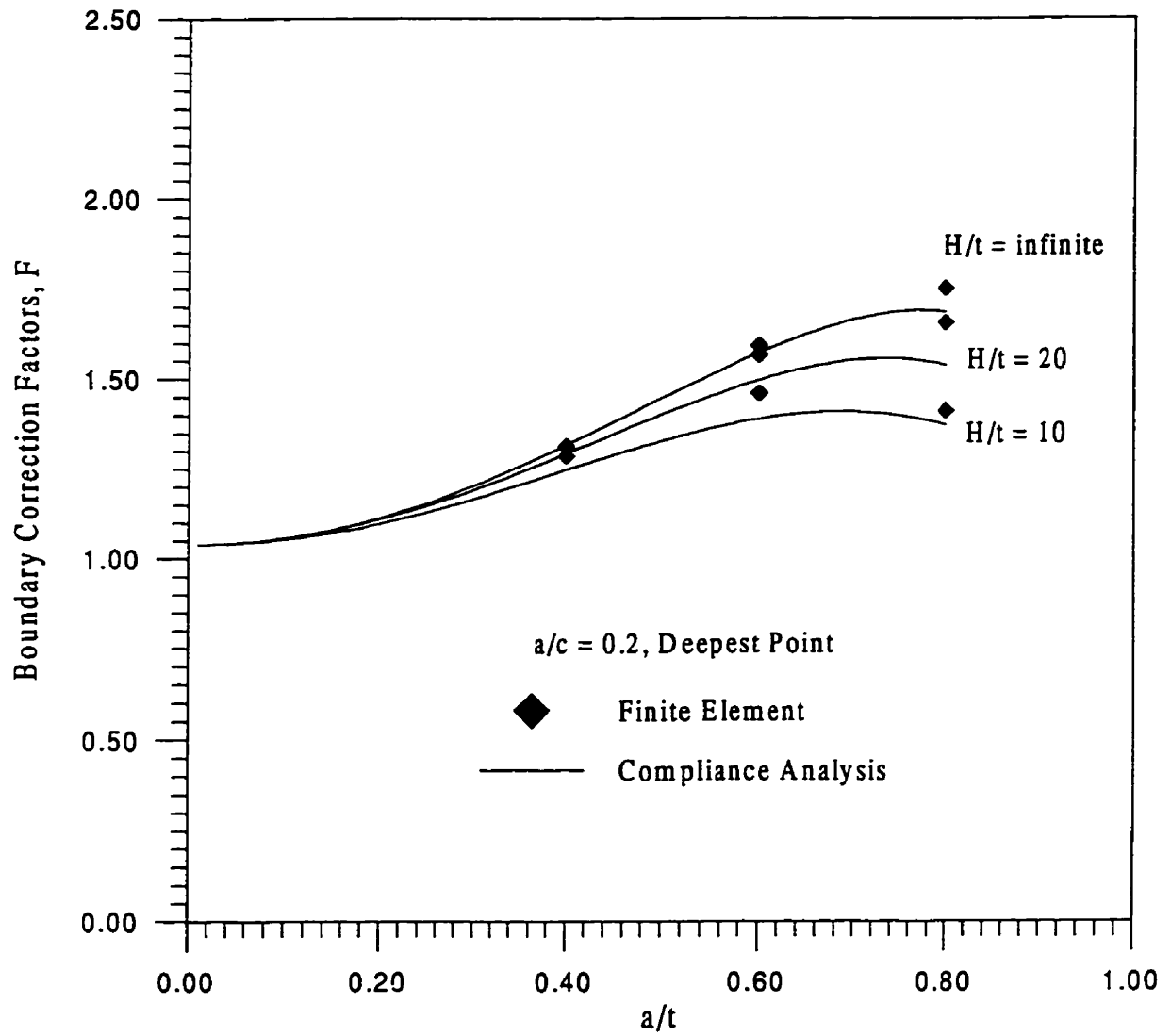


Figure 5.22 Comparison of the stress intensity factors from compliance analysis and finite element data for constant stress distribution $\sigma = \sigma_0$, $a/c = 0.2$, surface point

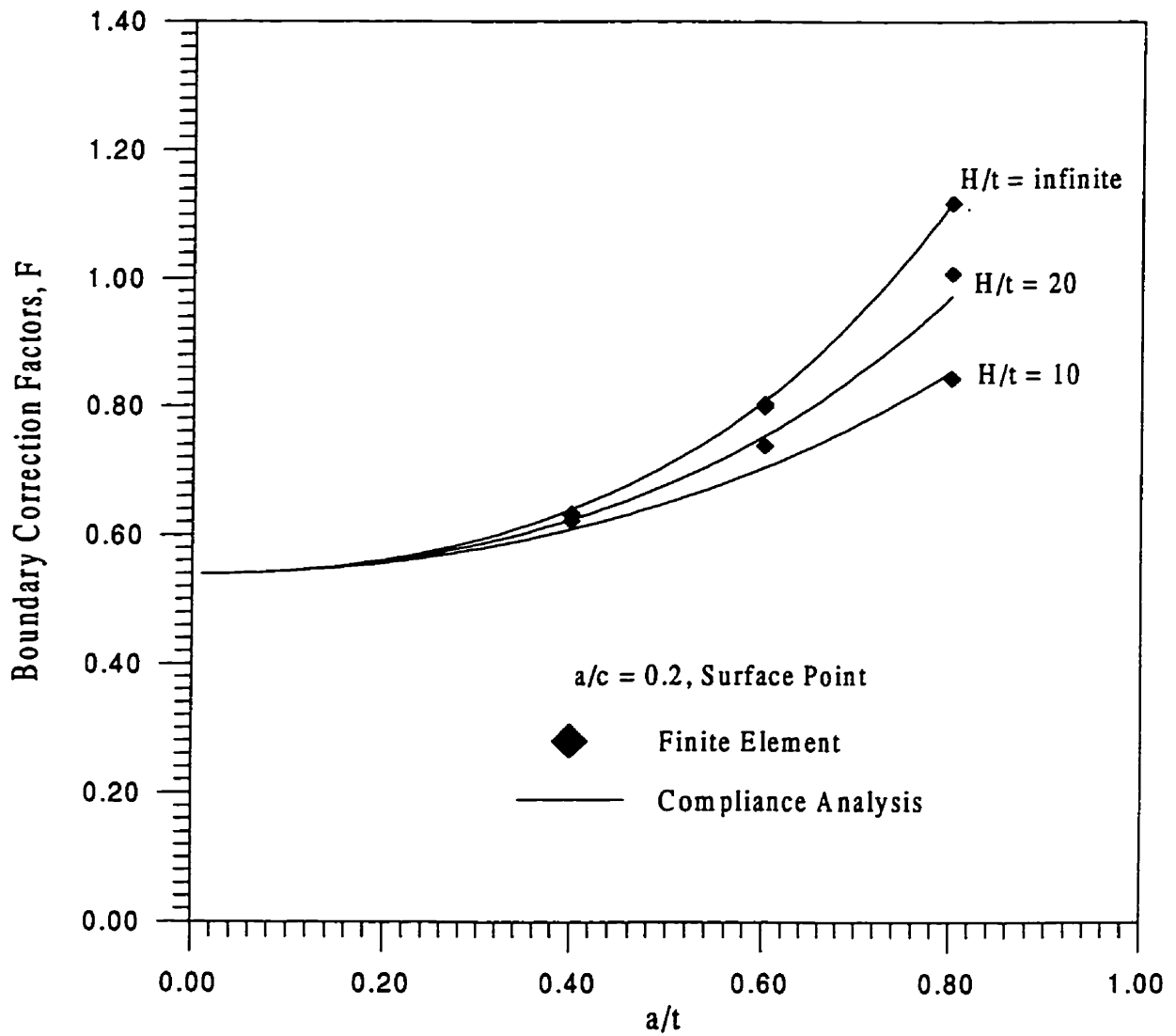


Figure 5.23 Comparison of the stress intensity factors from compliance analysis and finite element data for linear stress distribution $\sigma = \alpha(1-x/a)$, $a/c = 0.2$, deepest point

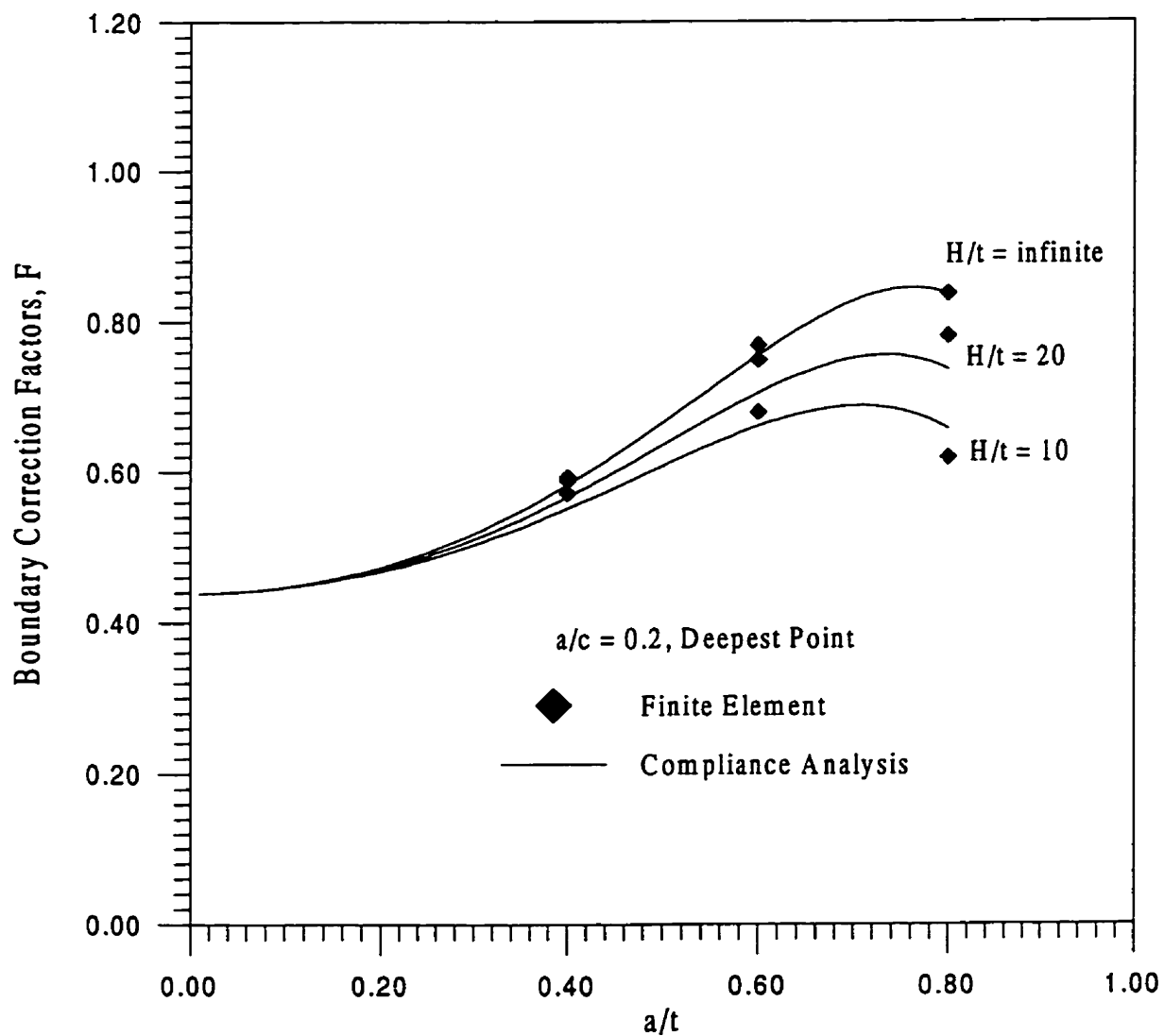


Figure 5.24 Comparison of the stress intensity factors from compliance analysis and finite element data for linear stress distribution $\sigma = \sigma_0(1-x/a)$, $a/c = 0.2$, surface point

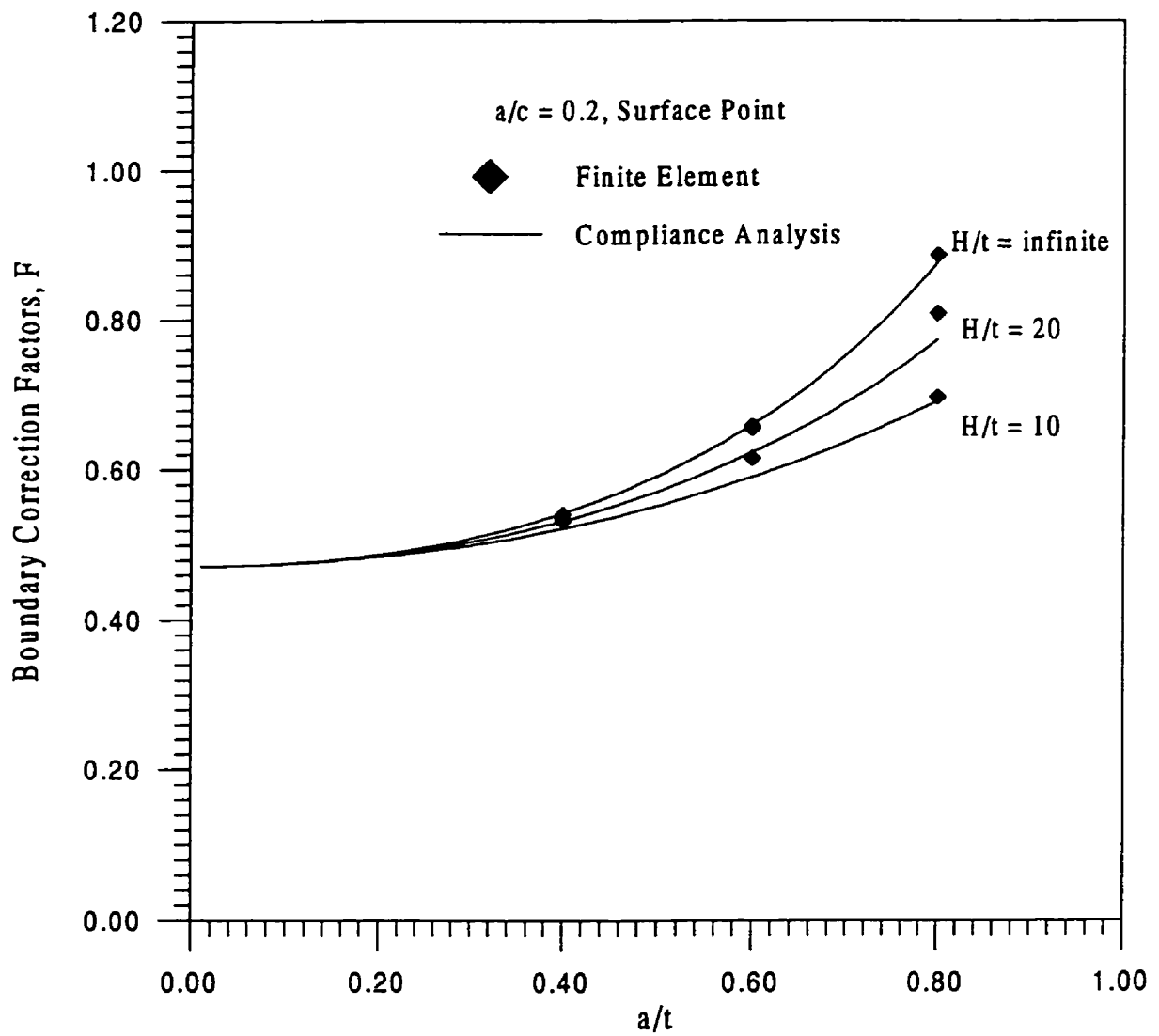


Figure 5.25 Comparison of the stress intensity factors from compliance analysis and finite element data for constant stress distribution $\sigma = \infty$, $a/c = 1.0$, deepest point

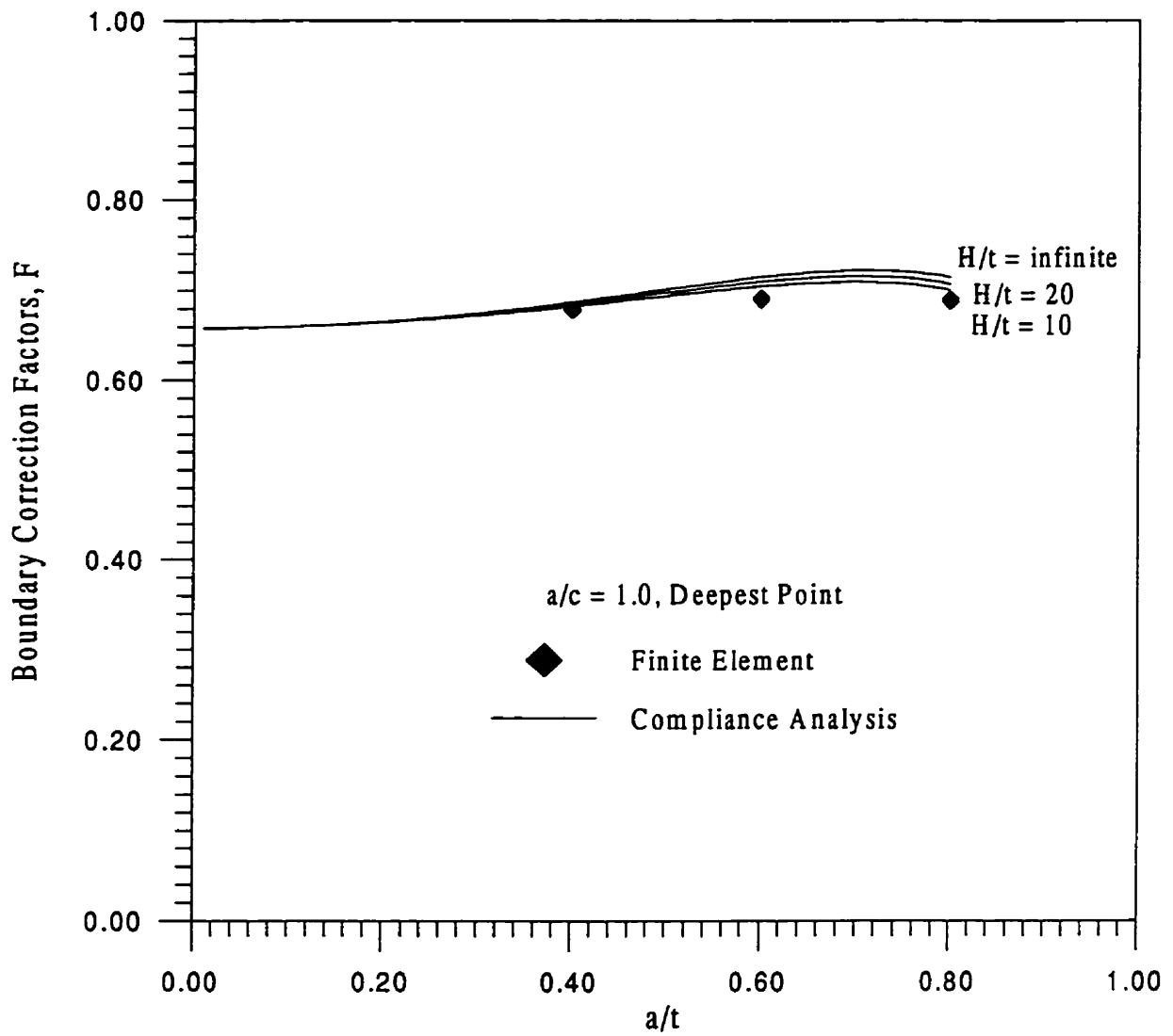


Figure 5.26 Comparison of the stress intensity factors from compliance analysis and finite element data for constant stress distribution $\sigma = \sigma_0$, $a/c = 1.0$, surface point

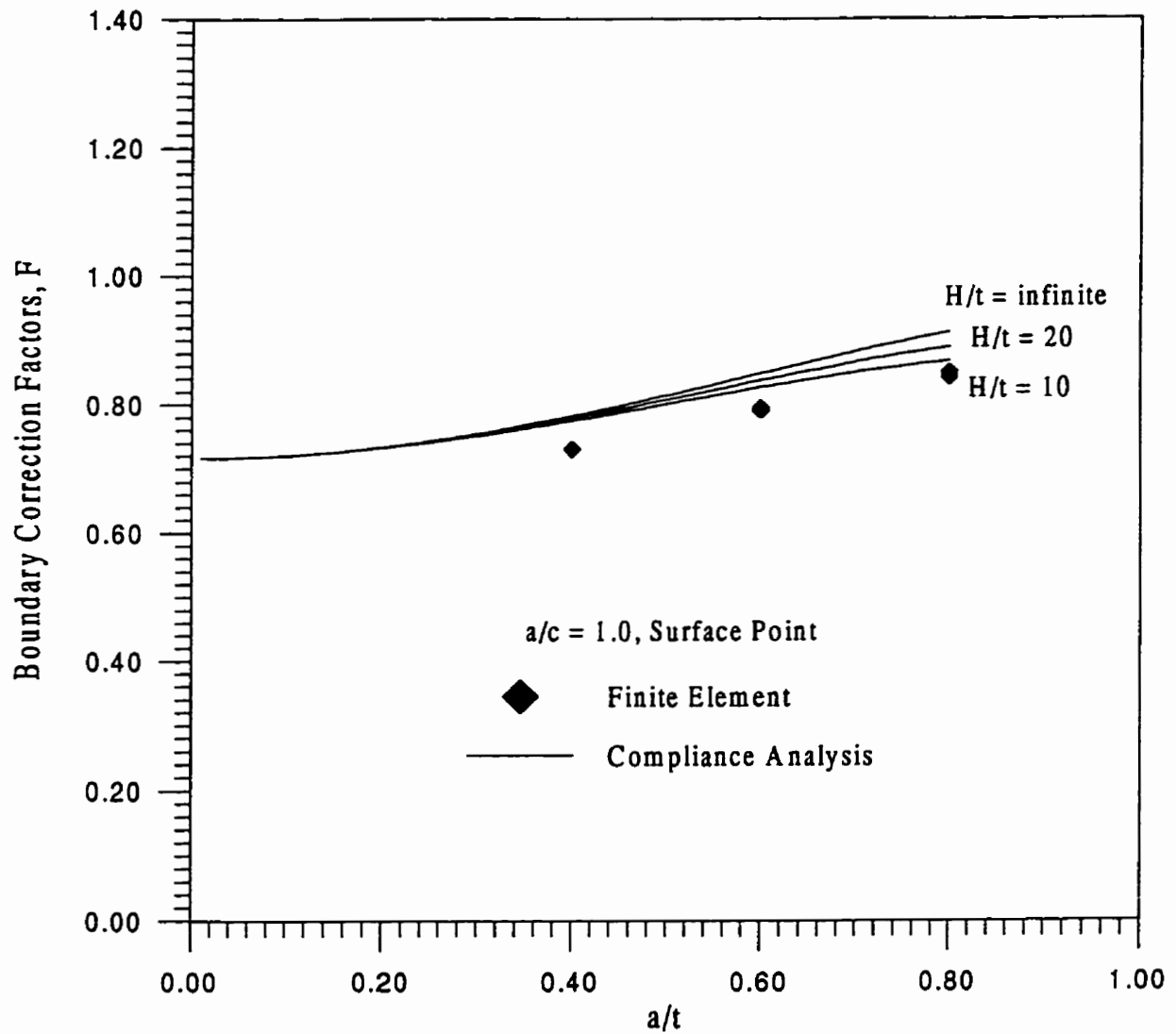


Figure 5.27 Comparison of the stress intensity factors from compliance analysis and finite element data for linear stress distribution $\sigma = \sigma_0(1-x/a)$, $a/c = 1.0$, deepest point

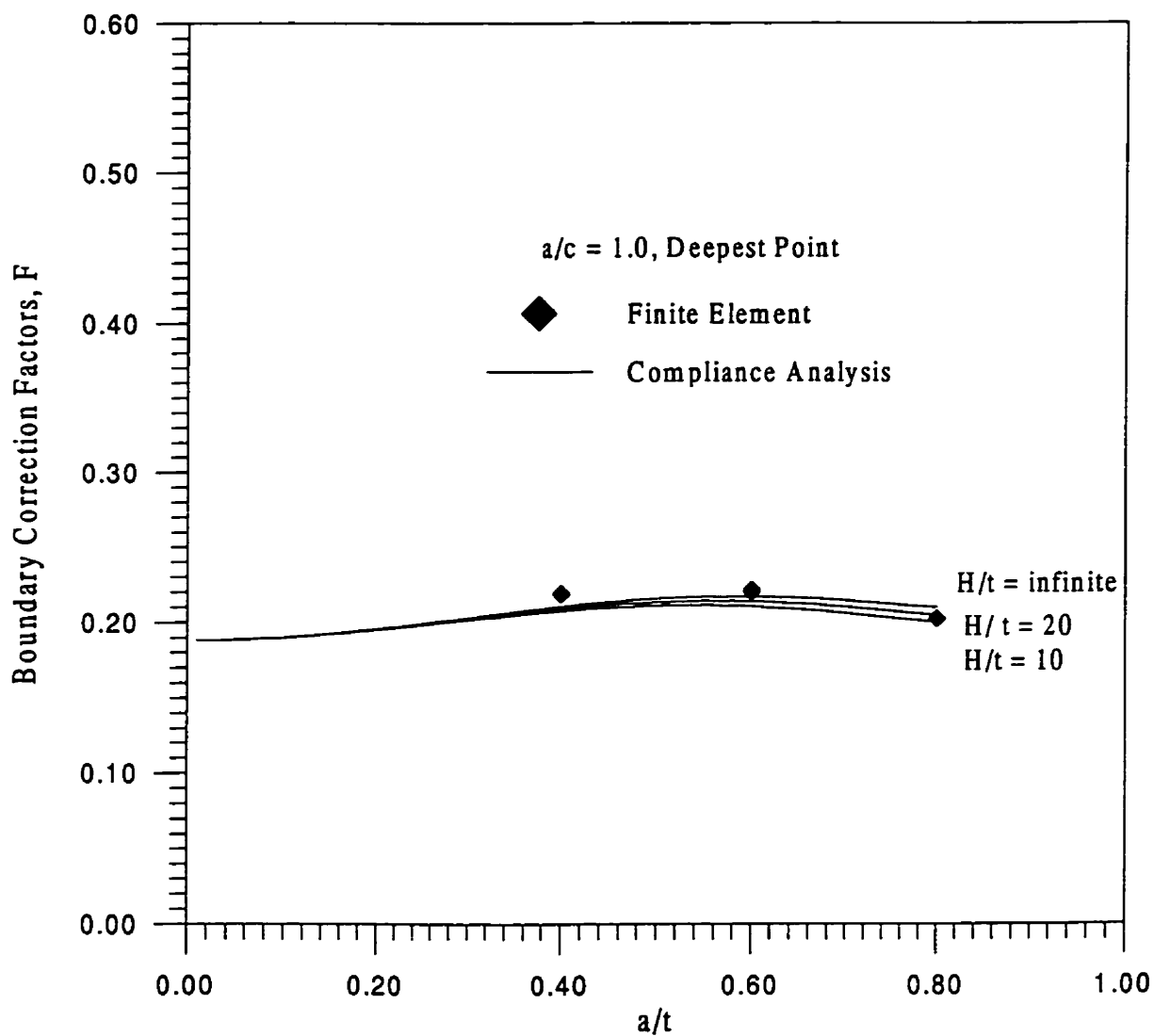


Figure 5.28 Comparison of the stress intensity factors from compliance analysis and finite element data for linear distribution $\sigma = \sigma_0(1-x/a)$, $a/c = 1.0$, surface point

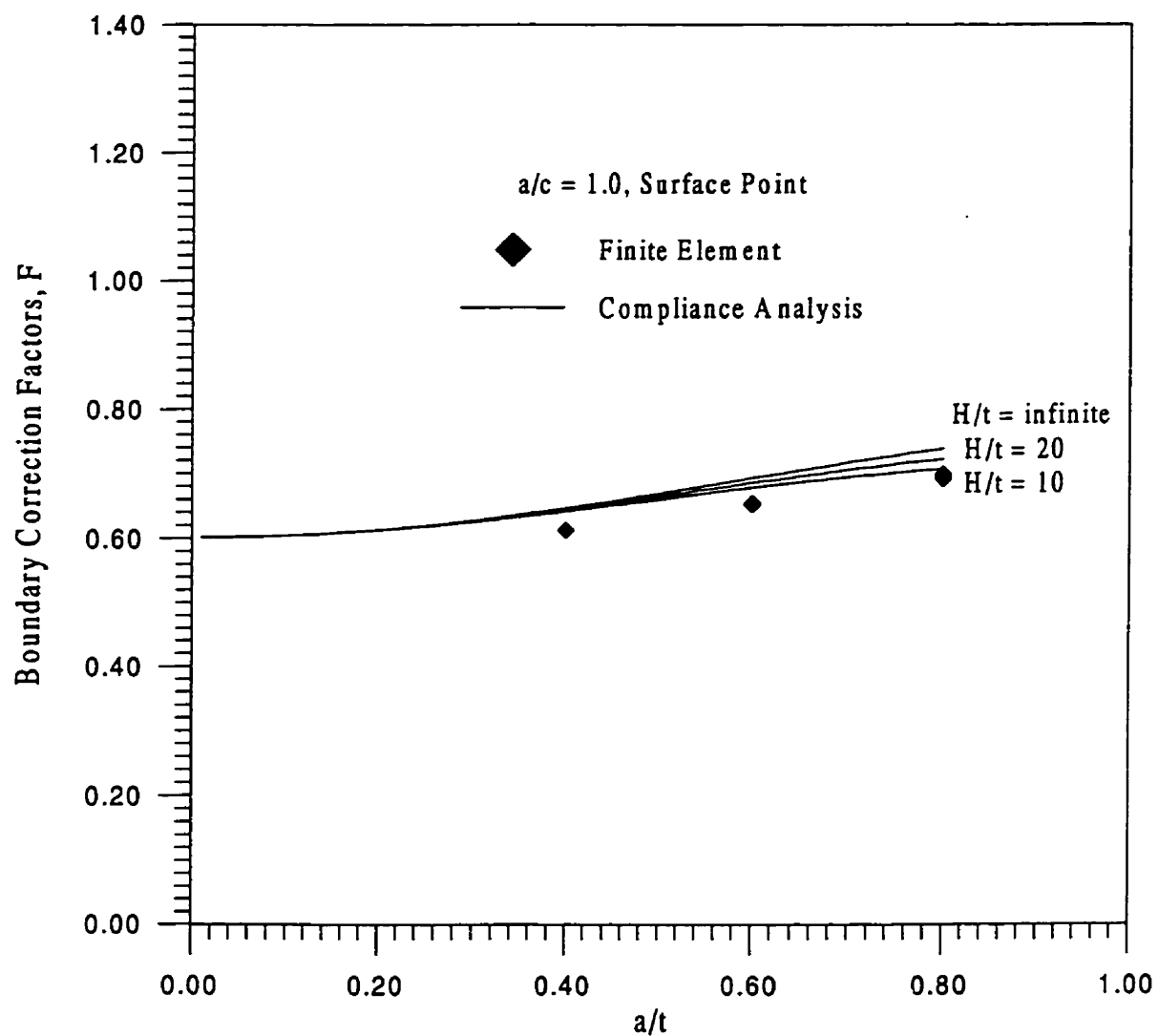


Figure 5.29 Comparison of the stress intensity factors from weight function and finite element data for parabolic stress distribution $\sigma = \alpha(1-x/a)^2$, $a/c = 0.1$, deepest point

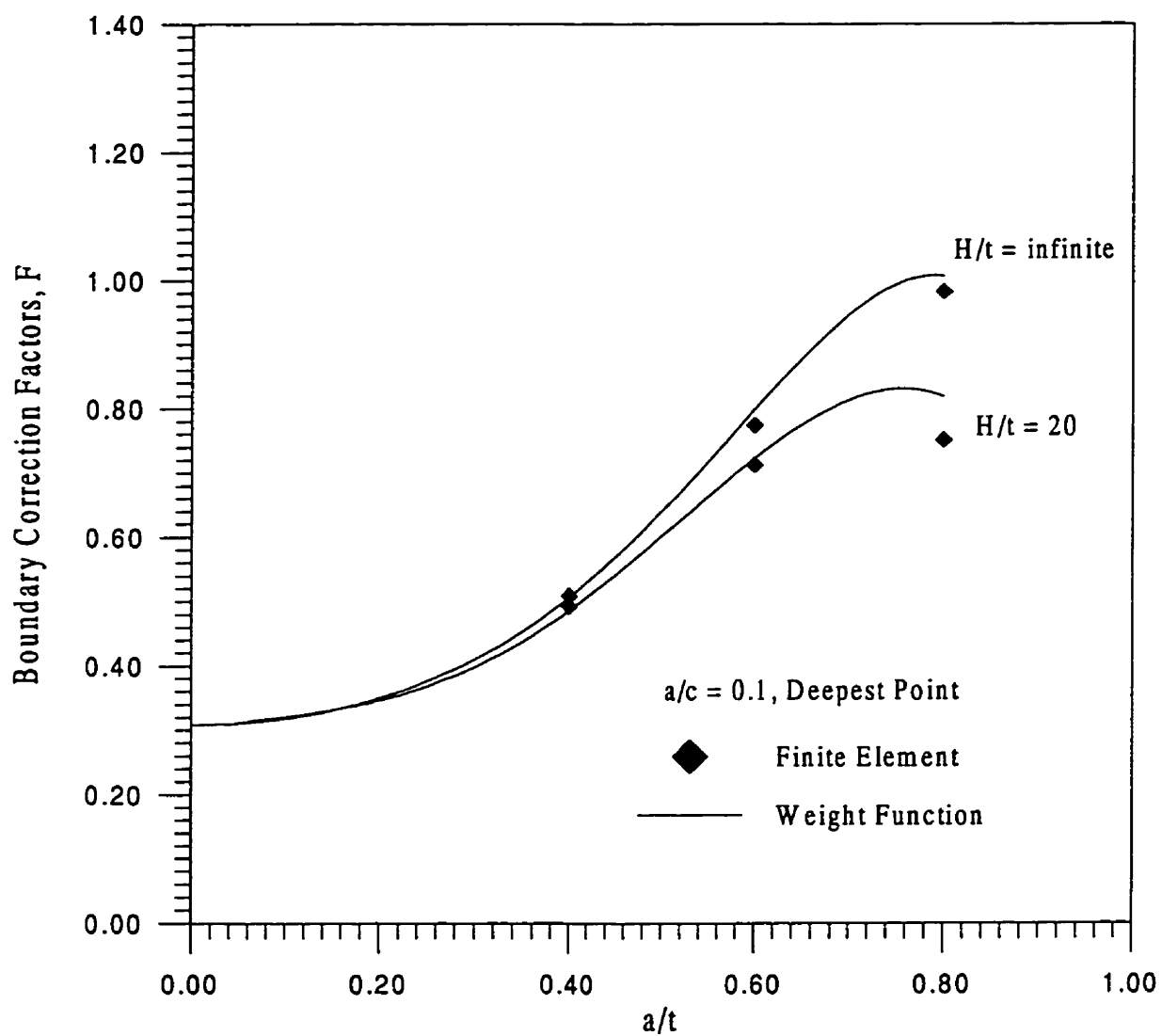


Figure 5.30 Comparison of the stress intensity factors from weight function analysis and finite element data for parabolic stress distribution $\sigma = \sigma_0(1-x/a)^2$, $a/c = 0.1$, surface point

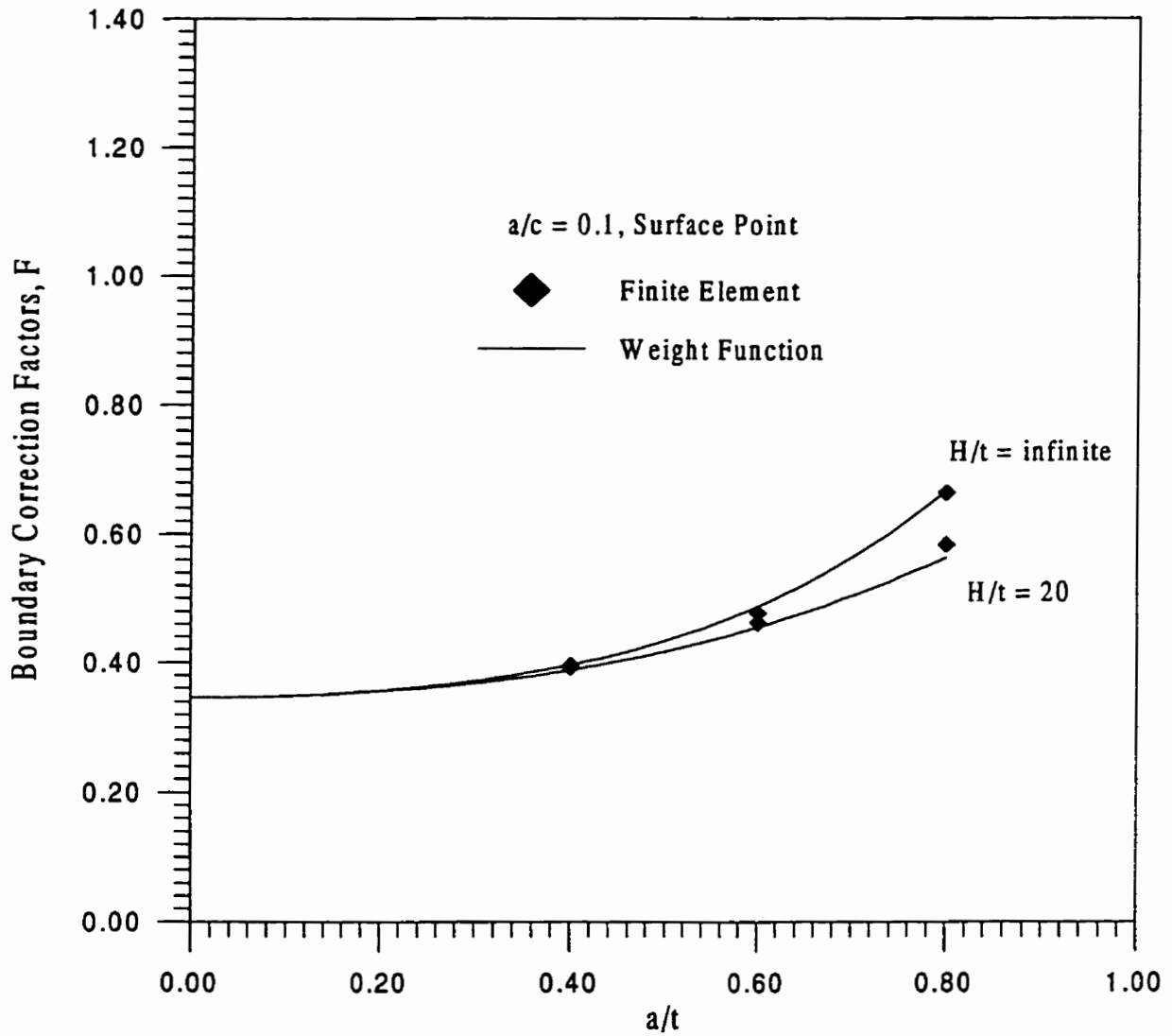


Figure 5.31 Comparison of the stress intensity factors from weight function and finite element data for cubic stress distribution $\sigma = \alpha(1-x/a)^3$, $a/c = 0.1$, deepest point

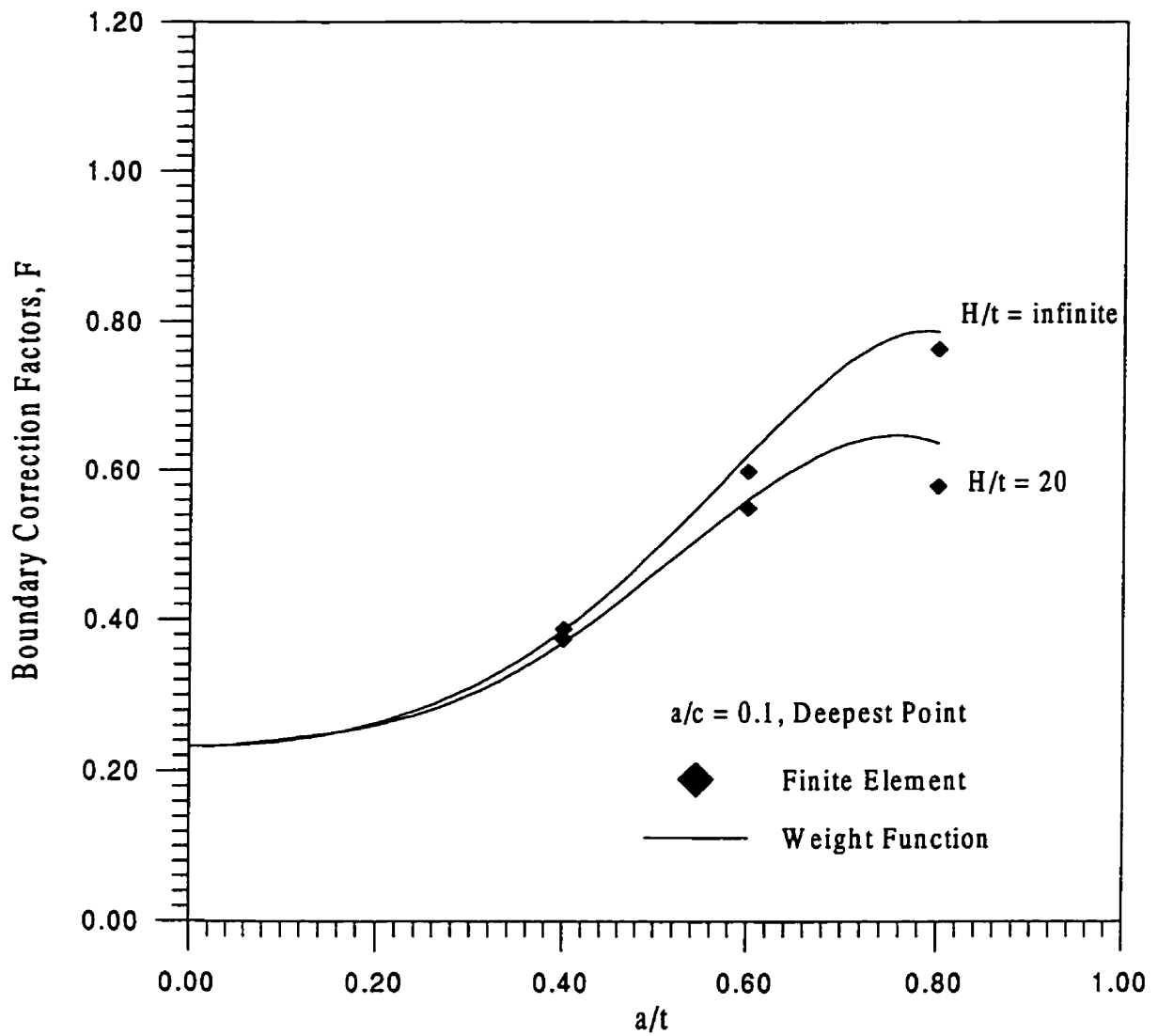
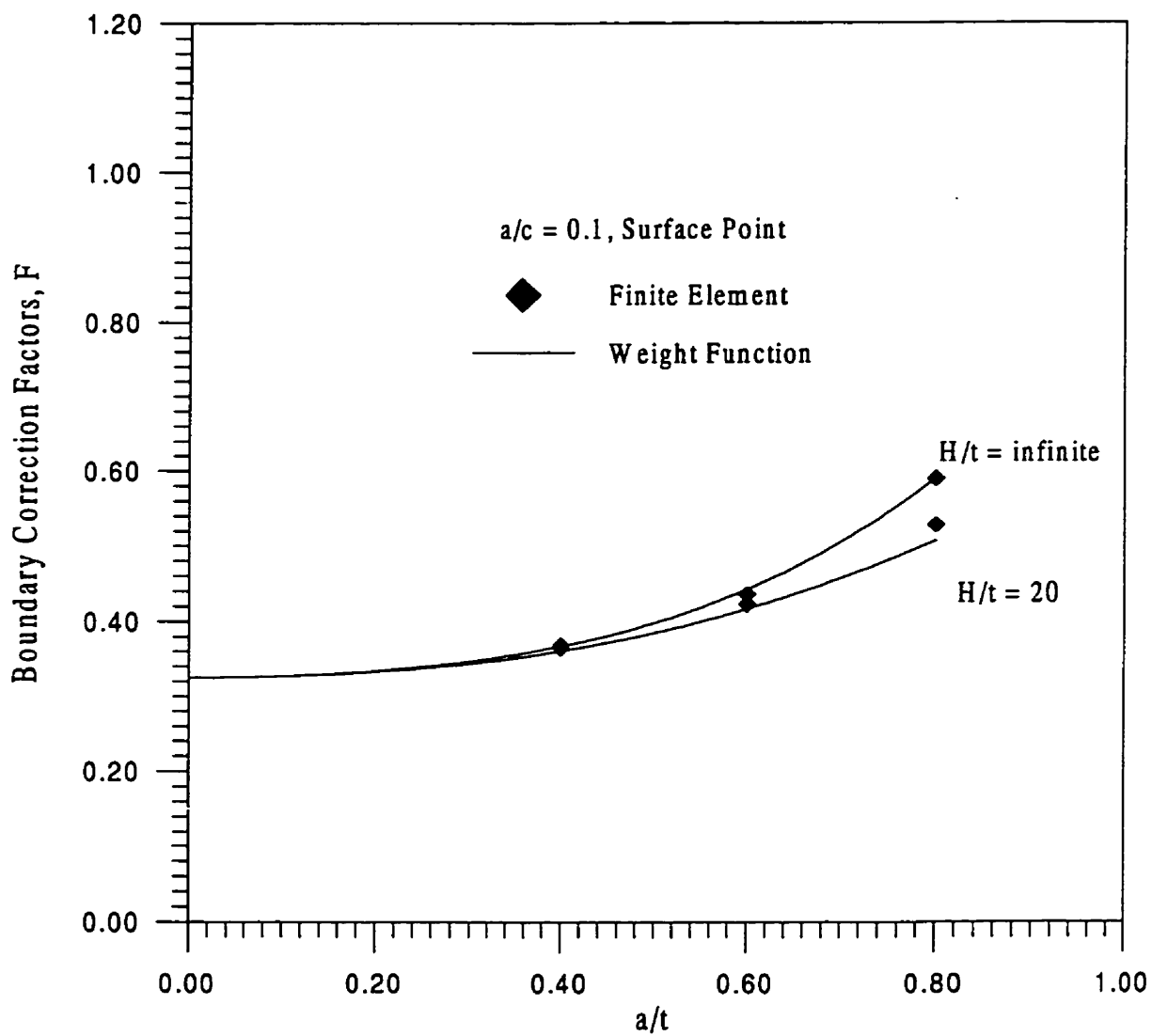


Figure 5.32 Comparison of the stress intensity factors from weight function and finite element data for cubic stress distribution $\sigma \propto (1-x/a)^3$, $a/c = 0.1$, surface point



Chapter 6

Surface Cracks in T-plate Joints

In this chapter, stress intensity factors and weight functions for surface cracks in T-plate joints with free-ends (section 6.1) or built-in ends (section 6.2) are presented.

6.1 Surface Cracks in T-plate Joints with Free Ends

As discussed in section 2.3.2, a T-plate welded joint represents a simple practical welded joint which may be used as a model for more complex welded joint behavior. The calculation of stress intensity factors for surface cracks at the weld toe of these joints is very difficult due to the complex geometry. Several authors (most recently, Fu et al., 1993; Bowness and Lee, 1995; 1996) have conducted detailed 3-D finite element calculations for simple loading conditions, i.e., far field tension and bending. However, in instances where cracks are subjected to thermally induced stresses or residual stresses (which is often the case for weld toe cracks), more complex stress distributions must be considered.

To date, the only weight functions developed specifically for semi-elliptical surface cracks in T-plate joints are those of Niu and Glinka (1990a, b). Weight functions at the deepest point of a surface crack in T-plate joints with a weld angle of 45 degrees were developed based on approximate stress intensity factor solutions. These solutions are restricted to the deepest point of the surface crack; no solutions are available for the surface points. In the absence of such data, most researchers (Lecsek et al., 1995; Brennean et al., 1996) use weight functions developed for flat plates in conjunction with T-plate stress distributions to estimate required stress intensity factors. While it is expected that such estimates will improve as the welded angle is decreased, little data is available to quantify these errors.

In the present section, weight functions at the deepest and surface points of a semi-elliptical surface crack in T-plate joints with weld angle between 0 and 45° are derived. Stress intensity factors for any one-dimensional stress field can be calculated from Eq.(2.6):

$$K(P') = \int_0^a \sigma(x)M(x;P')dx \quad (2.6)$$

Here P' is the general point along crack front, either A or B in Figure 6.1 in this case.

Weight functions $M(x; A)$ and $M(x; B)$ were derived in the form of Eqs.(2.11) and (2.12):

$$M(x, a; A) = \frac{2}{\sqrt{2\pi(a-x)}} \left[1 + M_{1A} \left(1 - \frac{x}{a}\right)^{\frac{1}{2}} + M_{2A} \left(1 - \frac{x}{a}\right) + M_{3A} \left(1 - \frac{x}{a}\right)^{\frac{3}{2}} \right] \quad (2.11)$$

$$M(x, \alpha; B) = \frac{2}{\sqrt{\pi a}} \left[1 + M_{1B} \left(\frac{x}{a} \right)^{\frac{1}{2}} + M_{2B} \left(\frac{x}{a} \right) + M_{3B} \left(\frac{x}{a} \right)^{\frac{3}{2}} \right] \quad (2.12)$$

The parameters were determined from two reference stress intensity factors and the conditions represented by Eqs.(2.13) and (2.14):

$$M_{2A} = 3 \quad (2.13)$$

$$M_{1B} + M_{2B} + M_{3B} + 1 = 0 \quad (2.14)$$

In order to determine and validate the weight functions, $M(x; A)$ and $M(x; B)$, reference stress intensity factors were required. Three dimensional finite element calculations were conducted to calculate stress intensity factors of surface cracks in T-plate joints. In all cases, the weldment located at one side only, the attachment plate thickness plus the weld leg length was equal to the base plate thickness, and overall weld angles was 30° or 45° (Figure 6.1). The resulting stress intensity factors for two basic loading cases were used as reference solutions to derive the weight functions. These weight functions were then validated using solutions for other loading cases.

6.1.1 Stress Intensity Factor Solutions

Finite Element Model

Three dimensional finite elements were used to model the symmetric half of a T-plate joint containing a semi-elliptic surface crack. Figure 6.1 shows the geometry and the co-ordinate system used. As for the flat plate analyses (Chapter 5), the finite element analyses were made

using ABAQUS version 5.4 (HKS, 1996) with 20-noded isoparametric three-dimensional solid elements and reduced integration. In order to model the square root singularity at the crack tip, three-dimensional prism elements with four mid-side nodes at the quarter points (a degenerate cube with one face collapsed) were used and the separate crack tip nodal points were constrained to have the same displacement (Barsoum, 1977).

The stress intensity factor, K , was calculated from the J -integral which in turn was calculated using the domain integral method (Moran and Shih, 1987). The plane strain relationship between J and K was used to calculate K . The analyses were made with a linear elastic material model with a Young's modulus, E , of 207 GPa and Poisson's ratio, ν of 0.3.

The loads were applied directly to the crack surface. Two types of loading, corresponding to $n = 0$ or 1 in the following equation, were applied to each crack geometry:

$$\sigma(x, y) = \sigma_0 \left(1 - \frac{x}{a}\right)^n \quad (6.1)$$

where σ_0 is the nominal stress, a is the crack depth and x is the distance from the weld toe. In addition, for the purpose of verification of the finite element models and validation of the weight functions, four more types of load were applied for certain geometries: stresses applied to the crack face using $n = 2$ or 3 in Eq. (6.1), or far field tension or bending.

Note that due to the lack of symmetry on the crack plane in the T-plate joint geometry, mode-II and mode-III singularities exist along the crack front. The J -integral estimation will include their effects. However, in the present T-plate geometries, the mode-I singularity dominates, and the J estimation is based on a mode-I crack increment. Therefore, the stress

intensity factor results determined from J were regarded as mode-I stress intensity factor values (Fu *et al.*, 1993).

The mesh generator developed for surface cracked plate was modified to generate all required input files for the analysis. First, the mesh for a surface crack in a flat plate was developed. Then the weld toe and attachment were added to the flat plate mesh. A typical model for the present analysis is illustrated in Figure 6.2 and used about 30,000 degrees-of-freedom.

The stress intensity factor results have been normalised as follows,

$$F = \frac{K}{\sigma_0 \sqrt{\pi a} / Q} \quad (6.2)$$

where F is the boundary correction factor, Q is the shape factor of an ellipse, given by the square of the complete elliptic integral of second kind. The empirical equation for Q , Eq. (2.3) was used

$$Q = 1.0 + 1.464 \left(\frac{a}{c}\right)^{1.65}, \quad \text{for } 0 \leq a/c \leq 1.0: \quad (2.3)$$

Verification of the Finite Element Model

The present finite element model for surface cracks in T-plate joints used a similar degree of refinement to that used for surface cracks in flat plates (Chapter 5). Stress intensity factors were calculated for several geometries ($a/c = 0.2$ or 1.0 and $a/t = 0.1, 0.2, 0.4$ or 0.6 with a 45° weld angle) under far field tension and bending. The resulting stress intensity factors were used

to calculate weld toe magnification factors for comparisons with published results from Bowness and Lee (1996). The differences were generally within 10%, which is comparable to their stated accuracy (Bowness and Lee, 1995). Figures 6.3-6.7 show comparisons at the deepest point and at the surface point for tension and bending cases. Based on these results and previous experience, the accuracy of the present finite element calculations is expected to be within 10 percent of the actual solutions.

Results for Stress Intensity Factors

Stress intensity factors for semi-elliptical surface cracks ($a/c = 0.05, 0.1, 0.2, 0.4, 0.6$ or 1.0) in a T-plate joint with a 30 or 45 degree weld angle with relative crack depths, a/t , of 0.1, 0.2, 0.4, or 0.6, subjected to stress distributions corresponding to $n = 0$ or 1 as expressed in Eq. (6.1) were determined to facilitate the generation of suitable weight functions. The results are summarised in Tables 6.1 and 6.2. In addition, stress intensity factors for cracks with aspect ratios of $a/c = 0.2$ or 1.0 in a T-plate joint with a 30 or 45 degree weld angle and relative crack depths, a/t , of 0.1, 0.2, 0.4 or 0.6 subjected to stress distributions corresponding to $n = 2$ or 3 as expressed in Eq. (6.1) or subjected to far field tension or bending were also determined to assist in the verification of the weight functions derived from the above results. These results are summarised in Tables 6.3 to 6.5.

Note that the stress intensity factors for a surface crack in a flat plate geometry correspond to a T-plate joint with a 0 degree weld angle. Stress intensity factors for surface cracks in flat plates obtained by the author (Wang and Lambert, 1995) were used in the present work.

6.1.2 Derivation of Weight Functions

Determination of $M(x; A)$ and $M(x; B)$.

Weight functions $M(x; A)$ and $M(x; B)$ were derived in the form of eqs.(2.11) and (2.12). The parameters were determined from reference stress intensity factors and the conditions represented by eqs.(2.13) and (2.14).

The weight function at the deepest point: $M(x; A)$

In order to determine $M(x; A)$ using Eq.(2.11), two reference solutions were used to determine M_{1A} , M_{2A} and M_{3A} : constant or linearly decreasing stress through the thickness corresponding to $n = 0$ or $n = 1$ in Eq. (6.1).

Reference stress intensity factors. For the deepest point of a surface crack, the numerical solutions for T-plate joints with weld angles of 30 degrees ($\pi/6$) and 45 degrees ($\pi/4$) presented previously, together with the flat plate results from Wang and Lambert (1995), were approximated by empirical formulas fitted with an accuracy of 5% or better. The results for an a/t ratio of 0 were obtained by smooth extrapolation. The choice of equations for the extrapolation was based on engineering judgement, but relied heavily on the forms used by Newman and Raju (1981). The range of applicability for these equations is $0.05 \leq a/c \leq 1.0$, $0 \leq a/t \leq 0.6$ and weld angles from 0 to 45 degrees.

The results for a stress distribution constant through the thickness

$$\sigma(x, y) = \sigma_0 \tag{6.3}$$

are

$$K_{Ir}^A = \sigma_0 \sqrt{\frac{\pi a}{Q}} Y_0\left(\frac{a}{c}, \frac{a}{t}\right) \cdot M_{A0}\left(\phi, \frac{a}{c}, \frac{a}{t}\right) \quad (6.4)$$

where Y_0 represents the boundary correction factors for cracks in a flat plate:

$$Y_0\left(\frac{a}{c}, \frac{a}{t}\right) = B_0 + B_1\left(\frac{a}{t}\right)^2 + B_2\left(\frac{a}{t}\right)^4 + B_3\left(\frac{a}{t}\right)^6$$

$$B_0 = 1.0929 + 0.2581\left(\frac{a}{c}\right) - 0.7703\left(\frac{a}{c}\right)^2 + 0.4394\left(\frac{a}{c}\right)^3$$

$$B_1 = 0.456 - 3.045\left(\frac{a}{c}\right) + 2.007\left(\frac{a}{c}\right)^2 + \frac{1.0}{0.147 + \left(\frac{a}{c}\right)^{0.688}}$$

$$B_2 = 0.995 - \frac{1.0}{0.027 + \left(\frac{a}{c}\right)} + 22.000\left(1.0 - \frac{a}{c}\right)^{9.953}$$

$$B_3 = -1.459 + \frac{1.0}{0.014 + \frac{a}{c}} - 24.211\left(1.0 - \frac{a}{c}\right)^{8.071}$$

and M_{A0} accounts for the effect of the attachments with different weld angles:

$$M_{A0}\left(\phi, \frac{a}{c}, \frac{a}{t}\right) = \frac{(\phi - 45)(\phi - 30)}{1350} - \frac{\phi(\phi - 45)}{450} M_{A0}^{\pi/6}\left(\frac{a}{c}, \frac{a}{t}\right) + \frac{\phi(\phi - 30)}{675} M_{A0}^{\pi/4}\left(\frac{a}{c}, \frac{a}{t}\right)$$

$$\begin{aligned}
M_{\lambda_0}^{\pi/6} \left(\frac{a}{c}, \frac{a}{t} \right) &= 0.9037 + 0.2624 \left(\frac{a}{t} \right) - 0.1294 \left(\frac{a}{c} \right) + 0.1173 \left(\frac{a}{t} \right)^2 \\
&+ 0.4350 \left(\frac{a}{c} \right)^2 - 0.4415 \left(\frac{a}{t} \right) \left(\frac{a}{c} \right) - 0.3409 \left(\frac{a}{t} \right)^3 - 0.2428 \left(\frac{a}{c} \right)^3 \\
&+ 0.02994 \left(\frac{a}{t} \right) \left(\frac{a}{c} \right)^2 + 0.3122 \left(\frac{a}{t} \right)^2 \left(\frac{a}{c} \right)
\end{aligned}$$

$$\begin{aligned}
M_{\lambda_0}^{\pi/4} \left(\frac{a}{c}, \frac{a}{t} \right) &= 0.8727 + 0.5252 \left(\frac{a}{t} \right) - 0.2497 \left(\frac{a}{c} \right) - 0.3144 \left(\frac{a}{t} \right)^2 \\
&+ 0.7695 \left(\frac{a}{c} \right)^2 - 0.81028 \left(\frac{a}{t} \right) \left(\frac{a}{c} \right) - 0.16645 \left(\frac{a}{t} \right)^3 - 0.44419 \left(\frac{a}{c} \right)^3 \\
&+ 0.2454 \left(\frac{a}{t} \right) \left(\frac{a}{c} \right)^2 + 0.5457 \left(\frac{a}{t} \right)^2 \left(\frac{a}{c} \right)
\end{aligned}$$

The results for a stress distribution linearly decreasing through the thickness

$$\sigma(x, y) = \sigma_0 \left(1 - \frac{x}{a} \right) \quad (6.5)$$

are

$$K_{2r}^A = \sigma_0 \sqrt{\frac{\pi a}{Q}} Y_I \left(\frac{a}{c}, \frac{a}{t} \right) M_{\lambda_1} \left(\phi, \frac{a}{c}, \frac{a}{t} \right) \quad (6.6)$$

where Y_I represents the boundary correction factors for cracks in a flat plate:

$$Y_I\left(\frac{a}{c}, \frac{a}{t}\right) = A_0 + A_1\left(\frac{a}{t}\right)^2 + A_2\left(\frac{a}{t}\right)^4 + A_3\left(\frac{a}{t}\right)^6$$

$$A_0 = 0.4537 + 0.1231\left(\frac{a}{c}\right) - 0.7412\left(\frac{a}{c}\right)^2 + 0.4600\left(\frac{a}{c}\right)^3$$

$$A_1 = -1.652 + 1.665\left(\frac{a}{c}\right) - 0.534\left(\frac{a}{c}\right)^2 + \frac{1.0}{0.198 + \left(\frac{a}{c}\right)^{0.846}}$$

$$A_2 = 3.418 - 3.126\left(\frac{a}{c}\right) - \frac{1.0}{0.041 + \frac{a}{c}} + 17.259\left(1.0 - \frac{a}{c}\right)^{9.286}$$

$$A_3 = -4.228 + 3.643\left(\frac{a}{c}\right) + \frac{1.0}{0.020 + \frac{a}{c}} - 21.924\left(1.0 - \frac{a}{c}\right)^{9.203}$$

and M_{A1} accounts for the effect of the attachment with different weld angles:

$$M_{A1}\left(\phi, \frac{a}{c}, \frac{a}{t}\right) = \frac{(\phi - 45)(\phi - 30)}{1350} - \frac{\phi(\phi - 45)}{450} M_{A1}^{\pi/6}\left(\frac{a}{c}, \frac{a}{t}\right) + \frac{\phi(\phi - 30)}{675} M_{A1}^{\pi/4}\left(\frac{a}{c}, \frac{a}{t}\right)$$

$$M_{A1}^{\pi/6}\left(\frac{a}{c}, \frac{a}{t}\right) = 0.8310 + 0.4932\left(\frac{a}{t}\right) - 0.2219\left(\frac{a}{c}\right) + 0.4913\left(\frac{a}{t}\right)^2$$

$$+ 0.9663\left(\frac{a}{c}\right)^2 - 0.9405\left(\frac{a}{t}\right)\left(\frac{a}{c}\right) - 1.2018\left(\frac{a}{t}\right)^3 - 0.5336\left(\frac{a}{c}\right)^3$$

$$+ 0.02560\left(\frac{a}{t}\right)\left(\frac{a}{c}\right)^2 + 0.8159\left(\frac{a}{t}\right)^2\left(\frac{a}{c}\right)$$

$$\begin{aligned}
M_{A1}^{\pi/4} \left(\frac{a}{c}, \frac{a}{t} \right) &= 0.79844 + 0.81134 \left(\frac{a}{t} \right) - 0.36419 \left(\frac{a}{c} \right) - 0.35084 \left(\frac{a}{t} \right)^2 \\
&+ 1.2286 \left(\frac{a}{c} \right)^2 - 1.0992 \left(\frac{a}{t} \right) \left(\frac{a}{c} \right) - 0.5184 \left(\frac{a}{t} \right)^3 - 0.6557 \left(\frac{a}{c} \right)^3 \\
&+ 0.1472 \left(\frac{a}{t} \right) \left(\frac{a}{c} \right)^2 + 0.87011 \left(\frac{a}{t} \right)^2 \left(\frac{a}{c} \right)
\end{aligned}$$

Weight function. By substituting eqs (6.3) - (6.6) into Eq. (2.6) together with the condition represented by Eq. (2.13), three equations with three unknowns were established. The parameters in the weight function expressions were solved for and are

$$M_{1A} = \frac{\pi}{\sqrt{2Q}} (4Y_0 \cdot M_{A0} - 6Y_1 \cdot M_{A1}) - \frac{24}{5} \quad (6.7)$$

$$M_{2A} = 3 \quad (6.8)$$

$$M_{3A} = 2 \left(\frac{\pi}{\sqrt{2Q}} Y_0 \cdot M_{A0} - M_{1A} - 4 \right) \quad (6.9)$$

The weight function for the deepest point of a semi-elliptic surface crack can then be determined directly from Eq. (2.11).

The weight function for the surface point: $M(x; B)$

The two reference stress intensity factor solutions used to determine the weight function $M(x; B)$ in the form of Eq. (2.12), corresponded to stress fields which were constant or linearly

decreasing through the thickness. These same stress fields were used for the determination of $M(x; A)$.

Reference Stress Intensity Factors. For the surface point of the surface crack, the finite element results presented previously for surface cracks in T-plate joints with a weld angle of 30 and 45 degrees together with the results for a flat plate from Wang and Lambert (1995) were approximated as follows, with an accuracy of 5% or better. The range of applicability for these equations is $0.05 \leq a/c \leq 1.0$, $0 \leq a/t \leq 0.6$, and weld angles between 0 and 45 degrees.

The results for a stress distribution constant through the thickness

$$\sigma(x, y) = \sigma_0 \quad (6.10)$$

are:

$$K_{I, r}^B = \sigma_0 \sqrt{\frac{\pi a}{Q}} F_0\left(\frac{a}{c}, \frac{a}{t}\right) M_{B0}\left(\phi, \frac{a}{c}, \frac{a}{t}\right) \quad (6.11)$$

where F_0 represents the boundary correction factors for cracks in a flat plate

$$F_0\left(\frac{a}{c}, \frac{a}{t}\right) = \left[C_0 + C_1\left(\frac{a}{t}\right)^2 + C_2\left(\frac{a}{t}\right)^4 \right] \sqrt{\frac{a}{c}}$$

$$C_0 = 1.2972 - 0.1548\left(\frac{a}{c}\right) - 0.0185\left(\frac{a}{c}\right)^2$$

$$C_1 = 1.5083 - 1.3219\left(\frac{a}{c}\right) + 0.5128\left(\frac{a}{c}\right)^2$$

$$C_2 = -1.101 + \frac{0.879}{0.157 + \frac{a}{c}}$$

and M_{B0} accounts for the effect of an attachment with different weld angles

$$M_{B0}\left(\phi, \frac{a}{c}, \frac{a}{t}\right) = \frac{(\phi - 45)(\phi - 30)}{1350} - \frac{\phi(\phi - 45)}{450} M_{B0}^{\pi/6}\left(\frac{a}{c}, \frac{a}{t}\right) + \frac{\phi(\phi - 30)}{675} M_{B0}^{\pi/4}\left(\frac{a}{c}, \frac{a}{t}\right)$$

$$\begin{aligned} M_{B0}^{\pi/6}\left(\frac{a}{c}, \frac{a}{t}\right) &= 0.8689 + 0.2130\left(\frac{a}{t}\right) + 0.0596 \ln\left(\frac{a}{c}\right) - 0.6162\left(\frac{a}{t}\right)^2 \\ &+ 0.0931\left[\ln\left(\frac{a}{c}\right)\right]^2 - 0.2956\left(\frac{a}{t}\right) \ln\left(\frac{a}{c}\right) + 0.9321\left(\frac{a}{t}\right)^3 + 0.05162\left[\ln\left(\frac{a}{c}\right)\right]^3 \\ &- 0.1592\left(\frac{a}{t}\right)\left[\ln\left(\frac{a}{c}\right)\right]^2 - 0.06520\left(\frac{a}{t}\right)^2 \ln\left(\frac{a}{c}\right) \end{aligned}$$

$$\begin{aligned} M_{B0}^{\pi/4}\left(\frac{a}{c}, \frac{a}{t}\right) &= 0.8615 + 0.2410\left(\frac{a}{t}\right) + 0.1587 \ln\left(\frac{a}{c}\right) - 0.64955\left(\frac{a}{t}\right)^2 \\ &+ 0.1775\left[\ln\left(\frac{a}{c}\right)\right]^2 - 0.3313\left(\frac{a}{t}\right) \ln\left(\frac{a}{c}\right) - 0.7929\left(\frac{a}{t}\right)^3 + 0.01811\left[\ln\left(\frac{a}{c}\right)\right]^3 \\ &- 0.2125\left(\frac{a}{t}\right)\left[\ln\left(\frac{a}{c}\right)\right]^2 - 0.3553\left(\frac{a}{t}\right)^2 \ln\left(\frac{a}{c}\right) \end{aligned}$$

The results for a stress distribution linearly decreasing through the thickness

$$\sigma(x,y) = \sigma_0 \left(1 - \frac{x}{a}\right) \quad (6.12)$$

are:

$$K_{2r}^B = \sigma_0 \sqrt{\frac{\pi a}{Q}} F_I\left(\frac{a}{c}, \frac{a}{t}\right) M_{BI}\left(\phi, \frac{a}{c}, \frac{a}{t}\right) \quad (6.13)$$

where F_I represents the boundary correction factors for cracks in a flat plate:

$$F_I\left(\frac{a}{c}, \frac{a}{t}\right) = \left[D_0 + D_1 \left(\frac{a}{t}\right)^2 + D_2 \left(\frac{a}{t}\right)^4 \right] \sqrt{\frac{a}{c}}$$

$$D_0 = 1.2687 - 1.0642\left(\frac{a}{c}\right) + 1.4646\left(\frac{a}{c}\right)^2 - 0.7250\left(\frac{a}{c}\right)^3$$

$$D_1 = 1.1207 - 1.2289\left(\frac{a}{c}\right) + 0.5876\left(\frac{a}{c}\right)^2$$

$$D_2 = 0.190 - 0.608\left(\frac{a}{c}\right) + \frac{0.199}{0.035 + \frac{a}{c}}$$

and M_{BI} accounts for the effect of an attachment with different weld angles

$$M_{B1}(\phi, \frac{a}{c}, \frac{a}{t}) = \frac{(\phi - 45)(\phi - 30)}{1350} - \frac{\phi(\phi - 45)}{450} M_{B1}^{\pi/6}(\frac{a}{c}, \frac{a}{t}) + \frac{\phi(\phi - 30)}{675} M_{B1}^{\pi/4}(\frac{a}{c}, \frac{a}{t})$$

$$\begin{aligned} M_{B1}^{\pi/6}(\frac{a}{c}, \frac{a}{t}) &= 0.8483 + 0.1317(\frac{a}{t}) + 0.03697 \ln(\frac{a}{c}) - 0.387(\frac{a}{t})^2 \\ &+ 0.08202[\ln(\frac{a}{c})]^2 - 0.2261(\frac{a}{t}) \ln(\frac{a}{c}) + 0.7143(\frac{a}{t})^3 + 0.002463[\ln(\frac{a}{c})]^3 \\ &- 0.1209(\frac{a}{t})[\ln(\frac{a}{c})]^2 - 0.07085(\frac{a}{t})^2 \ln(\frac{a}{c}) \end{aligned}$$

$$\begin{aligned} M_{B1}^{\pi/4}(\frac{a}{c}, \frac{a}{t}) &= 0.8344 + 0.09865(\frac{a}{t}) + 0.07959 \ln(\frac{a}{c}) - 0.023849(\frac{a}{t})^2 \\ &+ 0.10558[\ln(\frac{a}{c})]^2 - 0.2268(\frac{a}{t}) \ln(\frac{a}{c}) + 0.11467(\frac{a}{t})^3 + 0.00211[\ln(\frac{a}{c})]^3 \\ &- 0.1562(\frac{a}{t})[\ln(\frac{a}{c})]^2 - 0.29802(\frac{a}{t})^2 \ln(\frac{a}{c}) \end{aligned}$$

Weight Function. By substituting Eqs. (6.10)-(6.13) into Eq. (2.6), and applying the condition represented by Eq. (2.14), three equations with three unknowns were established. The weight function parameters for the surface point were solved for and are

$$M_{1B} = \frac{\pi}{\sqrt{4Q}} (30F_1 \cdot M_{B1} - 18F_0 \cdot M_{B0}) - 8 \quad (6.14)$$

$$M_{2B} = \frac{\pi}{\sqrt{4Q}} (60F_0 \cdot M_{B0} - 90F_1 \cdot M_{B1}) + 15 \quad (6.15)$$

$$M_{3B} = - (1 + M_{1B} + M_{2B}) \quad (6.16)$$

The weight function for the surface point can then be determined directly from Eq. (2.12).

6.1.3 Validation of Derived Weight Functions

First, the weight functions for the deepest and surface points derived above were validated using finite element results for two non-linear stress fields. Using Eq. (2.6), stress intensity factors were calculated for the following stress fields:

$$\sigma(x, y) = \sigma_0 \left(1 - \frac{x}{a}\right)^2 \quad (6.17)$$

$$\sigma(x, y) = \sigma_0 \left(1 - \frac{x}{a}\right)^3 \quad (6.18)$$

The stress intensity factors for the deepest and surface points calculated from weight functions and from the present finite element calculations for the above stress distribution are shown in Figures 6.7-6.10. For both weld angles, 30° and 45°, the difference between the boundary correction factors calculated from the weight function and the finite elements results were less than 4% for the surface point and 6% for the deepest point.

The weight functions were then used to calculate stress intensity factors under far field tension and bending cases. Two dimensional finite element analyses were performed to calculate the stress distribution on the prospective crack plane. The resulting stress distributions, $\sigma(x)$, for tension and bending were used to calculate the stress intensity factors using Eq.(2.6). The resulting stress intensity factors were then normalised to obtain M_k factors, Eqs.(2.20) and (2.21). Figures 6.11-6.14 show the comparison between the finite element results and the

weight functions. Good agreement was achieved with a maximum difference of 10%. No finite element results are available for shallow cracks. However, the weight function results for M_k factor at the deepest point appear to approach the stress concentration factor for this geometry as a/t approaches zero, as suggested by Maddox (1975).

6.1.4 Discussion

It is common practice to calculate stress intensity factors for surface cracks in T-plate joints by using weight functions derived for flat plates in conjunction with stress distributions from corresponding uncracked T-plate joints (Lecsek et al., 1995; Brennan et al., 1996 and Forbes et al., 1991). It is argued that by using the stress distribution, $\sigma(x)$, calculated for the uncracked T-joints and the weight function for flat plates, the effect of the weldment geometry on the stress intensity factor is accounted for satisfactorily.

From the present work, it was found that at the deepest point, the weight function for a flat plate always over-estimates the stress intensity factor at the deepest point in T-plate joints; these conservative results were also observed by Niu and Glinka (1987) and Fu et al. (1993). For the case of a stress distribution linearly decreasing through the thickness, the maximum difference is 19% (45 degree weld angle), and occurs for low aspect ratio, shallow cracks ($a/c = 0.05$ and $a/t = 0.1$). At the surface point, the flat plate weight function will provide either an over-estimation or an under-estimation depending on the aspect ratio of the crack. For cracks with aspect ratios less than 0.4, the flat plate weight function will under-estimate the stress intensity factors at the surface point; the maximum difference in the present case, for a stress distribution linearly decreasing through the thickness, is as much as 40% ($a/c = 0.05$, $a/t = 0.1$). For cracks with aspect ratios larger than 0.4, the flat plate weight function will over-estimate the stress intensity factor at the surface point; the

maximum difference in the present case is 18% ($a/c = 1.0$, $a/t = 0.1$). Similar trends were also found for the case of constant loading applied to the crack face.

In the present analysis, a sharp weld toe was used for all calculations. Since stress intensity factors for surface cracks under crack face uniform and linearly varying loads were used to derive weight functions, the sharp weld toe effect was minimised. Niu and Glinka (1990) have pointed out that, for different local weld toe radii, the weight function tends to be the same as long as the nominal weld angle is the same. Therefore, the weight functions derived from the present analysis can be used to calculate stress intensity factors for finite radius weld toe geometries, provided the appropriate stress distribution is used.

The effect of the local weld radius, ρ , on the stress distribution is restricted to a shallow region near the weld toe (2% of t for a typical weld toe radii $t/15 \geq \rho \geq t/50$, Niu and Glinka, 1987). For the deepest point, this has a significant effect on the stress intensity factor only for shallow cracks ($a/t < 0.1$). For deeper cracks ($a/t > 0.1$), the results are not sensitive to the local weld toe radius and hence the particular stress distribution used, since the singularity point of the weight function is at the deepest point of the crack and farther away from the weld toe as the crack becomes deeper. For the surface point, the weld radius has a significant effect on the stress intensity factor for all crack depths since the singularity point of the weight function is at the surface point, which is always at the weld toe.

The weld geometry in the present model is on one side of the attachment only. However, under the same loading system, and for the same attachment thickness, the difference between the stress intensity factors for the same crack geometry in T-plate joints welded on one side or welded on both sides of the attachment is expected to be insignificant (Niu and Glinka, 1990). The present weight functions can therefore also be applied to T-plate joints with welds on both sides of the attachment.

The attachment thickness in the present model was half of the base plate thickness. However, the difference in the weight functions for different attachment thicknesses was expected to be insignificant (Niu and Glinka, 1990). Therefore, the present weight function can also be applied to T-plate joints with a different attachment thickness. Since the stress distributions will be different for different attachment thickness, the stress intensity factors will still be different as expected.

6.2 Surface Cracks in T-plate Joints with Built-in Ends

In section 6.1, stress intensity factors and weight function solutions for surface cracks in T-plate joints with free ends were presented. As discussed in Chapters 2 and 3, T-plate joints with built-in ends are more realistic models for pipe-plate and tubular joints, since load redistribution (load shedding) effects can be accounted for in T-plate joints with built-in ends. In the present section, a method for calculating stress intensity factors for surface cracks in T-plate joints with built-in ends is proposed. The geometry and boundary conditions considered are shown in Figure 6.15. The method was based on weight function solutions for surface cracks in flat-plates with free ends and built-in ends, and weight functions for surface cracks in T-plate joints with free ends. The method was verified using finite element data.

6.2.1 Proposed Stress Intensity Factor Solutions

Although extensive finite element calculations can be conducted to obtain stress intensity factor solutions for any geometry, the analysis will be time consuming and very demanding because the geometric combinations include different values for a/c , a/t and H/t in the present problem (Figure 6.15). In the present study, it is proposed that stress intensity factors for any stress distribution $\sigma(x)$ can be calculated from stress intensity factor

solutions for surface cracks in T-plate joints with free ends for the same stress distribution and a correction factor α :

$$K_{built-in\ ends}(P') = \alpha(P') \cdot K_{free\ ends}(P') \quad (6.19)$$

where the stress intensity factor for free ends in the T-plate joints can be calculated from the corresponding weight functions

$$K_{free\ ends}(P') = \int_0^a \sigma(x) M_{free\ ends}(x; P') dx \quad (6.20)$$

The correction factor, α , accounts for the effect of the built-in ends (load shedding). It is assumed to be the same as the factor for surface cracks in flat plates, which can be calculated from

$$\alpha(P') = \frac{\int_0^a \sigma(x) M_{built-in\ ends}^{flat\ plate}(x; P') dx}{\int_0^a \sigma(x) M_{free\ ends}^{flat\ plate}(x; P') dx} \quad (6.21)$$

Note that α depends on $\sigma(x)$ and will be, therefore, different for remote tension and bending. Weight functions for surface cracks in T-plate joints with free ends, $M_{free\ ends}(x; P')$, in Eq. (6.20) were developed in section 6.1. Weight functions for surface cracks in flat plates with free ends, $M_{free\ ends}^{flat\ plate}(x; P')$, are also available from previous work (Wang and Lambert, 1995a). Weight functions for surface cracks in flat plates with built-in ends, $M_{built-in\ ends}^{flat\ plate}(x; P')$, were developed in section 5.2. Therefore, all weight functions involved in the calculation of Eq. (6.19) are available.

The physical assumption made here is that the effect of the built-in ends on stress intensity factors in T-plates is the same as for surface cracks in flat plates, as shown in Figure 6.16. Note that the resulting stress intensity factors from Eq. (6.19) will depend on a/c , a/t , the weldment angle, ϕ , and H/t . This method was verified using finite element data.

6.2.2 Verification of Proposed Stress Intensity Factor Solution

In order to verify the proposed stress intensity factor solutions, three-dimensional finite element calculations were conducted to calculate stress intensity factors for surface cracks in T-plate joints with built-in ends, welded at one side only, with attachment thickness of half base plate thickness, and overall weld angles of 45 degrees. The resulting stress intensity factors were compared with predictions from the present method.

Finite Element Model

The same models used in the calculation for T-plate joints with free ends in section 6.1 were used except that fixed boundary conditions were applied at the ends. Figure 6.15 shows the geometry and boundary conditions. Bending loads were applied via a tension applied to the welded attachment.

As before, the stress intensity factor results were normalised as follows,

$$F = \frac{K}{\sigma_0 \sqrt{\pi a} / Q} \quad (6.22)$$

Results for Stress Intensity Factors

Stress intensity factors for cracks with aspect ratios, a/c , of 0.1, 0.2 or 1.0 and relative crack depths, a/t , of 0.4, 0.6 or 0.8 in a T-plate joint with a 45 degree weld angle, and a H/t ratio of 10, subjected to bending loads were determined to verify the proposed stress intensity factor solutions. These results are summarised in Tables 6.6.

The stress intensity factors for the deepest and surface points calculated from the proposed stress intensity factor solutions, Eq. (6.21), and from finite element calculations are shown in Figures 6.17 – 6.22. Good agreement was achieved. The differences were within 10% for the deepest points, and within 15% for the surface points. It can be concluded that the proposed solution provides good solutions for surface cracks in T-plate joints with built-in ends.

Note that if the weight functions for T-plates with free ends were used (i.e., ignoring the effects of the built-in ends), the differences between the predictions and finite element results can be as large as 100% (see Figure 6.17 – 6.22).

6.2.3 Discussion

The Flat Plate Weight Function

Note that the proposed stress intensity factor expression, Eq.(6.19), can be re-written as

$$K_{built-in\ ends}^{T-plate}(P') = \left[\int_0^a \sigma(x) M_{built-in\ ends}^{flat\ plate}(x; P') dx \right] \frac{\int_0^a \sigma(x) M_{free\ ends}^{T-plate}(x; P') dx}{\int_0^a \sigma(x) M_{free\ ends}^{flat\ plate}(x; P') dx} \quad (6.23)$$

If we introduce a new correction factor $\beta(P')$:

$$\beta(P') = \frac{\int_0^a \sigma(x) M_{free\ ends}^{T-plate}(x; P') dx}{\int_0^a \sigma(x) M_{free\ ends}^{flat\ plate}(x; P') dx} \quad (6.24)$$

then the proposed equation is equivalent to

$$K_{built-in\ ends}^{T-plate}(P') = \beta(P') \cdot \int_0^a \sigma(x) M_{built-in\ ends}^{flat\ plate}(x; P') dx \quad (6.25)$$

If the factor $\beta(P')$ equals 1, then Eq. (6.25) becomes

$$K_{built-in\ ends}^{T-plate}(P') = \int_0^a \sigma(x) M_{built-in\ ends}^{flat\ plate}(x; P') dx \quad (6.26)$$

This implies that the weight function for surface cracks in flat plates with built-in ends can be used to calculate stress intensity factors for surface cracks in T-plate weld joints with built-in ends. However, $\beta(P')$ is not 1. Its' value was discussed in section 6.1.4, and is the difference between predictions for flat plate and T-plate weight functions. At the deepest point, $\beta(P')$ is always smaller than 1, with a minimum value of 0.8 for most stress distributions. At the surface point, $\beta(P')$ can either be smaller or larger than 1. For the case of low aspect ratio cracks, it can be as large as 1.4.

From these comparisons, it is clear that we can use Eq. (6.26) for the calculation of stress intensity factors at the deepest point of a surface crack in T-plate joints with built-in ends. Note that equation (6.26) will generally over-estimate the stress intensity factor by a few percent. Eq.(6.26) is not recommended for the surface point, since it may underestimate the stress intensity factor solution by as much as 40%.

The Load Shedding Effect

The finite element results for surface cracks in T-plate joints with built-in ends are compared with predictions from weight functions for T-plate joints with free ends in Figures 6.17-6.22. Since these weight functions do not account for load redistribution (load shedding), they always give an over-estimation of the stress intensity factors, as expected.

However, the degree of reduction of stress intensity factors due to built-in ends depends on several parameters. For low aspect ratio cracks ($a/c = 0.1, 0.2$), the decrease in stress intensity factor is higher than for higher aspect ratio cracks ($a/c = 1$). This drop also depends on a/t , increasing when a/t increases. The decrease also depends on the H/t ratio; the smaller the H/t ratio, the larger the drop. In addition, the effect on the deepest and surface points is also different. Overall, the load shedding effect depends on a/c , a/t , H/t and the position along the crack front.

Available models for load shedding effects can only model certain aspects of load shedding for surface cracks. The simple moment release model proposed by Aaghaakouchak *et al.* (1989) discussed in Chapter 2

$$\sigma_b = \sigma_b^0(1 - a/t) \quad (2.22)$$

can only model the effect of a/t on stress intensity factors. Figures 6.17 – 6.22 show predictions of this model along with the present results. Although reasonable predictions are given for the deepest point, their predictions severely under-estimate the results at the surface point.

Forbes (1991) proposed using an edge crack model with built-in ends to model load shedding for tubular joints. In addition to the effect of a/t , Forbes' method also accounts for the effect of H/t , but it cannot account for different load shedding for different aspect ratios, a/c . Only the present method is capable of accounting realistically for load shedding effects for surface cracks, which depend on all these parameters.

a/c	n	Position	a/t = 0.1	a/t=0.2	a/t=0.4	a/t=0.6
0.05	0	surface	0.4042	0.4229	0.4340	0.6329
		deepest	1.0863	1.2331	1.7579	2.6735
	1	surface	0.3863	0.5276	0.4222	0.5824
		deepest	0.4348	0.4807	0.8619	1.4515
0.1	0	surface	0.5026	0.4807	0.5320	0.7822
		deepest	1.0559	1.1625	1.5427	2.1138
	1	surface	0.4589	0.4377	0.4876	0.6751
		deepest	0.4207	0.4909	0.7407	1.1109
0.2	0	surface	0.5701	0.5886	0.7592	1.0381
		deepest	1.0281	1.0963	1.3355	1.6439
	1	surface	0.4934	0.4982	0.6167	0.8136
		deepest	0.3982	0.4432	0.5996	0.7961

Table 6.1. Boundary correction factors F for semi-elliptical surface cracks ($a/c = 0.05, 0.1, 0.2, 0.4, 0.6, 1.0$) in T-plate joints with $\pi/6$ weld angle under stress distributions of $\sigma(1-x/a)^n$, $n = 0, 1$, $F = K/\sigma\sqrt{\pi a/Q}$.

a/c	n	position	a/t = 0.1	a/t=0.2	a/t=0.4	a/t=0.6
0.4	0	surface	0.6953	0.7492	0.9344	1.1805
		deepest	1.0045	1.0357	1.1629	1.3005
	1	surface	0.5769	0.6146	0.7391	0.9111
		deepest	0.3699	0.3909	0.4739	0.5564
0.6	0	surface	0.8157	0.8624	0.9896	1.2350
		deepest	0.9966	1.0157	1.0768	1.1746
	1	surface	0.6671	0.6999	0.7855	0.9562
		deepest	0.3467	0.3596	0.3991	0.4542
1.0	0	surface	1.001	1.0350	1.1319	1.2764
		deepest	0.9934	1.0032	1.0344	1.0640
	1	surface	0.8143	0.8386	0.9052	1.0083
		deepest	0.3047	0.3112	0.3307	0.3395

Table 6.1. (Continue) Boundary correction factors F for semi-elliptical surface cracks ($a/c = 0.05, 0.1, 0.2, 0.4, 0.6, 1.0$) in T-plate joints with $\pi/6$ weld angle under stress distributions of $\sigma(1-x/a)^n$, $n = 0, 1$, $F = K/\sigma\sqrt{[\pi a/Q]}$.

a/c	n	position	a/t = 0.1	a/t=0.2	a/t=0.4	a/t=0.6
0.05	0	surface	0.4135	0.4379	0.4669	0.6962
		deepest	1.0667	1.2230	1.7429	2.6482
	1	surface	0.3860	0.4102	0.4421	0.6231
		deepest	0.4259	0.5219	0.8534	1.4361
0.1	0	surface	0.5015	0.5159	0.5650	0.9360
		deepest	1.0437	1.1529	1.5192	2.1003
	1	surface	0.4482	0.4424	0.5055	0.7429
		deepest	0.4074	0.4862	0.7265	1.0846
0.2	0	surface	0.5679	0.5867	0.7992	1.0812
		deepest	1.0118	1.0767	1.3351	1.6088
	1	surface	0.4884	0.4938	0.6400	0.8391
		deepest	0.3884	0.4304	0.5995	0.7740

Table 6.2. Boundary correction factors F for semi-elliptical surface cracks ($a/c = 0.05, 0.1, 0.2, 0.4, 0.6, 1.0$) in T-plate joints with $\pi/4$ weld angle under stress distributions of $\sigma_0(1-x/a)^n$, $n = 0, 1$, $F = K/\sigma_0\sqrt{[\pi a/Q]}$.

a/c	n	position	a/t = 0.1	a/t=0.2	a/t=0.4	a/t=0.6
0.4	0	surface	0.6810	0.7368	0.9230	1.1512
		deepest	0.9917	1.0235	1.1390	1.2507
	1	surface	0.5631	0.6027	0.7275	0.8875
		deepest	0.3626	0.3820	0.4567	0.5244
0.6	0	surface	0.7939	0.8439	0.9871	1.2042
		deepest	0.9870	1.0083	1.0738	1.1556
	1	surface	0.6478	0.6837	0.7793	0.9302
		deepest	0.3415	0.3534	0.3949	0.4395
1.0	0	surface	0.9750	1.0146	1.1281	1.2730
		deepest	0.9891	1.0026	1.0399	1.0695
	1	surface	0.7922	0.8221	0.8986	1.0009
		deepest	0.3029	0.3075	0.3301	0.3397

Table 6.2. (Continue) Boundary correction factors F for semi-elliptical surface cracks ($a/c = 0.05, 0.1, 0.2, 0.4, 0.6, 1.0$) in T-plate joints with $\pi/6$ weld angle under stress distributions of $\sigma\sqrt{1-x/a}$, $n = 0, 1$, $F = K/\sigma\sqrt{[\pi a/Q]}$.

a/c	n	position	a/t = 0.1	a/t=0.2	a/t=0.4	a/t=0.6
0.2	2	surface	0.4397	0.4374	0.5267	0.6786
		deepest	0.2410	0.2740	0.3895	0.5388
	3	surface	0.3991	0.3929	0.4637	0.5868
		deepest	0.1749	0.2009	0.2924	0.4120
1.0	2	surface	0.6975	0.7154	0.7655	0.8459
		deepest	0.1628	0.1672	0.1812	0.1924
	3	surface	0.6134	0.6272	0.6663	0.7319
		deepest	0.1116	0.1150	0.1259	0.1362

Table 6.3. Boundary correction factors F for semi-elliptical surface cracks ($a/c = 0.2, 1.0$) in T-plate joints with $\pi/6$ weld angle under stress distributions of $\sigma_0(1-x/a)^n$, $n = 2, 3$, $F = K/\sigma_0\sqrt{[\pi a/Q]}$.

a/c	n	position	a/t = 0.1	a/t=0.2	a/t=0.4	a/t=0.6
0.2	2	surface	0.4336	0.4314	0.5414	0.6956
		deepest	0.2344	0.2654	0.3897	0.5225
	3	surface	0.3926	0.3861	0.4731	0.5990
		deepest	0.1699	0.1943	0.2926	0.3991
1.0	2	surface	0.6779	0.7011	0.7576	0.8360
		deepest	0.1622	0.1661	0.1818	0.1928
	3	surface	0.5963	0.6141	0.6570	0.7202
		deepest	0.1116	0.1146	0.1267	0.1367

Table 6.4. Boundary correction factors F for semi-elliptical surface cracks ($a/c = 0.2, 1.0$) in T-plate joints with $\pi/4$ weld angle under stress distributions of $\sigma(1-x/a)^n$, $n = 2, 3$, $F = K/\sigma\sqrt{[\pi a/Q]}$.

a/c	load	position	a/t = 0.1	a/t=0.2	a/t=0.4	a/t=0.6
0.2	tension	surface	2.7231	2.1665	1.9251	1.8077
		deepest	1.0246	0.9638	0.9469	0.9747
	bending	surface	3.0259	2.3698	2.0360	1.9622
		deepest	1.0558	0.9373	0.8967	0.8925
1.0	tension	surface	1.9001	1.5177	1.2769	1.2123
		deepest	1.0083	0.9232	0.9064	0.9113
	bending	surface	2.1008	1.6772	1.3920	1.2848
		deepest	1.0349	0.8908	0.7856	0.6964

Table 6.5. Weld toe magnification factors Mk for semi-elliptical surface cracks ($a/c = 0.2, 1.0$) in T-plate joints with $\pi/4$ weld angle under far field tension and bending.

a/c	position	a/t = 0.2	a/t=0.4	a/t=0.6	a/t=0.8
0.1	surface	1.0377	0.8451	0.8211	0.9122
	deepest	0.9342	0.8268	0.6665	0.2694
0.2	surface	1.146	1.0377	1.0229	1.0062
	deepest	0.8461	0.6797	0.5089	0.2053
1.0	surface	1.9052	1.5466	1.6919	1.2798
	deepest	0.6826	0.3812	0.1326	-0.1691

Table 6.6. Boundary correction factors F for semi-elliptical surface cracks ($a/c = 0.1, 0.2, 1.0$) in T-plate joints with $\pi/4$ weld angle and built-in ends under bending, $F = K/\infty\sqrt{[\pi a/Q]}$.

Figure 6.1 Geometry and co-ordinate system

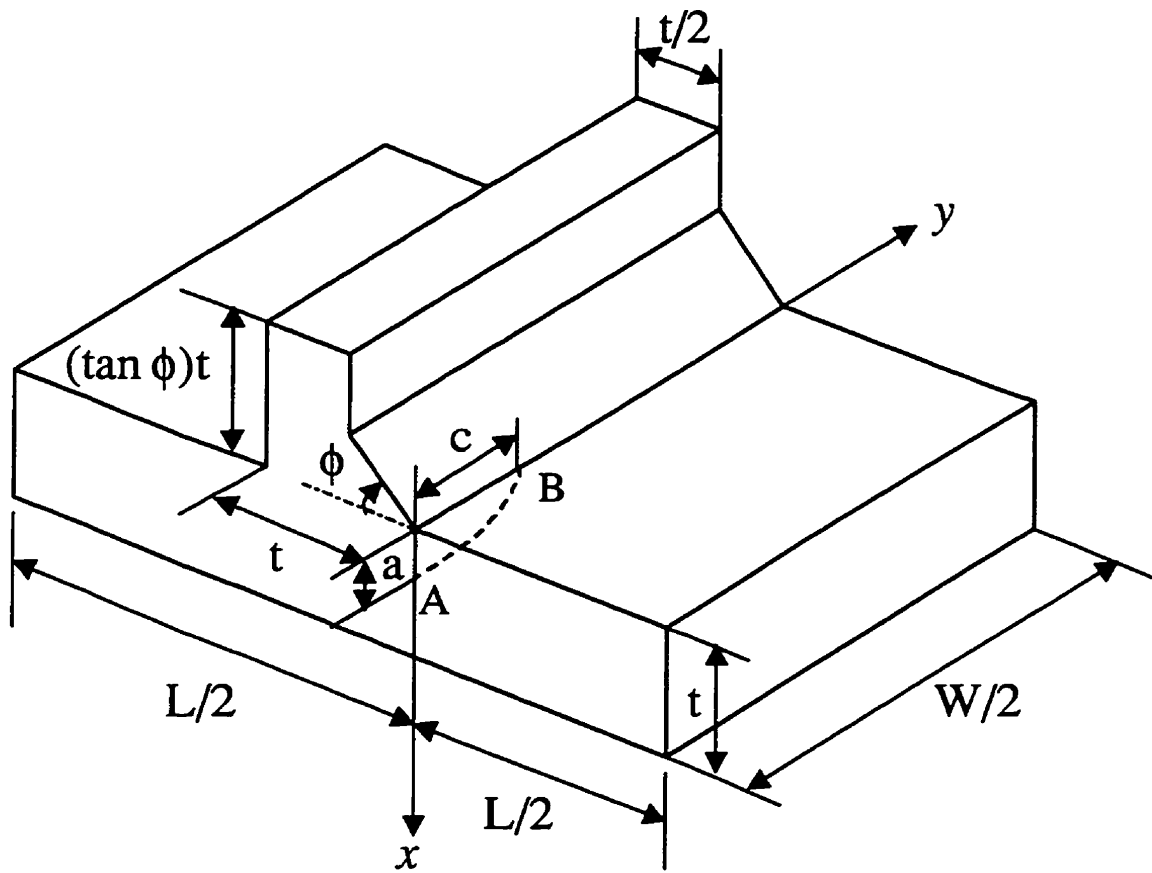


Figure 6.2 Typical finite element mesh (part), $a/c = 0.2$, $a/t = 0.2$, 45 degree weld angle

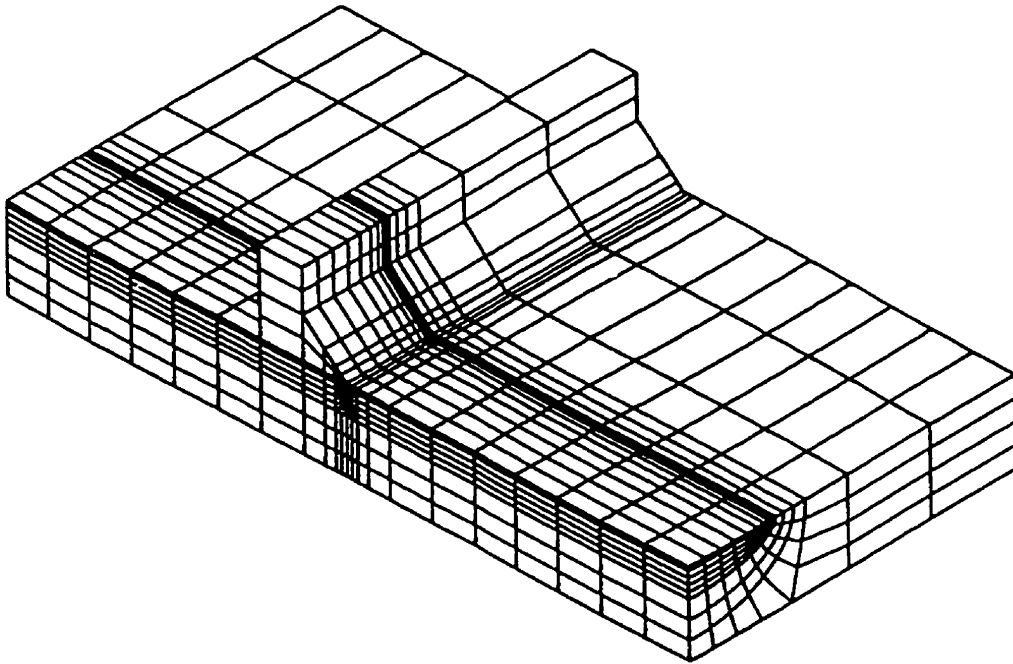


Figure 6.3 Comparison of the weld toe magnification factor from the present FE calculation and Bowness and Lee (1996), (far field tension, $\pi/4$ weld angle, deepest point).

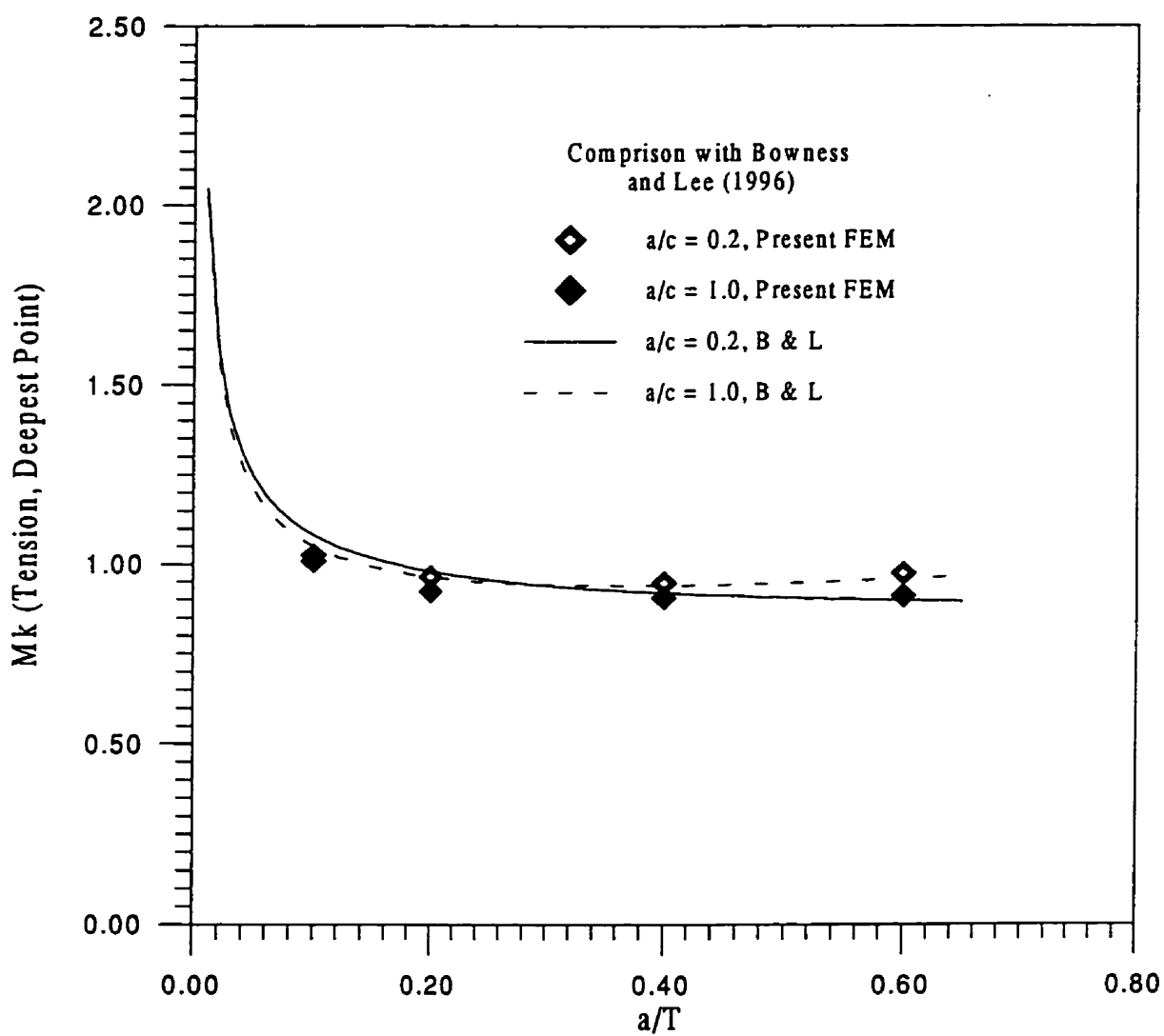


Figure 6.4 Comparison of the weld toe magnification factor from the present FE calculation and Bowness and Lee (1996), (far field tension, $\pi/4$ weld angle, surface point).

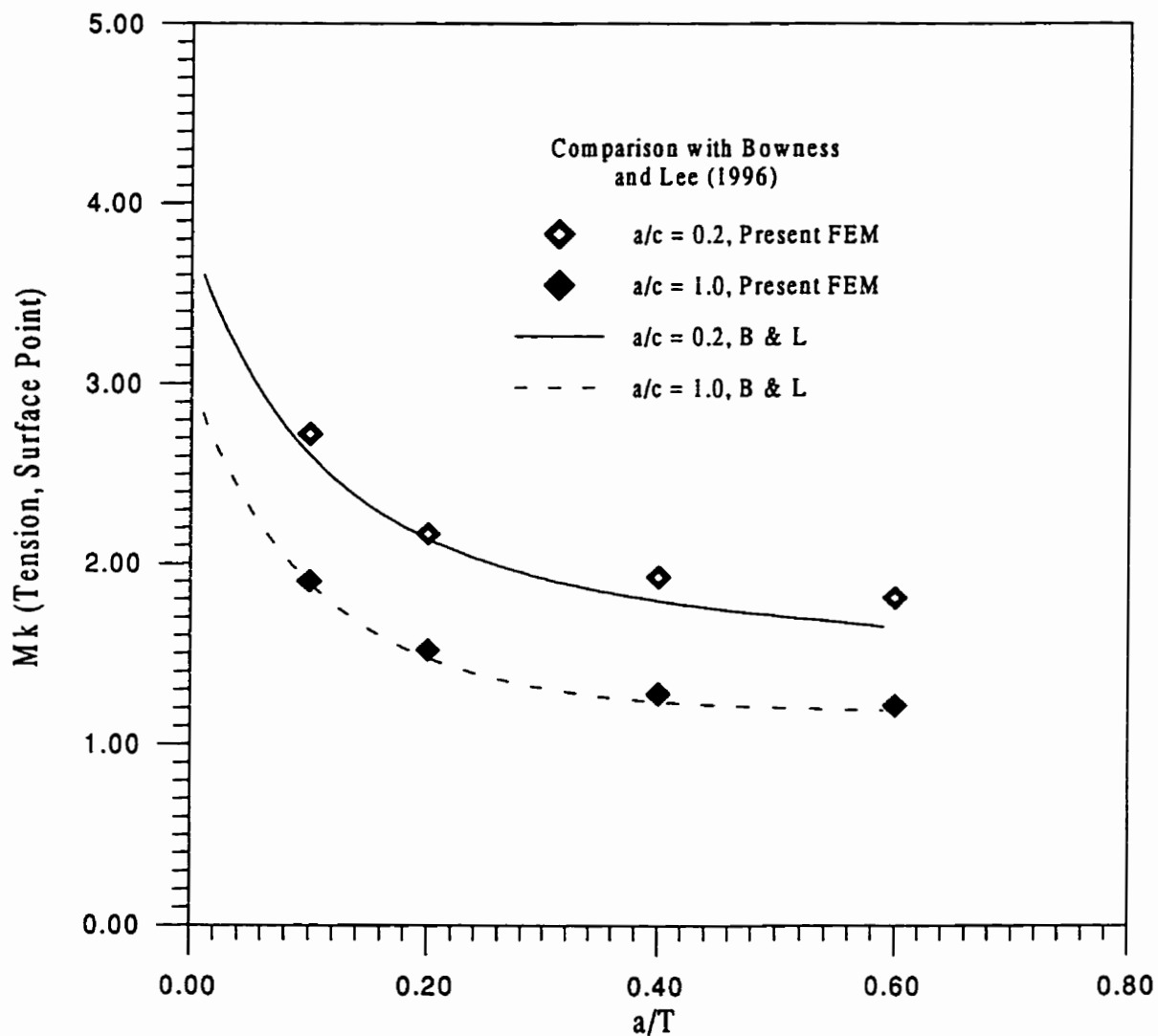


Figure 6.5 Comparison of the weld toe magnification factor from the present FE calculation and Bowness and Lee (1996), (far field bending, $\pi/4$ weld angle, deepest point).

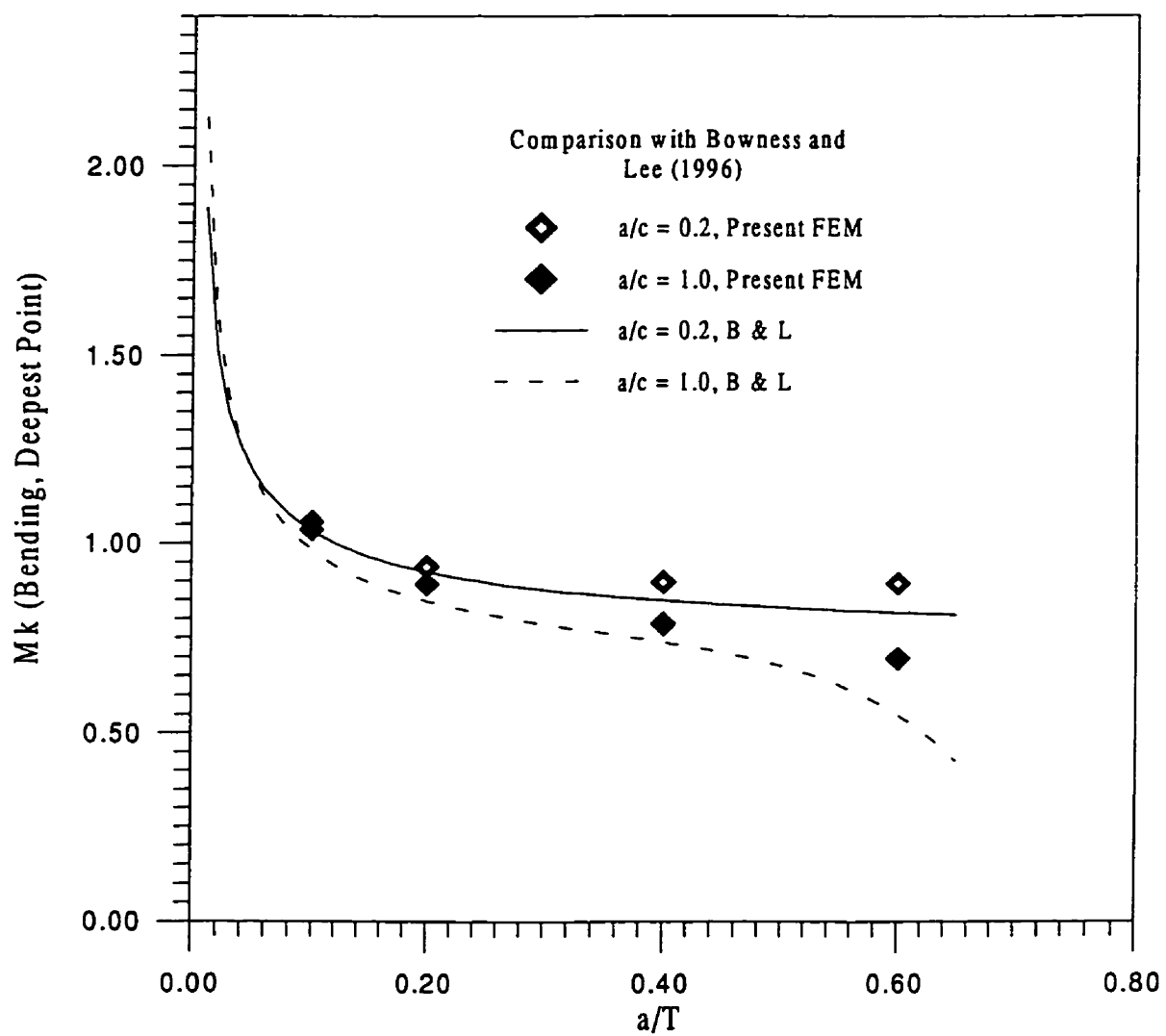


Figure 6.6 Comparison of the weld toe magnification factor from the present FE calculation and Bowness and Lee (1996), (far field bending, $\pi/4$ weld angle, surface point).

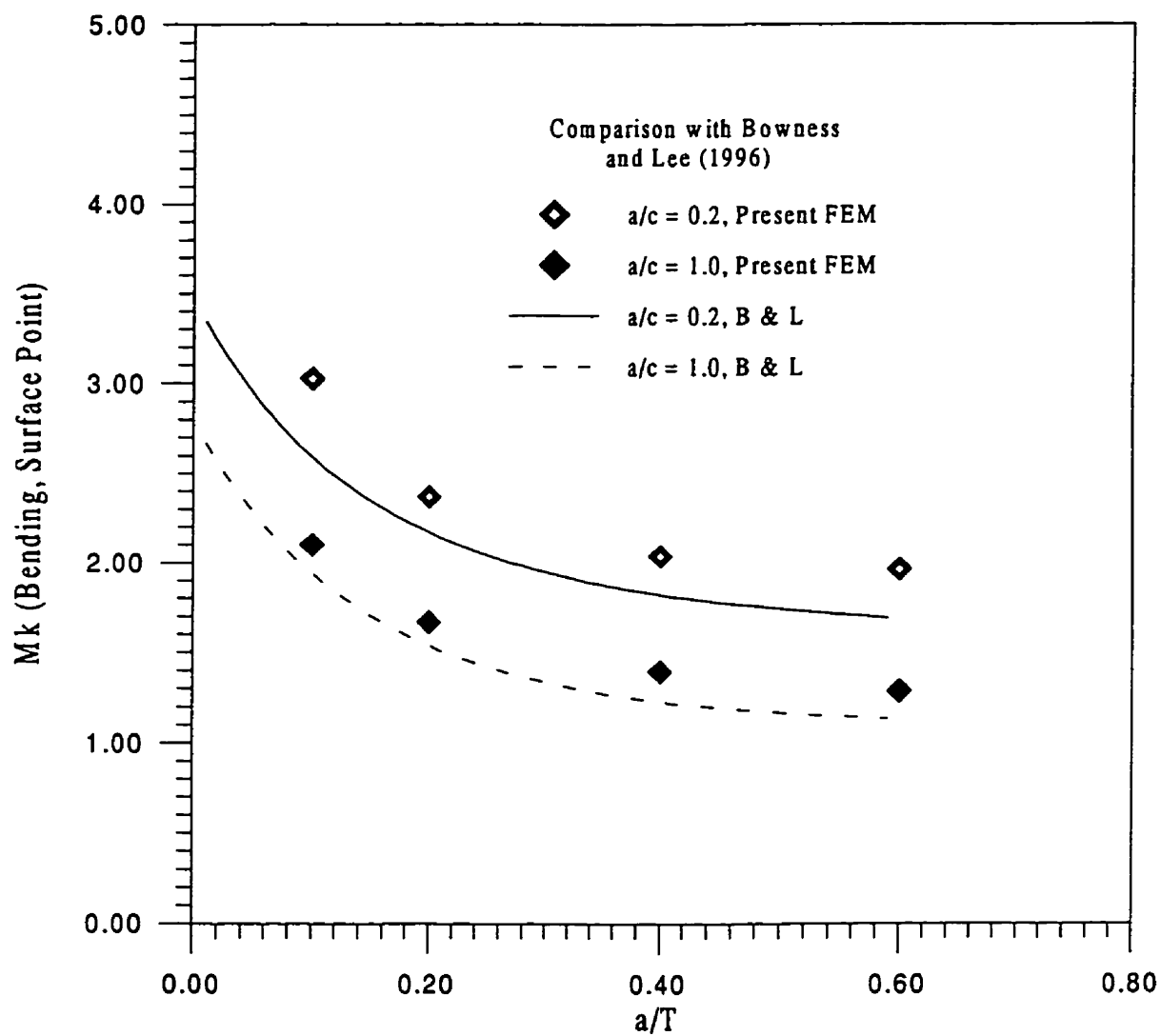


Figure 6.7 Comparison of the weight function based stress intensity factor and FEM data for stress distribution $\sigma(1-x/a)^2$ ($\pi/4$ weld angle, deepest point).

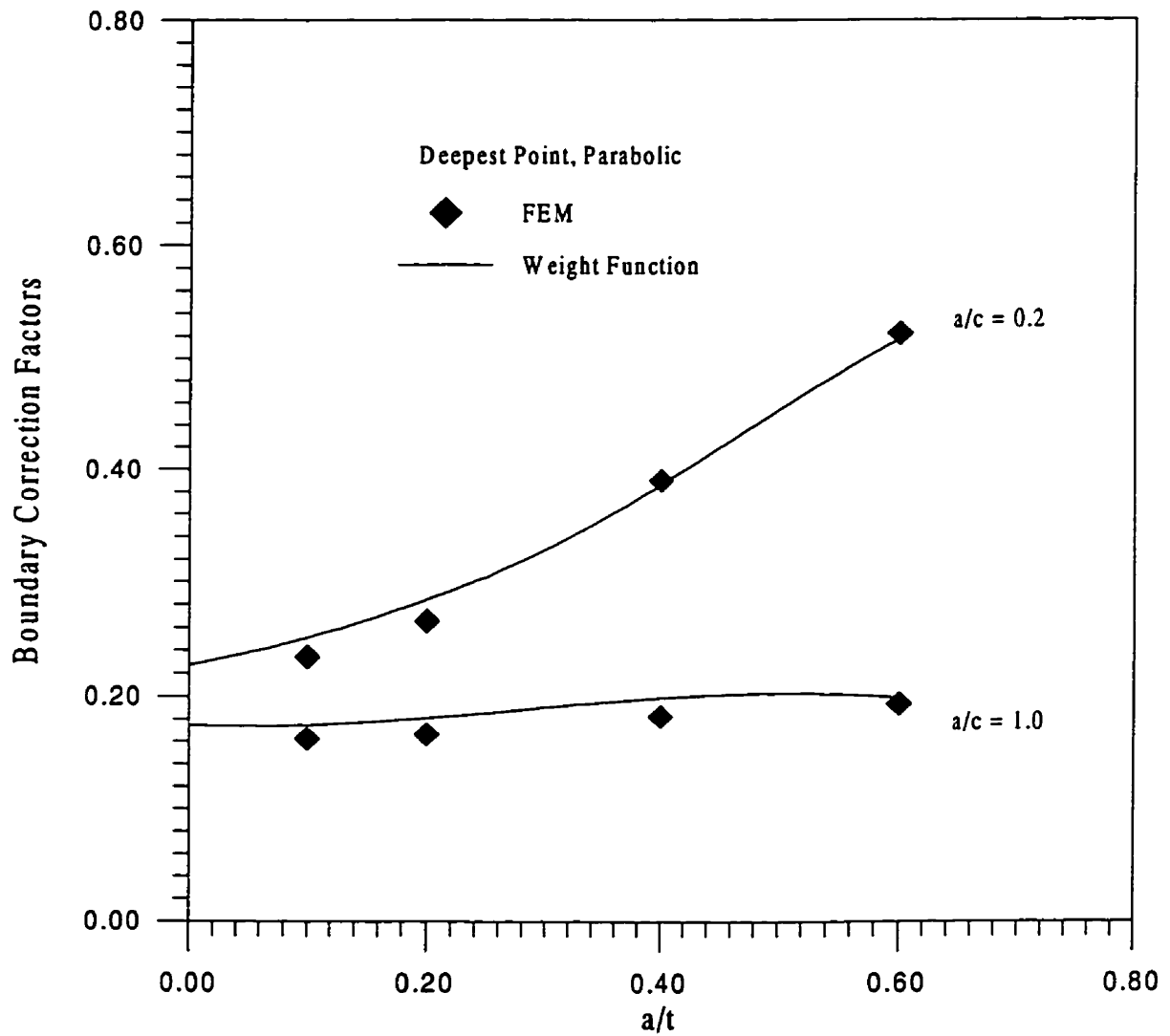


Figure 6.8 Comparison of the weight function based stress intensity factor and FEM data for stress distribution $\propto (1-x/a)^2$ ($\pi/4$ weld angle, surface point).

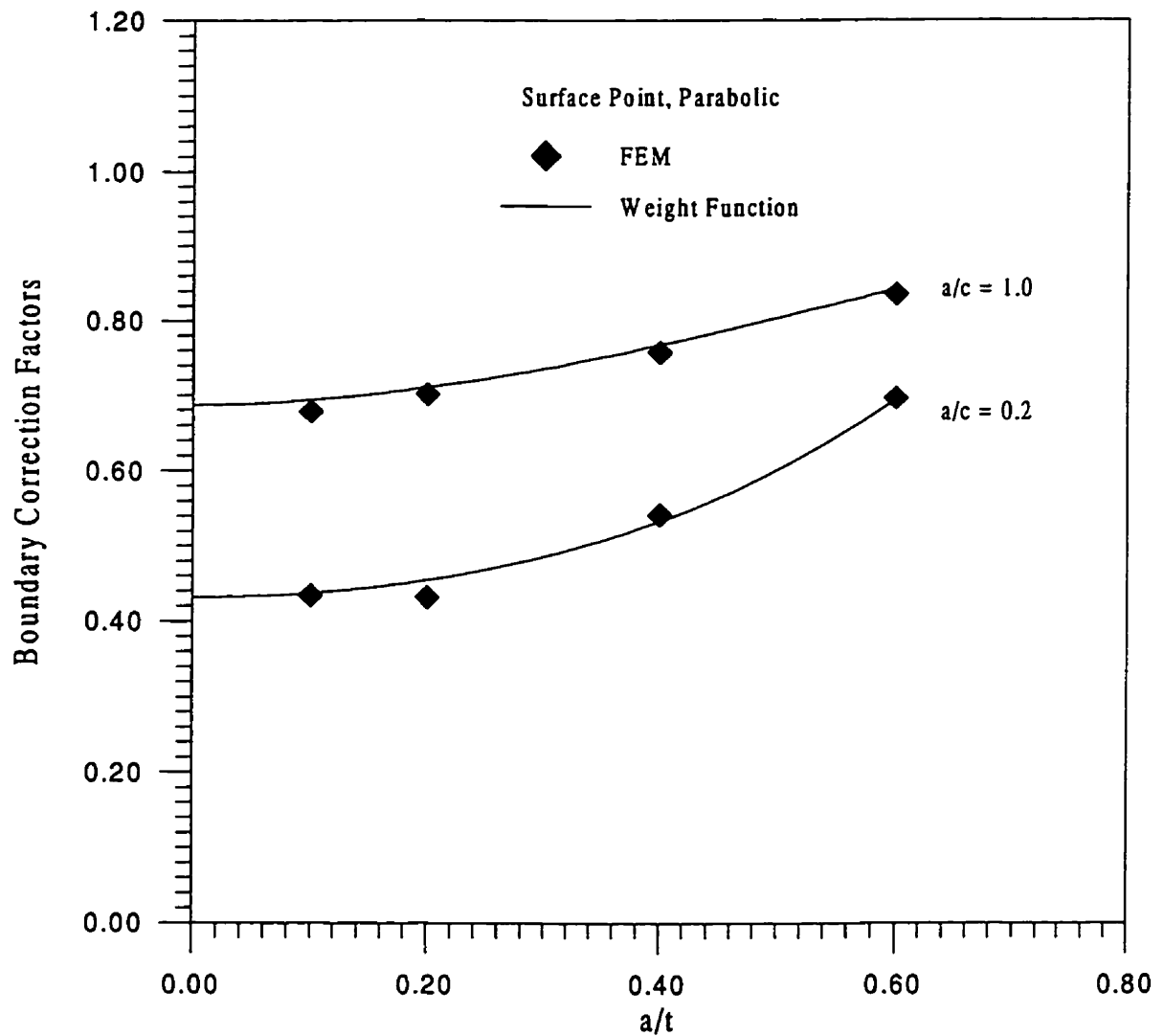


Figure 6.9 Comparison of the weight function based stress intensity factor and FEM data for stress distribution $\propto (1-x/a)^3$ ($\pi/4$ weld angle, deepest point).

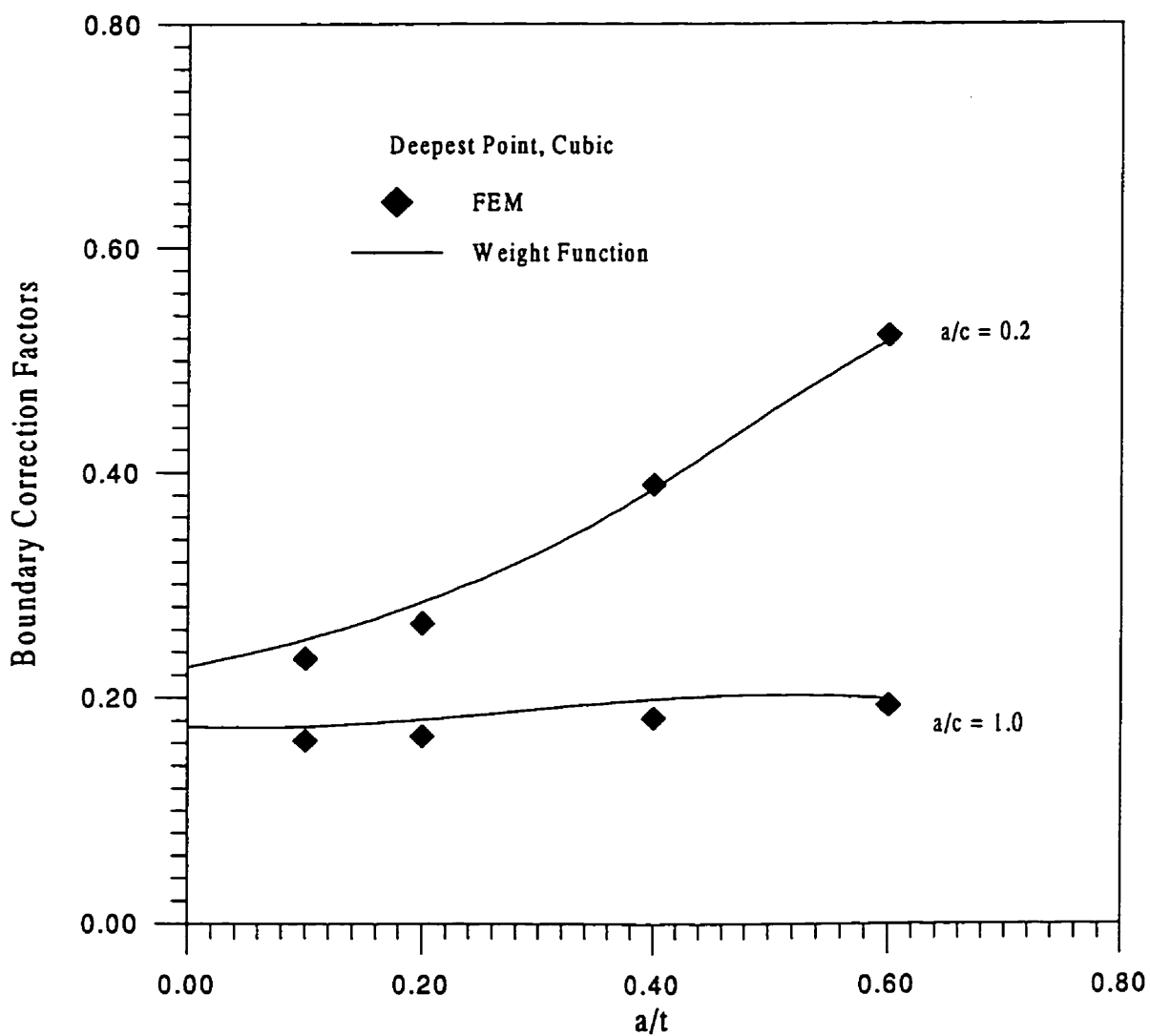


Figure 6.10 Comparison of the weight function based stress intensity factor and FEM data for stress distribution $\propto (1-x/a)^3$ ($\pi/4$ weld angle, surface point).

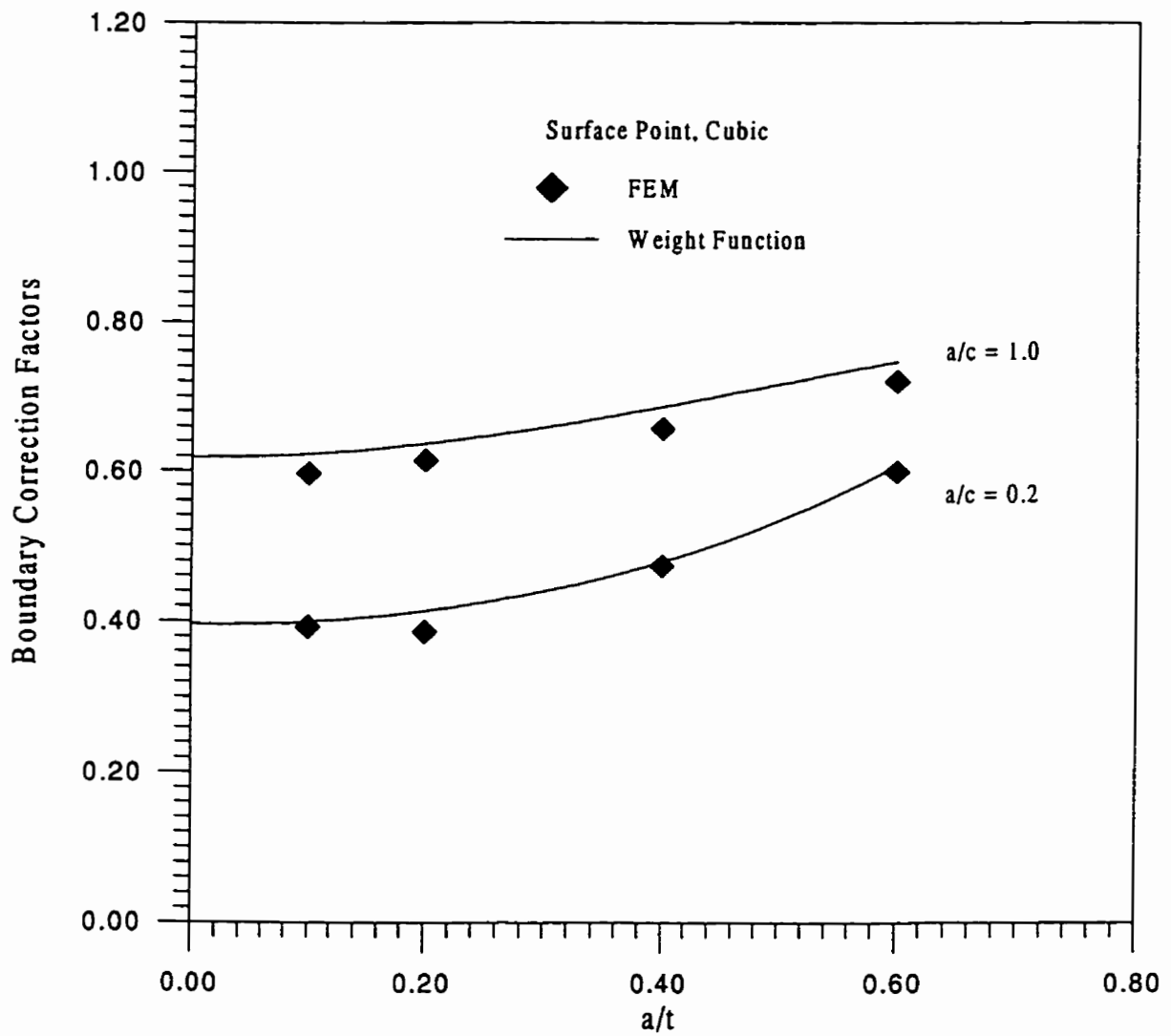


Figure 6.11 Comparison of the weight function based weld toe magnification factor and FEM data (far field tension, $\pi/4$ weld angle, deepest point).

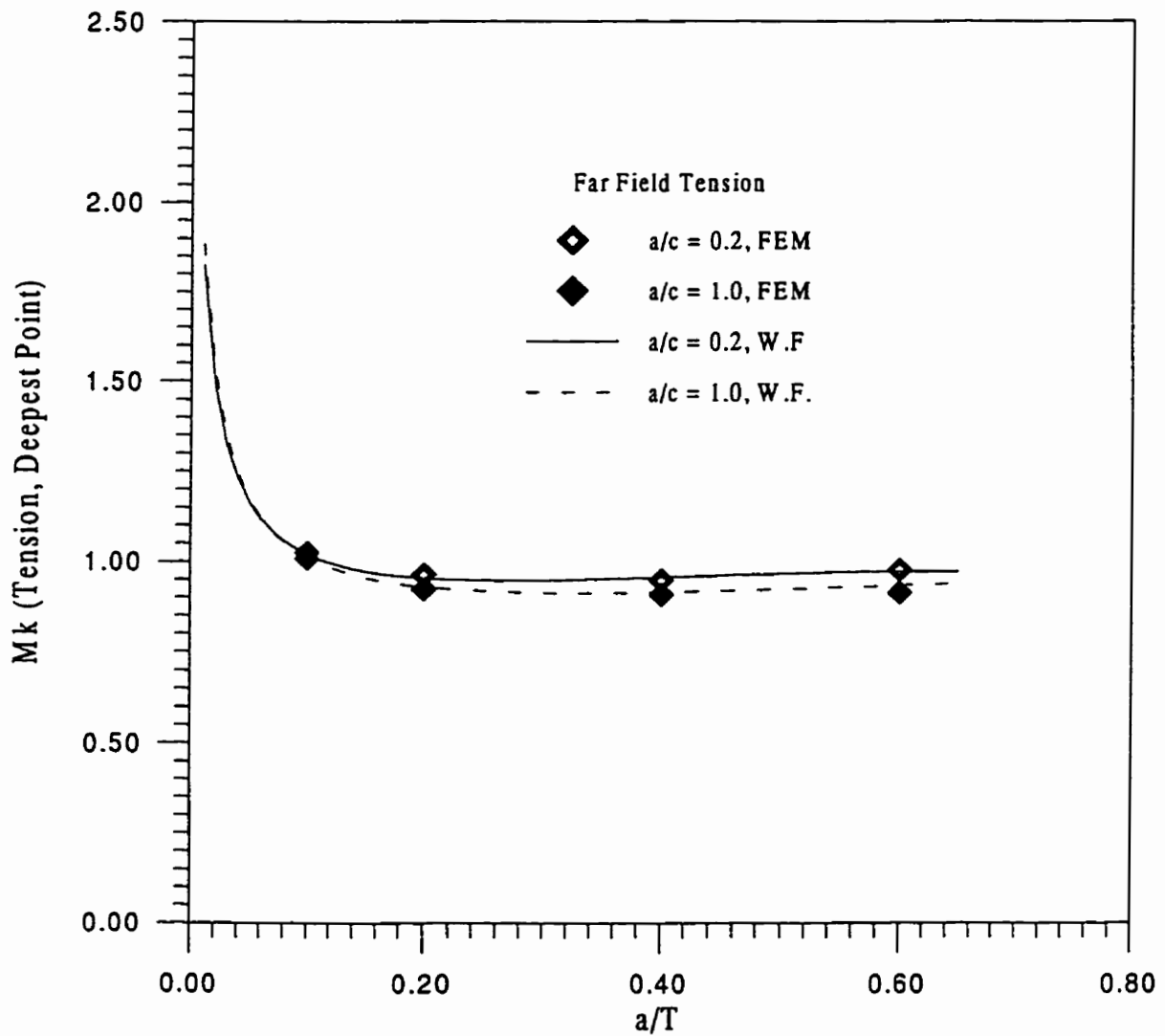


Figure 6.12 Comparison of the weight function based weld toe magnification factor and FEM data (far field tension, $\pi/4$ weld angle, surface point).

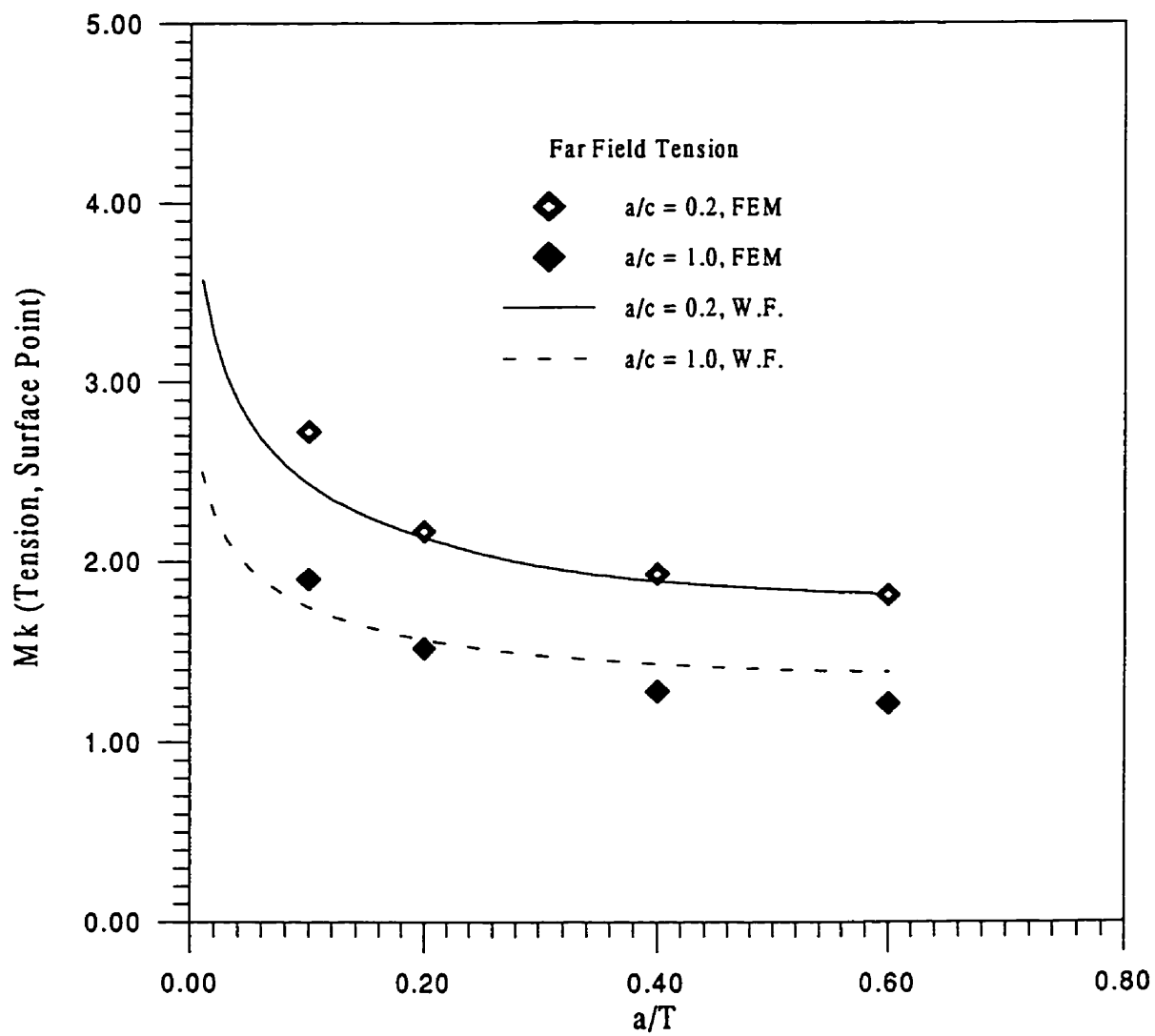


Figure 6.13 Comparison of the weight function based weld toe magnification factor and FEM data (far field bending, $\pi/4$ weld angle, deepest point).

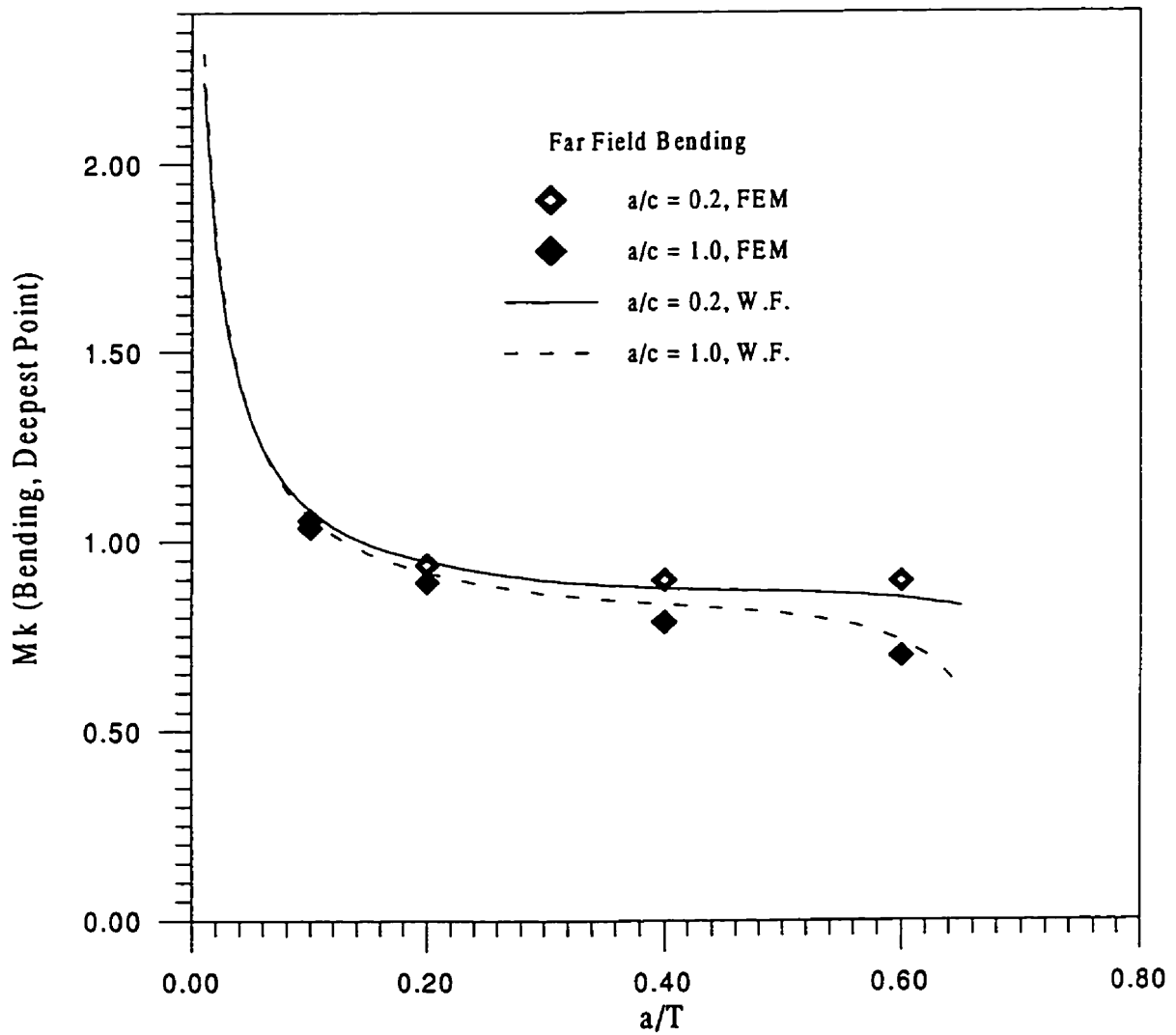


Figure 6.14 Comparison of the weight function based weld toe magnification factor and FEM data (far field bending, $\pi/4$ weld angle, surface point).

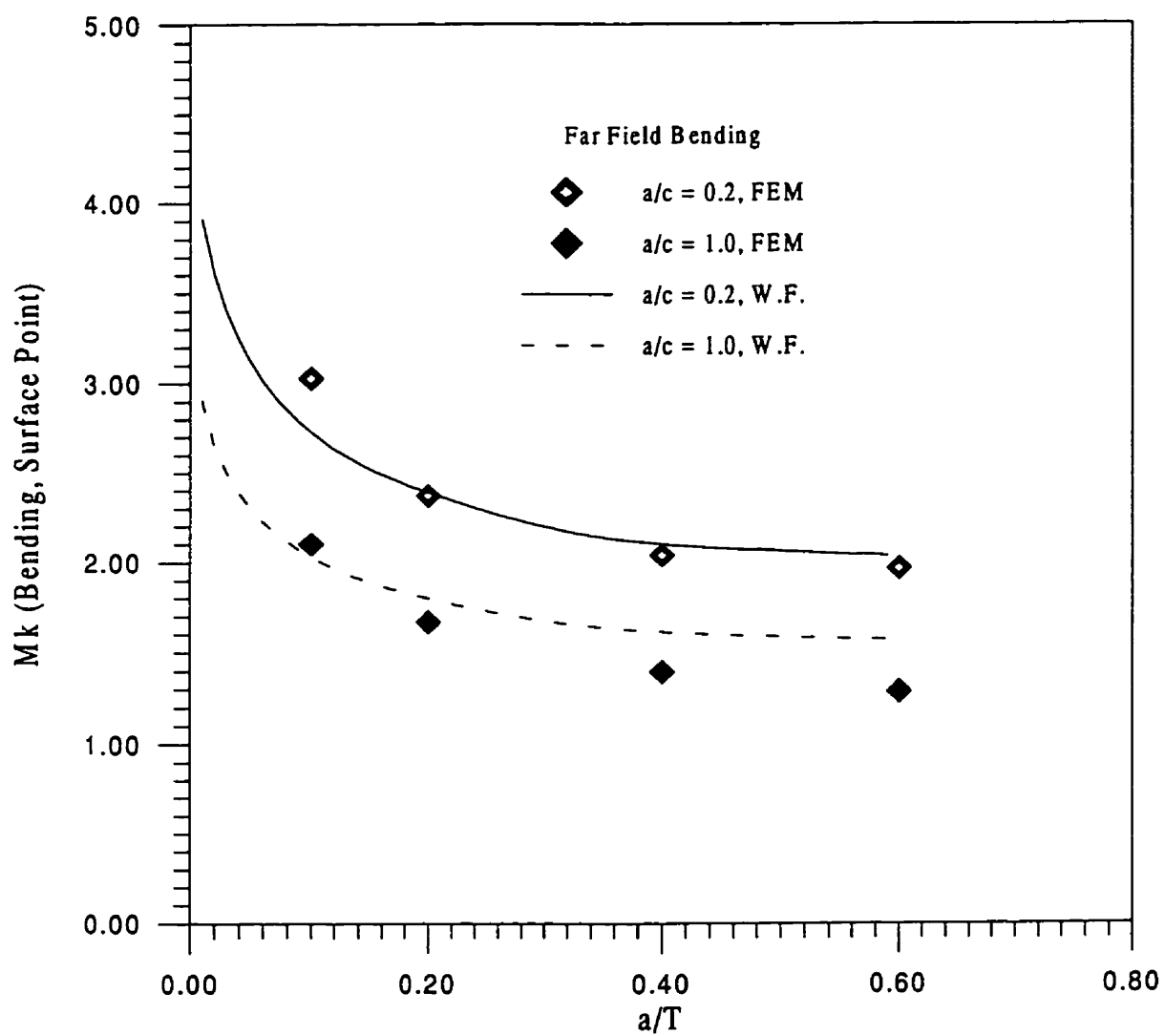


Figure 6.15 Geometry, boundary condition and load

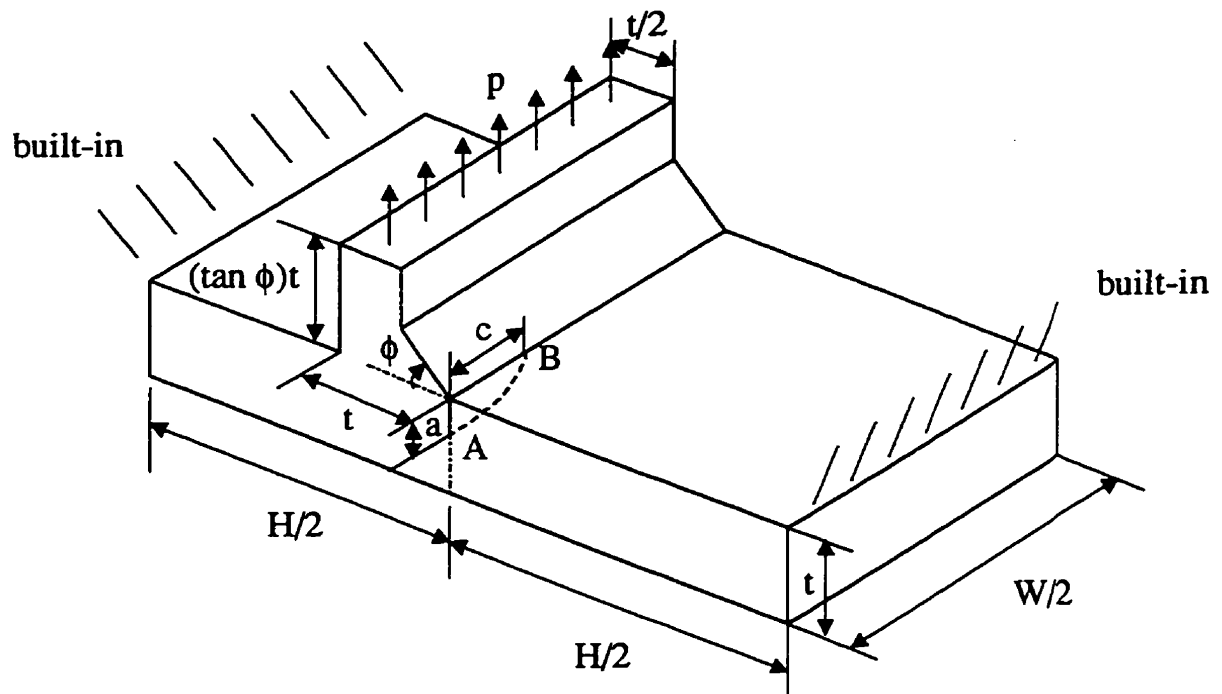


Figure 6.16. Proposed solution

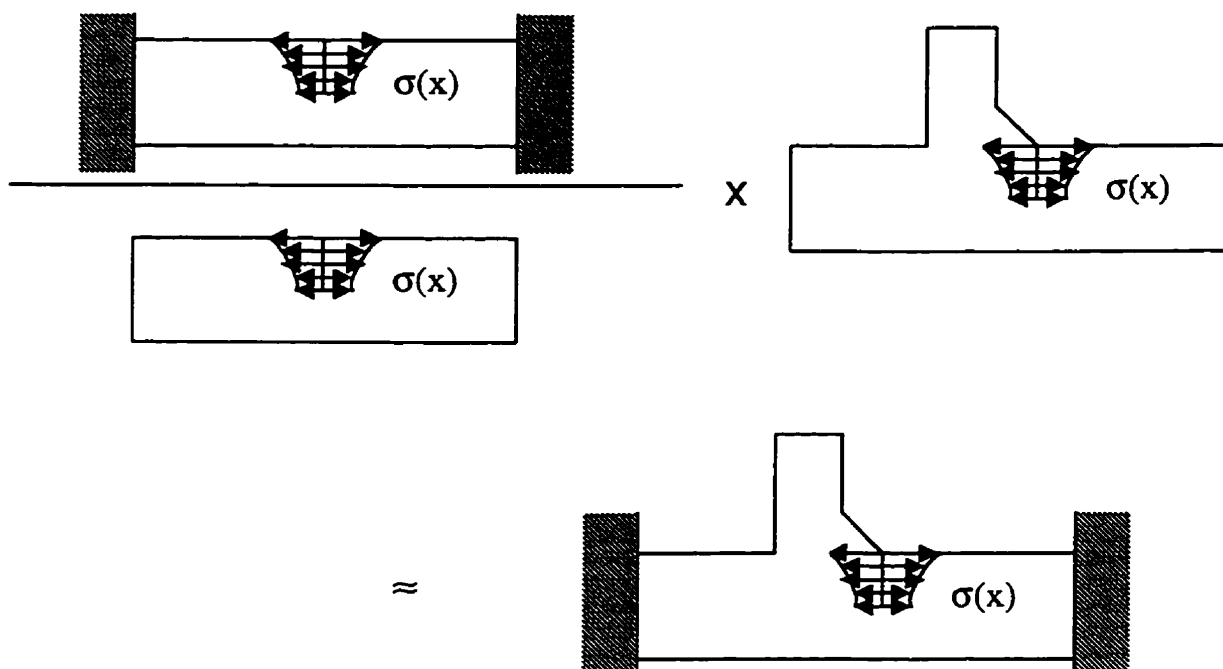


Figure 6.17 Stress intensity factors for surface cracks in T-plate joints with built-in ends under bending, $\pi/4$ weld angle, ($a/c = 0.1$, $H/t = 10$, deepest point).

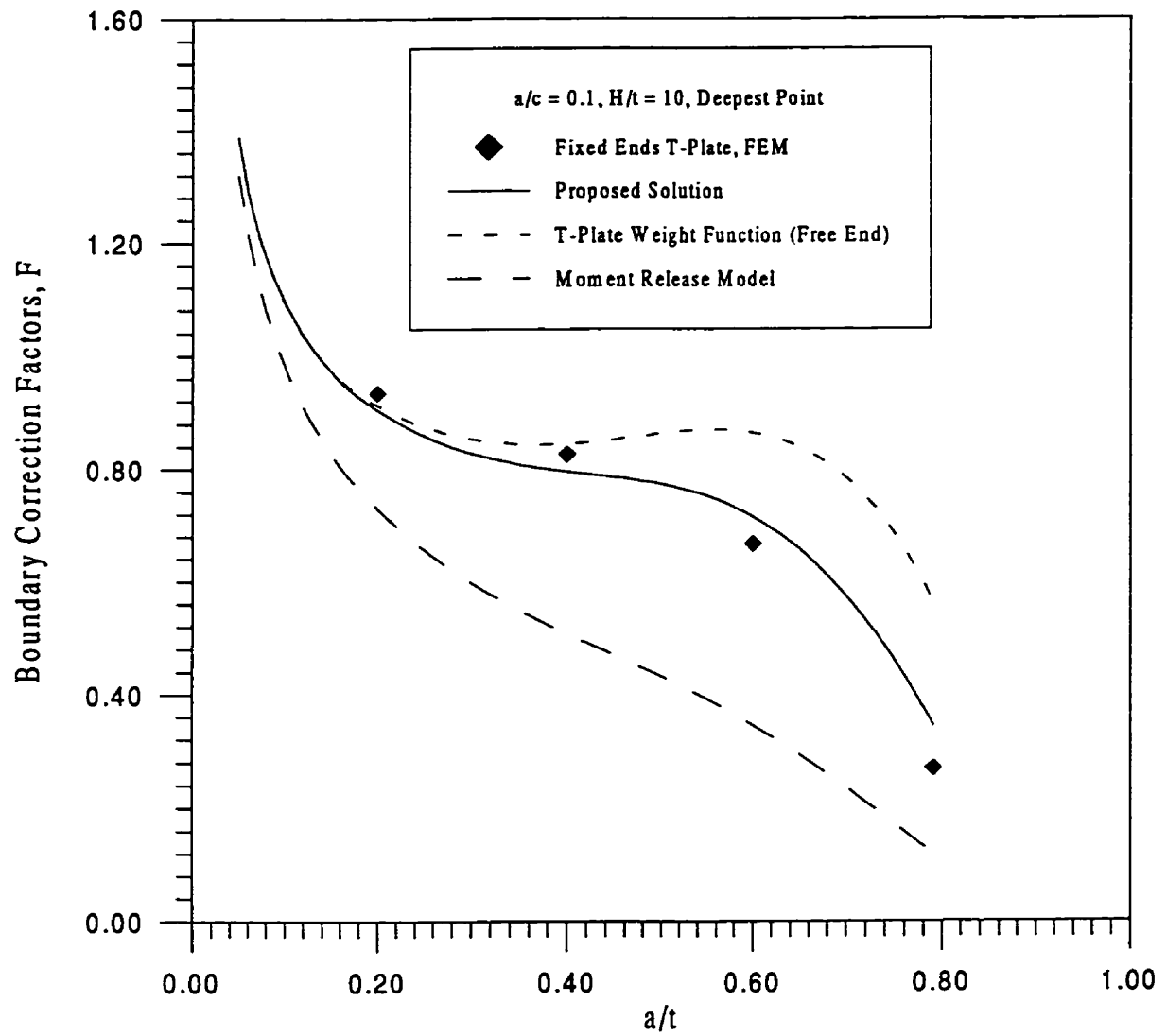


Figure 6.18 Stress intensity factors for surface cracks in T-plate joints with built-in ends under bending, $\pi/4$ weld angle, ($a/c = 0.1$, $H/t = 10$, surface point).

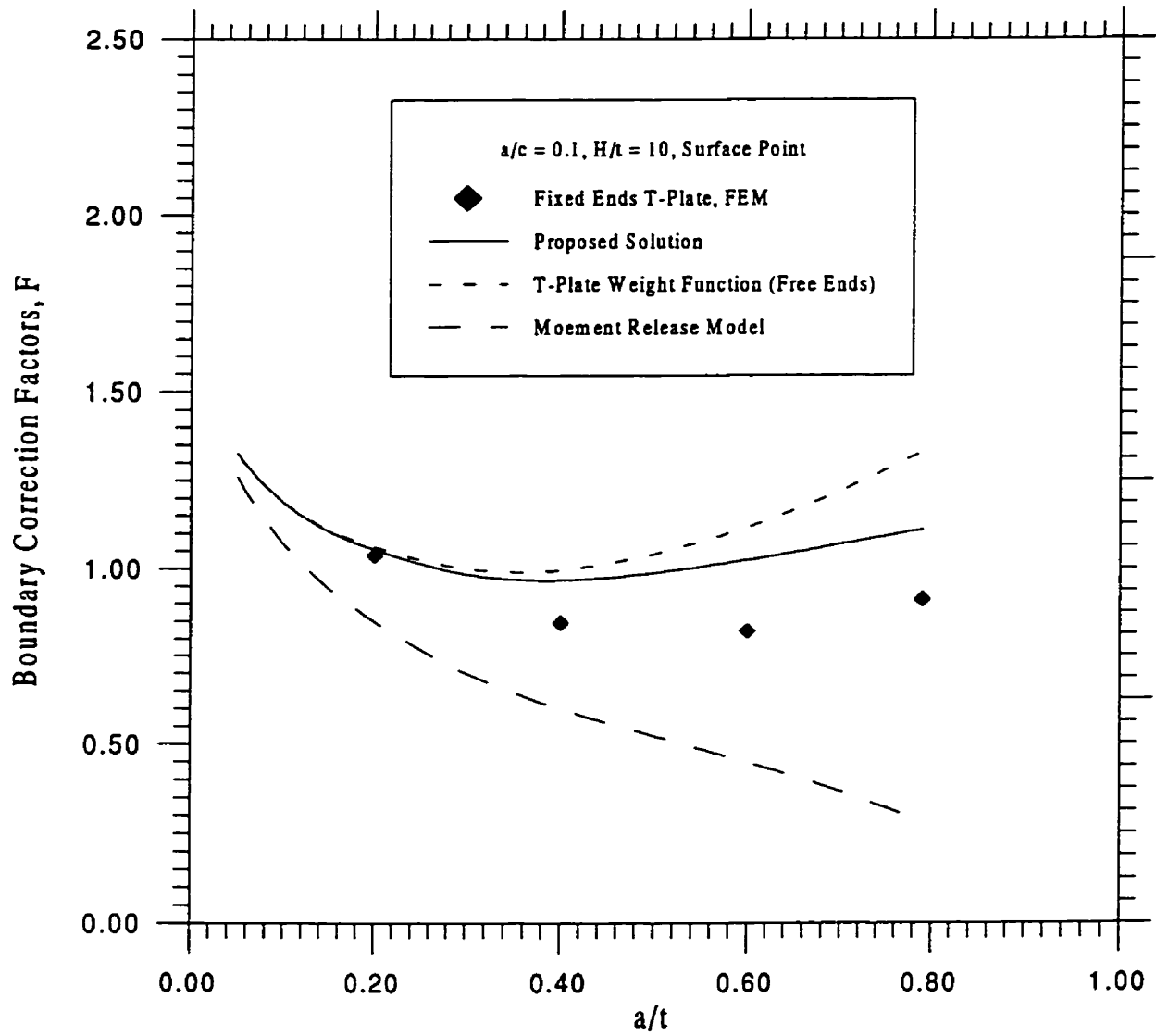


Figure 6.19 Stress intensity factors for surface cracks in T-plate joints with built-in ends under bending, $\pi/4$ weld angle, ($a/c = 0.2$, $H/t = 10$, deepest point).

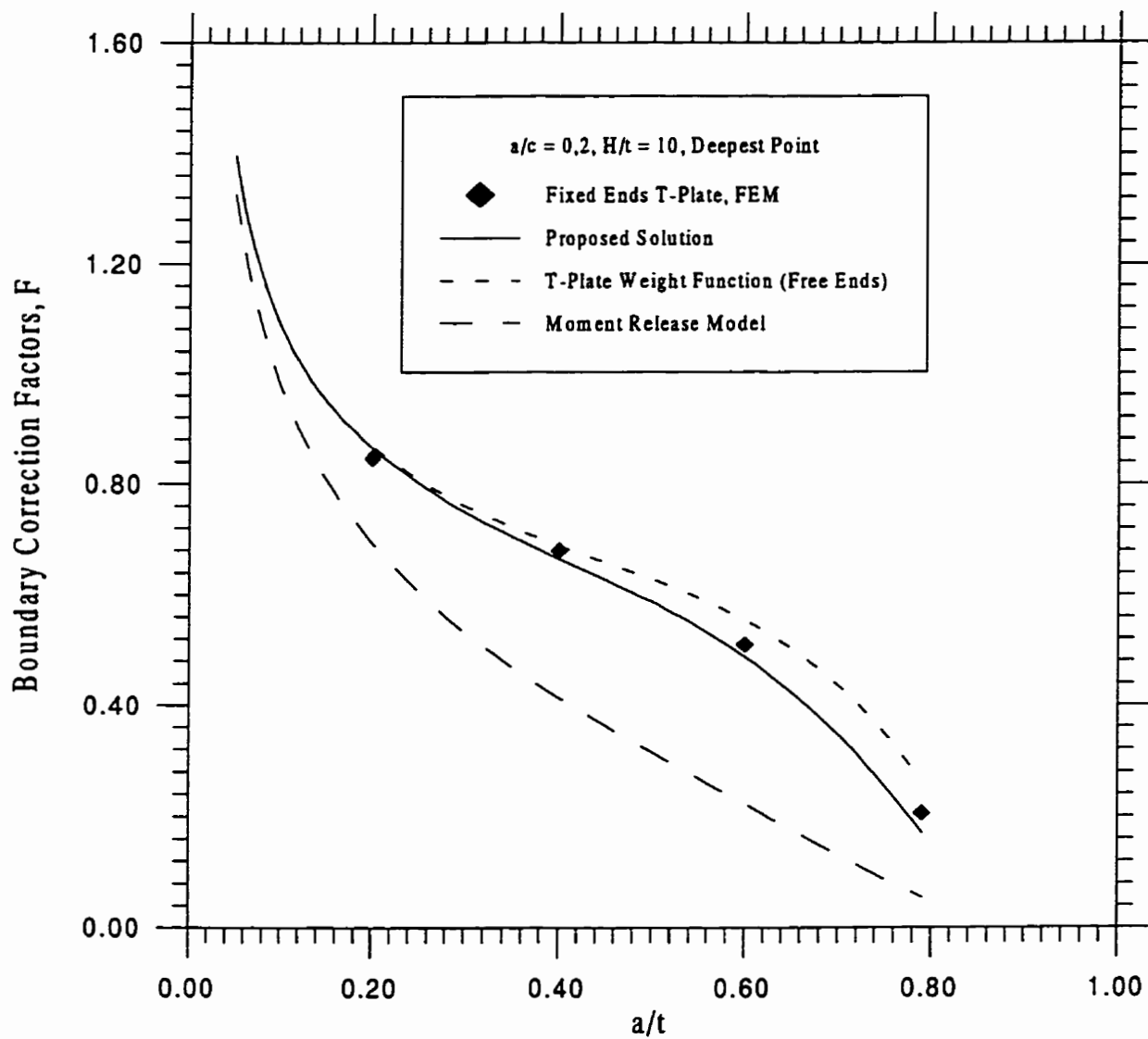


Figure 6.20 Stress intensity factors for surface cracks in T-plate joints with built-in ends under bending, $\pi/4$ weld angle, ($a/c = 0.2$, $H/t = 10$, surface point).

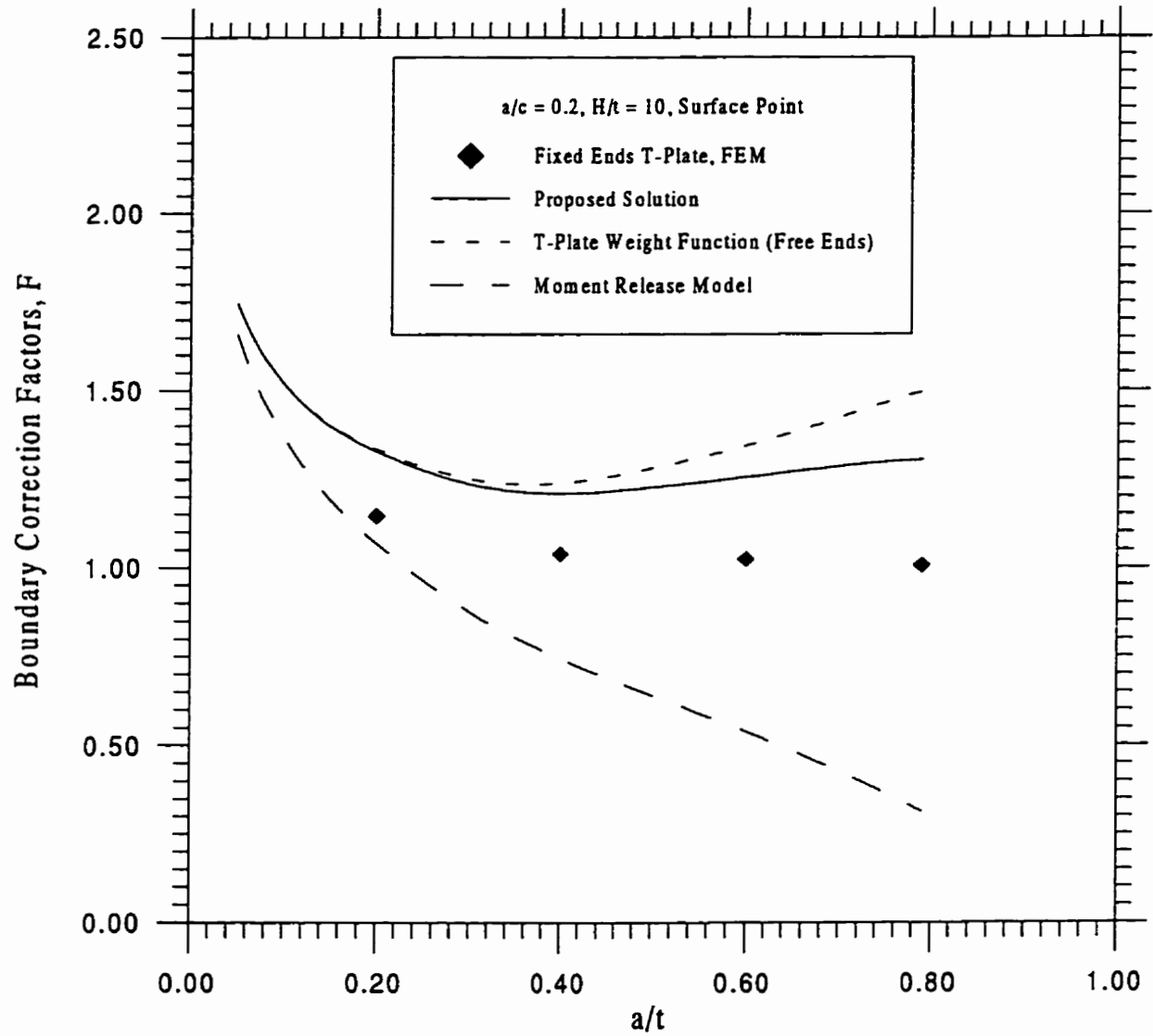


Figure 6.21 Stress intensity factors for surface cracks in T-plate joints with built-in ends under bending, $\pi/4$ weld angle, ($a/c = 1.0$, $H/t = 10$, deepest point).

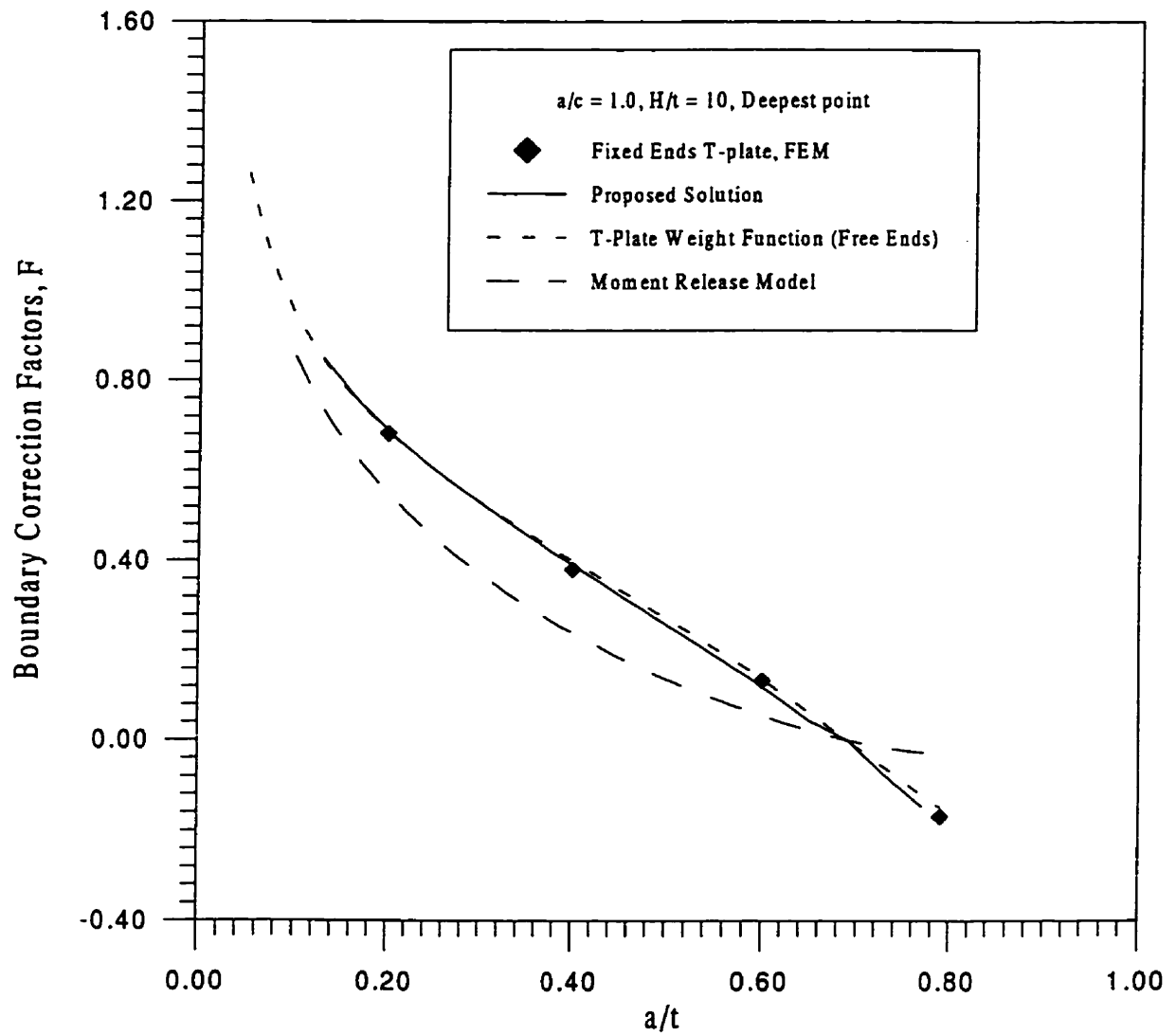
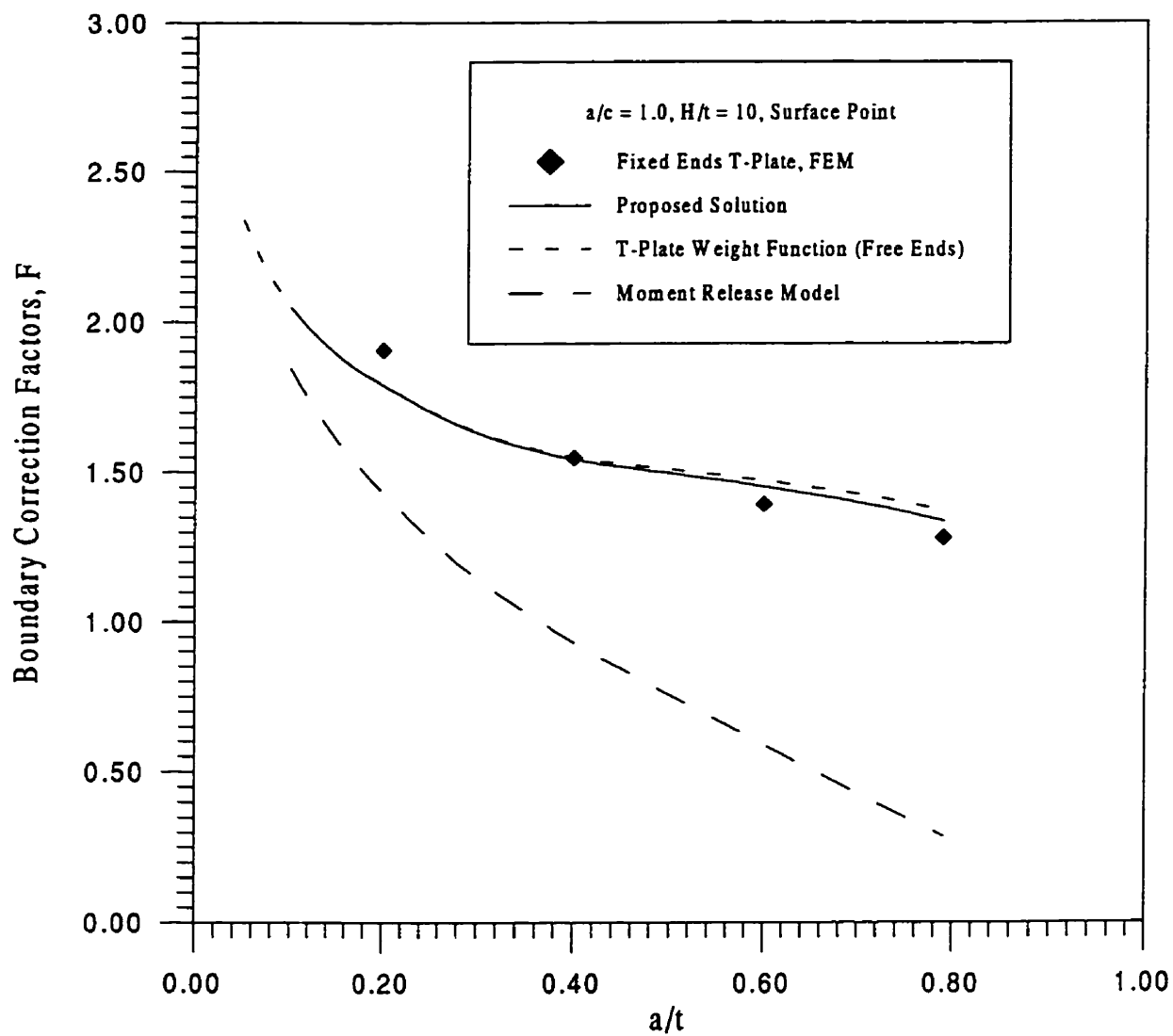


Figure 6.22 Stress intensity factors for surface cracks in T-plate joints with built-in ends under bending, $\pi/4$ weld angle, ($a/c = 1.0$, $H/t = 10$, surface point).



Chapter 7

Surface Cracks in Pipe-Plate and Tubular Joints

In this chapter, methods to determine stress intensity factors for surface cracks in pipe-plate and tubular joints are discussed. A new model for the calculation of stress intensity factors for surface cracks in pipe-plate and tubular joints was developed. The results are compared with available numerical and experimental data.

7.1 Surface Cracks in Pipe-plate Joints

As discussed in section 2.3.3, the pipe-plate specimen has been considered as a simplified model for a tubular joint (Lambert *et al.*, 1987). Figure 7.1 shows the geometry of a pipe-plate joint. Two different types of loading are usually considered, bending and tension, as shown in Figure 7.1. In this section, approximate stress intensity factor solutions for surface cracks in pipe-plate joints are proposed. The results are compared with available finite element and experimental data.

7.1.1 Proposed Stress Intensity Factor Solution

Lambert (1988) used stress intensity factor solutions developed for T-plate joints with free ends, Eq.(2.17), to calculate the stress intensity factors for surface cracks in the pipe-plate specimen. Because of the differences in boundary conditions and geometry between T-plate and pipe-plate joints, such empirical equations resulted in conservative estimates for stress intensity factors for deep cracks, $a/t > 0.5$, and hence underestimated fatigue life. This effect was attributed to load shedding. This is not addressed in stress intensity factor solutions T-plate joints with free ends.

In the present research, it is proposed that the stress intensity factor solutions for surface cracks in T-plate joints with built-in ends developed in Chapter 6 be used to estimate the stress intensity factors for surface cracks in pipe-plate joints.

For a surface crack in a pipe-plate joint (Figure 7.1), a T-plate model with built-in ends and the same crack geometry (a/c , a/t and ϕ), under the same crack face stress distribution, $\sigma(x)$, is used to calculate stress intensity factors, Figure 7.2. The stress distribution, $\sigma(x)$, is the stress distribution on the prospective crack plane for the uncracked pipe-plate joint.

Note that the parameter, H , the span for the T-plate joint with built-in ends, requires more attention. An appropriate H must be chosen to account for the effects of the plate boundary and the pipe (brace) geometry. Because of differences in the geometries between T-plate and pipe-plate joints, several different choices for H parameters were examined. Since the radius of the brace plays a major role on the constraint of the crack in the pipe-plate geometry (Figure 7.2), the following expression for H was used:

$$H(R_{pipe}) = \lambda \cdot R_{pipe} \quad (7.1)$$

where R_{pipe} is the radius of the pipe, as shown in Figure 7.1, and λ is a constant. Note that while it may reasonably be expected that H will depend on plate thickness, only one pipe-plate geometry was considered herein, and therefore no information was available to indicate this effect.

Stress intensity factors for surface cracks in pipe-plate joint can now be calculated for different values for λ using the procedures in Chapter 6, Eqs. 6.19-6.21:

$$K_{built-in\ ends}^{T-plate}(P') = \alpha(P') \cdot K_{free\ ends}^{T-plate}(P') \quad (6.19)$$

The stress intensity factor for a T-plate joint with free ends, $K_{free\ ends}^{T-plate}(P')$, can be calculated from the corresponding weight functions

$$K_{free\ ends}^{T-plate}(P') = \int_0^a \sigma(x) M_{free\ ends}^{T-plate}(x; P') dx \quad (6.20)$$

The correction factor, $\alpha(P')$, to account for the effect of the built-in ends, is based on the factor for surface cracks in flat plates:

$$\alpha(P') = \frac{\int_0^a \sigma(x) M_{built-in\ ends}^{flat\ plate}(x; P') dx}{\int_0^a \sigma(x) M_{free\ ends}^{flat\ plate}(x; P') dx} \quad (6.21)$$

7.1.2 Comparisons with Experimental and Finite Element Data

Experimental and Finite Element Results

Experimental stress intensity factors were determined on the basis of measured crack growth rates in pipe-plate joints (Lambert, 1988). The geometry of the pipe-plate is shown in Figure 7.3. The pipe had a 417mm diameter, with 32 mm wall thickness, and was welded to the centre of a 26 mm thick flat plate using a 45° flat fillet weld. The plate was 1.5m long by 1m wide, and was clamped along the edges. A cyclic in-plane-bending load was applied. Periodical crack measurements were made using a pulsed D.C. potential drop technique (Yee and Lambert, 1995). The crack growth rates da/dN were obtained from these results. The corresponding stress intensity factors were determined from Paris' equation:

$$\Delta K = \left(\frac{1}{C} \cdot \frac{da}{dN} \right)^{1/m} \quad (7.2)$$

where C and m are material constants ($C = 2.4 \times 10^{-12}$ and $m = 3$). The resulting stress intensity factors were normalised as follows:

$$Y = \frac{\Delta K}{\Delta \sigma_{HS} \sqrt{\pi a}} \quad (7.3)$$

where σ_{HS} is the hot spot stress in the pipe-plate joint, obtained by linearly extrapolating the top surface stresses to the weld toe. The resulting experimental stress intensity factor solutions were plotted in Figure 7.4.

Lambert and Bell (1993) also conducted three-dimensional finite element calculations for this pipe-plate specimen. They analysed six different crack geometries observed during the experiments. The resulting stress intensity factors are presented in Table 7.1, and plotted in Figure 7.4. They also presented the stress distribution on the perspective cracked plane obtained from a detailed 2D finite analysis of the uncracked geometry.

Comparisons with Proposed Solution

Stress intensity factors were calculated using the procedure described in section 7.1.1 for these crack geometries for different values of λ . Comparisons of the results for the present method, experimental and finite element calculations at the deepest point are shown in Figure 7.4. The proposed method gave the best predictions for $\lambda = 1/2$. The difference between this solution and finite element calculations was about 10%. There was also good agreement with the experimental data.

The predictions from the moment release model (Aaghaakouchak *et al.*, 1989) are also plotted in Figure 7.4. It under-estimates the stress intensity factors. This is not surprising since the moment release model was developed based on results for tubular joints, which usually experience more load shedding than the pipe-plate joint (Forbes, 1991).

7.2 Surface Cracks in Tubular Joints

Figure 7.5 shows the geometry for a tubular joint used in the Canadian Offshore Research Program (Forbes *et al.*, 1992). Three different types of loading were considered:

in-plane bending, out-of-plane bending, and tension, as shown in Figure 7.5. In this section, a solution for stress intensity factors for surface cracks in tubular joints is proposed. The results are compared with experimental data from Forbes (1991), and to approximate load shedding solutions proposed by Aaghaakouchak *et al.* (1989).

7.2.1 Proposed Stress Intensity Factor Solution

In the present research, it is proposed that stress intensity factor solutions for surface cracks in T-plate joints with built-in ends can be used to calculate stress intensity factors for surface cracks in tubular joints.

For a surface crack in a tubular joint (Figure 7.5), a T-plate model with built-in ends and the same crack geometry (a/c , a/t and ϕ), under the same crack face stress distribution, $\sigma(x)$, is used to calculate stress intensity factors in tubular joints, as shown in Figure 7.6. The stress distribution, $\sigma(x)$, is the stress distribution on the prospective crack plane for the uncracked tubular joint.

In this case, a similar expression for the equivalent span for the T-plate joint with built-in ends, H , as was used for the pipe-plate analysis, is used:

$$H = \lambda \cdot R_{brace} \quad (7.4)$$

where R_{brace} is the radius of the brace, as shown in Figure 7.5, and λ is a constant. The value of λ will depend on the overall geometry of the tubular joints, but will be less than 1 to reflect the increased stiffness of the joint due to the brace curvature. Since only one

geometry was used, no information was available to investigate the effects of other parameters such as thickness, length, etc.

Based on those assumptions, stress intensity factors for surface cracks in tubular joints can now be calculated using Eqs. 6.19 - 6.21.

7.2.2 Comparisons with Experimental Data

Experimental Data

Stress intensity factor solutions for surface cracks in a tubular joint were obtained from experimental observations by Forbes (1991). The geometry of the tubular is shown in Figure 7.7. Cyclic axial or in-plane bending loads were applied to the brace, and surface crack propagation was observed. The brace had a 457mm diameter, with a 19 mm wall thickness. The brace was welded to the centre of a chord having a 1067 mm diameter and 19 mm wall thickness using a 45°, flat, full penetration fillet-like weld. Experimental stress intensity factors for surface cracks in this geometry were obtained from the measured crack growth rates. The resulting stress intensity factors were normalised according to Eq. (7.3), and are plotted in Figures 7.8 and 7.9. From the crack shape development observations, a matrix of crack geometries for the two specimens is presented in Table 7.2 (Forbes, 1991). The stress distribution on the prospective crack plane was obtained by Forbes (1991) using two-dimensional finite element analysis.

Comparisons with Proposed Solution

Stress intensity factors were calculated using the procedure described in section 7.2.1 for the cracks geometries presented in Table 7.2. Comparisons of the results between the proposed solution and experimental data at the deepest point are shown in Figure 7.8 and 7.9. The present method gave the best predictions for both axial and in-plane bending cases when λ was $1/3$. The results from the moment release model (Aaghaakouchak *et al.*, 1989) and from Forbes (1991) model are also plotted in Figures 7.8 and 7.9. The moment release model gave good predictions for axial loads but under-estimated the in-plane bending case. Forbes' model gave fairly good predictions for both axial and in-plane bending loads. Forbes' model involved experimental measurement of the actual load shedding in the specimens, and therefore is not as generally applicable as the present method.

Compared with pipe-plate joints, the λ value for tubular joint was found to be smaller, $1/3$ versus $1/2$. The reason for this is assumed to be that the chord of the tubular joint provides more constraint than the flat base plate of pipe-plate joint. This is consistent with the observation by Forbes (1991) that tubular joints generally experience more load shedding than pipe-plate joints.

7.3 Discussion

A T-plate welded joint model with built-in ends was used to model surface cracks in pipe-plate and tubular joints. Load shedding effects were included because of the built-in ends. This model accounts for different load shedding effects resulting from different ratios of a/c , a/t , H/t at different positions along the crack front. This is a more sophisticated

model than those proposed by Aaghakouchak *et al.* (1989) and Forbes (1991), but much simpler to implement than a three-dimensional finite element analysis.

Some uncertainties remain in the present model. One of these is the value for λ in the expression for the parameter H . Values were chosen for λ for one pipe-plate and one tubular joint geometry only; it will certainly depend on other geometric parameters of the joints, including T , t , R_{chord} , and L . More extensive finite element/experimental analyses are required to examine the range of λ values, and to relate these to joint geometry.

A second issue is the curvature of the fatigue surface crack as it grows through the thickness. In the present model, semi-elliptical cracks are modelled as planar and normal to the base plate (for pipe-plate joints) or to the chord wall (for tubular joints). Only mode I stress intensity factors were considered. In reality, because the geometry is not symmetric about the crack plane, mode II stress intensity factors exist, and the crack front will curve in such a way as to maximise the mode I stress intensity factor component (Figure 7.10(a)). Du and Hancock (1989) conducted finite element analyses for stress intensity factors for curved and planar surface cracks in tubular joints using both line-spring and three-dimensional finite element analysis. They concluded that the stress intensity factors for curved surface cracks were similar to those for straight cracks normal to the chord wall, as long as the same a/t ratio was used. Bowness and Lee (1995) also conducted detailed three-dimensional finite element analyses for curved and planar surface cracks in tubular joints. They agreed that planer surface cracks could be used if the resulting stress intensity factors were treated as $K_{\text{effective}}$, which include the effect of the mode II stress intensity factor components:

$$K_{\text{effective}} = \sqrt{K_I^2 + K_{II}^2 + \frac{K_{III}^2}{1-\nu}} \quad (7.5)$$

Therefore, using mode I stress intensity factors and the assumption of a planar crack face in the present model appears justified.

Note that the T-plate model used in the present analysis had an equal base plate length on either side of the crack, as shown in Figure 7.10 (b). It may be more effective to use a T-plate model with built-in ends of different lengths, a and b , as illustrated in Figure 7.10 (c). The existence of the brace will provide more constraint than the flat plate (for pipe-plate joint) or chord (for tubular joint), and therefore a will be smaller than b . Further finite element calculations are required to determine appropriate values for a and b , and whether this approach will offer significant improvements over the present method where $a = b$.

The another effect which was not included in the present model is the effect of a two-dimensional stress distribution. Only variations in the stress distribution through the thickness were considered in the present model. As discussed in section 2.3, the stress distribution on the uncracked plane is two-dimensional, $\sigma(x, y)$, and changes along the weld toe. Typical stress distributions along the weld toe for pipe-plate and tubular joints are plotted in Figure 7.11. T-plate joints with built-in ends subject to two-dimensional stress distributions, $\sigma(x, y)$, as shown in Figure 7.12(a), can be used to model this effect. The Fourier series approach presented in Chapter 5 can be used to estimate the stress intensity factors required for the model in Figure 7.12(a). However, from the estimation by Desjardins *et al.* (1991), the difference between the predictions from the models shown in Figures 7.12 (a) and (b) were within a few percent for the present surface cracks geometries and the typical stress distributions shown in Figure 7.11. Therefore, in the present analysis, the simple one-dimensional stress distribution model shown in Figure 7.12(b) was used.

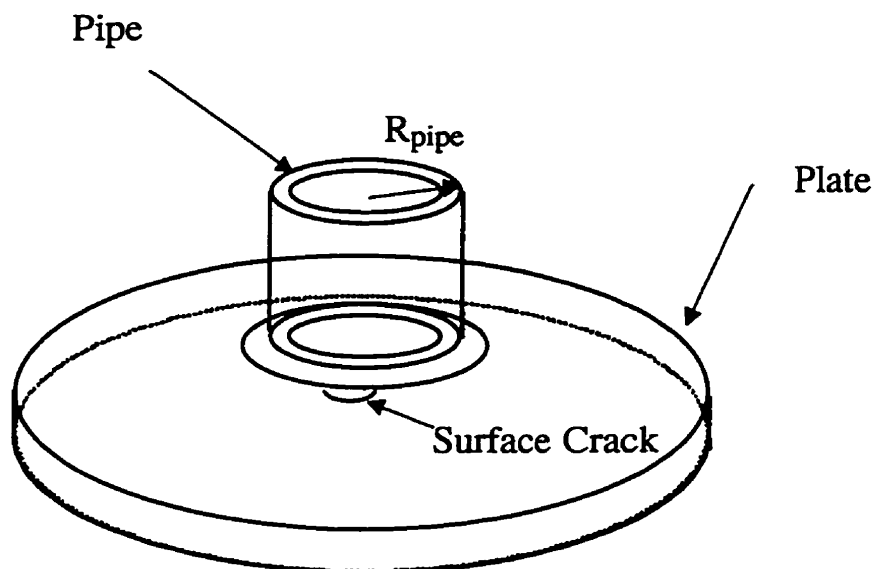
Table 7.1 Y factor for cracks in the pipe-plate weld joint (Lambert and Bell, 1993)

a/t	a/c	Y
0.25	0.1969	0.813
	0.1225	0.896
0.5	0.103	0.751
	0.090	0.786
0.6	0.121	0.613
	0.105	0.645

Table 7.2 Crack Shape in the Pipe-plate Weld Joint (Forbes, 1991)

Axial Load		In Plane Bending	
<i>a/t</i>	<i>a/c</i>	<i>a/t</i>	<i>a/c</i>
0.2	0.0490	0.2	0.0516
0.4	0.0671	0.4	0.0464
0.6	0.0800	0.6	0.0671
0.8	0.0903	0.8	0.0697

Figure 7.1 Pipe-plate joint



Pipe-Plate Geometry

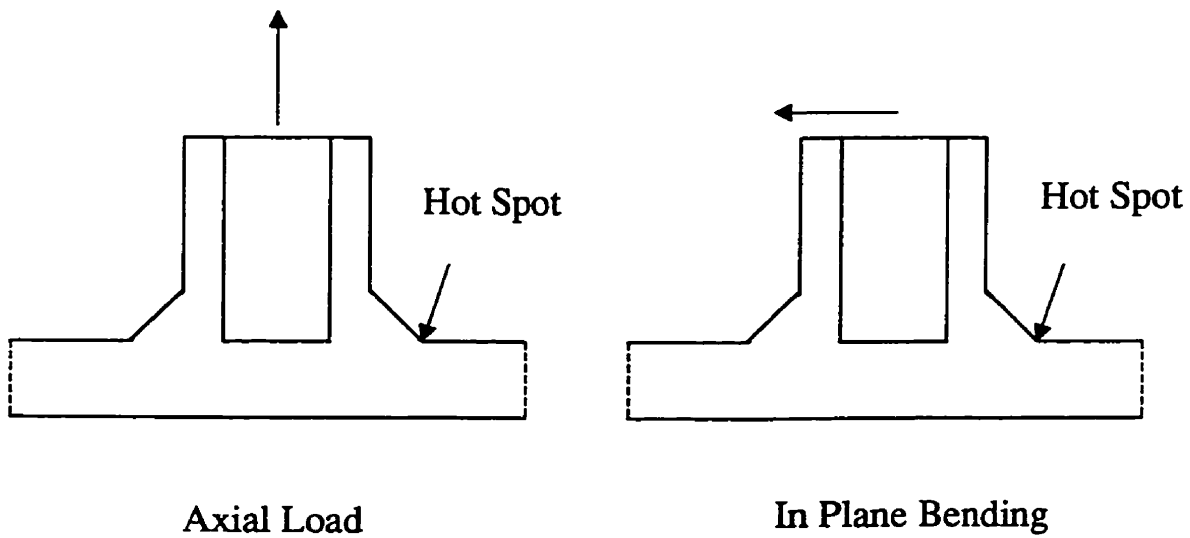


Figure 7.2 T-plate with built-in ends model for pipe-plate joints

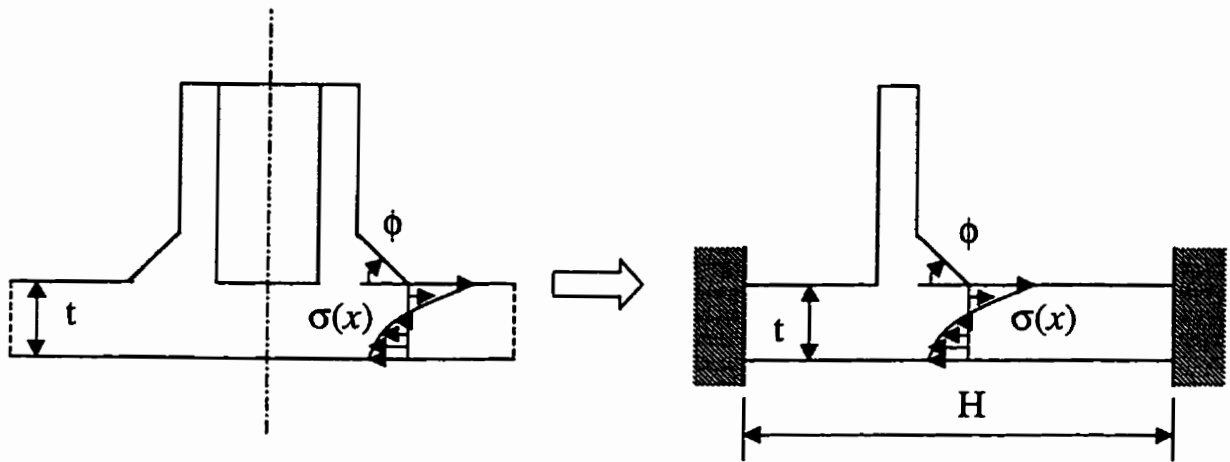


Figure 7.3 The pipe-plate specimen (Lambert, 1988)

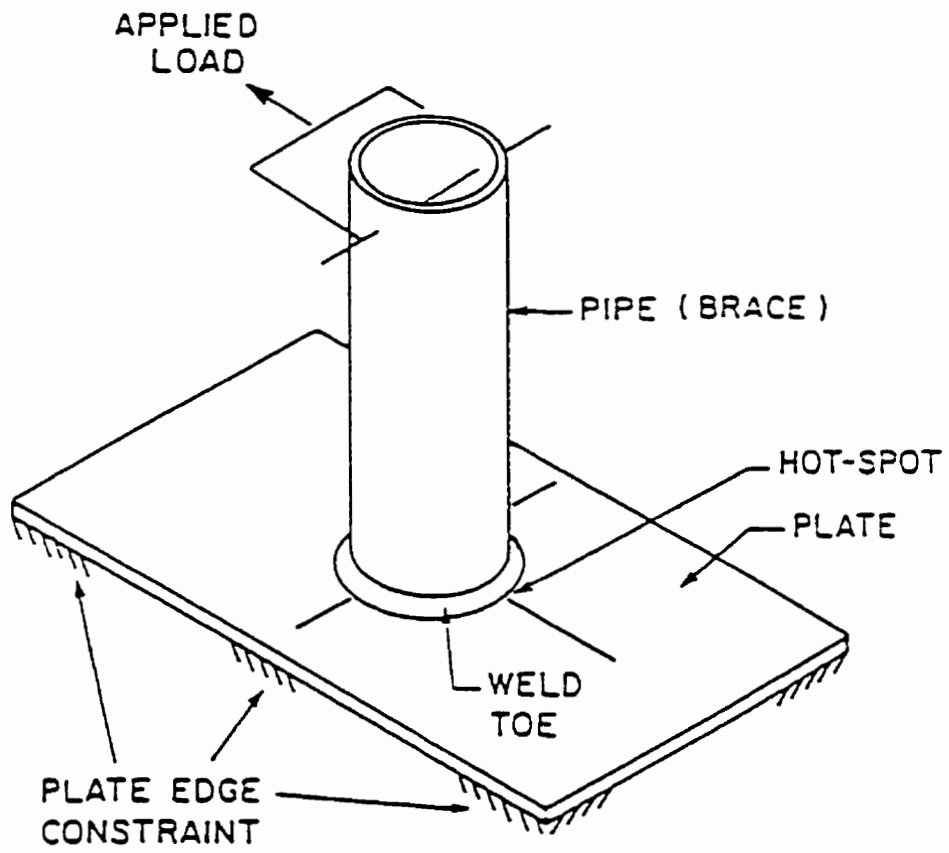


Figure 7.4 Results for stress intensity factors for surface cracks in pipe-plate joints

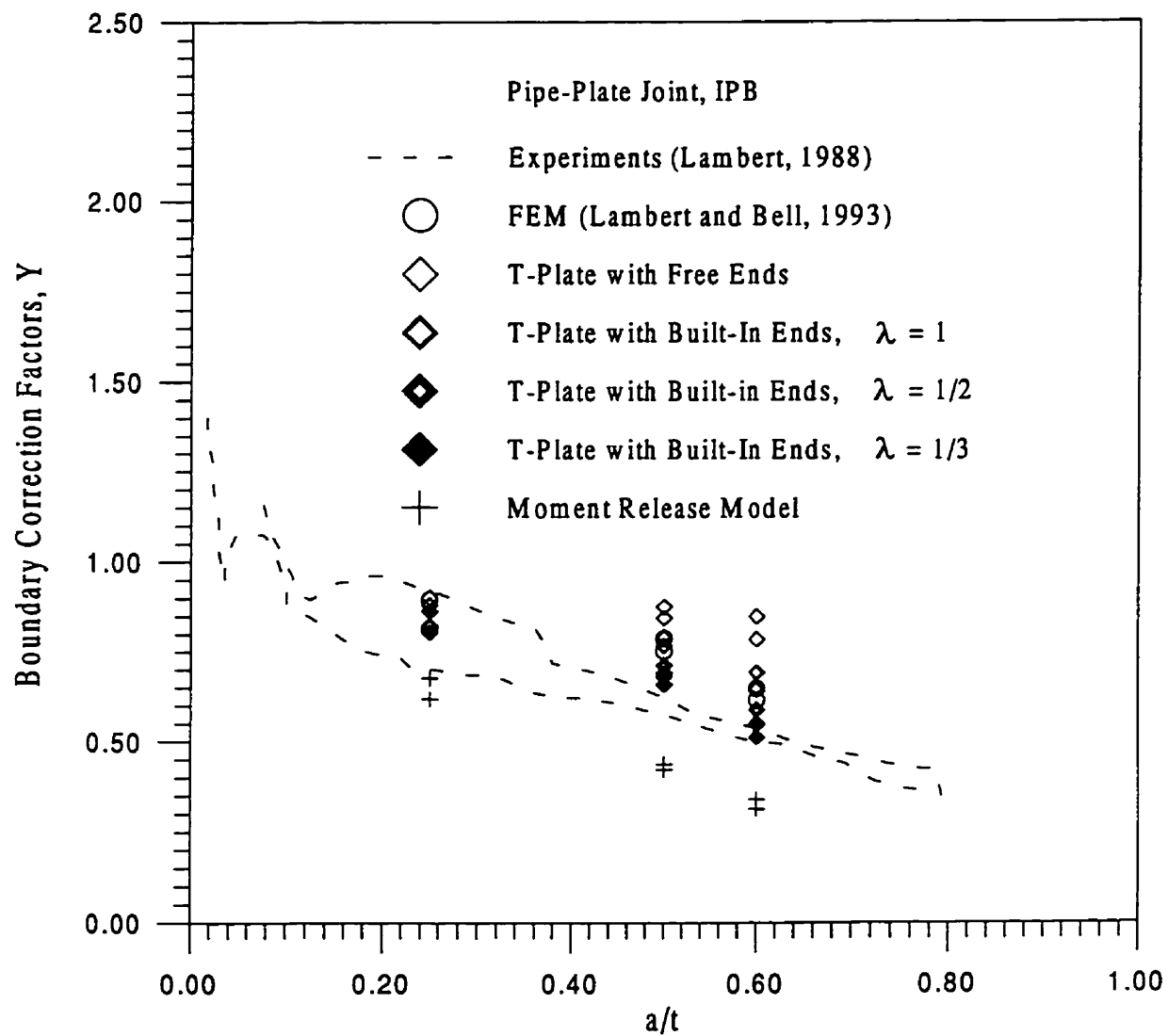


Figure 7.5 Geometry of tubular joint

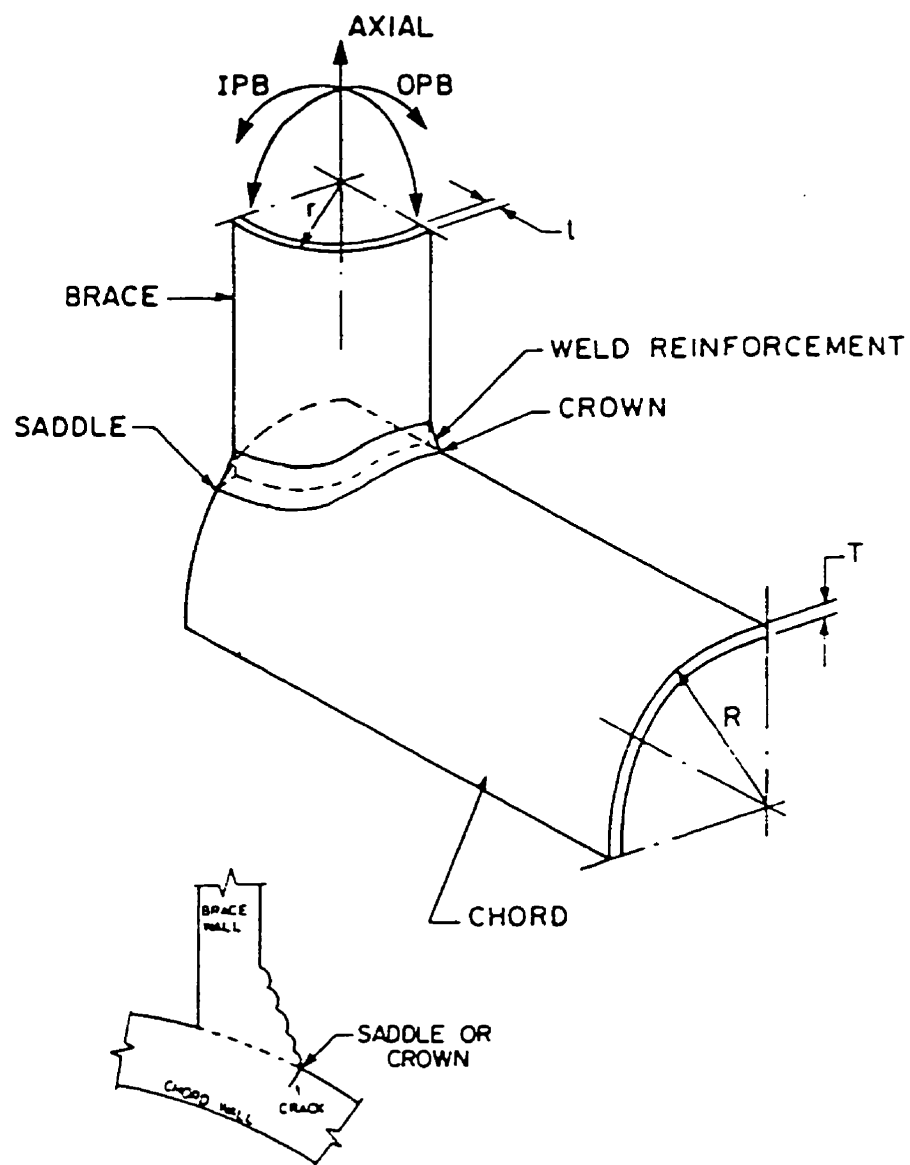


Figure 7.6 T-plate with built-in ends model for tubular joints

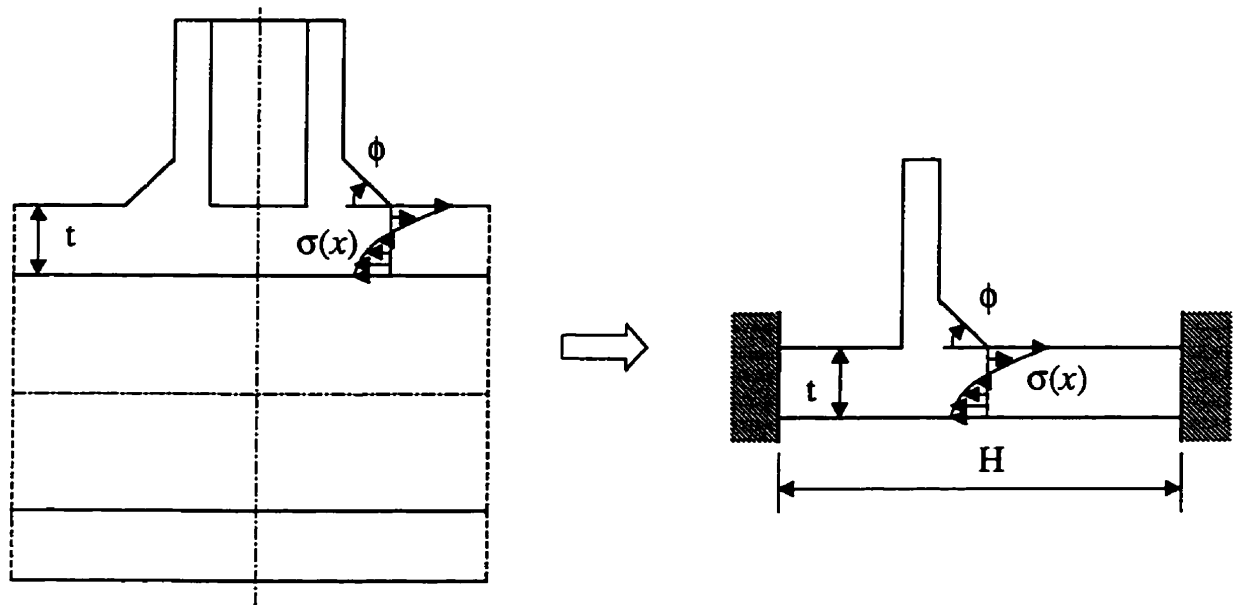


Figure 7.7 The tubular specimen (Forbes, 1991)

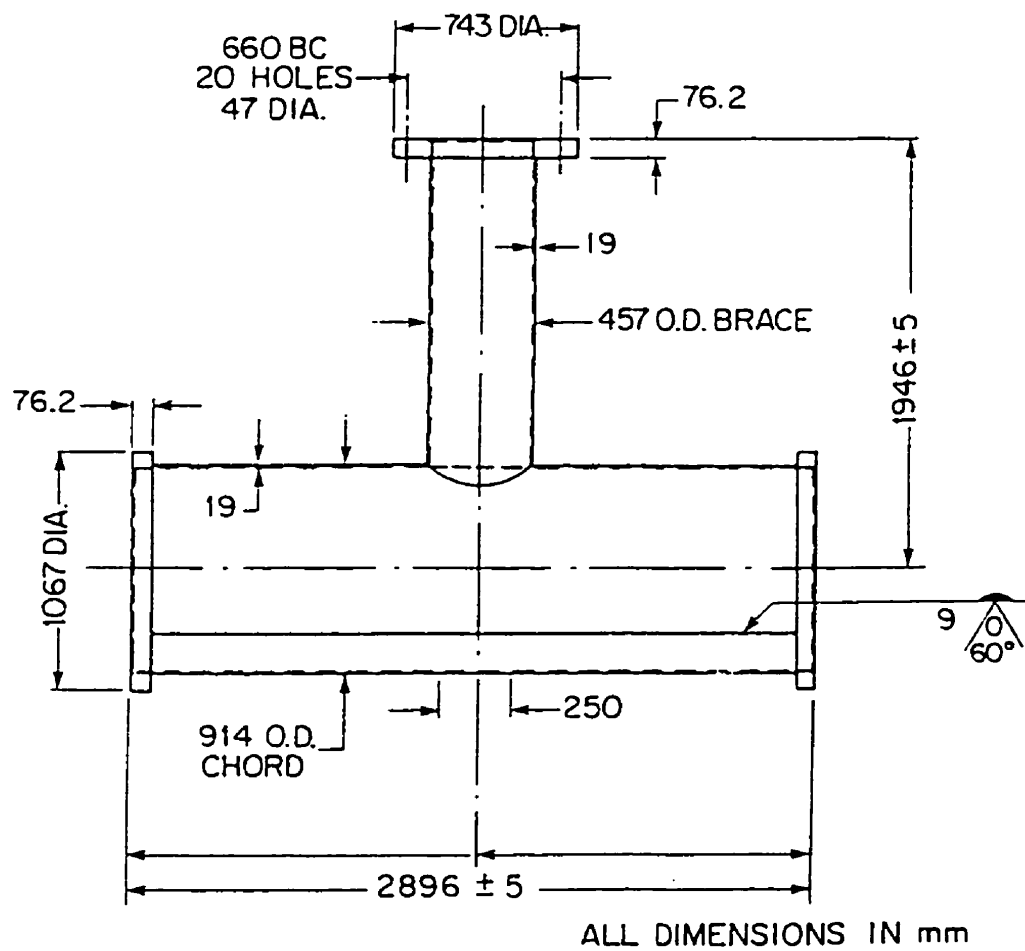


Figure 7.8 Results for stress intensity factors for surface cracks in tubular joints (axial loads)

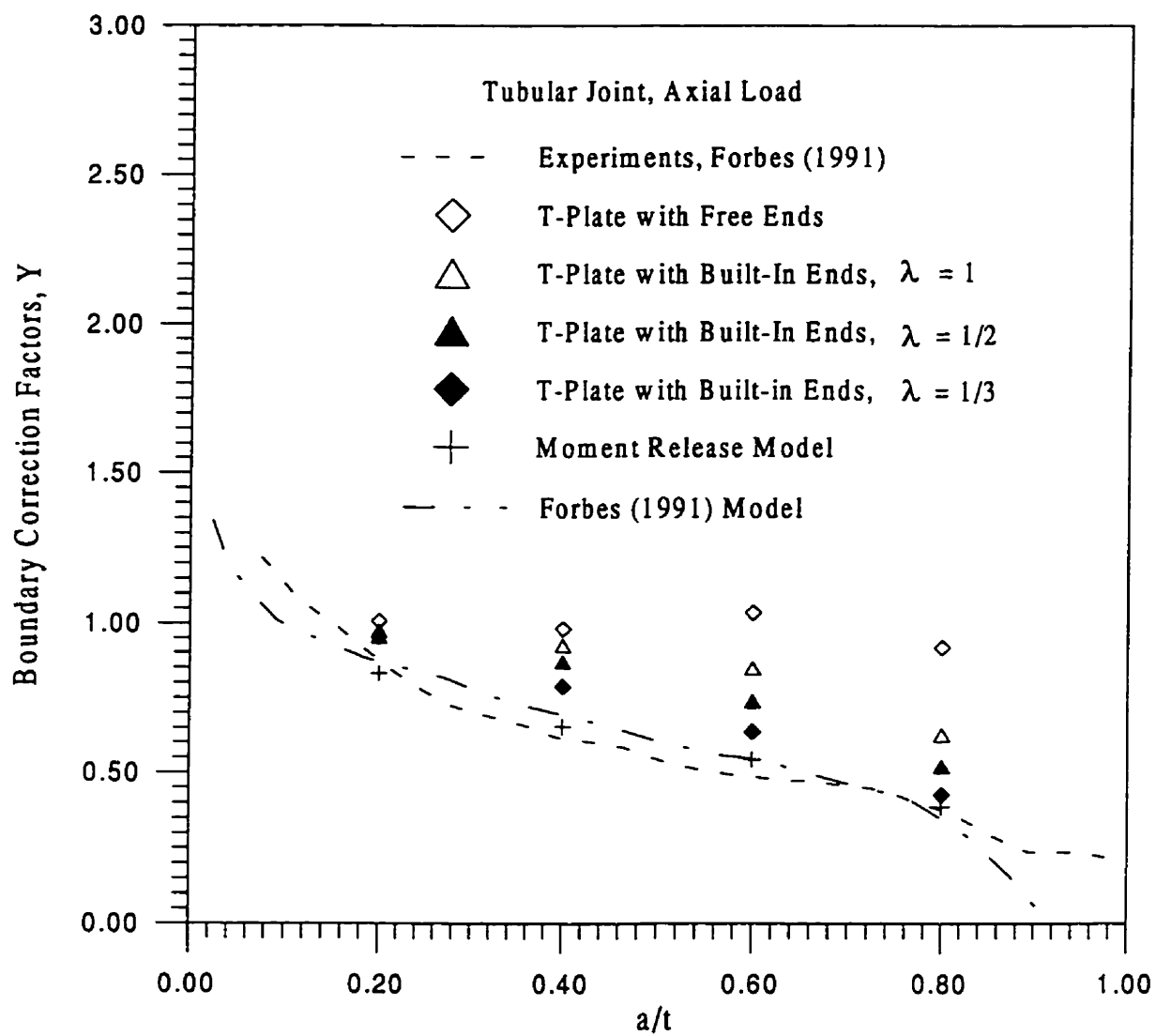


Figure 7.9 Results for stress intensity factors for surface cracks in tubular joints (in plane bending loads)

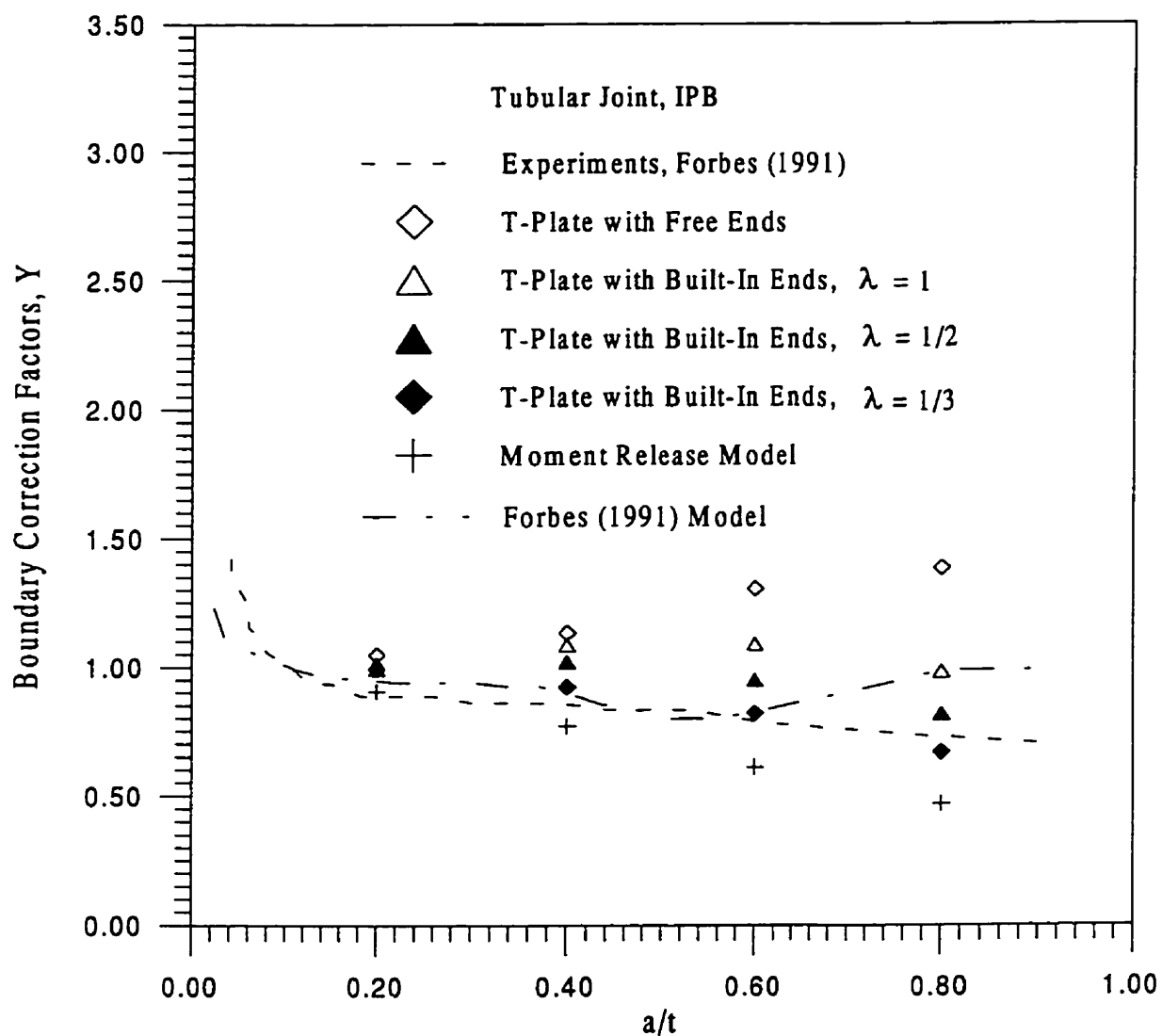


Figure 7.10 Curvature of the surface crack

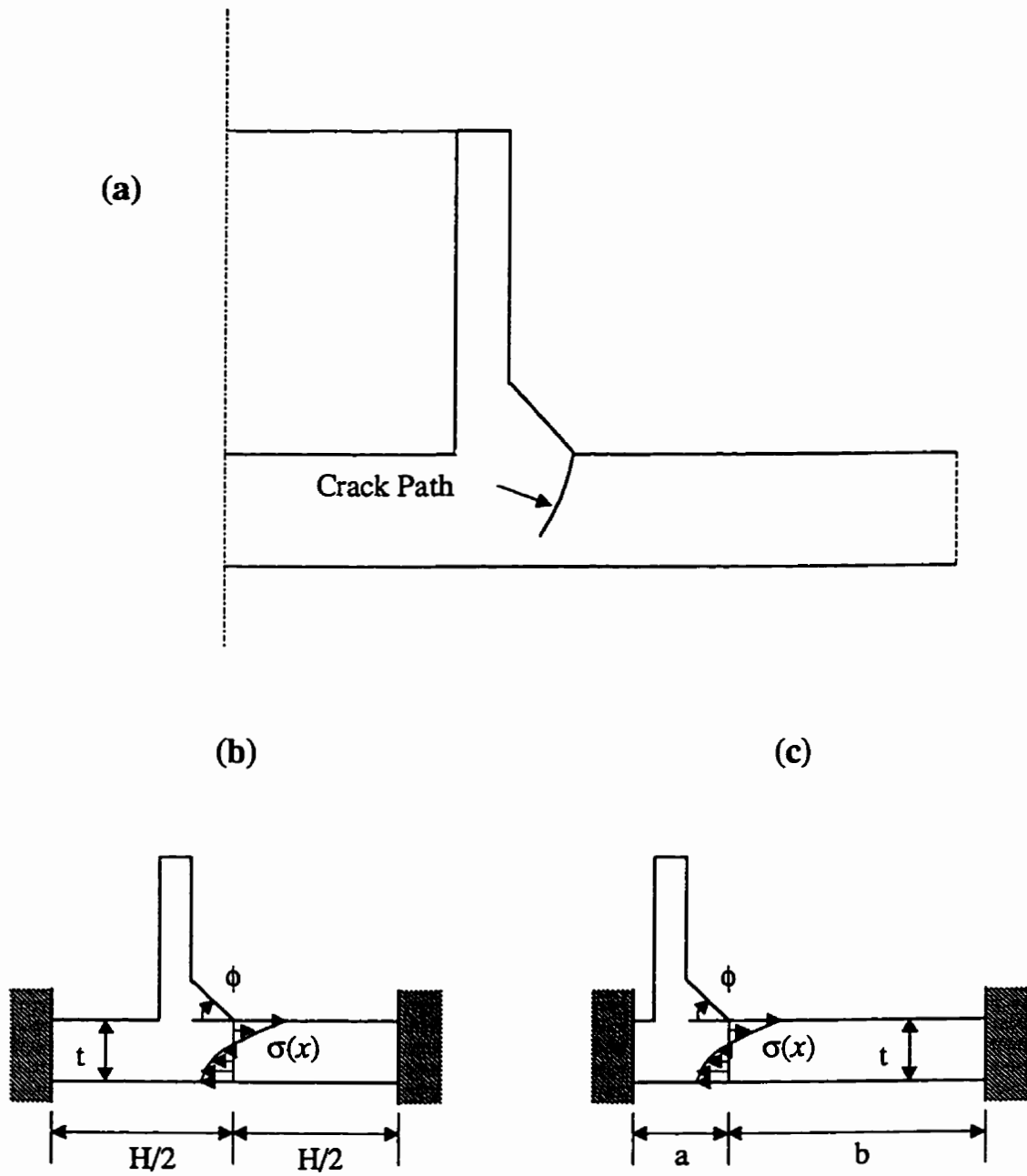


Figure 7.11 Typical two-dimensional stress distribution for pipe-plate and tubular joints

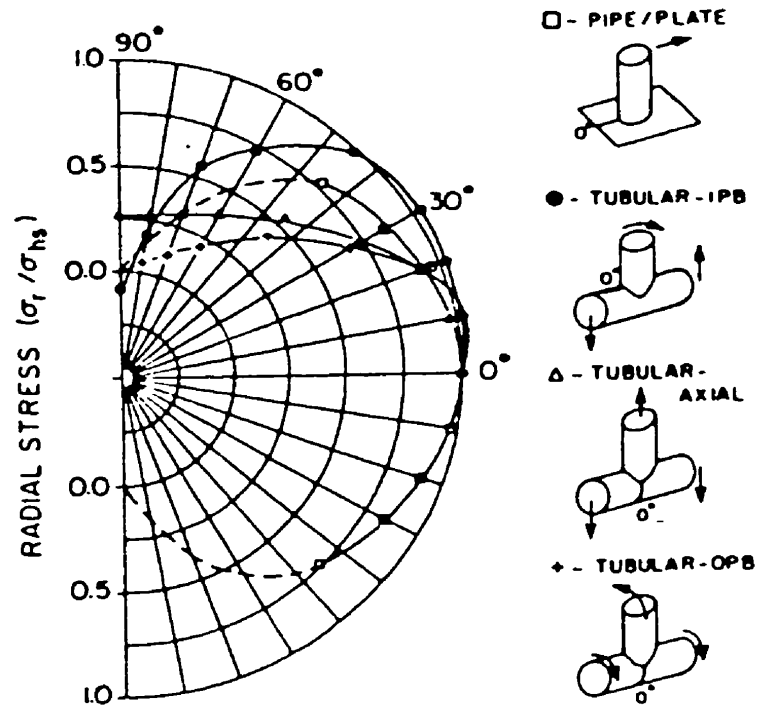
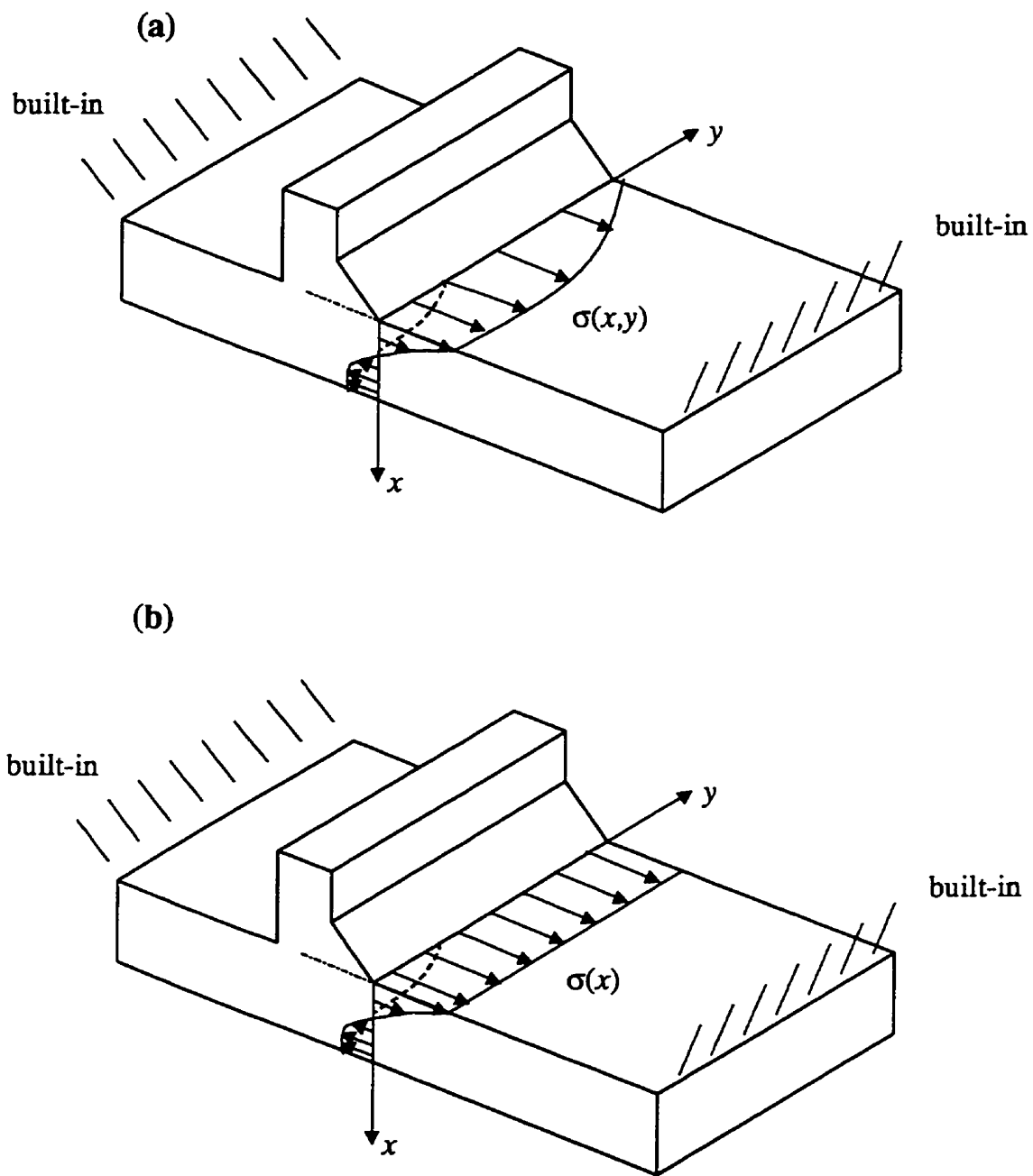


Figure 7.12 T-plate with built-in ends model, (a) two dimensional stress distribution, (b) one dimensional stress distribution



Chapter 8

Conclusions and Recommendations

8.1 Conclusions

In the present research, weight function and stress intensity factor solutions for semi-elliptical surface cracks in flat plates and welded joints were developed. These solutions can account for the effect of two-dimensional stress distributions, and load shedding. They can be used for fatigue life prediction and fracture assessment of these structures. This present approach will be more efficient (in terms of computing time and cost) than three-dimensional finite element analyses, yet more accurate and widely applicable than available empirical solutions.

Theory and Development

Two methods were proposed by the author to derive weight functions for the calculation of stress intensity factors for two-dimensional cracks under two-dimensional stress distributions: the general point load weight function approach and the Fourier series approach. Both methods can calculate stress intensity factors efficiently for surface cracks under two-dimensional stress distributions.

In order to accommodate the effects of fixed boundary conditions into weight functions, a method to obtain stress intensity factor solutions for situations with fixed displacement boundary conditions was developed for surface cracks based on a compliance analysis. This method can provide stress intensity factor solutions for components with built-in ends from available solutions for the same geometry with free end boundary conditions. This dramatically reduced the efforts required for the analysis of stress intensity factors for problems with built-in ends.

Embedded Elliptical Cracks

The proposed general weight function approach for two-dimensional cracks was applied to develop approximate weight functions for embedded elliptical cracks. These weight functions were validated with analytical solutions for different two-dimensional stress distributions. Good accuracy was achieved for a wide range of crack aspect ratios.

Semi-elliptical Cracks in Flat Plates

A Fourier series approach was applied to develop weight functions for semi-elliptical surface cracks in flat plates under two-dimensional stress distributions. The weight functions were derived from reference stress intensity factors obtained from three dimensional finite element analyses. Validation of these weight functions was also conducted. The approximate closed form weight functions derived are suitable for the calculation of stress intensity factors for semi-elliptical surface cracks in flat plates with aspect ratios in the range $0.1 \leq a/c \leq 1$ and relative depths $0 \leq a/t \leq 0.8$ under two dimensional stress distributions.

A compliance analysis method was applied to calculate stress intensity factors for semi-elliptical surface cracks in flat plates with built-in ends. The resulting stress intensity factors were used as reference stress intensity factors to derive weight functions for semi-elliptical surface cracks in flat plates with built-in ends. The stress intensity factor and weight function solutions were verified with three-dimensional finite element calculations. The weight functions derived are suitable for the calculation of stress intensity factors for semi-elliptical surface cracks in flat plates with aspect ratios in the range $0.1 \leq a/c \leq 1$ and relative depths $0 \leq a/t \leq 0.8$.

Semi-elliptical Cracks in T-plate Joints

Weight functions at the deepest and surface points of a semi-elliptical surface crack in T-plate joints with weld angle between 0 and 45° were derived. These weight functions were derived from reference stress intensity factor solutions, which were obtained from three-dimensional finite element calculations, and verified using stress intensity factors for different non-linear stress fields and for far field tension and bending cases. The differences between the weight function prediction and the finite element data were within 10%. The

closed form weight functions derived here make them suitable for fatigue crack growth analysis and fracture assessment for T-plate joints. The weight function can be used to calculate stress intensity factors for any stress field $\sigma(x)$. They are suitable for semi-elliptical surface cracks with aspect ratios $0.05 \leq a/c \leq 1$, relative crack depths $0 \leq a/t \leq 0.6$ and weld angles $0 \leq \phi \leq 45^\circ$.

A method for calculating stress intensity factors for surface cracks in T-plate joints with built-in ends was proposed. The method was based on the weight function solutions for surface cracks in flat-plates with free ends and built-in ends, and the weight functions for surface cracks in T-plate joints with free ends. The method was verified using finite element data. The method can be used to calculate stress intensity factors for any stress field, and are suitable for semi-elliptical surface cracks with aspect ratios $0.05 \leq a/c \leq 1$, relative crack depths $0 \leq a/t \leq 0.6$ and weld angles $0 \leq \phi \leq 45$.

Semi-elliptical Cracks in Pipe-plate and Tubular Joints

A method to determine stress intensity factors for surface cracks in pipe-plate and tubular joints was presented. A T-plate welded joint with built-in ends was used to model pipe-plate and tubular joints. For a surface crack in a pipe-plate or tubular joint, a T-plate model with the same crack geometries of a/c , a/t , ϕ , with built-in ends, under the same crack face stress distribution, $\sigma(x)$ was used to calculate the stress intensity factors in pipe-plate or tubular joints. Different λ values in the H expression were found to give the best results for the given pipe-plate and tubular joints. These different values were required to model the appropriate degree of load shedding in these joints resulting from differences in joint stiffness. The results were compared with available numerical and experimental data.

8.2 Recommendations

The general point load weight function approach for two-dimensional cracks was only applied to embedded elliptical cracks in the present research. This proposed weight function for embedded elliptical cracks can also serve as the foundation for further development of weight functions for two-dimensional surface cracks, corner cracks and other part-through cracks in engineering structures.

The proposed stress intensity factor solutions for surface cracks in pipe-plate and tubular joints were based on limited numerical and experimental stress intensity factor solutions. The λ values were found for one pipe-plate and one tubular joint geometry. Since no solutions are available at the surface point, the proposed solution was not verified at the surface point. Further three-dimensional finite element/experimental analyses are required to examine the range of the λ values, to relate the λ values to the joint geometries, and to further verify the proposed solutions at the surface points.

References

Aaghaakouchak, A., Glinka, G., and Dharmavasan, S., (1989), "A load shedding model for fracture mechanics analysis of fatigue cracks in tubular joints", *OMAE* pp.159-165.

ABAQUS User's Manual, version 5.4 , Hibbit, Karlsson and Sorenson, Providence, R.I., 1994.

Aliabadi, M.H. and Rooke, D.P., (1991), *Numerical Fracture Mechanics*, Kluwer Academic Publishers, Boston.

Banks-Sills, L., (1991), "Application of the Finite Element method to Linear Elastic Fracture Mechanics," *Applied Mechanics Review*, Vol. 44, pp. 447 - 461.

Barsoum, R. S., (1977), "Triangular Quarter-Point Elements as Elastic and Perfectly-Plastic Crack Tip Elements," *International Journal for Numerical Methods in Engineering*, Vol. 11, pp. 85 - 98.

Bell, R., (1985), "Determination of stress intensity factors for welded toe defects", Phase II, DSS contract OST 84-00125 report.

Bowie, O.L. and Freese, C.E., (1981), "Cracked-Rectangular Sheet with Linearly Varying End displacements", *Engineering Fracture Mechanics*, Vol. 14, pp. 519-526.

Bowness, D. and Lee, M.M.K., (1995), "The Development of an Accurate Model for the Fatigue Assessment of Doubly Curved Cracks in Tubular Joints", *International Journal of Fracture*, Vol 73, pp. 129-147.

Bowness, D. and Lee, M.M.K., (1996), "Stress Intensity Factors for Semi-Elliptical Weld-Toe Cracks in T-Butt Geometries", *Fatigue & Fracture of Engineering Materials & Structures*, Vol 19, pp. 787-797.

Brennan, F.P., Dover, W.D., Kare, F. and Hellier, A.K., (1996), "Development of Parametric Equations for Weld Toe Stress Intensity Factors", *Report to the Health and Safety Executive*.

Bueckner, H. F., (1970), " A Novel Principle for the Computation of Stress Intensity Factors," *Z. Agew. Math. Mech.*, Vol 50, pp. 129 - 146.

Bueckner, H. F., (1970), " A Novel Principle for the Computation of Stress Intensity Factors," *Z. Agew. Math. Mech.*, Vol 50, pp. 129 - 146.

Bueckner, H.F., (1987), "Weight Functions and Fundamental Fields for the Penny-Shaped and the Half-plane Crack in Three-Space". *International Journal of Solids and Structures*, Vol 23, pp. 57 - 93.

Burdekin, F.M., Chu, W.H., Chan, W.T.W and Manteghi, S., (1986), "Fracture Mechanics Analysis of Fatigue Crack Propagation in Tubular Joints", *International Conference on Fatigue and Crack Growth in Offshore Structures*, April, Institute of Mechanical Engineers, C133/86.

Burns, D.J., Lambert, S.B., and Mohaupt, U.H., (1987), "Crack growth behavior and fracture mechanics approach", paper PS6, *Int. Conf. Steel in Marine Structures*, Delft, The Netherlands.

Cheaitani, M.J., Thurlback, S.D. and Burdekin, F.M., (1995), "Fatigue, fracture, and plastic collapse of offshore tubular joints using BSI PD 6493", *Proceedings of the 14th International Conference on Offshore Mechanics and Arctic Engineering*, ASME, Vol. III, pp. 41-54.

Desjardins, J.L., (1988), "Stress Intensity Factors for Surface Cracks in Complex Stress Fields", *M.A.S. Thesis, University of Waterloo*, Waterloo, Canada.

Desjardins, J.L., Lambert, S.B., Burns, D.J. and Thompson, J.C., (1991), "A Weight Function Technique for Estimating Stress Intensity Factors for Cracks in High – Pressure Vessel", *Journal of Pressure Vessel Technology*, Vol. 113, pp. 10-21.

Dijkstra, O.D, Snijder, H.H., and Straalen, I.J. Van, (1989), "Fatigue crack growth calculations using stress intensity factors for welded toe geometries, *OMAE*, pp. 137-143.

Dover, W.D. and Connolly, M., (1986), "Fatigue Fracture Mechanics Assessment of Tubular Welded Y and K-Joints", *International Conference on Fatigue and Crack Growth in Offshore Structures*, April, Institute of Mechanical Engineers, C14/86.

Dover, W.D., (1978), "Fatigue Crack Growth in T-Joints, out-of-plane Bending", *Proceedings of the 10th Offshore Technology Conference(OTC-78)*, Houston, OTC 3252.

Du, Z.Z. and Hancock, J.W., (1989), "Stress Intensity Factors of Semi-Elliptical Cracks in a Tubular Welded Joint Using Line Springs and 3D Finite Elements", ASME, *Journal of Pressure Vessel Technology*, Vol. 111, pp. 247-251.

Fett, T., Mattheck C., and Munz, D., (1989), "Approximate Weight Function for 2D and 3D-problems", *Engineering Analysis with Boundary Elements*, Vol. 6, pp. 48-63.

Fett, T., Mattheck, C. and Mune, D., (1987), "On the Evaluation of Crack Opening Displacement from the Stress Intensity Factor", *Engineering Fracture Mechanics*, Vol. 27, pp. 697-715.

Forbes, J., Glinka, G. and Burns, D.J., (1992), "Fracture Mechanics Analysis of Fatigue Cracks and Load Shedding in Tubular Welded Joints", *OMAE*, Vol. III-B, pp. 307-313.

Forbes, J.W., (1991), "Fatigue in Stiffened T-Tubular Joints for Offshore Structures", Ph. D. Thesis, University of Waterloo, Waterloo, Canada.

Forbes, J.W., Desjardins, J.L., Glinka, G. and Burns, D.J., (1991), "Stress Intensity Factors for Semi-Elliptical Surface Cracks in Weldments," *Proceedings of the 10th International Conference on Offshore Mechanics and Arctic Engineering*, ASME, Vol III-B, pp. 529 - 534.

Fu, B., Haswell, J.V., and Bettess, P., (1993), "Weld magnificant factors for semi-elliptical surface cracks in fillet welded T-butt joint models", *International Journal of Fracture*, Vol. 63, pp.155-171.

Glinka, G. and Shen, G., (1991), "Universal Features of Weight Functions for Cracks in Mode I," *Engineering Fracture Mechanics*, Vol. 40, pp. 1135 - 1146.

Green, A. E. and Snedden, I.N., (1950), "The Distribution of Stress in the Neighborhood of a Flat Elliptical Crack in an Elastic Solid." *Proc. Camb. Phil. Soc.*, Vol. 46, pp. 159-163.

Grueter, L., Huget, W. and Kylla, H., (1981), "Weight Functions and Stress Intensity Magnification Factors for Elliptical and Semi-Elliptical Cracks Under Variable Normal Stresses", Interatom Report INTAT no. 32.05095.0.

Haswell, J. and Hopkins, (1991), "A review of fracture mechanics models of tubular joints", *Fatigue and Fracture of Engineering Materials and Structures*, Vol. 14, pp. 483-497.

Hellier, A.K., Connolly, M.P.m Kare, R.F. and Dover, W.D., (1990), "Prediction of the Stress Distribution in Tubular Y- and T-Joints", *Int. J. Fatigue*, Vol. 12, pp 25-33.

Hibbit, Karlsson and Sorenson, (1996) *ABAQUS User's Manual*, version 5.4 , Pawtucket, R.I.

Irwin, G.R., (1962), "The Crack Extension Force For a Part-Through Crack in a Plate." *ASME Journal of Applied Mechanics*, Vol. 29, pp. 651-664.

Kassir M.K. and Sih, G.C., (1967), "Three Dimensional Stress Distribution around an Elliptical Crack under Arbitrary Loadings." *ASME Journal of Applied Mechanics*, Vol. 33, pp. 601-611.

Kiciak, A., Glinka, G. and Burns, D.J., (1995), "Weight Functions and Stress Intensity Factors for Longitudinal Semi-Elliptical Cracks in Thick-Wall Cylinders", *J. Press. Vess. Technol.*, to be published.

Lambert, S.B. and Bell, R., (1993), "Stress Intensity Factors for a Pipe-Plate Welded Joint", *International Journal of Pres. Ves. & Piping*, Vol. 53, 525-542.

Lambert, S.B., (1988), "Fatigue Crack Growth in Welded Joints in Seawater", Ph.D. Thesis, Univeristy of Waterloo, Waterloo, Canada.

Lambert, S.B., Mohaupt, U.H., Burns, D.J. and Vosikovsky, O., (1987), "Simulation of Fatigue Behaviour of Tubular Joints Using a Pipe-to-Plate Specimen", In *Steel in Marine Structures, SIMS'87*, pp. 489-500.

Lecsek, R.L., Yee, R., Lambert, S.B. and Burns, D.J., (1995), "A Probabilistic Model for Initiation and Propagation of Surface Cracks in Welded Joints", *Fatigue & Fracture of Engineering Materials & Structures*, Vol. 18, pp. 821-831.

Lecsek, R.L., (1993), "Fatigue Crack Initiation and Propogation in Notched Plates and Welded T-Joints", M.A.S. Thesis, Univeristy of Waterloo, Waterloo, Canada.

Maddox, S.J., (1975), *International Journal of Fracture*, Vol. 11, pp.221-243.

Maddox, S.J., (1997), "Development in Fatigue Design Codes and Fitness-for-Service Assessment Methods", *Proceedings of the IIW International Conference on Performance of Dynamically Loaded Welded Structures*, San Francisco. pp. 22-41.

Marchand, N., Parks, D.M. and Pelloux, R.M., (1986), " K_I -Solutions for Single Edge Notch Specimens under Fixed End Displacements", *International Journal of Fracture*, Vol. 31, pp. 53-65.

Mettheck, C., Munz, D. and Stamm, H., (1983), "Stress Intensity Factor for Semi-Elliptical Surface Cracks Loaded by Stress Gradients", *Engineering Fracture Mechanics*, Vol. 18, pp. 633-641.

Miller, A.G., (1988), "Review of Limit Loads of Structure Containing Cracks", *Int. J. Pres. Vessel & Piping*, Vol. 32, pp. 197-327.

Moran, B. and Shih, C.F., (1987), "Crack Tip Associated Domain Integrals from Momentum and Energy Balance", *Engineering Fracture Mechanics*, Vol. 27, pp. 615 - 642.

Newman Jr., J. C. and Raju, I. S., (1979), "Analyses of Surface Cracks in Finite Plates under Tension and Bending Loads," *NASA TP-1578*.

Newman Jr., J.C., and Raju, I.S., (1981), "An Empirical Stress Intensity Factor Equation for the Surface Crack," *Engineering Fracture Mechanics*, Vol. 15, pp. 185-192.

Nishioka, T. and Atluri, S.N., (1983), "An Alternating Method for Analysis of Surface Flawed Aircraft Structure Components", *AIAA J.* Vol. 21, pp. 749-757.

Nishioka, T. and Atluri, S.N., (1983), "Analytical Solutions for Embedded Elliptical Cracks, and Finite Element Alternating Method for Elliptical Surface Cracks, Subjected to Arbitrary Loadings." *Engineering Fracture Mechanics*, Vol. 17, pp. 267-288.

Niu, X. and Glinka, G., (1987), "The Weld Profile Effect on Stress Intensity Factors in Weldments," *International Journal of Fracture*, Vol. 35, pp. 3-20.

Niu, X. and Glinka, G., (1990), "Weight Functions for Edge and Surface Semi-Elliptical Cracks in Flat Plates and Plates with Corners," *Engineering Fracture Mechanics*, Vol. 36, pp. 459 - 475.

Niu, X. and Glinka, G., (1990), "Theoretical and Experimental Analyses of Surface Fatigue Cracks in Weldments", *Surface-Crack Growth: Models, Experiments, and Structures*, ASTM STP 1060, W.G. Reuter et al. Eds., ASTM, pp.390-413.

Okamura, H., Watanabe, K. and Takano, T., (1975), "Deformation and Strength of Cracked Member under Bending and Axial Force", *Engineering Fracture Mechanics*, Vol. 7, pp. 531-539.

Oore, M. and Burns, D.J., (1980a), "Estimation of Stress Intensity Factors for Embedded Irregular Cracks Subjected to Arbitrary Normal Stress Fields", *ASME Journal of Press. Ves. Tech.*, Vol. 102, pp. 202-211.

Oore, M. and Burns, D.J., (1980b), "Estimation of Stress Intensity Factors for Irregular Cracks Subjected to Arbitrary Normal Stress Fields", *Proc. 4th Int. Conf. Pres. Ves. Tech., London, I. Mech. E.*, Vol 1, pp. 139-147.

Petroski, H.J. and Achenbach, J.D., (1978), "Computation of the Weight Function from a Stress Intensity Factor", *Engineering Fracture Mechanics*, Vol. 10, pp. 257-266.

Raju, I.S. Mettu, S.R. and Shivakumar, V., (1994), "Stress intensity factor solutions for surface cracks in flat plates subjected to non-uniform stresses", *Fracture Mechanics: Twenty-Fourth Volume, ASTM STP 1207*, Landes et al. Eds, ASTM, Philadelphia, pp. 560-580.

Rhee, H.C., (1989), "Fatigue crack growth analyses of offshore structural tubular joints", *Engineering Fracture Mechanics*, Vol. 34, pp. 1231-1239.

Rice, J., (1972), "Some Remarks on Elastic Crack Tip Field," *International Journal of Solids and Structures*, Vol 8, pp. 751 - 758.

Rice, J., (1989), "Weight Function Theory for Three-dimensional Elastic Crack Analysis", *Fracture Mechanics, Perspectives and Directions (Twentieth Symposium) ASTM STP 1020*, pp. 29 - 57.

Ritchie, D. and Voermans, C.W.M., (1987), "Stress intensity factors in an offshore tubular joint test", *Proc. 3rd Int. Symp. on Numerical Fracture Mechanics*, San Antonio, Texas.

Shah, R.C. and Kobayashi, A.S., (1971), "Stress Intensity Factor for an Elliptical Crack under Arbitrary Normal Loading". *Engineering Fracture Mechanics*, Vol. 3, pp 71-96.

Shen, G. and Glinka G., (1991a), "Weight Function for a Surface Semi-Elliptical Crack in a Finite Thickness Plate," *Theoretical and Applied Fracture Mechanics*, Vol 15, pp. 247 - 255.

Shen, G. and Glinka, G. (1991b), "Determination of Weight functions from Reference Stress Intensity Factors," *Theoretical and Applied Fracture Mechanics*, Vol. 15, pp. 237 - 245.

Shih, C.F., Moran, B. and Nakamura, T., (1986), "Energy Release Rate along a Three-Dimensional Crack Front in a Thermally Stressed Body," *International Journal of Fracture*, Vol. 30, pp. 79-102.

Shiratori, M., Niyoshi, T. and Tanikawa, K., (1987), "Analysis of Stress Intensity Factors Surface Cracks Subjected to arbitrarily distributed surface stresses", in *Stress Intensity Factors Handbook* (Edited by Murakami, Y. et al.), Vol. 2, pp. 698-705.

Shirotori, M., (1986), "Analysis of Stress Intensity Factors for Surface Cracks Subjected to Arbitrarily Distributed Stresses", *Bulletin of the Faculty of Engineering, Yokohama National University*, Vol. 35, 1-25.

Sih, G. C and Lee, Y. D., (1989), "Review of Triaxial Crack Border Stress and Energy Behaviour," *Theoretical and Applied Fracture Mechanics*, Vol. 12, pp. 1 - 17.

Sih, G.C., Paris, P.C. and Erdogan, F., (1962), "Crack Tip Stress Intensity Factors for Plane Extension and Plate Bending Problems, *ASME Journal of Applied Mechanics*, Vol. 29, pp.306-312.

Smith, L.F., (1984), "The effect of geometry changes upon the predicted fatigue strength of welded joints", *Proc. 3rd Int. Conf. on Numerical Methods in Fracture Mechanics* (Edited by Luxmoore and Owen), pp. 561-574.

Spiegel, M. R., (1992), *Mathematical Handbook of Formulas and Tables*. McGraw-Hill Inc.

Tan, P.W., Raju, I.S., Shivakumar and Newman, J.C, (1988), "An Evaluation of Finite Element Models and Stress Intensity Factors for Surface Cracks Emanating from Stress Concentrations", *NASA Technical Memorandum* 101527.

Vainshtok, V.A., (1991), "Some applications of the weight function theory to the analysis of cracks", *Computational Mechanics*, Vol8, pp. 319-329.

Vainshtok, V.A., and Varfolomeyev, I.V., (1990), "Stress Intensity Factor Analysis for Part-Elliptical Cracks in Structures", *International Journal of Fracture*, Vol. 46, pp. 1-24.

Vijayakumer, K. and Atluri, S.N., (1981), "An Embedded Elliptical Flaw in an Infinite Solid Subject to Arbitrary Crack Face Traction." *ASME Journal of Applied Mechanics*, Vol. 48, pp. 88-98.

Wang, X. and Lambert, S.B., (1995a), "Stress Intensity Factors for Low Aspect Ratio Semi-Elliptical Surface Cracks in Finite Thickness Plates Subjected to Nonuniform Stresses", *Engineering Fracture Mechanics*, Vol 51, pp. 517-532.

Wang, X. and Lambert, S.B., (1995b), "Local Weight Functions for Semi-Elliptical Surface Cracks in Finite Thickness Plates", *Theoretical and Applied Fracture Mechanics*, Vol. 23, pp. 199 - 208.

Wang, X. and Lambert, S.B., (1997), "Stress Intensity Factors and Weight Functions for High Aspect Ratio Semi-Elliptical Surface Cracks in Finite-Thickness Plates", *Engineering Fracture Mechanics*, Vol 57, pp. 13-24.

Wang, X., and Lambert, S.B., (1996), "Stress intensity factors and weight functions for longitudinal semi-elliptical surface cracks in thin pipes", *Int. J. Pres. Vessel & Piping*, Vol. 65, pp. 75-87.

Wu, X.R. and Carlsson, A.J., (1991), *Weight Functions and Stress Intensity Factor Solutions*. Pergamon Press, Oxford

Wu, X.R., 1984, "Stress intensity factors for half-elliptical surface cracks subjected to complex crack face loadings", *Engineering Fracture Mechanics*, Vol. 19, pp. 387 - 405.

Yee, R. and Lambert, S.B., (1995), "A Reversing Direct Current Potential Drop System for Detecting and Sizing Fatigue Cracks along Weld Toes", *Journal of Testing and Evaluation*, Vol. 23, pp. 254-260.

Zheng, X. J. and Glinka, G., (1995), "Weight functions and stress intensity factors for longitudinal semi-elliptical cracks in thick-wall cylinders", *Journal of Pressure Vessel Technology*, Vol. 117, pp. 383-389.

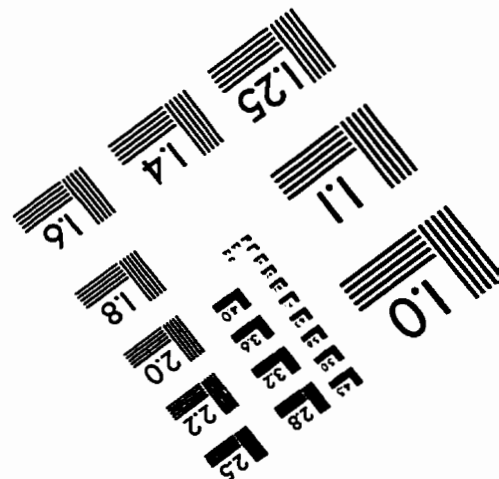
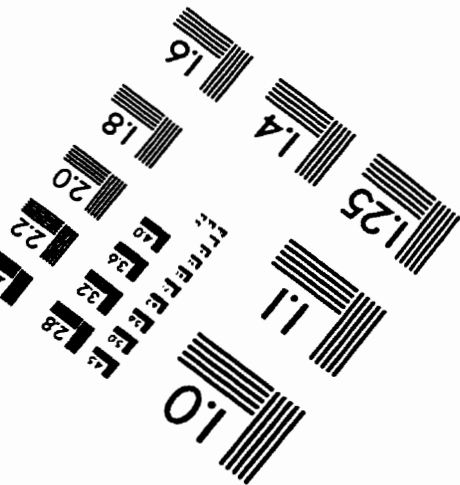
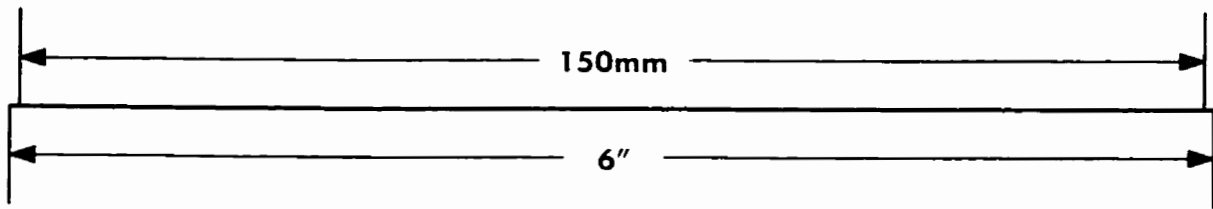
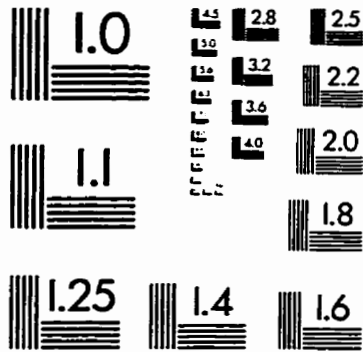
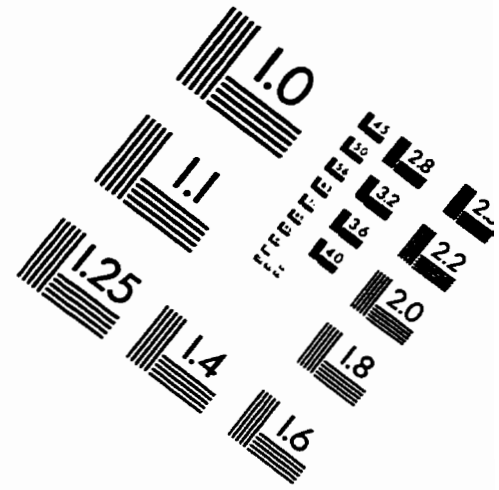
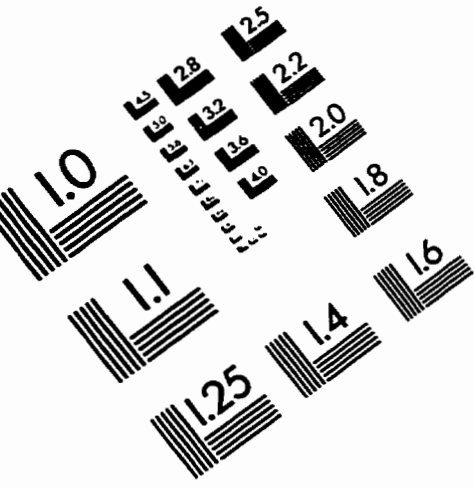
Appendix:

List of relevant papers published by the author

- Xin Wang, S.B. Lambert and G. Glinka, “Approximate Weight Functions for Elliptical Embedded Cracks”, *Engineering Fracture Mechanics*, in press, 1998
- Xin Wang and S.B. Lambert, “Weight Functions and Stress Intensity Factors for Semi-Elliptical Cracks in T-Plate Welded Joints”, *Fatigue & Fracture in Engineering Materials & Structures*, in press, 1998
- Xin Wang and S.B. Lambert, “Stress Intensity Factors and Weight Functions for Semi-Elliptical Surface Cracks in Finite-Thickness Plates under Two-Dimensional Stress Distributions”, *Fatigue & Fracture in Engineering Materials & Structures*, Vol. 20, pp. 1637-1655, 1997
- Xin Wang and S.B. Lambert, “Stress Intensity Factors and Weight Functions for High Aspect Ratio Semi-Elliptical Surface Cracks in Finite-Thickness Plates”, *Engineering Fracture Mechanics*, Vol. 57, pp. 13-21, 1997
- Xin Wang and S.B. Lambert, “Stress Intensity Factors and Weight Functions for Longitudinal Semi-Elliptical Cracks in Thin Pipes”, *International Journal of Pressure Vessel and Piping*, Vol. 65, pp. 75-87, 1996
- Xin Wang and S.B. Lambert, “Stress Intensity Factors for Low Aspect Ratio Longitudinal Surface Cracks in Thin Pipes”, *ASME PVP-Vol. 331, Pressure Vessels and Piping Design, Analysis, and Severe Accidents*, pp. 39-45, 1996
- Xin Wang and S.B. Lambert, “Local Weight Functions for Semi-Elliptical Surface Cracks in Finite Thickness Plates”, *Theoretical and Applied Fracture Mechanics*, Vol. 23, pp. 199-208, 1995

- Xin Wang and S.B. Lambert, "Stress Intensity Factors for Low aspect Ratio Semi-Elliptical Surface Cracks in Finite Thickness Plates Subjected to Non-Uniform Stresses", *Engineering Fracture Mechanics*, Vol. 51, pp. 517-532, 1995

IMAGE EVALUATION TEST TARGET (QA-3)



APPLIED IMAGE, Inc
1653 East Main Street
Rochester, NY 14609 USA
Phone: 716/482-0300
Fax: 716/288-5989

© 1993, Applied Image, Inc. All Rights Reserved